THE UNIVERSITY
of EDINBURGH

Microbial weathering of shale rock in natural and historic industrial environments

Toby Samuels

Doctor of Philosophy

The University of Edinburgh

April 2018

Lay Summary

The rock weathering activity of microorganisms within shale is something that concerns research scientists, civil engineers and resource geologists, among others, due to its impact on natural and manmade environments. Shale forms roughly 70 % of all sedimentary rocks within the Earth's crust and has vast economic value. Fracking and shale gas provide a contemporary example, but shale forms cap formations over oil and gas deposits and is a major source of valuable heavy metals. Furthermore, crushed shale is extensively used within the construction industry for a range of purposes including building foundations and roadside embankments. Therefore, microbial weathering of shale can be the basis of valued resources or the cause of financial damages.

A previously unconsidered consequence of microbial shale weathering is in the erosion of soft rock cliffs and coastline recession. Coastal erosion is a major issue worldwide, yet the mechanisms controlling erosion and their relative contribution in differing environments is poorly understood. Microbial weathering activity has previously been disregarded as too slow and ephemeral to have any real impact on shaping landscapes, but this viewpoint has become increasingly challenged.

In this thesis, I have addressed the following questions:

- Which rock weathering microbial species are present in weathered shale environments, and what rock weathering capabilities do they have?
- What impact do rock weathering microbial communities have on the breakdown of shale?
- Which components of shale are susceptible to microbial rock weathering processes?
- Does shale elicit physiological or growth responses in microbes that inhabit weathered shale environments?

To answer these questions, I have used the North Yorkshire coastline and its range of weathered shale environments, including natural cliffs and manmade industrial locations, as sample sites to isolate and study rock weathering organisms. Using a range of techniques both in the field and in the laboratory, I show that microbial communities within weathered shale have rock diverse weathering capabilities and that they can use these to change their geochemical environment.

Numerous bacterial isolates with one or more weathering capabilities, such as the production of acid or the oxidation of iron, were identified. One bacterial isolate, *Variovorax paradoxus,* was demonstrated to have complex interactions with its geological environment that affected both its growth and motility. Microbial iron oxidation was shown to be a dominant biogeochemical process within a simulated weathered shale environment, and both bacteria and fungi were shown to weather and morphologically alter the iron-based mineral pyrite. However, despite identifying rock weathering microbes with a range of capabilities not related to iron oxidation, no clear evidence of their weathering activity could be discerned from the data collected.

These results support the role of iron oxidizing microbes as important weathering agents within shale rock cliffs and other weathered shale environments. Previous studies have shown that microbial iron oxidation can act via numerous mechanisms to structurally weaken rock, and I hypothesise that the activity of iron oxidizing microbes within shale rock cliffs could play a role in accelerating erosive processes. Future work should focus on the role of other microbial weathering mechanisms in shale rock degradation. The presence of organisms with the capabilities to enact these mechanisms is indicative of their potential, but alternative methodologies may need to be devised to elucidate their actual impact.

Abstract

The weathering of shales is a globally important process affecting both natural and built environments. Shales form roughly 70 % of worldwide sedimentary rock deposits and therefore the weathering of these rocks has substantial effects on the geochemical cycling of elements such as carbon, iron and sulfur. Microbes have been shown to play a key role in weathering shales, primarily through the oxidation of the iron and sulfur of embedded pyrite and the resultant production of sulfuric acid.

Despite significant interest in the microbial weathering of shales within industrial sectors such as biohydrometallurgy and civil engineering, comparatively few studies have investigated microbial shale weathering in natural environments. Furthermore, the role of microbes in natural shale weathering processes beyond iron oxidation has largely remained unexplored.

In this thesis, the weathering capabilities of microbial communities from natural weathered shale was investigated. The North Yorkshire coastline was used as a study location, due to the abundance and diversity of natural cliffs and historic, disused industrial sites. Cliff erosion and recession on the North Yorkshire coastline is a major concern for local authorities and is the focus of current research. The aim of this work has been to evaluate microbial shale weathering processes within these environments, and hypothesise the possible contribution they may have to erosive processes.

Phenotypic plate assays inoculated with weathered shale material were used to obtain rock weathering bacterial isolates that tested positive for a specific weathering phenotype, such as iron oxidation or siderophore production. Subsequent 16S rRNA sequencing enabled genera level identification, revealing 15 genera with rock weathering capabilities with several being associated with multiple weathering phenotypes including *Aeromonas sp*., *Pseudomonas sp.* and *Streptomyces sp.*. Shale enrichment liquid cultures were incubated with shale rock chips to simulate natural biological weathering conditions, and the concentration of rock-leached elements in the fluid measured. No evidence of microbially-enhanced leaching was found

consistently for any element, however the significant reduction in leachate iron concentration under biological conditions indicates that iron precipitation occurred via microbial iron oxidation.

Enrichment cultures inoculated with weathered shale and containing organic matter (OM) rich rocks in water or M9 medium, both liquids lacking an organic carbon source, were grown over several months. The cultures yielded microbial isolates that could utilise rock bound OM sources and one bacterial isolate, *Variovorax paradoxus*, was taken forward for ecophysiological study. The shale rock that the organism was isolated from, along with other OM rich rocks (mudstones and coals), elicited complex responses from *V. paradoxus* including enhanced growth and motility.

Finally, mineral microcosms *in vitro* and mesocosms *in situ* investigated microbial colonization and weathering of shale-comprising minerals (albite, calcite, muscovite, pyrite and quartz). Microcosms were established using iron oxidizing enrichment cultures, as based on the results of the simulated rock weathering experiments, while the *in situ* mesocosms were buried within weathered shale scree within a disused mine level. Levels of colonization significantly varied between minerals within the microcosms (pyrite>albite, muscovite>quartz>calcite). Although differences in mineral colonization were seen in the mesocosms, they did not match those in the microcosms and were not statistically significant. Pyrite incubated in the microcosms became significantly weathered, with extensive pit formation across the mineral surface that is consistent with microbial iron oxidation. In the mesocosms, pit formation was not identified on pyrite surfaces but dark etchings into the pyrite surface were found underneath fungi hyphal growth.

The results of this thesis highlights that a range of microbial rock weathering mechanisms are abundant across weathered shale environments. Microbial iron oxidizing activity was a dominant biogeochemical process that altered rock-fluid geochemistry and weathered pyrite surfaces. However, the impact on rock or mineral weathering of other microbial mechanisms was not elucidated by this work. Given the known capabilities of these mechanisms, the conditions under which they are active may not have been met within the experimental setup used.

Microbial iron oxidation in shale and shale-derived materials has previously been demonstrated to weaken rock structure through acid production and secondary mineral formation. From the results of this thesis, it is clear that microbial iron oxidation is an active process within some of the weathered shale environments studied, including cliff surfaces. Therefore, it can be hypothesised that microbial activity could play a role in structurally weakening shale rock within cliffs and accelerate their erosion. Future work should attempt to quantify the rate and extent of microbial iron oxidizing activity within shale cliff environments and investigate its contribution to erosive processes.

Declaration

This thesis has been solely composed by the candidate. Unless clearly stated, this work is the candidate's own. Where results have been obtained through collaborations with other researchers, their precise contributions are made clear in the text as appropriate.

This work has not been submitted for any other degree or professional qualification.

Candidate's signature……..……..Date……

Acknowledgments

Over the past four years, various individuals and groups have enabled me to produce the work in this thesis. I would broadly like to thank the many students and researchers I have interacted with throughout the course of my PhD, you have provided me with the inspiration and support to get this project to the finish line. There are however several specific acknowledgements I would like to make.

Firstly, I would like to thank Israeli Chemicals Limited (formerly Cleveland Potash Limited), for providing the funding for this project. David Pybus, my point of contact with ICL, has been an exemplary industrial supervisor, guiding me in my field work and the project as a whole. His drive and passion to understand coastal erosion on the North Yorkshire coastline has been motivational.

I am hugely indebted to my principal supervisor Charles Cockell whose enthusiasm, optimism and boundless energy has kept me afloat. His ability to always see the bigger picture and to broaden my mind has been inspirational. Undertaking my PhD at the UK Centre for Astrobiology (UKCA) has provided me with numerous fantastic opportunities, from exploring the subterreanean world of Sardinia to talking to primary school children about Tim Peake and the International Space Station. I am grateful both to Charles and to all members of the UKCA, for making my PhD experience memorable.

I would also like to thank Mark Wilkinson, my second supervisor, for his support and guidance in all matters geological. Thank you for your never-ending patience! There is a long list of other researchers at the University of Edinburgh that I would like to acknowledge for the help they provided me, particularly with regards to instrument use. These include Nick Odling (XRD), Nicola Cayzer (SEM-EDS), Mike Hall (rock cutting and polishing), Lorna Eades (ICP-OES), Ingo Loa (Raman) and Andy Schofield (SEM). I would like to make a special thanks to Angela Dawson, for her expertise in microbiology and for all her hard work in keeping me, and many others, safe while working.

I would like to acknowledge Wren Montgomery of Imperial College London for her contribution to this project, providing me both with geological samples and organic geochemistry data.

I was lucky enough to meet Penny Boston (now director of the NASA Astrobiology Institute) while at a meeting. She provided me with new insights into geomicrobiology and cave microbiology that would have a lasting effect on both my interests and my doctoral work. As such, she is another that I would like to say a special thanks to.

My colleagues at the UKCA and the University of Edinburgh have been a fun and friendly group to work with, many of who have helped me through the past four years. I would specifically like to thank Casey Bryce, Hanna Landenmark, Claire-Marie Loudon, Tasha Nicholson, Petra Schwendner, Adam Stevens and Jenn Wadsworth for proof reading my thesis and providing useful comments and edits. I would also like to thank Sophie Nixon, Mark Fox-Powell and Sam Paylor in particular for their guidance and support when things got difficult!

The completion of this thesis has been greatly aided by the generosity and flexibility of my current employers, Nick Colegrave and Peter Keightley, in allowing me to work on my thesis when time permitted. Thank you to both for being so understanding.

The support and love of my friends and family has played a major role in keeping me happy and (largely) sane since moving to Edinburgh. Special thanks go to Bius for listening to my complaints, to Einstein for his midnight antics, to Houdini for his continual amusement and to Luna for her endless joy for everything and everyone.

Finally, thank you to you, my examiners, for agreeing to read this thesis!

List of contents

List of figures

List of tables

Glossary of terms

AMD – acid mine drainage

ARD – acid rock drainage

CFU – colony forming unit

DNA - deoxyribonucleic acid

EDS – energy dispersive spectroscopy

EPS – exopolymeric substances

GC-MS – gas chromatography – mass spectrometry

ICP-OES – induced coupled plasma – optical emission spectroscopy

IFT – interfacial tension

OD – optical density

PBS – phosphate buffered saline

PCR (cPCR) – polymerase chain reaction (colony polymerase chain reaction)

PHA – polyhydroxyalkanoates

RNA (rRNA) - ribonucleic acid (ribosomal ribonucleic acid)

SEM – scanning electron microscopy

SOM – sedimentary organic matter

XRD – x-ray diffraction

YC1 – Yorkshire coast 1 – strain of *Variovorax paradoxus*

Chapter 1 – Introduction

1.1 Geomicrobiology and microbial rock weathering

Microbial rock weathering is a fundamental aspect of geomicrobiology, the field of science that investigates microbial interactions with geological materials such as minerals and rocks. Rock weathering is the geological process that alters the geochemical and mineralogical components of a rock through i) dissolution, whereby constituent molecules are released from the rock or ii) transformation, primarily of minerals that through chemical reaction are converted into another mineral type (Konhauser, 2006). Biological, chemical and physical processes all contribute to the overall geological process of rock weathering, although these different processes can often act via the same mechanisms. For example, acids are primary agents of mineral dissolution and rock weathering, but the source of these acids can come from both abiotic (geochemical) and biotic (biogeochemical) activity (Drevers and Stillings, 1997). Microbial rock weathering specifically refers to the impact that microbial biomatter, microbially-released molecules and microbial activity have on the weathering of geological materials (Konhauser, 2006).

Microorganisms from all domains of life (Archaea, Bacteria and Eukaryotes) contribute to rock weathering processes in a diverse range of terrestrial and marine environments (Akob and Küsel, 2011). These microbes play a vital role in sustaining the biosphere, driving biogeochemical cycles by liberating or transforming elements such as carbon, phosphorus, sulfur and iron from minerals and rocks (Falkowski *et al*.; 2008; Uroz *et al*., 2009). Rock weathering, including microbial rock weathering, also plays a major role in regulating atmospheric concentrations of CO_2. Carbonate ions derived from dissolved CO_2 can react with free cations liberated from dissolved minerals, making rock weathering a geological CO_2 sink. However, microbial weathering processes can also contribute to CO_2 release through the dissolution of carbonate rocks and the degradation of sedimentary organic matter (Konhauser, 2006).

1.2 Shale – a naturally important rock and industrial resource

1.2.1 Shale petrology and introduction to weathering processes

One such rock that is known to be weathered by microbial activity is shale, a fine grained sedimentary rock whose lithology covers 25 % of the exposed continental land mass (Amiotte-Suchet *et al*., 2003) and forms two thirds of all sedimentary rock deposits (Ilgen *et al*.. 2017). Shale is a mudstone rock formed from marine or lacustrine sedimentary deposits and is comprised of silt-sised clasts of quartz, clay minerals and other sedimentary material. It is also composed of variable amounts of sedimentary organic matter, which makes it a source rock for the formation of oil and gas reservoirs (Nichols, 2009). Depending upon definition, the term shale can be used interchangeably with mudstone, the term used for sedimentary rocks that are composed by 50 % or more of particles less than 62.5 μm in average diameter. Alternatively, it can specifically refer to fissile mudstones, rocks with visible laminations that run parallel with the sedimentation orientation and are planes of structural weakness (Ilgen *et al*., 2017).

The weathering of shale rock within the natural environment has a range of important consequences including nutrient release (Tuttle and Breit, 2009), pollution of soils and freshwater (Kwong *et al*., 2009), heaving of bedrock below infrastructure resulting in structural damage (Anderson, 2008), triggering of slope landslides (Bhattarai *et al*., 2006) and regulation of atmospheric CO_2 levels (Jin *et al*., 2014). Microbial rock weathering processes have a significant impact on shale weathering and in many cases play a key role in the above outlined issues (Pye and Miller, 1990; Schillawski and Petsch, 2008; Cockell *et al*., 2011; Zhu and Reinfelder, 2012; Stasiuk *et al*., 2017). The best studied microbial process in shale rock weathering is the oxidation of iron and sulfur within the mineral pyrite (FeS_2), resulting in the formation of sulfuric acid (H_2SO_4) (Li *et al*., 2014). This process, among others, will

feature throughout the following sections on the significance of shale and shale weathering.

1.2.2 Shale weathering and the global carbon cycle

Where shale bedrock meets the Earth's surface in the critical zone (where rocks, atmosphere, water and life interact), it becomes oxidised and weathered to form regolith. This subsequently degrades, and with the addition of dead organic matter, becomes shale-derived soils that provide nutrients and habitats for ecosystems (Ma *et al.*, 2010). The weathering of shale bedrock has two opposing effects on atmospheric CO_2 regulation, a) cations leached from the weathered rock can become complexed with dissolved CO_2 to form carbonates (CO_2 sink) and b) organic matter within shale is oxidised to CO_2 and released (CO_2 source). The relative contribution and the net effect of these two processes are debated in the literature (Petsch *et al*., 2005; Schillawski and Petsch, 2008; Jin *et al*., 2014), but the role of shale in regulating CO_2, particularly in the context of future climate change, is widely acknowledged (Bouchez *et al*., 2010; Beaulieu *et al*., 2012).

Microbial communities have been demonstrated to weather both minerals and organic matter within shale, and hence contribute to CO_2 fixation/release (Schillawski and Petsch, 2008). Microbial iron oxidation and the mineral weathering of pyrite has been demonstrated to be a dominant process in natural shale weathering environments, producing sulfuric acid which accelerates the weathering of other minerals (Joeckel *et al*., 2005; Tuttle and Breit, 2009; Zhu and Reinfelder, 2012; Li *et al*., 2014). Furthermore, microbial weathering of shale organic matter has been elucidated in several environments and potential weathering mechanisms proposed (Petsch *et al*., 2001a, Berlendis *et al*., 2014, Stasiuk *et al*., 2017).

1.2.3 Shale weathering, acid rock drainage and environmental pollution

The weathering of shale rock and shale-derived soils, in addition to releasing/absorbing CO_2 and releasing nutrients, leaches potentially harmful

elements previously contained within shale comprising minerals or metallo-organic complexes. Potentially harmful elements (PHEs) can be defined as elements that are toxic at certain concentrations to one or more species, but in many cases are also essential nutrients at lower concentrations (e.g. Fe) (Bini and Wahsha, 2014). Most PHEs released by shale are heavy metals that are found at high concentrations within the rock such as Cu, Fe, Mn (Kwong *et al*., 2009).Acid rock drainage (ARD), the release of acidic, metalliferous fluids from rocks, is prevalent in shale lithology due to the oxidation and weathering of pyrite. The oxidation of sulfur within the pyrite results in the production of sulfuric acid, which then leaches heavy metals such as As, Cu, Co, Fe, Mn, Ni, U and Zn into the surrounding environment, often with a profound polluting effect (Langan *et al*., 1996; Joeckel *et al*., 2005; Kwong *et al*., 2009). PHE pollution from shale is best known from the industrial mining of shale (both historic and modern), either for shale-bound resources or as a conduit to other lithologies, with resultant acid mine drainage (AMD) (Johnson and Hallberg, 2005; Espana *et al*., 2005). A report released in 2008 stated that nine percent of rivers in England and Wales and 2 % of rivers in Scotland have been at risk of failing to meet the EU Water Framework Directive due to AMD from abandoned mines, posing serious threats to both ecosystem and human health (Johnston and Rolley, 2008).

Although both ARD and AMD are recognised to contribute to environmental pollution, AMD is considered to have a greater impact (Simate and Ndlovu, 2014). Mining activity produces large volumes of crushed rock mine tailings, mined rock or ore that has either been already processed for resource extraction or that has no financial worth, which are commonly heaped in areas surround the mine (Naciker *et al*., 2003). These heaps have a substantial potential for AMD, with increased rock surface area (due to crushing) exposed to factors that enhance weathering rates (e.g. oxygenated rain water) (Naicker *et al*., 2003).

A well-known case example of AMD is that of Iron Mountain mining complex in California, US (Jacobs *et al*., 2016). At one point one of the largest copper producing mines in the US, the mining complex became the source of environmental pollution only a few years after mining activity began in the late 19th century, polluting local freshwater and causing large kills of Salmon in the surrounding area. In the proceeding ~70 years of mining activity, AMD pollution from Iron mountain had a

dramatic impact on the health of the local environment, and in 2000 $1 billion US dollar settlement was agreed between the US environmental protection and the responsible parties. The case of iron mountain demonstrates how quickly AMD problems can arise from mining activity, and the large financial costs that can be occurred by required environmental remediation (Jacobs et al., 2016).

Microbes are significant drivers of ARD and AMD through pyrite oxidation, acid production and altering the mobility of PHEs (Baker and Banfield, 2003; Méndez-García *et al*., 2015). Bacterial species such as *Acidithiobacillus ferrooxidans*, *Leptospirillium ferrooxidans* and *Sulfobacillus thermosulfidooxidans* are dominant members of AMD microbial communities, oxidizing both iron and sulfur to produce iron (hydr)oxides and sulfuric acid (Baker and Banfield, 2003). The microbial oxidation of other metal sulfides, such as sphalerite (Zn,FeS_2) and chalcopyrite (Cu,FeS_2) (Rodríguez *et al*., 2003; Vera *et al*., 2013), mobilises these metals from the bedrock into the aqueous environment (Benner *et al*., 2000). Studies of microbial processes within modern AMD environments is also enhancing our understanding of geobiological processes in paleoenvironments, such as the oxidation of pyrite in the Great Oxidation Event (Fru *et al*., 2016; Havig *et al*., 2017).

1.2.4 Shale weathering – impact on the human environment

Shale lithology covers 25 % of the Earths continental surface (Amiotte-Suchet *et al*., 2003) and as such comprises the bedrock below and outcrops surrounding human infrastructure in many locations worldwide (Bhattarai *et al*., 2006). Crushed shale is also a significant source of construction aggregate, used for a wide array of construction projects including infrastructure foundation laying (Anderson, 2008) and creating roadside embankments (Pye and Miller, 1990). The weathering of shale, both in natural lithology and manmade structures therefore is a major concern to civil engineers and local government.

The oxidation of pyrite and other shale comprising minerals results in the formation of sulfuric acid, which reacts with calcite to form gypsum ($CaSO_4$) and with illite to form jarosite ($KFe^{3+}_3(OH)_6(SO_4)_2$). The density of these secondary minerals is lower than that of reactant minerals, resulting in a volumetric increase within the rock

(Taylor, 1988). This volumetric expansion within shale is called pyritic heave, and has been identified as the major cause of bedrock (Anderson, 2008; Hoover and Lehmann, 2009), shale floor slab (Gratten-Bellew and Eden, 1975; Wilson, 1987) and crushed shale fill, collapse (Pye and Miller, 1990; Anderson, 2008). Within buildings, pyritic heave can cause major structural damage that requires either expensive repair or demolition of the building. In Ireland, more than 10,000 homes built in the early 1990s in the city of Dublin and surrounding suburban areas have been affected by pyritic heavage (Hawkins, 2014). Remediation expenses have already cost local councils more than €12 million with further expenses expected for the future (The Irish Times, 7th July 2017).

Microbial catalysis of pyrite oxidation reactions can increase reaction rate by over 10^6 -fold, meaning that microbial activity can have a significant impact on pyritic floor heaving. Many acidophilic microbes capable of pyrite oxidation, such as *Acidithiobacillus ferrooxidans*, are mildly thermophilic and are believed to play a greater role in pyritic heaving in warmer climates or in buildings with underfloor heating (Hawkins, 2014).

1.2.5 Shale rock and industrial resources

The composition and properties of shale rock make it a valuable resource in several modern industries including shale gas (fracking) and heavy metal extraction (Wang *et al*., 2014; Kutschke *et al*., 2015). Shale gas is formed when organic matter (0.5-25 % of rock composition) undergoes thermal maturation due to geothermal pressures, resulting in the conversion of solid organic matter into natural gas contained within nanopores (Loucks *et al*., 2009). Today, unconventional shale gas (USG) is extracted from shale rock through hydraulic fracturing (fracking), the process of injecting high volumes of fluid into a horizontally drilled well through the shale formation, cracking the rock and releasing the gas (Wang *et al*., 2014). The USG industry has undergone significant expansion in the last decade due to advancements in fracking technology and decreasing production of conventional natural gas (Wang and Krupnik, 2013). In 2012, USG comprised 34 % of US natural gas production with this figure expected to increase to ~50 % by 2035 (Vengosh *et al*., 2014). Worldwide, USG has become a significant global market comprising 174 trillion

cubic metresof estimated extractable gas worth $105 billion (USD) by 2020, with significant reservoirs in China, Argentina, Algeria, Canada, US and the EU (Allied Market Research, 2016; Wang *et al*., 2014; Vengosh *et al*., 2014).

Microbial activity is increasingly being recognised as an important contributor to shale gas formation (Colosimo *et al*., 2016). Bacterial communities can initiate the degradation of sedimentary organic matter through the breakdown of complex organic geopolymers found within the rock. Degradation products, derived either from biotic or abiotic processes can then be transformed by methanogenic archaea to methane gas. Bacterial members of the *Actinobacteria*, *Bacteroidetes*, *Firmicute* and *Proteobacteria* phyla have been identified in degrading shale organic matter within subsurface shale lithology (Meslé *et al*., 2013). These organisms degrade large, insoluble organic polymers into smaller soluble organic molecules that can be used by methanogenic archaea (Colosimo *et al*., 2016). USG reservoirs with greater proportions of biologically sourced methane have been proposed to be more economically productive. δC^{13} CO_2 values can be used to determine proportions of biogenic methane within extracted shale gas, making microbial studies of USG reservoirs an increasingly valuable investment (Martini *et al*., 2008).

Shale rock is also extracted and processed as a metalliferous ore, supplying numerous heavy metals including cobalt, copper, nickel and zinc to global markets (Watling, 2014; Kutschke *et al*., 2015). Metals within shale are commonly within the form of metal sulphides that are formed and preserved within the reducing conditions of the aqueous sedimentary environment (Klein and Phillpots, 2012). To extract these metals, the mining industry puts rock ore through a grinding and then a flotation step, producing a concentrated heavy metal fluid. Unrefined metals can then be extracted from this fluid through pyrometallurgical smelting. Within Europe, the Kupferschiefer black shale formation within Germany (historical) and Poland (current mining operations - KGHM) has been mined for copper and silver (Kutschke *et al.*, 2015). Over three mining sites (Lubin, Polkowice-Sieroszowice and Rudna), KGHM extract 550,000 tonnes of Cu and 1344 tonnes of Ag per annum (for 2005), making it the 6th largest refined copper and 3rd largest refined silver suppliers worldwide in 2005 (Kable, 2017).

The decreasing number of discoveries of high-grade metal ore deposits is putting increasing pressure on mining industries to increase extraction efficiency, particularly from mining wastes (Watling, 2014). Biohydrometallurgy, the use of biological processes to improve metal extraction from ore, is already used extensively within the copper mine industry (Schippers *et al*., 2013). Development of biohydrometallurgical processes for mining wastes and low grade ores, including metalliferous black shales, is becoming increasingly important to meet future demand and reverse current deficits (Watling, 2014).

Microbial weathering of Kupferschiefer black shale and the development of biohydrometallurgical processes has been the focus of the international working groups Bioshale (2004-2008), ProMine (2009-2013) and Ecometals (2014-2017) (Kutschke *et al*., 2015). Work from these projects has led to greater understanding of microbial mineral weathering (Matlakowska *et al*., 2012), leaching of heavy metals (Włodarczyk *et al*., 2015) and degradation of organic matter in black shales (Stasiuk *et al*., 2017).

1.3 Thesis scope and gap in knowledge

Section 1.2 provides a wide overview of the relevance of microbial rock weathering studies in shale rock, both to our understanding of natural and manmade environments. A previously unconsidered aspect of microbial rock weathering of shale is its potential to physically shape environments; altering the geomorphology of an exposed rock face.

This doctoral research project has been funded by formerly Cleveland Potash Limited (CPL), now a subsidiary of Israeli Chemicals Limited (ICL). ICL have an active potash and polyhalite mine at Boulby, a small coastal hamlet in North Yorkshire approximately 1 km from the cliff edge (see map in figure 4.3, Chapter 4). For 15 years, CPL have collaborated with researchers at the University of Durham in a project entitled COBRA (COastal Behaviour and Rates of Activity), investigating geomorphological processes and cliff erosion on the North Yorkshire coastline between Skinningrove and Whitby. Some this collaboration's most recent work can

be found within Rosser *et al*. (2013), Brain *et al*. (2014) and Vann Jones *et al*. (2015).

In 2008, Professor Charles Cockell (Open University) joined COBRA to investigate the role of *in situ* microbial communities to alter the geological microenvironment of shale cliffs (Cockell *et al*., 2011). Microbiological (16S rRNA sequencing and fluorescence microscopy) and mineralogical (XRD, Raman, XAS and SEM) characterisation of geological samples revealed a diverse microbial community associated with a range of weathered mineral products including iron oxyhydroxides and gypsum. Microbial genera associated with iron oxidation, methanotrophy, phosphate solubilisation and nitrogen cycling were all identified (Cockell *et al*., 2011).

The scope of this project has been to continue the investigation into microbial rock weathering processes within shale cliffs, but primarily using culture-based techniques. In particular, the author of this work wanted to investigate the role of other rock weathering processes beyond iron and sulfur oxidation in weathered shale environments. Previous studies have largely concluded that redox reactions and mineral transformations of Fe and S dominate in natural weathered shale environments (Joeckel *et al*., 2005; Li *et al*., 2014), yet the role of other rock weathering activities (e.g. phosphate solubilisation) remains relatively unknown. Cockell *et al*. (2011) revealed that heterotrophic microorganisms comprised the majority of the identified diversity in weathered shale samples taken from cliffs at Boulby. The role of heterotrophic microbes in shale rock weathering has been extensively studied in industrial contexts (see Kutschke *et al*., 2015, for a review) but has remained largely unexplored in the context of natural environments. This project therefore has aimed to elucidate the abundance, distribution and rock weathering capabilities of heterotrophic microbes in naturally weathering shale rock.

1.4 Research questions and thesis outline

The central questions of this thesis revolve around the rock weathering potential of natural microbial communities in weathered shale on the North Yorkshire coastline. Although the authors of Cockell *et al*. (2011) speculate on possible microbial

weathering activity within the shale environment they sampled, the study did not attempt to characterise the weathering capabilities of the microbial community (Cockell *et al*., 2011).

In this thesis, the following research questions will be addressed:

1) What is the distribution of rock weathering microbes in natural and historic industrial weathered shale environments?

2) Can microbial rock weathering activity in shale be demonstrated using *in vitro* and *in situ* methodologies?

3) Investigate which physiological adaptations rock-dwelling microbes have to colonise and survive in weathered shale rock habitats?

Most recent studies investigating microbial shale weathering in natural environments have used either culture-independent or geochemical methods, identifying microbial weathering processes indirectly (Cockell *et al*., 2011; Savage *et al*., 2012; Li *et al*., 2014; Berlendis *et al*., 2014). Other studies have used culture based approaches, but are often limited to the use of single (often model) organisms (Wengel *et al*., 2006; Kalinowski *et al*., 2006; Rhine *et al*., 2008; Liermann *et al*., 2011), or lack weathering capability assessment (Joeckel *et al*., 2005). Notable exceptions to this include the work of Petsch *et al*. (2001a, 2005), although this work entirely focused on organic matter degradation and did not explore other microbial shale weathering mechanisms.

This thesis focuses on the use of culture-based methodology, which has been used effectively within industrially focused studies (Matlakowska et al., 2010a; Matlakowska et al., 2012; Włodarczyk *et al*., 2015; Włodarczyk *et al*., 2015, Stasiuk *et al*., 2017), to investigate the potential for shale weathering activity in natural environments. Furthermore, it combines the use of *in vitro* culturing and *in situ* incubation of geological samples, to compare microbial weathering activity in the laboratory and in the environment. The results and knowledge gained from this thesis will then be used as a basis for understanding the possible role of microbial geomorphology in shale cliff environments on the North Yorkshire coastline. The first section of the thesis (Chapters 1-4) provides introductory knowledge required to

understand the content of this work, as well as information on how this work was carried out. Chapter two provides an overview of shale rock weathering processes, with particular focus on microbial shale weathering studies both from natural and industrial settings. Due to the economic relevance of biohydrometallurgy, studies investigating microbial shale weathering in artificial environments (e.g. bioreactors) are more abundant than studies of microbial activity in natural weathered shale. Valuable lessons can be learnt from this industrial literature for scientists interested in natural environments, so a review of these studies is included. Details of methodology used throughout the thesis can be found in Chapter three, with information on sampling field sites and the geology of shale lithology on the North Yorkshire coastline contained in Chapter four.

The scientific research carried for this thesis is presented across four results chapters (Chapters 5-8), which are summarised here:

Chapter 5: This chapter aimed to assess the rock weathering potential of microbial communities inhabiting weathered shale. Phenotypic plate assays were used to assess the occurrence and abundance of microbial isolates with rock weathering capabilities. Five rock weathering phenotypes were tested for: organic acid production, siderophore production, phosphate solubilisation, iron oxidation and manganese oxidation. 16S rRNA sequencing was used to phylogenetically identify over 30 rock weathering isolates.

Chapter 6: Ecophysiological responses of weathered shale isolate *Variovorax paradoxus* to organic rich rocks. A strain of *V. paradoxus,* a *β-Proteobacteria* with diverse heterotrophic metabolic capabilities, was isolated from a weathered shale inoculated medium lacking both a source of organic carbon and iron. Experiments revealed that this strain could grow within extremely low nutrient media lacking any added carbon source, indicating it could sustain growth on contaminating carbon within the media. The effect of organic rich geological substrates (shale and coal) on growth, surface motility and polymer production (polyhydroxyalkanoates and biosurfactants) was investigated.

Chapter 7: Biologically enhanced leaching of shale in batch cultures. The ability of an enrichment community to enhance elemental release from shale was assessed in

batch cultures over ~ 4 months. Two experimental set ups were used, a) shale rock chips inundated in liquid medium and b) moistened rock chips contained in a freely draining system. Elemental leaching was measured using ICP-OES over several time points within the course of the experiment. The work of this chapter takes the potential for microbial rock weathering explored in Chapter 5, and attempted to observe direct evidence of microbial shale weathering activity.

Chapter 8: Incubation of shale-comprising minerals in i*n vitro* and *in situ* shale weathering environments. Mineral samples of albite, calcite, muscovite, pyrite and quartz were incubated in iron oxidizing enrichment cultures *in vitro*, and were buried *in situ* in weathered shale scree. Both fluorescence and scanning electron microscopy were used to assess mineral colonization and weathering. This final chapter addressed the weathering capability of weathered shale communities, and determined the relative susceptibility of differing mineralogical groups to microbial weathering.

Finally, the thesis is concluded in Chapter 9, with key findings across the thesis brought together. A synthesis of knowledge on microbial shale weathering on the North Yorkshire coastline is presented, with suggestions for future research given.

Chapter 2 - Background

2.1 Petrology of shale

As briefly discussed in Chapter 1, shale is a geological term used either interchangeably with mudstone, or it can specifically refer to mudstones that display fissility. In this thesis, the first definition of the term will be used. The sedimentary geology of the Yorkshire coast has historically been classified in this way, for example, the Redcar Mudstone Formation is entirely comprised of members described as "shale" (see Chapter 4). Therefore, the term shale will be used to discuss all rocks sampled in the work for this thesis.

This section provides a brief overview of shale petrology. For further information, see Boggs (2009).

2.1.1 Sedimentology and diagenesis

Shale is sedimentary rock that is derived from aqueously deposited sediments either in lake/river (lacustrine) or marine environments. It is a fine-grained rock with a generalised composition that is roughly two parts silt (2-63 μm) to one part clay (< 2 μm diameter), with varyingly low amounts of sand (0.063-2 mm) (Boggs, 2009). Silt grains are generally angular, having been relatively unaltered (not rounded) by aeolian or fluvial transport abrasion after erosion from their parent body. Clay grains on the other hand form platy, flaky or acicular shapes (Boggs, 2009; Nichols, 2009).

Various processes influence the microfabric of shale. Physiochemical processes include the electrochemical forces that attract and bind minerals together and interface dynamics, the differences in motion and sedimentation of differing particles. Biological processes also occur within shale sedimentation and lithification, including biogeochemical processes that produce particular minerals (e.g. pyrite) or gas phases (e.g. H_2S or CH_4), and bioturbation by animals that burrow through, or die and become fossilised within, the sediment. Burial diagenesis includes processes that occur as a result of heat and pressure post-deposition and burial. These processes include cementation, the precipitation of minerals around

deposited grains, and compaction which rearranges particles due to pressure stress (Boggs, 2009).

Fissility, the ease with which planar, parallel surfaces within the rock can be split, is one of the main microfabric features of shale. At the micron scale, fissility is the alignment of platy clay mineral particles to the bedding orientation, producing laminae. Several processes are believed to play a role in the development of fissility, but the relationship between microfabric and depositional environment is complex and not easily generalised. One process involves organic compounds within depositional fluids that act as dispersing agents, breaking apart flocs of clay particles. These particles can then settle as single plates that roughly orientate with bedding. Upon burial, these clay plates become compacted and further aligned, producing fissility (Lash and Blood, 2004). Organic compounds are more abundant in anoxic, reducing depositional environments, indicating that geochemical parameters influence the likelihood of fissility development. Fissile shales can be classified based on the thickness of the layers they part into including flaggy (~10 mm), platy (~5 mm), fissile (~1 mm) and papery (~0.5 mm) (Boggs, 2009).

The anoxic nature of some lacustrine and marine depositional environments is a major defining factor in the composition and geochemistry of shale. This is discussed further in the next three sections (2.1.2 - 2.1.4).

2.1.2 Mineralogy

Shale mineralogy can be broadly split into two parts, 1) the deposition of detrital grains via fluvial processes and 2) the formation of authigenic minerals that have crystallised out of both depositional and post-depositional fluids. Quartz, feldspars, clay minerals and micas comprise the major mineralogical components of shale, all of which come from detrital sources. The respective abundances of these minerals vary significantly between lithologies, with quartz (15-54 %) and clay minerals (17-57 %) generally being the most abundant. A diverse variety of clay minerals can be found within shales including illite, kaolinite, smectite, chlorite and vermiculite (Boggs, 2009). The formation of authigenic minerals such as carbonates (e.g. calcite, dolomite, siderite, rhodochrosite) and sulfides (e.g. pyrite, marcasite, chalcopyrite)

are generally minor constituents that act to cement detrital grains together (cementation). Metal oxides such as the iron oxide mineral hematite can form at low concentrations in shales that have formed under relatively oxic conditions (Huckriede and Meischner, 1996). The phosphate-bearing mineral apatite occurs at low abundances within embedded nodules that form around areas of high biological activity within the deposited sediment (Skinner, 1993).

Oxygen concentration rapidly decreases with depth in some bodies of water, making most aqueous depositional environments relatively anoxic compared to surface conditions. This has numerous effects for the deposition of shale-comprising sediments. Firstly, the anoxic conditions enable the growth of anaerobic microbial communities that can reduce soluble, oxygenated compounds such as sulfates (SO_4^{2-}) to insoluble, reduced compounds such as sulfides (S^{2-}). Secondly, heavy metal compounds often have greater solubility in anoxic waters, allowing elevated heavy metal concentrations to accumulate within depositional fluids. Hydrogen sulfide gas produced by sulfate-reducing microbes can react with these dissolved heavy metals to form insoluble metal sulfides (e.g. FeS_2, $FeCuS_2$) (Skinner, 1993; Boggs, 2009).

2.1.3 Organic matter

Sedimentary organic matter (SOM) within shales is primarily derived from dead plant biomass that becomes trapped during sediment deposition. The anoxic conditions of deposition and subsequent burial significantly reduce the oxidation and degradation of SOM, allowing it to undergo fossilization and thermal maturation. In shales, this organic matter can be divided into a soluble fraction (5 %) and an insoluble fraction (95 %), otherwise known as bitumen and kerogen respectively. In the formation of kerogen, plant polymers such as lignin, cellulose and carotenoids are polycondensed into larger complexes (>1 kDa) that are both insoluble and non-hydrolyzable (Vandenbroucke, 2003). This makes kerogen recalcitrant and therefore difficult for microorganisms to access as a carbon or energy source (Petsch *et al.*, 2001a). As an estimated 10^{20} mols of carbon is locked into SOM, making it larger than any single surface reservoirs (e.g. oceans, atmosphere, biomass), its potential to support the microbial biosphere is vast (Hedges and Oades, 1997). A review of microbial degradation of kerogen can be found in sections 2.3.5.1 and 2.3.5.2.

Four types of kerogen can be classified based on the source of plant derived biomass: type I – lacustrine algae (sapropelic), type II – marine algae (planktonic), type III – terrestrial vascular plants (humic) and type IV – partially decomposed organic matter (residue). Any of these four kerogen types can be found in shale, but typically types I and II form the main kerogen components of shale rock. Kerogen types can be distinguished by their level of oxidation, assessed through both hydrogen/carbon and oxygen/carbon ratios. Type I kerogens are the most reduced (high H/C ratio, low O/C ratio), with a shift across types II to IV towards greater levels of oxidation, with type IV having the highest O/C ratio and lowest H/C ratio. Differences in O/C and H/C ratios in biological source material (e.g. between lacustrine and marine algae) are initially high, but decrease with the extent of thermal diagenesis until they form natural gas or oil (Vandenbroucke, 2003). A Van Krevelen diagram (O/C plotted against H/C) can be used to visualise these differences and the thermal evolution of each kerogen type (Seewald, 2003).

The four kerogen types can also be distinguished by their chemical structure. Although all kerogens are large macromolecular structures (see Behar and Vandenbrouke, (1986) for model diagrams) that are above 1 kDa in size, the internal structure of each kerogen type varies. Type I kerogens, being highly reduced and having a high H/C and low O/C ratios, are primarily comprised of connected, long chains of aliphatic hydrocarbons with some cyclic and aromatic moieties. Across the kerogen types with increasing O/C ratio, the proportion of cyclic and aromatic moieties increases. These structures can be elucidated through the use of organic chemistry techniques such as nuclear magnetic resonance (NMR) spectroscopy (Petsch *et al*., 2001b) and pyrolytic gas chromatography – mass spectrometry (pyGC-MS).

2.1.4 Metallurgy

The anoxic, reducing conditions under which shale-forming sediments are laid down are conducive to the accumulation of high concentrations of heavy metals. The metallic content of shales is stored in three main forms, a) within aluminosilicate minerals from detrital grains, b) metal sulfides, oxides and carbonates that have formed through geochemical and biogeochemical reactions within the sediment, and

c) complexed within sedimentary organic matter. Vine and Tourtelot (1970) classify trace metals within shale based on which of these three forms they are primarily found in, with Al, Ti, Ga, Zr and Sc being detrital, Ca, Mg, Mn and Sr in carbonates and Ag, Mo, Zn, Ni Cu, Cr and V being associated with organic matter.

Aluminosilicate minerals such as feldspars (e.g. albite, $NaAlSi_3O_8$) and clays (e.g. illite, $(K,H_3O)(Al,Mg,Fe)_2(Si,Al)_4O_{10}((OH)_2,(H_2O))$) are the most abundant source of aluminium in shales and also contain significant quantities of alkali metals (primarily Na, Mg, K and Ca) and trace amounts of heavy metals (e.g. Fe) (Boggs, 2009). Metals can be released from these minerals through weathering mechanisms such as proteolysis and chelation (more detail in section 2.3.3).

Metal sulfides of As (arsenopyrite – AsFeS), Cu (chalcopyrite - $CuFeS_2$), Fe (pyrite – FeS_2), Ni (Ni-sulfides - NiFeS) and Zn (sphalerite - ZnFeS) are common constituents of shale mineralogy (Anjum *et al*., 2012). The formation of these minerals is derived from bio/geochemical reactions (e.g. sulfate reduction) within the depositional waters of the sediment. The iron mineral haematite (Fe_2O_3) is the most abundant metal oxide mineral within most shales, but other metal oxides include additional iron oxyhydroxides (e.g. ferrihydrite) and manganese oxyhydroxide minerals (e.g. birnessite). Microbial redox activity is an important process in the accumulation of these oxide minerals within sediments (Polgári *et al*., 2012). Furthermore, the metal oxides can bind to other metal ions in the surrounding solution, contributing to the enrichment of numerous metallic elements such as Ni and Zn (Manceau *et al*, 2007).

Some studies suggest that rhodocrosite ($MnCO_3$) is accountable for the majority of the Mn component of shales, formed from reduced manganese in seawater reacting with dissolved CO_3^{2-} to form carbonate nodules (Calvert and Pederson, 1996). Other studies indicate that Mn is primarily associated with calcite as a minor element (Leventhal and Hosterman, 1982). Calcite ($CaCO_3$), dolomite ($Ca,Mg(CO_3)_2$) and Siderite ($FeCO_3$) can be major carbonate constituents within shales (Littke *et al*., 1991; Friedman and Murata, 1979; Mozley and Wersin, 1992).

Organic matter can also act as a major sink for metal immobilisation within shale-forming sediments for metals such as vanadium and rare earth elements. Radioactive elements such as uranium can also be enriched in shale, often associated with

kerogen (Leventhal, 1991; Kalinowski *et al*., 2006). Metalloporphyrins (also known as geoporphyrins when identified in rocks) are heterocyclic organic compounds that are commonly found within shale kerogen. In structure, they resemble a ring of connected cyclic hydrocarbons (comprised of four pyrrole units), with a central space in which four nitrogen residues protrude. These nitrogen residues have a δ^- charge that attracts and binds to cationic metals. Metalloporphyrins bind to several different metals, but form particularly strong complexes with vanadium and nickel (Baker and Louda, 1986, Matlakowska *et al*., 2010).

2.2 Overview of shale weathering

Weathering is the breakdown or dissolution of minerals and rocks at the Earth's surface, via a range of physical, chemical and biological processes. It should be distinguished from erosion, which is the removal of broken down material from the source to another location (Nicols, 2009). The weathering of shale is driven by numerous factors that are influenced by the environmental and geochemical conditions surrounding the rock.

The most obvious sign of weathering on a shale outcrop, when compared to un-weathered bedrock, is the fractured and fragmented fabric of the rock surface. This can be seen in Figure 2.1, where platy hexagonal structures (platy saprolites) project out of the rock surface. This morphology arises from slaking, the expansion and splitting of shale along planes of weakness within the rock (bedding planes and fissile laminae) due to hydration-dehydration cycling of expandable clay minerals. These minerals can absorb or desorb water depending on surrounding moisture levels, resulting in significant volumetric changes (i.e. expansion and shrinking) (Sadisun *et al*., 2000; Boggs, 2009).

All clay minerals are composed of layered aluminosilicate sheets that are either tetrahedral or octahedral in structure. The layers of these sheets can either have a 1:1 (matched pairs) or 2:1 ratio (octagonal sheets sandwiched between tetrahedral sheets). Smectite minerals (2:1 ratio) such as montmorillonite have the most extensive shrink-swell capacity, but their abundance within shale lithology varies (Karpiński and Szkoda, 2015**)**. Sodium cations present between aluminosilicate

sheets in clay minerals attract anions within the sheets and shields anionic repulsion between them. The replacement of Na ions with other ions such as Li, K and Ca reduces the swelling potential of expanding clays (Koncagül and Santi, 1999).

Figure 2.1¦ Shale cliff surface. Hydration-dehydration cycling (slaking) has resulted in the splitting of the rock into layers of platy saprolites (hexagonal platy fragments). This image was taken by the author at cliffs by Hole Wyke mine adit, North Yorkshire.

Slaking substantially reduces the shear strength, compressive strength and durability of shales, as can be determined by shearing devices, unconfined compression strength tests and slake durability tests (to be distinguished from slaking as a weathering process) (Huang *et al*., 1995; Koncagül and Santi, 1999; Bhattarai *et al*., 2006). However, slaking does not alter the rock hardness, which is largely controlled by the moisture content of the rock (Koncagül and Santi, 1999).

The effect of slaking on shale cliffs on the North Yorkshire coastline is readily visible by the accumulation of platy saprolites (rock chips) that have eroded from the cliff surface (Fig. 2.2)

Figure 2.2¦ Accumulation of platy saprolites (rock chips) that have eroded from the cliff face onto the foreshore. Wave and tidal action, the erosive mechanisms that transport rock chips, can act to remove rock chips from the foreshore at high tide. Above the water line, these erosive mechanisms are not in play, resulting in the accumulation of shale rock scree layer coating the cliffs. Image taken by the author at Keldhowe Steel cliffs, North Yorkshire.

Chemical weathering processes play a more dramatic role in altering the composition and microstructure of shale rock. The effect chemical weathering has on shale can be conceptualised through the separation of distinct weathered zones within a rock profile (Chigira and Oyama, 2000; Tuttle and Breit, 2009; Li *et al*., 2014). These zones (from surface to deepest subsurface) are the oxidised zone, the dissolved zone, the illuviated zone and the reduced (or fresh bedrock) zone. The oxidation front lies at the boundary between the oxidised and dissolved zone, while the dissolution front lies at the boundary between the dissolved/illuviated zone and the reduced zone. The illuviated zone within a shale profile has a similarly acidic pH to the dissolved zone, but has not yet undergone extensive dissolution of minerals and SOM (Li *et al*., 2014). All or a subset of these zones can be present within a weathered shale rock profile, dependent upon rock geochemistry and the surrounding environmental conditions.

A weathered shale rock profile can be defined by gradients of (H_2O), (O_2) and (H_2SO_4) across these zones. The (O_2) is highest at the rock-atmosphere interface and decreases with increasing rock depth, while the (H_2O) gradient increases with increasing depth as the water table is approached. Sulfuric acid (H_2SO_4) is produced below the oxidation front within the dissolved zone and is neutralised at the dissolution front. The extent of weathering and rock alteration is highest within the oxidised zone and decreases with decreasing depth (Chigira and Oyama, 2000; Li *et al*., 2014).

At the dissolved front, sulfuric acid significantly enhances dissolution of susceptible minerals within the reduced zone such as carbonates, and to a lesser extent aluminosilicates (Tuttle and Breit, 2009). This first stage of rock weathering increases rock porosity and alters mineralogical composition. Within the dissolved zone, the iron sulfide minerals (primarily pyrite, FeS_2) becomes oxidised by oxygen within the groundwater to form iron oxyhydroxides and sulfuric acid. The oxidation of pyrite within this zone occurs under relatively anoxic conditions compared to the oxidised zone (see fig. 2.3), and is facilitated by the activity of anaerobic iron-oxidizing microorganisms such as *Acidithiobacillus ferrooxidans* (Li *et al*., 2014). Details of the chemical and biochemical reactions that drive pyrite oxidation will be given in section 2.3.4. Li *et al*. (2014) separate the dissolved zone into two distinct layers, the dissolved zone (above) and the illuviated zone (below) for their study of a black shale weathering profile in Chengkou County, Southwest China. Sulfuric acid production primarily occurs within the dissolved zone and leaches down through the illuviated zone until the dissolution front, below which is unaltered fresh rock (reduced zone). They show that with increasing depth in the illuviated zone the concentrations of pyritic sulfur and organic matter increase, along with increasing pH to circumneutral pH at the dissolved front. A decreasing weathering gradient can therefore be described to exist with depth in the illuviated zone profile (Li *et al*., 2014).

Figure 2.3¦ Oxidised zone of a shale rock cliff profile. The rock surface is heavily slaked and coated in weathered mineral products of varying colours. Orange, red and brown colourings are likely to be crusts of iron oxyhydroxides, while yellow and white colourings are likely to be deposits of gypsum and jarosite. Image taken by the author at Saltwick Bay cliffs, North Yorkshire.

Within the oxidised zone, the pyrite content of the shale has been largely to completely oxidised, meaning that the potential for sulfuric acid production within this zone is low. As a result, decreasing depth through the oxidised zone corresponds with an increase in pH to circumneutral (Li *et al*., 2014). The high oxygen concentration within the oxidation zone is conducive to the further oxidation of iron oxyhydroxides (such as ferrihydrite, $Fe_2O_3.0.5H_2O$) to iron oxide minerals such as haematite (Fe_2O_3). The precipitation of sulfate weathered mineral products can also occur within the oxidised zone, such as gypsum ($CaSO_4$) and jarosite ($KFe^{3+}{}_3(OH)_6(SO_4)_2$) (Tuttle and Breit, 2009).

Figure 2.4¦ Crusts of weathered mineral products coating a weathered shale rock surface. Large (>1 mm) acicular crystals comprised the crust and are tentatively identified as gypsum crystals. The crystals appear to be impregnated with iron oxyhydroxides, providing the orange/red colouring.

Weathering indices have been produced to visually assess samples of shale rock and give a qualitative grading of weathering extent (Spink and Norbury, 1993; Sadisan *et al*., 2000; Hobbs *et al*., 2012). Gradings go from one (fresh rock) to six (residual soil), with five being completely weathered rock. The indices describe how fresh rock becomes slaked and fractured initially (grade 2) before a thin layer of the rock surface undergoes colour changes from grey/black to red/brown (grade 3). More extensive colour change and the formation of mineral crusts coating the weathered rock surface (see fig. 2.4) indicate that extensive weathering has occurred (grades 4 - 5) (Sadisan *et al.,* 2000).

Microbial rock weathering processes play a significant role in the weathering of shale, both in natural and anthropogenic environments. This will be explored in depth in section 2.4. Before this, a more general review of microbial rock weathering is provided in section 2.3.

2.3 Principles and mechanisms of microbial rock weathering

2.3.1 Introduction

When considering microbial weathering of minerals and rocks, it is useful to frame thoughts around the scale at which that interaction is being studied. Interactions can involve single microbial species or a larger microbial community, and can involve single minerals or whole rocks. Experimentally, both laboratory and field studies can be used to study these types of interactions. Naturally occurring *in situ* communities within a field site can be used to study community interactions with a mineral or rock, or a microbial community could be enriched in a growth medium within a laboratory setting. Studies investigating the interaction of a single species with a mineral or rock tend to be confined to laboratory work, where the exclusion of other microbial species within the experimental set up can be controlled.

An example of a single species – single mineral interaction is between *Acidithiobacillus ferroxidans* and pyrite, where the bacteria oxidise the iron within the mineral to obtain energy (autolithotrophy) (Mielke *et al.,* 2003). This interaction has been extensively studied in both naturally occurring and anthropogenic environments, and the microbial mechanisms of weathering and the adaptive advantage of the activity is well understood. This is not the case for many microbial weathering interactions, where a lack of extensive research or difficulties in studying the interaction mean the factors constraining it are not fully understood. However, initial work often highlights possible mechanisms of action and putative reasons for the microbes weathering activity.

This last point about discerning the adaptive advantage behind the microbial mineral/rock weathering behaviour, is challenging within most study systems and in many cases is overlooked. Such behaviour must increase the fitness of the organism through enhancing growth, survival or both. For many specific mineral interactions, such as iron oxidation of pyrite, the biogeochemical reaction provides metabolic energy for *A. ferroxidans* which supports growth. In other cases of more general rock

weathering, the weathering activity leaches minerals and components within the rock releasing nutrients which subsequently enhances growth (Rogers *et al*., 2004).

When considering individual mechanisms within a weathering behaviour, it is useful to consider whether they are active or passive, i.e. whether they require direct energy expenditure for the rock weathering mechanism (Viles, 2012). This consideration allows greater comprehension of the conditions under which an activity will be carried out and the factors that might constrain it. For example, an active weathering mechanism of an organism is more likely to be a necessary requirement for growth, and therefore that organism will always be associated with that weathering activity. In contrast, a passive mechanism might only be carried out under specific environmental conditions, or might be a bi-product of another cellular process (Viles, 2012). For example, Taunton *et al*. (2000) hypothesise that the passive microbial uptake of phosphate would alter the saturation of phosphate in fluids surrounding the cells, enhancing the dissolution of surrounding phosphate-bearing minerals. Ascertaining the active or passive nature of a microbial weathering mechanism is challenging; it requires a mechanistic understanding of the mechanism itself, along with the relative contribution (e.g. obligatory for growth) of that process to survival and growth of the weathering organism. Determining this relative contribution is particularly difficult, requiring the fitness (e.g. growth, fecundity) of the organism with and without the weathering mechanism to be quantified. Experimental control over weathering mechanism activation/inhibition is problematic, as the genetic and molecular basis that control weathering phenotypes remain largely unknown (Uroz *et al*., 2009).

Microbial weathering processes can also be categorised by their contribution to a weathering process relative to any abiotic mechanism, (Viles, 2012). Microbially-induced weathering is where microbial biomass or products (such as organic acids or exopolymeric substances) directly contribute to a weathering process and significantly enhance the rate of that process compared to baseline abiotic mechanisms. Microbially-influenced weathering does not directly contribute to the weathering process, but the organism's presence within the environment facilitates the abiotic process to occur and/or enhances the rate of that process. These processes become prominent upon extensive microbial colonization of rock surfaces, in

particular upon the formation of biofilms (Brehm *et al*., 2005). Biofilms are the growth of microbes, either as a single species or a community, within an extracellular matrix of exopolymeric substances (EPS). In addition, biofilms are commonly defined as being attached a surface, in which the extracellular matrix aids both cell adherence to the surface and surrounding cells (Kearns, 2010). The growth of biofilms on mineral surfaces has been shown to have a significant impact on mineral dissolution via numerous processes, including the production of acidic exopolysaccharides that etch the surfaces of plagioclase (Welch *et al*., 1999) and quartz (Brehm *et al*., 2005).

2.3.2 Mechanisms of microbial mineral and rock weathering

There is a diversity of mechanisms used by microbes to weather rocks and minerals, all of which vary in their specificity and their effectiveness in different geological substrates. It can be useful to classify these mechanisms into categories, so that the interactions between these mechanisms can be better considered (Uroz *et al*., 2009; Gadd, 2010). The alteration of the environmental pH surrounding the mineral, at either a microscopic or bulk-solution scale, is one of the main microbial contributions to mineral and rock weathering (Drevers and Stillings, 1997). Chelation, the removal of elements (particularly heavy metals) from within a mineral matrix or a bulk rock by a chelating factor, is another important weathering process (Liermann *et al*., 2000; Włodarczyk *et al*., 2015). A third category consists of all the known redox reactions involved in weathering, those that directly oxidise or reduce a specific mineral to form another (Barker *et al*., 1998; Gadd, 2010). A summary of microbial weathering systems can be found in Figure 2.6.

A distinction should be made here between those mechanisms that result in mineral or rock weathering and those that contribute to erosion. All of the weathering processes mentioned above contribute to erosion to some extent, but some purely bio-erosive processes also exist, such as the splitting of mineral planes by the mechanical force of fungal hyphal growth (Hutchens, 2009). Such bio-erosive processes physically break minerals and rock into smaller pieces but do not alter their geochemical composition, whilst also generally increasing the available surface area exposed to weathering processes.

Altering pH: Biologically produced organic acids and acidic extracellular polymeric substances (EPS) are one of the main ways that microbes alter the pH of their environment (Drevers and Stillings, 1997; Welch *et al*., 1999). Organic acids are often produced as a byproduct of cellular metabolism, oxidizing carbon sources to form carboxylic acids such as citrate and oxalate. Other organic acids are actively synthesised, such as amino acids or phenolic acids, but their primary purpose is generally not weathering related. Regardless, the release of these acids into the surrounding environment can make a direct contribution to mineral dissolution and rock weathering.

When considering organic acids as acids (proton donators) rather than chelators, they can act via several mechanisms to enhance mineral dissolution. Acid-derived protons can cleave bonds such as siloxane (Si-O-Si) or aluminosilicate bonds (Al-O-Si) in silicates, weakening the mineral matrix these bonds support and facilitating dissolution (Gadd, 2010). Furthermore, metal cations (such as K, Al and Fe) within aluminosilicate mineral matrices can be displaced by these protons, releasing the metal ions into the surrounding solution. These displacing protons are subsequently oxidised to form hydroxyl ions or water, which diffuse out of the matrix, leaving a gap (Bennett, 1991; Bennett *et al*., 2001).

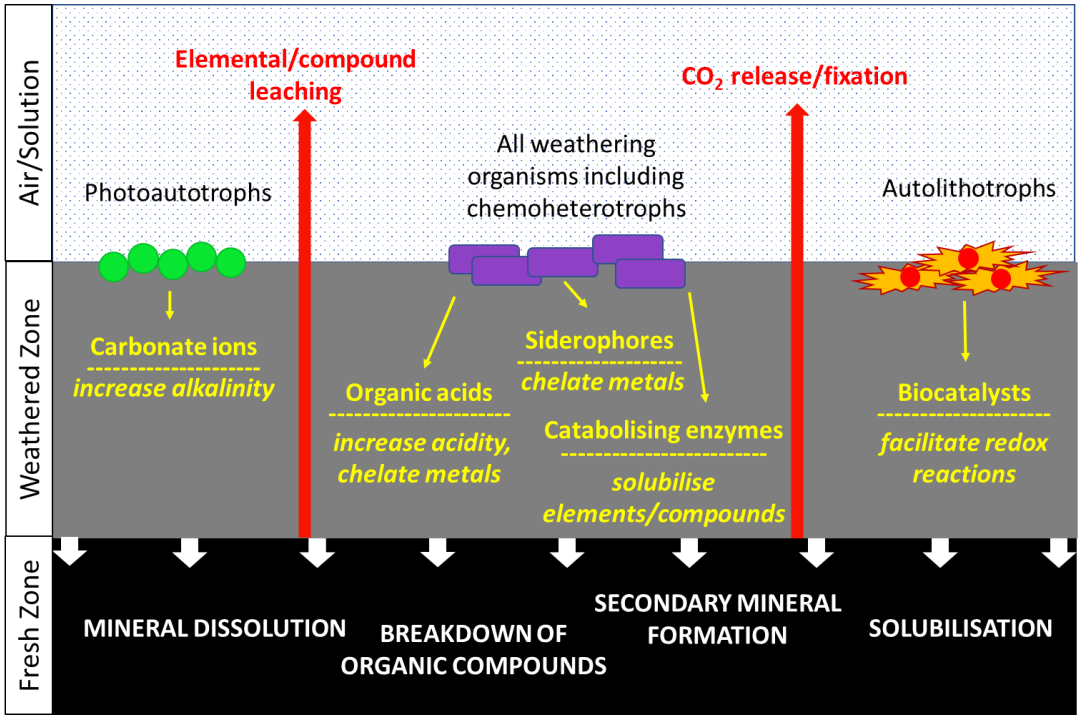

Figure 2.5¦ A summary of important microbial weathering mechanisms and their impact on geological substrates. Different microbial groups are present on the interface between air or water and a substrate, with the grey layer indicating the weathered zone of the substrate. Beneath this is the weathering front, where fresh rock below (black layer) is being actively weathered and releasing weathering products. Yellow labels within the weathered zone are examples of microbial weathering mechanisms, while the white capitalised labels within the fresh zone are the weathering processes that these mechanisms contribute to. Labels in red in the air/solution zone are weathering products that are released from the rock through the weathered zone into the surrounding environment or absorbed in the case of carbon fixation. Note that solubilization in this diagram can refer to elemental release from mineralogical or organic components.

Away from the mineral surface, acids also act to reduce pH which alters the solubility of ions (e.g. Fe^{3+}) within the solution surrounding the mineral. This disrupts ion concentration equilibria at the mineral-solution interface, resulting in enhanced mineral dissolution to restore equilibrium. The pH itself can also alter the redox states of the ions within those solutions (e.g. Fe^{2+}/Fe^{3+}), again disrupting ion equilibria and enhancing mineral dissolution (Drevers and Stillings, 1997). These

various mechanisms of action can act in unison to enhance weathering, or can actually oppose each other, depending upon the environmental conditions and local geochemistry.

Organic acids form only one part of biologically sourced acidity within a weathering environment, with the others including acidic EPS and production of inorganic acids (such as sulfuric acid) from biogeochemical processes. Almost all microbial species produce and excrete EPS onto their substrate and into the environment for a range of purposes including attachment and adherence to physical surfaces, protection from stressors and facilitating the formation of biofilms (Hall-Stoodley *et al*., 2004). However, the biochemical properties of some EPS molecules provide them with weathering capabilities. Welch *et al*. (1999) found that a variety of acidic EPS molecules (including starch, xanthan, pectin and alginate polymers) all increased weathering of feldspar by a factor of 50-100 compared to abiotic controls.

One of the main sources of biologically generated inorganic acid is from microbially mediated pyrite (FeS_2) oxidation, which produces sulfuric acid from the oxidation of liberated sulfur (Nordstrom and Southam, 1997). Species such as *Acidothiobacillus ferroxidans* can oxidise both the iron and sulfur components that are released from weathered pyrite, forming a range of oxidised sulfur compounds including thiosulfate and sulfuric acid (Schippers *et al*., 1996). Rocks rich in pyrite therefore can become significant sources of acid rock drainage which, although often attributed to mining activity (Baker *et al*., 2003; Johnson and Hallberg, 2005), is also found in undisturbedenvironments (Kwong *et al*., 2009; Konhauser *et al*., 2011). This type of microbial acid production can have profound weathering affects, for example, in a natural shale weathering profile pyrite derived sulfuric acid reduced bulk rock pH from circumneutral (pH 6-7) to highly acidic (~ pH 2.5). The pH gradient across this rock profile strongly correlated with its weathering intensity index (Li *et al*., 2014).

Photosynthetic microbes can also influence rock weathering processes through raising environmental pH rather than reducing it, which occurs because photosynthetic mechanisms produce carbonate ions. For example, the growth of cyanobacterial species *Anabaena cylindrica* was shown to increase the pH of solution-rock mixtures (basalt and rhyolite) from 6.5 to 8.5, which subsequently

enhanced the release rate of Ca, Mg, Si and K from these rocks (Olsson-Francis *et al*., 2012).

Metal chelation: As previously mentioned, acidic organic compounds have additional weathering properties due to their ability to chelate metal cations, which acts to enhance mineral dissolution (Bennett *et al*., 2001). 3,4 Dihydroxybenzoic acid (DHBA) is a commonly found organic acid in mineral weathering environments (Hiebert and Bennett, 1992) and has been used as a microbially produced model ligand for mineral weathering studies (Rogers and Bennett, 2004). Rogers and Bennett (2004) found that DHBA enhanced the dissolution of numerous feldspars, and microbial communities that produced DHBA also enhanced the dissolution of these minerals. Furthermore, when the weathering activity of the microbial community was tested on similar feldspar minerals, those with high concentrations of phosphorus were more strongly weathered, suggesting that their weathering activity is an active process in nutrient acquisition. The organic acids produced from this activity form soluble or insoluble complexes with a range of metal cations.. In both cases, the metals are essentially removed from the solution and therefore enhance mineral dissolution to re-establish concentration equilibria (Rogers and Bennett, 2004; Drevers and Stillings, 1997).

A specific group of organic compounds with an incredibly high affinity for Fe^{3+} are known as siderophores, and they are released by a diverse range of microorganisms to complex Fe along with other heavy metals (including Cu, Co, Mn and Ni) to increase their solubility and biological availability (Gadd, 2004; Gadd, 2010). Ferric Fe and other metal oxides have low solubility indices at circumneutral pH, so the use of siderophores to obtain iron and other biological utilised metals such as Mn and Cu is vital for growth in natural environments. Siderophores are active weathering agents identified in the environment and are produced by a range of organisms (Liermann *et al*., 2000; Kalinowski *et al*., 2006; Matlakowska and Sklodowska, 2009; Włodarczyk *et al*., 2015). Liermann *et al*. (2000) demonstrated that a *Streptomyces sp.* soil isolate could weather hornblende. The authors hypothesised that the organisms production of a siderophore molecule, desferrioxamine mesylate (DFAM) was primarily responsible for this weathering activity. When purified DFAM (24 μM) was added to a solution containing hornblende, the resulting mineral

dissolution rates were similar to that of hornblende weathered by the *Streptomyces sp.* isolate (Liermann *et al*., 2000). Metals such as uranium (Kalinowski *et al*., 2006) and arsenic (Matlakowska *et al*., 2008) are also chelated by siderophore molecules.

Redox reactions: Pyrite dissolution and the subsequent oxidation of sulfur to sulfuric acid has already been highlighted as an important mechanism of mineral/rock weathering via redox reactions. Although important, it is just one from a large array of biogeochemical reactions involving a large number of elements across the periodic table. Metallic elements such as Fe, Mn and Cu, and non-metals such as C, S, N and P all undergo redox cycling within geological environments (Falowski *et al*., 2008; Gadd, 2010), with individual microbial species contributing to oxidative or reductive (or in some cases both) processes.

Manganese redox reactions provide a good case study for biogeochemical cycles within natural geological environments. Numerous informative review articles on manganese oxidation can be found in the literature (Tebo *et al*., 2004; Tebo *et al*., 2005; Geszvain *et al*., 2012). Mn can form (II), (III) and (IV) compounds, with (II) being more soluble than (III) and (IV) compounds. The rates of abiotic manganese oxidative processes are slow compared to those of microbial processes, and as such biogeochemical cycling of Mn dominates Mn redox reactions. Mn oxidation occurs in a phylogenetically diverse microbial group including both bacteria and fungi (Gadd, 2007). For the bacterial members of this group the primary mechanism for oxidative activity is multi-copper oxidase-like enzymes, that can be found intracellularly, in the cell wall, or in spore coats (Tebo *et al*., 2004). Mn- oxidation, although thermodynamically favourable, has not been directly shown to provide energy through a lithoautotrophic metabolism in any organism. Despite this, there are several adaptive purposes that the Mn oxidation pathway may have, including storage of an electron acceptor for Mn reduction (which does drive known metabolisms) and Mn-oxide coatings that shield cells from radiation. Furthermore, manganese oxides are known catalysts for the degradation of organic matter, so Mn oxidation potentially plays a role in organic carbon weathering and subsequent nutrient acquisition for Mn-oxidizing heterotrophs. Strains of *Leptothrix discophora, Pseudomonas putida* and *Bacillus subtilis* are among the best-characterised bacterial Mn oxidisers, occuring in a range of natural geological settings harbouring

manganese oxides including carbonate cave walls (Carmichael *et al*., 2013), desert rock varnish (Kuhlman *et al*., 2006) and marine sediments (Francis *et al*., 2002), including ferromanganese nodules within the sediment (Stein *et al*., 2001). These microbial species, among others within the weathering community, actively weather the rock which causes reduced manganese (II) minerals such as rhodochrosite ($MnCO_3$) to dissolve, following which the leached Mn (II) becomes oxidised to produce oxide minerals such as birnessite (MnO_2) (Marshall, 1979; Tebo *et al*., 2004; Ehrlich *et al*., 1998).

Breakdown of organic compounds: Although minerals form the bulk composition of most rock forms, organic matter (OM) from various sources can be found in all types of sedimentary rock. The amount of OM can vary, from trace amounts in volcanic rocks to minor amounts (~10 %) in black shales, or can comprise the majority of the rock in the case of coal (Nichols, 2009). Microbes are able to transform or degrade such organic matter, contributing to biological weathering processes. The type of transformation/degradation is dependent on a number of variables including the composition of the OM, environmental conditions and the types of microbes involved. For example, under anaerobic conditions in the subsurface, rock-bound OM can be transformed by methanogens to form gaseous methane (Meslé *et al*., 2013). At the Earth's surface, aerobic conditions enable microbes to obtain energy from oxidative breakdown of OM in rocks including shales and coal (Petsch *et al*., 2001a; Wengel *et al*., 2006, Berlendis *et al*., 2014).

OM formed in sedimentary deposits is primarily in the form of a kerogen, a macromolecular structure of OM above one kDa in size and largely non-hydrolysable and insoluble. Due to these properties kerogen is highly recalcitrant to microbial degradation but, despite this numerous species have been found associated with sedimentary OM and are thought likely to use it as a sole carbon source (Petsch *et al*., 2001a). Although the mechanisms used by these microbes to degrade kerogen remain largely unknown, several studies suggest that enzymes that degrade other forms of recalcitrant OM (such as polycyclic aromatic hydrocarbons) may be used (Berlendis *et al*., 2014).

2.3.3 Biosignatures of microbial mineral and rock weathering

Within laboratory conditions, experimental design can include abiotic controls so that biological and geochemical weathering processes and their effect on the mineral/rock can be determined. However, geomicrobiologists working with samples that have been extracted from the environment do not have the luxury of abiotically treated samples for comparison. This is true both of geological samples that have undergone recent weathering processes, or weathered rock that has been preserved through geological time. As such, biological markers are required to confidently associate a microbial weathering process with a weathered geological substrate. Ideally, abiotic geochemical processes should not be able to replicate such a marker. In reality, many biosignatures are not uniquely biological in their formation, meaning numerous biosignatures must be combined to confidently associate microbial activity with mineral/rock weathering (Gorbushina *et al*., 2002).

Biosignatures are normally specific to the microbial process and the mineral/rock involved, although some biosignatures can be associated with multiple mineral or rock types. Morphological biosignatures provide some of the most compelling evidence of microbial activity within a weathering zone. Pitting and etching of mineral surfaces is a commonly cited example of morphological alteration from biological activity in minerals such as quartz, feldspar minerals and pyrite (Bennett *et al*., 2001; Buss *et al*., 2007; Mielke *et al*., 2003). These features are normally associated with attached microbes either within or to the side of the pit/etch and often with weathering mineral product precipitated on the outer microbial surface (Bennett *et al*., 2001). The size of pits and etch marks vary significantly between minerals and between studies, but in combination with sterile controls lacking these alterations, they provide strong evidence of microbially-faciliated mineral dissolution. Scanning electron microscopy (SEM) imaging of pits, combined with mineralogical analysis and identification of microfossils, was used to identify microbial iron oxidation and weathering of pyrite in ~3.4 Ga old rocks, one of the oldest recorded instances of microbial weathering activity (Wacey *et al*., 2011). Boring through mineral/rock surfaces is another morphological alteration mediated by microbes such as

cyanobacteria, chlorophyta (algae) and fungi in minerals such as carbonates and volcanic glasses (Cockell and Herrera, 2008). Exact adaptive advantages of specific cases of boring have not yet been identified, but several proposals such as nutrient acquisition, protection from radiation or predation and escape from entrapment during mineralization have all been proposed. Care should be taken when analyzing unknown morphological features before associating them with biological activity, as features that have previously been believed to be purely biological in origin have been shown to form under abiotic conditions (Edwards *et al*., 2001). Ferric iron produced from either biotic or abiotic ferrous iron oxidation can react with pyrite (see section 2.4.2) to produce cell shaped pits. These pits look as if they have formed from a direct microbially induced surface reaction, but can be formed in the complete absence of cells (Edwards *et al.,* 2001).

Biogenic minerals, those that are formed through biological processes, can be biosignatures of microbial processes that use leached elements or compounds from a weathered surface. For example, the rate of abiotic manganese oxidation is comparatively very slow compared to microbially-mediated manganese oxidation, so natural deposits of manganese oxide minerals are generally assumed to be at least partially biologically formed (Tebo *et al.,* 2005). Boston *et al*., (2001) reviewed microbial biosignatures within cave environments, in which they highlight numerous biosignatures including manganese oxide "snow". This snow, which visibly falls from the roof of the cave, is a corrosion residue formed from bedrock weathering where microbial processes contribute both to rock weathering and to iron and manganese hydr(oxide) mineral formation (Northup *et al*., 2000). Biogenic mineral formation can also occur directly onto biological material such as cellular surfaces or EPS, which act as nucleation sites for mineral growth. Numerous mineral types have been found to form on fungal hyphae, such as magnesium oxalate dihydrate on *Penicillium simplicissimum* and calcite on *Serpula himantioides* (Gadd, 2007).

There are problems with the use of biogenic minerals as signatures of microbial weathering processes. Firstly, it is often not possible (without additional information) to determine if the microbes involved in biogenic mineral formation were also directly involved in the primary mineral weathering. Secondly, like other

biosignatures, biogenic minerals are not formed from biological processes alone, so other biosignatures (such as the direct association with biomatter) must be used in conjunction with biogenic minerals to be confident of their microbial origin (Gorbushina *et al*., 2002).

2.4 Microbial shale weathering

2.4.1 Introduction

Microbial weathering of shale has been studied extensively in both natural and anthropogenic environments. Although many of these studies attempt to address fundamental questions in geomicrobiology and rock weathering, a significant proportion of studies have focused on the role microbial shale weathering has, or could have, within industry and infrastructure.

Chapter 1 introduced the industries investigating the role microbial biotechnology could play in future development, including oil and gas extraction (Jiang *et al*., 2015; Colosimo *et al*., 2016) and heavy metal mining (Anjum *et al*., 2012; Włodarczyk *et al*., 2016). The damaging impact of microbial activity on infrastructure through the weathering of shale bedrock below structures (Hoover and Lehmann, 2009) and crushed shale material within structures (Hawkins, 2014) has also been covered.

However, the microbial weathering activity that interests shale-related industries also has a significant impact on shale weathering in range of natural environments (Joeckel *et al*., 2005; Cockell *et al*., 2011; Yesavage *et al*., 2012; Schlegel *et al*., 2013; Li *et al*., 2014). Shale lithology covers over 25 % of the Earth's continental surface (Amiotte-Suchet *et al*., 2003) and, as such, shale weathering plays a substantial role in soil formation globally (Jin *et al*., 2010). The metalliferous nature of shale makes it a valuable resource, but can also be a dangerous source of environment pollution. Microbial weathering of shale has been implicated in acid rock drainage, releasing acidic, metalliferous solutions containing heavy and radioactive metals (Wengel *et al*., 2006; Kalinowski *et al*., 2006) resulting in

vegetation retardation,soil salinization and degradation of water resources (Joeckel *et al*., 2005).

The focus of this thesis is on the natural weathering of shale rock in cliffs and at historic industrial sites on the North Yorkshire coastline, UK. In this section, the literature on microbial shale weathering in both natural environments and under industrial conditions will be reviewed. Although studies from these two areas of microbial shale weathering research vary in their methodology and approach, the knowledge gained and the underlying weathering mechanisms elucidated are broadly applicable.

2.4.2 Microbial pyrite oxidation and shale weathering

The earliest investigations linking microbial activity with shale weathering were in relation to the damage shale weathering caused to human infrastructure (Penner *et al*., 1970; Quigley *et al*., 1973; Grant-Bellew and Eden, 1975). These studies, among others, identified that microbial oxidation of pyrite was a primary agent of shale bedrock heaving below buildings. Grant-Bellew and Eden (1975) indicated that microbial pyrite oxidation resulted in acid production and subsequent weathering of shale bedrock below a church in Ottawa, Canada. The acid also leached into the carbonate-rich concrete laid on top of the shale bedrock, resulting in significant dissolution and structural weakening of the concrete (Grant-Bellew and Eden, 1975).

This research in biogeochemical shale weathering coincided with progress made in understanding the biochemical mechanisms of pyrite oxidation at low pH of the *Ferrobacillus- Thiobacillus* bacterial group (Silverman 1967; Singer and Stumm, 1970; Groudev, 1979), many of which were later reclassified as strains of the species *Acidithiobacillus ferrooxidans* (Kelly and Wood, 2000; Karavaiko *et al.,* 2003). Reviews of bacterial mechanisms of pyrite oxidation at low pH as it is currently understood can be found in Sand *et al*. (2001), Konhauser (2006) and Vera *et al*. (2013).

Historically, pyrite oxidation at low pH has been believed to occur via direct and indirect leaching. The direct leaching mechanism involves the attachment of the bacterial cell to the pyrite surface, where an electron transfer from the iron to oxygen

was enzymatically facilitated at the cell surface. The indirect leaching mechanism occurs when ferric (III) ions react with pyrite resulting in the minerals dissolution, with ferric (III) ions produced by microbial oxidation of ferrous (II) ions (Larsson *et al*., 1990; Mustin *et al*., 1992).

The chemical equations for direct (Eq. 1-2) and indirect leaching (Eq. 3) are detailed below:

Direct leaching

(1) $4FeS_2 + 14O_2 + 4H_2O = 4Fe^{2+} + 8SO_4^{2-} + 8H^+$

(2) $4Fe^{2+} + O_2 + 4H^+ = 4Fe^{3+} + 2H_2O$

Indirect leaching

(3) $FeS_2 + 14Fe^{3+} + 8H_2O = 15Fe^{2+} + 2SO_4^{2-} + 16H^+$

Microbial iron oxidizing activity has been demonstrated to be particularly important in the catalysis of reaction 2, enhancing the reaction rate by up to 10^6-fold (Lacey and Lawson, 1970).

The direct/indirect leaching paradigm has come into question in the last two decades, largely due to a lack of evidence to support the proposed mechanism for direct leaching (Vera *et al.,* 2013). For an enzyme catalysed oxidation of iron (pyrite) by oxygen (cell), a nanowire or another conductive filament would be required to shuttle the electron from the pyrite surface to the enzyme embedded within the cellular membrane.. Until recently, no evidence for a nanowire producing iron oxidizing bacteria existed, indicating that direct bioleaching should be disregarded (Vera *et al*., 2013). However, in 2014 Li and Li discovered that the type IV pili of *Acidithiobacillus ferrooxidans* were electrically conductive. The authors further suggested that *A. ferrooxidans* could use their type IV pili to shuttle electrons from iron minerals to the cell membrane (Li and Li, 2014; Sure *et al*., 2016). Future research will be required to determine if type IV pili can be used in the direct leaching mechanism of pyrite oxidation.

Further research into the indirect leaching mechanism has demonstrated that in fact two indirect mechanisms exist for pyrite oxidation, the thiosulfate and polysulfide

mechanisms respectively (Vera *et al*., 2013). Only the thiosulfate mechanism is directly applicable to pyrite (the polysulfide mechanism being applied to other metal sulfides), so only the reaction details are shown for this in equations 4-5..

Thiosulfate mechanism (indirect leaching)

(4) $FeS_2 + 6Fe^{3+} + 3H_2O \rightarrow S_2O_3^{2-} + 7Fe^{2+} + 6H^+$

(5) $S_2O_3^{2-} + 8Fe^{3+} + 5H_2O = 2SO_4^{2-} + 8Fe^{2+} + 10H^+$

This mechanism demonstrates that sulfate ions are not produced directly from pyrite oxidation, but via an intermediate in the form of thiosulfate ($S_2O_3^{2-}$), a commonly identified sulfur product in iron-oxidizing cultures (Balci *et al*., 2007).

Due to the acidic conditions of shale weathering environments, it is generally considered that the above-mentioned mechanisms are predominant in pyritic shale weathering environments (Taylor, 1988; Pye and Miller, 1990; Joeckel *et al*., 2005; Anderson, 2008; Hoover and Lehmann, 2009; Tuttle and Breit, 2009; Li *et al*., 2014).

Joeckel *et al*. (2005) used geochemical, mineralogical and microbiological techniques to analyse sulfate mineral crusts coating a weathered Graneros shale outcrop in Nebraska, USA. The results of the study indicated that microbial iron oxidation by *Acidithiobacillus ferrooxidans* was primarily responsible for the dissolution of pyrite within that environment. The liberated sulfur from the dissolved pyrite was subsequently oxidised to sulfuric acid (H_2SO_4) and reacted with calcite ($CaCO_3$) to form gypsum ($CaSO_4 \cdot 2H_2O$). Further reaction of sulfuric acid with aluminosilicates resulted in the formation of hydrated aluminium and iron sulfates, such as alunogen ($Al_2(SO_4)_3 \cdot 17H_2O$), copiapite ($Fe^{2+}Fe_4^{3+}(SO_4)_6(OH)_2 \cdot 20H_2O$) and jarosite ($KFe_3(SO_4)_2(OH)_6$) (Joeckel *et al*., 2005).

Li *et al.* (2014) carried out a community analysis and geochemical characterisation of a black shale weathering profile, with specific focus on the cycling of iron and sulfur. They found that *Ferrithrix*, an aerobic iron oxidizing bacteria, dominated in the surface oxidised zone (see section 2.2 for shale weathering zone descriptions), while the abundance of other iron oxidisers such as *Acidithiobacillus* and *Ferrimicrobium* (anaerobic iron oxidisers) increased with depth into the dissolved and illuviated

zones. The abundance of sulfur-oxidizing bacteria such as *Sulfobacillus* and *Thiobacillus* also significantly increased with depth into the dissolved and illuviated zones. Decreasing concentrations of pyritic sulfur and decreasing pH upwards through these two zones towards the oxidised zones indicates that *Sulfobacillus* and *Thiobacillus* are the likely agents of sulfur oxidation and acid production. The study demonstrated that the abundance of differing genera and microbial metabolic groups varies through a shale weathering profile, and that these organisms possibly respond and contribute to the formation of distinct weathering zones (Li *et al*., 2014).

The use of *Acidithiobacillus sp*. for the weathering and bioleaching of shale has been explored over several decades. The primary purpose of bioleaching was either to extract the shale organic components bitumen and kerogen (Findley *et al*., 1974; Vrvíc *et al*., 1988; Zhang and Li, 2017) or metals such as Cu, Fe, Mo, U and V (Mishra *et al*., 1984; Tasa *et al*., 1997; Farbiszewska *et al*., 2003; Lee *et al*., 2005; Grobelski *et al*., 2007). The use of two strains of *Acidithiobacillus sp.* (referred to as *Thiobacillus ferroxidans* and *Thiobacillus thiooxidans*) enhanced Fe leaching by up to 50-fold from black shale pulp taken from Toolse phosphorite deposit, Estonia. Pyrite oxidation was determined to be the primary agent of Fe release, facilitated by the activity of *T. ferrooxidans*. Analysis of the release of valuable elements such as Mo and V was also assessed, but biological activity of the *A. ferrooxidans* strains did not enhance their concentration in the leachate (Tasa *et al*., 1997).

Increasing evidence supports pH circumneutral mechanisms for pyrite oxidation within shale weathering environments (Rhine *et al*., 2008; Zhu *et al*., 2008; Zhu and Reinfelder, 2012; Li *et al*., 2014). Zhu and Reinfelder (2012) incubated pyrite rich black shale in a circumneutral pH groundwater for 4-5 weeks. Post-incubation image analysis revealed preferential colonization of weathered pyrite within the shale, with both pitting and secondary mineral formation visible on the pyrite surface. Culture independent analysis of the surface community did not reveal the presence of common iron oxidizing organisms, which the authors suggested points towards indirect leaching (Eq. 3) of the pyrite. Microbial iron oxidation within the groundwater could therefore contribute to the pyrite dissolution. Alternatively, genera identified on the pyrite such as *Dechloromonas*, which has been previously indicated in iron oxidation, might be active in direct pyrite leaching. Other work

supports the role of aerobic pH neutral microbial iron oxidation in groundwater (Rhine *et al*., 2008; Zhu *et al*., 2008).

Although the exact mechanisms of microbial pyrite oxidation at circumneutral pH remain unknown, Percak-Dennett *et al.* (2017) have provided a contemporary review of potential processes that could contribute to this phenomenon. The authors demonstrate that a microbial community dominated by two *Rhizobiales* species enhanced pyrite oxidation by one order of magnitude at circumneutral pH *in vitro*. They review a range of proposed Fe and S related mechanisms for iron oxidation in pyrite at circumneutral pH and highlight the indirect polythionate intermediate model as a likely mechanism to explain their results. Polythionate ions (e.g thiosulfate, S_2O_3) are liberated from pyrite through abiotic processes at circumneutral pH and is an important component of pyrite dissolution. Microbial utilisation of these ions in fluids surrounding pyrite could act to keep polythionate concentrations low, and hence maintain pyrite dissolution. As liberated iron from pyrite is rapidly oxidised abiotically at circumneutral pH, microbial utilisation of polythionates can enhance iron oxidation under these conditions. Shotgun sequencing of the microbial community used in Percak-Dennett *et al*. (2017) revealed that complete metabolic pathways for carbon assimilation and polythionate oxidation were present, supporting the plausibility of these processes contributing to iron oxidation at circumneutral pH in their study (Percak-Dennett *et al*. 2017).

2.4.3 Microbial degradation of shale organic matter

The first evidence of shale organic matter (SOM) being utilised for microbial metabolism was within the pores of sandstone interbedded with shale. Bitumen (soluble) organic matter seeped from the shale into the sandstone, and provided an electron donor for sulfate reduction and acetogenesis (Chapelle and Lovley, 1990; Krumholz *et al*., 1997). Krumholz *et al*. (2002) further identified that crushed shale material could directly support the growth of the acetogen *Acetobacterium psammolithicum*, indicating that SOM within shale was bioavailable for anaerobic metabolism.

The degradation of SOM by aerobic heterotrophic bacteria was first demonstrated by Petsch *et al*. (2001b), who used $\delta^{13}C$ and $\delta^{14}C$ analysis of phospholipid fatty acids (PLFA) to show direct uptake of SOM by the microbial community *in vitro* (Petsch *et al*., 2001b). Further PLFA analysis within shale rock *in situ* revealed that the abundance of SOM-derived carbon assimilated by anaerobic microbes varied from trace amounts up to 74-94 % (Petsch *et al*., 2003; Petsch *et al*., 2005). The distinct structures of SOM derived PLFA molecules were used to provide chemotaxonomic data, which indicated that the extracted PLFA was derived from a range of aerobic and anaerobic bacteria along with eukaryotic (possibly fungal) organisms (Petsch *et al*., 2003). Sequence data (16S rRNA) of organisms from shale enrichment cultures revealed the presence of both aerobic and anaerobic bacteria including *Acinetobacter*, *Clostridium*, *Comamonas*, *Dechloromonas* and *Pseudomonas* (Petsch *et al*., 2005).

Work within the BIOSHALE project (see Chapter 1) investigated the microbial degradation and assimilation of SOM from Kupferschiefer black shale, mined within Poland for the extraction of copper and silver. Initial work isolated neutrophilic, heterotrophic bacterial strains from black shale mining waste that could degrade metalloporphyrins, organic compounds that have strong ligand-binding to metals such as Fe, Co, Cu and V. Across two studies, they identified the following genera: *Acinetobacter*, *Aeromonas*, *Bacillus*, *Brevibacillus*, *Microbacterium* and *Pseudomonas* (Farbiszewska-Kiczma and Farbiszewska, 2005; Matlakowska and Sklodowska, 2009).

Eight microbial strains isolated by Matlakowska and Sklodowska (2009) for their rock weathering and SOM degrading capabilities, have been used in mixture culture to biologically weather the SOM and mineral content of black shale. The results of this work in relation to SOM weathering has been released in a series of papers over the last eight years (Matlakowska *et al*., 2010; Matlakowska and Sklodowska 2010; Matlakowska *et al*., 2011; Matlakowska *et al*., 2013; Włodarczyk *et al*., 2016; Stasiuk *et al*., 2017). The mixture includes four strains of *Pseudomonas*, two strains of *Microbacterium* and singular strains of *Bacillus* and *Acinetobacter* (Matlakowska and Sklowdowska, 2009).

The group's initial work demonstrated that this mixture of heterotrophic organisms could grow using black shale as a sole energy and carbon source. Microbial activity increased the dissolved organic carbon (DOC) content of the fluid in contact with the rock, with UV-visible spectroscopy used to confirm biological degradation of released aromatic, aliphatic and metalloporphyrin (complexed with V) hydrocarbons (Matlakowska *et al*., 2010). The biological degradation of artificial metalloporphyins complexed with Co and Cu was also confirmed (Matlakowska and Sklodowska, 2010). Włodarczyk *et al.* (2016) carried out proteomic analysis of the cellular and extracellular proteins from a culture containing black shale, and identified a range of hydrocarbon-degrading enzymes and metal uptake proteins. They additionally demonstrate that the extractable organic composition of black shale is modified by microbial activity, with a significant decrease in unsaturated aliphatic hydrocarbons (35 % to 17 %) and an increase in the abundance (5.4 % to 27 %) and diversity (9 to 24 compounds) of carboxylic acids (Stasiuk *et al*., 2017).

Wengel *et al*. (2006) demonstrated that the wood-rotting fungus *Schizophyllum commune* could biologically weather black shale, leaching DOC and heavy metals from the rock into solution. The degradation of SOM by *S. commune* was shown, with benzenes, phenols, carboxylic groups and long chain alkanes all suggested products of SOM degradation (Wengel *et al*., 2006).

2.4.4 Bioleaching of shale – organic acids and siderophores

The action of organic acids and siderophores, primarily produced by heterotrophic bacteria and fungi, can significantly enhance elemental leaching from weathered shale. As covered in section 2.3.2, organic acids can act both as agents of pH reduction and metal chelation, while siderophores specifically chelate iron and other transition metals with great affinity. The study of heterotrophic microbial weathering of shale has been particularly focused on industrial applications, such as the desilicification of oil shale (Vrvić *et al*., 1989; Cvetković *et al*., 2001; Dragutinović *et al*., 2012; Zhang *et al*., 2013; Zhang and Li, 2017) and the enhanced leaching of heavy metals from metalliferous black shales (Farbiszewska-Kiczma *et al*., 2004; Anjum *et al*., 2010; Nouren *et al*., 2011; Kostudis *et al*., 2015; Włodarczyk *et al*., 2015).

The production of organic acids is the main mechanism via which fungi can actively weather shale (Anjum *et al*., 2009, Anjum *et al*., 2010; Nouren *et al*., 2011; Anjum *et al*., 2012; Rajpert *et al*., 2013). Fungal species such as *Penicillium notatum* and *Aspergillus niger* are common inhabitants of soil, where they are often associated with the production of organic acids such as citric, malic and oxalic acids. Fungal organic acids in geological environments are known to both facilitate metal mobility and transform minerals, such as formation of metal oxalate hydrates when oxalic acid reacts with aluminosilicate minerals (Gadd, 2007). Anjum *et al*. (2009, 2010) investigated growing *P. notatum* and *A. niger* on different agricultural waste substrates to produce organic acid rich solutions, which were subsequently used for the leaching of black shale. Fungal growth on molasses or mango peel produced cultures that yielded maximum enhancement of metal release by ~25-fold for Cu (*A. niger*), Co and Zn (*P. notatum*). These studies demonstrate the potential of biohydrometallurgy to reduce the cost and environmental pollution of metal extraction from low grade ores (Anjum *et al*., 2009; Anjum *et al*., 2010).

Within the natural environment, the microbial production of siderophores in shale rock can significantly enhance metal mobility, with consequences for environmental pollution. Kalinowski *et al*. (2006) investigated the role of siderophore production by *Pseudomonas fluorescens* in the mobilization of uranium from black shale crushed tailings, left behind after operations closed at Ranstad mine, Sweden. *P. fluorescens* grown in a suspended crushed shale liquid medium increased pH from 4.7 to 9.3 in unbuffered media, and caused leaching of uranium (up to 0.6 μM m^{-2} of rock) which was undetectable in sterile controls. The activity of *P. fluorescens* also leached U (up to 0.04 μM m^{-2}) out of pre-treated acid leached ore; pre-treatment extracted all labile U, leaving only residual U that should be firmly bound to the rock. These results demonstrate that microbial activity can significantly contribute to rock leaching beyond inorganic geochemical processes, indicating their importance to environmental pollution (Kalinowski *et al*., 2006).

Across the USA nine co-ordinated, interdisciplinary environmental research sites have been established, entitled Critical Zone Observatories (CZO). Research at these sites focus on interconnected biological, chemical and physical processes that contribute to the formation of the critical zone. The Susquehanna Shale Hills CZO is

a forested catchment on shale bedrock, in which biogeochemical processes that release and isotopically fractionate Fe and Mo have been explored (Liermann *et al*., 2011; Yesavage *et al*., 2012). Batch culture experiments and geochemical analyses in the field demonstrated that released Fe and Mo was isotopically lighter and heavier respectively, compared to parent material. Released Fe and Mo was derived from pyrite and clay minerals within the shale, in which microbial iron oxidation and microbial secretion of organic ligands, such as DFAM, enhanced leaching. The distinct isotopic signature of microbial weathering of shale provides a useful tool to monitor microbial shale weathering activity in natural environments (Liermann *et al*., 2011; Yesavage *et al*., 2012).

The work of Matlakowska *et al.* within the BIOSHALE collaboration has also focused on the role of microbially produced metal binding ligands in shale weathering (Matlakowska and Sklodowska, 2010; Matlakowska *et al*., 2012; Rajpert *et al*., 2013; Matlakowska *et al*., 2014; Włodarczyk *et al*., 2015). Włodarczyk *et al*. (2015) investigated the production of organic ligand production by microbial isolates (Matlakowska and Sklowdowska, 2009) grown with crushed black shale in medium lacking a source of Fe. Over the course of five days, the bacterial population (3.5 x 10^{10} CFU/mL) produced a medium rich in organic acids and siderophores (siderophore concentration - 1.5 mM). Bacterial activity and the production of these ligands resulted in simultaneous release of a range of metals, notably As, Al, Fe, K and Mg, from the black shale. GC-MS was used to analyse microbially-produced organic compounds, the results of which identified the organic ligands succinic and salicylic acids, and the siderophore precursor molecule 3-hydroxyhexanoic acid (Włodarczyk *et al*., 2015).

2.5 Microbial geomorphology

Previous sections have focused on microbial weathering of minerals and rocks from a molecular to microscopic level, the scale at which individual microbes interact with their surrounding environment. This section covers the novel field of microbial geomorphology (Viles, 2012), the study of how microbial activity alters the shape and structure of geological outcrops on the centimetre to kilometre scale, with a

specific focus on the contribution of microbial weathering processes. The field is itself a subfield of biogeomorphology, which primarily investigates how plants and animals (such as boring invertebrates) alter geomorphology.

Existing studies within microbial geomorphology have largely focused around microbial biomineralization and its contribution to creating geomorphic structures (such as cyanobacterial sheath calcification in tufa), rather than microbial rock weathering and degradation (Viles 2012; Coombes, 2016). However, these weathering processes can make significant contributions to geomorphology, such as speleothem formations within cave environments (Boston *et al*., 2001). Manganese "snow" was a previously given example. Sulfur caves provide another good example, where sulfuric acid production is the primary agent driving cave formation (Boston *et al*., 2006). Hydrogen sulphide gas emitted from springs becomes increasingly oxidised (elemental sulfur, sulfates) as it enters the cave. Within increased availability of sulfates, sulfate-reducing microbes such as *Thiobacillus* sp. can then act to form sulfuric acids as a bi-product of their metabolism. Whole cave systems are formed through these processes, showing that microbial weathering processes (inorganic acid production enhancing rock degradation) can play a significant role in karst geomorphology.

At the Earth's surface, the microbial contribution to saprolite (weathered rock) formation from a quartz diorite bedrock was investigated in the Luquillo Mountains, Puerto Rico (Buss *et al*., 2005). The authors identified that the abundance of aerobic iron oxidizing microbes increased with depth into the partially weathered zone, and correlated with HCl extractable iron (II). They further demonstrate that the autotrophic iron oxidizing community is the primary source of organic substrates for heterotrophic microbes. The combined activity of these microbial communities resulted in saprolite depletion of both Fe (II) and total organic carbon, from iron oxidation and CO_2 release respectively. The authors hypothesise, and support with numerical geochemical models, that microbial activity likely maintains a gradient of Fe (II) and organic carbon release from the bedrock, driving saprolite formation. This example demonstrates how microbial weathering activity can play a role in altering lithology on a landscape scale.

Viles (2012) highlights the role microbes can play in facilitating other bioweathering and bioerosive processes by plants or animals. Rock analysis from a limestone coastal platform revealed the presence of cyanobacteria produced endolithic boreholes. These tunnels act to increase porosity and reduce rock strength at the rock surface, enabling the activity of bioerosive animals such as grazing molluscs to erode the surface.

The field of microbial geomorphology is still in its infancy (Viles, 2012), but the increasing development of sophisticated techniques in microbiology and geomorphology will increasingly enable more ambitious and revealing studies (Viles, 2016).

Chapter 3 – Methodology

3.1 Introduction

In this chapter, details of methodology used throughout the thesis are provided. This includes both general methodology that is shared between chapters (e.g. media recipes) and general concepts for specific instruments, techniques and processes used (e.g. explanation of how XRD works). For the latter, only a general overview of how that instrument/technique/process works will be provided. Specific details such as settings used for particular analyses can be found within the individual methodology sections of each results chapter (Chapters 5-8).

3.2 Microbial culture techniques

Standard microbial techniques were used throughout the work in this thesis. Liquid and solid media were prepared using established recipes, and were sterilised by autoclaving at 121^{o} C for 20 minutes. Most equipment, including glassware and plastics, that needed to be sterilised was autoclaved under the same conditions. Some equipment or samples (such as mineral cubes) that needed to be sterilised under dry conditions, a kiln was used to heat the samples to 160^{o} C for 2 hours. In Chapter 6, glassware and tinfoil needed to be purified of organic contamination, so they were heated in a furnace at 500^{o} C for five hours. Above 350^{o} C, most organic compounds will readily breakdown into CO_2, purifying surfaces from organic contamination (Personal communication, Wren Montgomery, ICL).

In chapters 6 and 7, M9 medium is used as a standard medium for growth of both axenic (single strain) and community cultures. The recipe for M9 medium (Miller, 1972) is as follows (per L): 200 mL of sterile M9 5x salts (64 g/L $Na_2HPO_4{\cdot}7H_2O$, 15 g/L KH_2PO_4, 2.5 g/L NaCl, 5.0 g/L NH_4Cl), 2 mL of sterile 1M $MgSO_4$, 100 µL of sterile 1M $CaCl_2$, 20 mL of sterile 20 % glucose aqueous solution (optional, see methodology sections of chapters 6 and 7), topped up to 1 L total with sterile water (. The resulting pH of this medium is ~7.4. All solutions are sterilised by autoclaving.

All chemicals used to prepare media in this thesis were purchased from Sigma Aldrich.

To enumerate colony forming units (CFU) within a culture, an aliquot would be serially diluted (10-fold dilutions) and then plated onto agar plates. One CFU (normally assumed to be a single cell) forms one colony. By counting the number of grown colonies and then multiplying counts by the dilution factor, CFU/mL can be calculated.

Measurements of optical density (OD) were also used to obtain values of relative growth between bacterial cultures. A Biotek Synergy 2 Plate Reader was used to measure OD (600 nm absorption) in wells of Greiner 96-well flat-bottomed microplate.

Glycerol stocks were used for the long-term storage of *V. paradoxus*. Cultures were grown until they reached exponential phase and then diluted 1:1 into 50 % aqueous glycerol solution. Stocks were then frozen at -20^{o} C for long-term storage.

In Chapter 6, two types of bacterial motility were assayed: swimming and swarming. Swimming is the motility of a single bacterial cell using its flagella to propel itself through liquid medium. Swarming is defined as "rapid multicellular movement of bacteria across a surface, powered by rotating flagella" (Kearns, 2010), and is motility on a solid surface. Both swimming and swarming assays are done on agarose plates with varying concentrations of agarose (0.3-0.5 % swimming, 0.6-0.7 % swarming). For swim agarose plates, the low agarose concentration produces large, interconnected pores within the gel, allowing bacteria to swim through. On swarming plates, agarose concentration is high enough to inhibit swimming but low enough to reduce surface tension sufficiently to enable swarming (Kearns, 2010).

3.3 Field sampling methodology

Geological samples were collected from numerous field sites for the work carried out in this thesis. For further information and images of these field sites, see Chapter 4. All sampling was done using sterile techniques, to reduce risk of contamination to the samples collected.

A rock hammer was used to break or loosen samples from rock exposures, while a trowel was used to scoop weathered rock chips from scree. The trowel was also used to bury the field mesocosms into the scree floor of Assholm mine (Chapters 4 and 8). Samples collected in this thesis were stored in either sterile Whirlpak bags of varying sizes or in Sterilin 20 mL vials. Before sampling at each location, the rock hammer/trowel was cleaned, dowsed in ethanol and then flame sterilised. Sterile nitrile gloves were worn by the author throughout sampling. Goggles were also worn by the author when using the rock hammer or handling glutaraldehyde (see below). All geological samples were kept at ambient temperature until return to the laboratory, where they were stored in a cold room at 4^{o} C in the dark until use.

Storage of geomicrobiological samples altered environmental conditions surrounding the rock-inhabiting microbial communities collected, including the temperature, light and humidity and oxygen availability. The storage period of samples before use varied for the sets of samples collected for the work in this thesis, from a few days to three to four weeks. It is therefore possible that microbial taxa sensitive to these changes could be under-represented in this work. To limit this impact, samples were used for experimentation as quickly as possible post collection.

When collecting the field mesocosms from Assholm mine after one year of burial (see Chapters 4 and 8), sterilised tweezers (ethanol and flamed) were used to remove mineral samples from the Nalgene tubes. Mineral samples were transferred to cold phosphate buffered saline (PBS) supplemented with 2.5 % glutaraldehyde, and subsequently kept chilled (cool box with freezer packs) until return to the laboratory. The following recipe was used for the PBS solution (Cold Spring Harbour Laboratory Protocols, 2006): in 1 L of dH_2O 8 g NaCl, 0.2 g KCl, 1.44g $NaHPO_4$ and 0.24 g KH_2PO_4, adjust to pH 7.4 using HCl and then autoclave to sterilise. See Chapters 4 and 8 (methodology section) for more details on Assholm mine and the use of glutaraldehyde solution respectively.

3.4 Molecular biology techniques, Sanger sequencing and bioinformatics

Polymerase chain reaction (PCR) is a molecular technique used to amplify the number of copies of DNA molecules within a solution. For a detailed explanation of PCR, see McLennan *et al.* (2012). PCR was used in Chapter 5, to amplify 16S rDNA from bacterial isolates. Specific details of the PCR protocol used can be found in Chapter 5, section 5.2.3. Gel electrophoresis and Nanodrop DNA concentration quantification was used to test for successful PCR of individual isolates.

The 16S rDNA gene codes for a ribosomal RNA that is highly conserved between bacterial species. Divergences in 16S rDNA sequences between species can be used for phylogenetic species identification. PCR products of 16S rDNA were sent to Edinburgh Genomics (Ashworth Laboratories, University of Edinburgh) for Sanger sequencing. Briefly, Sanger sequencing allows the nucleotide sequence of DNA molecules to be discerned via the extension of the target DNA molecule (template) with a mixture of nucleotides and fluorophore labelled dideoxynucleotide (ddN) chain terminators. As the template becomes extended by DNA polymerase, either a normal nucleotide or a ddN can be incorporated into the synthesised strand. If a ddN is added the chain is terminated, producing DNA chains of varying length. Each ddN of the four bases (Adenine, Thymine, Cytosine and Guanine) is labelled with a unique fluorophore that emit at different wavelengths when excited. Separation of DNA chains on a gel and subsequent fluorescence imaging allows the DNA sequence of the template to be determined. Further information on Sanger sequencing can be found in McLennan *et al*. (2012).

Sequencing was carried out using both forward (27F) and reverse (1389R) primers, so contigs (contiguous DNA sequence) were prepared from the forward and reverse sequences of each isolate. Quality trimming of sequence reads was carried out by Edinburgh Genomics, so no modifications were made to the sequences before contig preparation. Contigs were prepared using DNA Baser Sequence Assembler (http://www.dnabaser.com/index.html).

Contigs were then queried through the BLASTn (Basic Local Alignment Search Tool - nucleotide sequences - https://blast.ncbi.nlm.nih.gov/Blast.cgi) database to resolve sequences to Genera taxonomic level. Genus level identification was made at 97 % or above similarity with a BLAST database sequence.

3.5 Preparation of mineral and rock samples

In chapters six and seven, shale rock materials collected from field sites were autoclaved to sterilise them. In these instances, rock powder or rock chips were autoclaved for 121 ^{o}C for 20 minutes. Autoclaved material was then used for both the sterile control and the biological test condition, where a microbial inoculum from an enrichment culture was added. This ensured that any geological alteration caused by autoclaving of the material did not influence experimental outcomes. XRD analyses of pre-autoclaved and autoclaved Redcar mudstone rock powder (Chapter 7) did not reveal any detectable differences (< 1 %) in mineralogical composition (data not shown).

Mineral samples were either donated to the author by Professor Charles Cockell (University of Edinburgh – supervisor) from previous purchases or were ordered from UKGE Limited.

The minerals albite, calcite, muscovite, pyrite and quartz, and the rock jet were prepared for experiments in Chapters 6 and 8. For all minerals (except muscovite) and jet, cubes roughly 2 cm^3 were cut using a rock axel saw. At least one face of each cube was ground on 74 μm and 20 μm diamond grinding discs, Buehler Ultra-prep, before polishing on Kemet PSU-M polishing cloth with 0.3 μm aluminium oxide and water. Fresh sheets of muscovite were cleaved from the mineral surface using tweezers. No further alteration was carried out to the surface. All mineral and rock samples were dry oven sterilised at 180 ^{o} C for 2 hours.

3.6 Fluorescence microscopy

Cell counts of both liquid cultures and solid surfaces were used for cell enumeration of axenic and community cultures. Rock particle suspensions and mineral surfaces

colonised by microbes were also imaged using fluorescence and bright-field microscopy (Chapters 6 and 8).

The fluorescent nucleic acid dye Acridine Orange (DNA excitation wavelength at 500 nm, emission wavelength at 526 nm) was used for all fluorescent microscopy in this thesis. Varying concentrations (see individual methodology chapters) of Acridine orange was used to stain microbial cultures for at least 15 minutes in the dark before imaging. For liquid cultures, an aliquot was mounted onto black 25 mm diameter polycarbonate filters to improve contrast (0.22 μm; Merck Millipore, Billerica, Massachusetts, USA). Cultures were visualised with a I3 fluorescence filter (blue laser, excitation filter BP 490/20;575/30, dichromatic mirror 505;600, suppression filter BP 525/20;635/40) on a Leica DM4000B digital microscope. Images were taken using a Leica DFC 450 C microscope-mounted camera.

For cell counting, a minimum of 200 cells were counted over at least 10 randomly chosen fields of view (100 μm^2 grid). For mineral surfaces, where the number of cells per field of view could not be reduced by dilution (as can be done for dense liquid cultures), images were taken for later analysis. For cultures of *Variovorax paradoxus*, automatic cell counting analysis was used in ImageJ. The following settings and analyses were used: 1) convert image to 8-bit, 2) invert, 3) adjustment of brightness/contrast 4) fill holes (if necessary), 5) Watershed, 6) analyse particles.

For mineral colonization in the microcosms and mesocosms (Chapter 8), images of the mineral surfaces were taken and then hand counted later. This allowed dense colonization to be counted when it was not possible to do the count directly at the microscope due to photobleaching.

3.7 SEM-EDS

Two scanning electron microscopes (SEM) were used for this thesis. Standard SEM without EDS was carried out using a JEOL JSM-6010PLUS LUS/LV Scanning Electron Microscope. This microscope is funded by the Soft Matter and Functional Interfaces Centre for Doctoral Training (SOFI-CDT). SEM with EDS was carried out on a Carl Zeiss SIGMA HD VP Field emission SEM with the Oxford AZtec EDS System.

A brief description of principles for SEM and EDS are included below. SEM is the use of electrons rather than photons to image a surface, in which a sample in a vacuum is targeted by an electron beam. Several types of signal can be returned to detectors from the sample. The most common type of signal used for imaging is the production of secondary electrons, where the electron beam (primary electrons) knocks electrons out of atomic orbitals (secondary electrons) within the sample, producing ionisation products. Most secondary electrons are produced at a very shallow depth within the sample (~10 nm), and can resolve features less than 1 nm in size. Secondary electron detection can therefore be used for fine detail imaging.

Energy dispersive spectroscopy (EDS) is the elemental analysis of a solid sample, through detection and analysis of X-rays radiated from the sample. In SEM-EDS, secondary electrons are generated from primary electron bombardment which leaves an electron hole within the shell. Electrons from outer, higher energy shells can drop down to fill the hole and energy (X-ray radiation) is released in the process. The number and energy of the X-rays released are characteristic of the energy difference between the two shells and the atomic structure of the emitting element. Analysis of emitted X-rays therefore allows elemental composition of a sample to be determined. For more details on SEM and SEM-EDS, see Reichelt (2007).

Preparation of material for SEM involved two steps, sample drying followed by gold coating. Colonies imaged in Chapter 5 were air dried on a glass slide, mineral samples in Chapters 6 and 8 were put through a chemical drying process. For chemical drying, samples were washed in increasing concentrations of ethanol-water solutions (30 %, 50 %, 70 %, 95 % twice and 100 % three times) for 5 minutes per wash. Samples were then washed in solutions of 2:1, 1:1 and 1:0 hexamethyldisilazane (HMDS) with ethanol for 10 minutes per wash. Samples were dried overnight in a laminar flow hood before being mounted on stubs and gold coated. A layer of gold coating was applied to samples roughly 10-15 nm in thickness.

A 20 kV accelerating voltage was used for most images taken on both microscopes. In some cases, 14 kV was used when either the gold coat was too thin on some spots of the sample, or charge accumulation occurred on topographic features. Working

distances varied substantially between samples analysed to obtain the highest quality images possible. Specific working distances of individual images can be seen in the information bar below SEM images or in the figure legend.

3.8 XRD

X-ray diffraction (XRD) is used to detect the presence of specific crystalline mineral phases within a solid sample. Characteristic scattering of X-rays through distinct crystalline structures allows individual minerals such as quartz to be identified. For more information on XRD, see Lavina *et al.* (2014).

In Chapter 7, shale rock samples were analysed using XRD to determine mineralogy. Samples were first coarsely crushed using a rock crusher, before being finely crushed (1 μm particle size or below) in a corundum bead grinder while suspended in ethanol. The ethanol-particulate suspension was then sprayed onto a sheet, the ethanol allowed to evaporate and the powder collected.

The sample was then loaded into the Bruker D8-Advance X-ray Diffractometer which employs a 2-theta configuration in which the X-rays are generated by a Cu-anode x-ray tube operating at 40 kV and a tube current of 40 mA. The diffracted x-rays were detected using a NaI scintillation detector. The samples were scanned from 2 to 60 degrees two theta at a scan rate of 0.02°/second and the resultant diffractograms compared with the 2012 issue of the International Centre for Diffraction Data (ICDD) diffractogram database library using the EVA analysis package. This procedure typically gives a detection limit for crystalline phases of approximately 1 wt.%.

To quantify percentage abundance of minerals present in the samples, diffractograms were imported into TOPAS analysis software for Rietveld analysis.

3.9 ICP-OES

Inductively coupled plasma optical emission spectroscopy (ICP-OES) provides elemental concentrations of cationic metallic elements and a restricted range of non-metal elements in a liquid sample. In Chapter 7, elemental leaching from shale rock into solution was determined using ICP-OES. The use of ICP-OES is a standard method for quantifying elemental concentrations in rock leachate (Olsson-Francis *et al*., 2012).

Principles of ICP-OES are briefly described here. The liquid sample is initially injected into an argon plasma where it becomes dried, vaporised and atomised. Heat is then used to excite and ionise the produced atoms. Ionization energy is released as radiation which is sampled for spectrometric measurements. Specific wavelengths are unique for individual elements, with wavelength intensity being proportional to elemental abundance. Further information on ICP-OES can be found in Hou *et al*. (2000).

Liquid samples were prepared for ICP-OES by filtering (0.22 μm filter) each solution twice to remove particulates and the addition of 2 drops (~100 μL) of 70 % nitric acid to inhibit precipitation. ICP-OES analysis was carried out using a Perkin Elmer Optima 5300 DV. Samples were loaded into the instrument through a peristaltic pump via a Gem Tip cross flow nebuliser and Scotts spray chamber at a rate of 1.5 mL min^{-1}. For all elements except Fe, measurements were taken in radial mode (Fe measurements taken in axial mode). Multi-elemental standard solutions were prepared from 1000 mg/L stock solutions (Fisher Scientific, UK). The concentration of these solutions ranged from 0.005-200 ppm, resulting in a lower detection limit of > 0.005 ppm. In cases where sample elemental concentrations were above 200 ppm, sample solutions were diluted to allow measurements to fall within the detection range. All measurements were taken in fully quantifiable mode (three points per unit wavelength). For calibration lines the correlation coefficients for the linear regression were 0.999 or better.

3.10 Raman spectroscopy

Raman spectroscopy is a technique that uses the interaction of electromagnetic radiation (the laser light) with molecular vibrations within a sample to create a fingerprint of its molecular composition and structure. The basic concepts of Raman spectroscopy are explained below.

Molecular bonds can absorb photons that interact with them, with the energy gained from that absorbed photon being subsequently released as an emitted photon. The release of emitted photons from an irradiated sample is called scattering, of which two types exist: elastic scattering (or Rayleigh scattering) and inelastic scattering (or Stokes-Raman scattering). Elastic scattering occurs when all the energy from the absorbed photon is released in an emitted photon, resulting in conservation of energy. Inelastic scattering occurs when conservation of energy does not occur, because the emitted photon has less (or more) energy than the photon absorbed. Generally, the reduction in energy results in a detectable shift in the wavelength of the emitted light compared to the irradiating light. This is called the Raman shift, and is given in units as the number of wavelengths shifted per centimetre (cm^{-1}).

In Raman spectroscopy, a monochromatic laser is used to irradiate a sample and the light returned from the sample directed to a detector. A holographic grating is used to disperse the scattered light to enhance detection resolution, and an edge filter is used to separate in-elastically from elastically scattered light. For more information on the theoretical principles and application of Raman spectroscopy, see Vandenabeele (2013). Raman spectroscopy can be used to determine mineralogy within geological samples, and has been specifically used to distinguish between iron minerals within complex samples (Das and Hendry, 2011; Cockell *et al*., 2011).

A LabRam 300 spectrometer (Jobin-Yvon/Horiba) with a helium-neon laser (632.81 nm) was used to obtain Raman spectra of iron oxidizing colonies in Chapter 5. The settings used to obtain measurements with this instrument are detailed below. A 500 µm diameter laser beam was directed onto the sample, with scattered radiation directed through a 100 µm slitand a 1800-g/mm grating before reaching the CCD (charge-coupled device) detector. Measurements of silica (521 cm^{-1} peak) were used

to calibrate the instrument before sample measurements were made. An acquisition time of 60 seconds was used at 10 % total laser power for all measurements taken. Five-point measurements were taken from each colony analysed and used to create an average Raman spectrum. Spectra were analysed using LabSpec (version 5) software.

3.11 Drop tensiometry

Amphipatic molecules, those that have both hydrophobic and hydrophilic moieties, can act as surfactants within a fluid by reducing surface and/or interfacial surface tension. Many microbially produced and secreted molecules, such as glycolipids and lipopolysaccharides, can act as surfactants (biosurfactants) within culture media (Cserháti *et al*., 2002). The release of these molecules can be a bi-product of metabolism and growth. However, some microbial species produce and excrete large quantities of biosurfactant as part of a physiological response. For example, a bacterial swarming colony can produce a wetting agent (containing biosurfactants) which reduces the interfacial surface tension between the agar and the culture medium (Jamieson *et al*., 2009). Biosurfactants have also been demonstrated to increase the solubility of insoluble compounds, such as aliphatic hydrocarbons, making them available for biological degradation and metabolism (Haddadin *et al.,* 2009).

In Chapter 6, the production of biosurfactants by *Variovorax paradoxus* is assessed using pendant drop tensiometry. This technique involves suspending a drop of fluid from the end of a needle in front of a camera, with regular imaging of droplet shape over time. Based upon the droplet shape and the contact angle of the droplet to the needle exuding it, a value for the interfacial surface tension (IFT, mN/m^2) at the droplet/air interface can be calculated. The presence of surfactants within a fluid reduces its IFT value. In drop tensiometry, surfactants within the fluid cause droplet contact angle to decrease and surface area to increase due to droplet elongation. Surfactants must accumulate at the fluid/air interface to affect the IFT, so after the droplet is exuded surfactants diffusing to the droplet surface alter the IFT over time.

This continues until surfactants become saturated at the fluid/air and therefore no longer alter IFT. For further information on drop tensiometry, see Lee *et al*. (2008).

For the work carried out in this thesis, a Krüss Easydrop tensiometer (Krüss GmbH, Germany) was used in combination with Drop Shape Analysis software. A 25 µL droplet was exuded from a 1.84 mm diameter needle at a rate of 400 mL min^{-1} into a covered glass cube. The point at which the droplet was fully formed was designated t=0 and images of the droplet were taken once per second for one hour. By this point, the droplet shape had become stable and no further changes in IFT were observed. Duplicate measurements were taken for each sample analysed, and duplicate samples were prepared for each condition tested.

3.12 Data and statistical analyses

General data analysis and the production of figures was carried out in Microsoft Excel. All error bars in figures represent standard error across replicate measurements, unless otherwise specified. Statistical package for social scientists (SPSS) and R (version 3.4.0) were used to carry statistical analyses.

Chapter 4 - Field work

4.1 Geology of the North Yorkshire coastline

4.1.1 Introduction

The Whitby coastline is found in the North East of England, UK, and is primarily comprised of soft rock cliffs whose geology stretches across the Jurassic period within the Mesozoic era. The sampling sites used in this thesis are from sedimentary strata within the Toarcian and Pliensbachian stages (190.8 – 175.6 Ma) (Powell, 1984; Powell, 2010; Rawson *et al.*, 2000). Classically these groups of shales, interbedded with sandstone and other sedimentary formations form part of the Lias Group, which spans the Rhaetian stage of the Triassic period to the Toarcian stage of the Jurassic period (Powell, 1984; Rawson *et al*., 2000). The group is formed of marine sediments that were deposited in a system of shallow, epeiric seas (ocean that is floored by a continental shelf) which included the Cleveland basin, which outcrops across modern day Northeast Yorkshire (Powell, 2010). A geological map of the area can be found in Figure 4.1, and the individual lithostratigraphical divisions within the Lias group can be found in Figure 4.2.

Weathered shale environments were sampled from various divisions within the Lias group, so a brief description of these divisions is included within sections 4.1.2 and 4.1.3. For more information on the Lias group see Hobbs *et al.* (2012), with additional information on lithostratigraphy and palaeontology within Rawson *et al.* (2000) and geochemistry within Gad *et al.* (1968) (only for Whitby Mudstone Formation). It should be noted that member and unit sizes (height in metres) are taken from Rawson *et al.* (2000) and that their values vary slightly from other descriptions (Howarth, 1962; Hobbs *et al*., 2012).

Figure 4.1¦ A geological map of the North Yorkshire area (Powell, 2010).

4.1.2 Redcar Mudstone Formation

This formation, otherwise known as the "Lower Lias", is comprised of four members (bottom to top): Calcareous shales, Siliceous shales, Pyritous shales and Ironstone shales. The shales overall are fossiliferous and are interbedded with limestone and contain sporadic nodules of argillaceous limestone (Hobbs *et al.*, 2012).

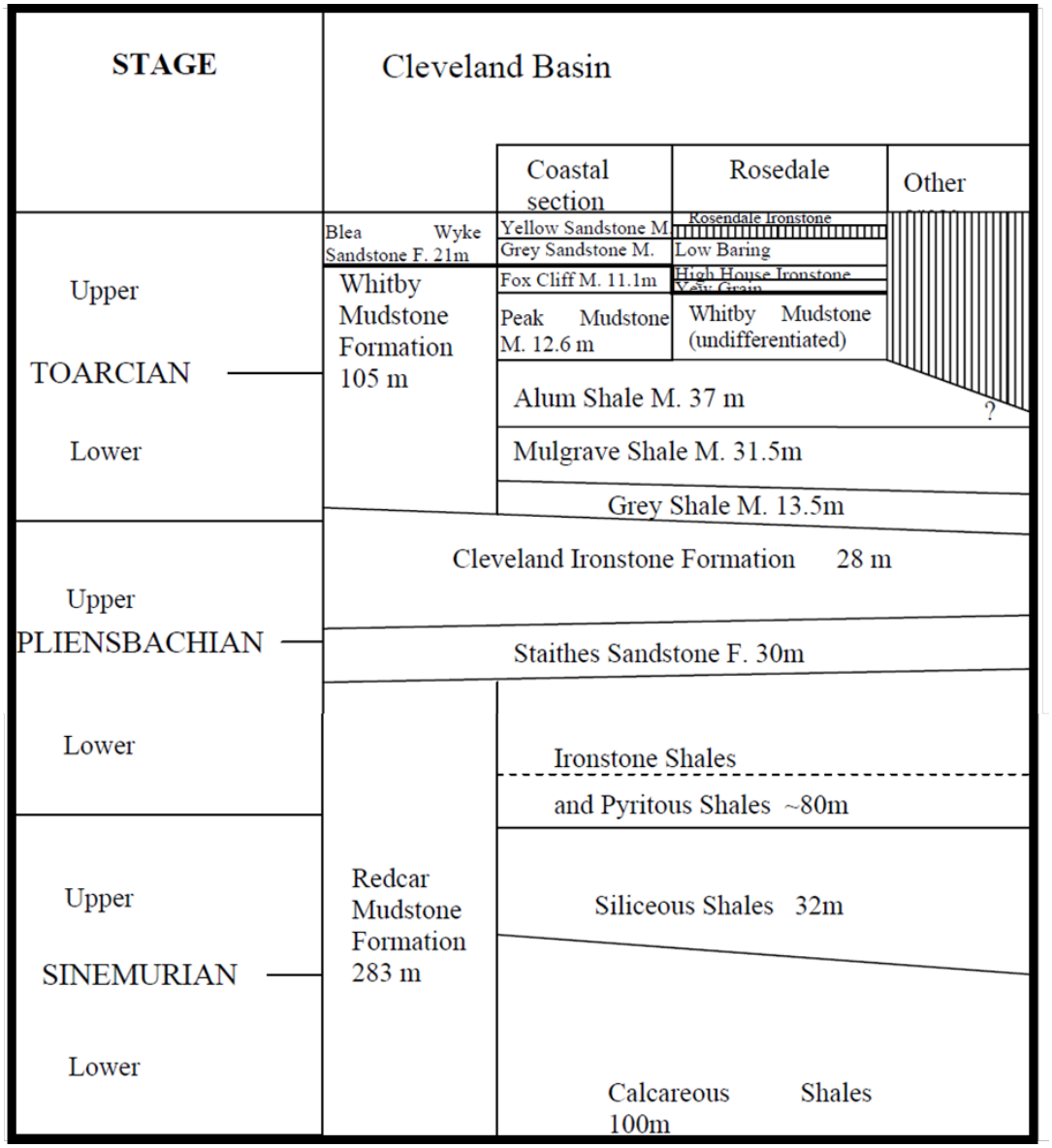

Figure 4.2¦ Lithostratigraphical diagram of the Lias Sediments that outcrop at the Yorkshire coastline (Coastal section) and the Yorkshire mainland (Rosedale) (Adapted from Hobbs *et al*., 2012).

In this study, samples were taken from both the pyritous (c. 27 m) and ironstone shale members (c. 64m) from cliff locations and a disused mining access tunnel at Hole Wyke near Staithes, North Yorkshire.

Hobbs *et al*. (2012) geochemically characterised the members of the Redcar mudstone formation. The Pyritous shale member has a 3 % pyrite content similar to that of the ironstone shale member (2 %), however the pyrite is in the form of visible

pyritic burrows. The ironstone shales contain hard sideritic ironstone nodules that are visible within the cliff surface. The mineralogy of these rock types are largely similar (pyritous – P, ironstone – I, percentage abundance) being primarily comprised of quartz (P – 29 %, I – 24 %), calcite (P – 8 %, I – 6 %), pyrite (P – 3 %, I – 2 %), mica (P – 37 %, I – 42 %) and kaolinite (both 21 %) (Hobbs *et al.*, 2012).

4.1.3 Whitby mudstone formation

The Whitby mudstone formation (WMF) was deposited within the Toarcian stage, a geological time which saw a rise in global sea levels (Hallam, 1997). Whitby mudstone formation sediments were therefore laid at the bottom of a deeper, marine water column within a more anoxic depositional environment than previous Lias sediments. The result of this change in depositional environment is that the rocks formed from this stage have greater abundances of "reduced" components that were not oxidised and degraded during sedimentation, such as sulphide minerals (e.g. pyrite) and sedimentary organic matter (Rawson *et al.,* 2000).

The WMF is comprised of five members (oldest to youngest): Grey shale member, Mulgrave shale member, Alum shale Member, Peak mudstone member and Fox cliff siltstone member. In this thesis, both the Mulgrave shale (c. 32 m) and Alum shale (c. 41 m) members were sampled at various locations, both on the coastline and at inland disused mine workings in North Yorkshire. The Mulgrave shale member is comprised of two lithological units, the jet rock shales (c. 8 m) and the overlying and larger unit of bituminous shales (c. 24 m). The Alum shale member is comprised of four units (oldest to youngest): Hard shales (c. 4 m), Main alum shales (c. 20 m), Cement shales (c. 13 m) and Peak shales (c. 4 m) (Howarth, 1962; Gad *et al.*, 1968; Rawson *et al.,* 2000).

Mineralogical (Hobbs *et al*., 2012) and chemical (Gad *et al*., 1968) data are available for both the Alum shale and Mulgrave shale members. The Jet rock and Bituminous units of the Mulgrave shale member have a higher average organic carbon content (5.54 % and 2.74 % respectively) than the alum shales (1.67 %), with the Jet rock unit in particular having a noticeably oily smell when fresh rock is cracked open (Gad *et al*., 1968; Rawson *et al.*, 2000). The Jet rock unit is named after the presence

of Jet (also called Whitby Jet) inclusions that occur as thin, elongate coal-like seams through the shale. These inclusions originate from fossilised material of flattened, drifted logs of wood closely related to that of modern *Auracarias* (Monkey Puzzle tree) (Rawson *et al.*, 2000).

In terms of mineralogy, both the Alum shale and Mulgrave shale members are similar to that of the Redcar mudstone formation members, with high contents of quartz (31 % and 25.6 %, respectively), mica (40 % and 34 %) and kaolinite (20.5 % and 16 %). However, Alum shale has a slightly higher pyrite content (5 %) than the Mulgrave shale (3.3 %) and the Redcar mudstone formation shale (2-3 %) (Hobbs *et al*., 2012). The mineralogical analysis of Hobbs *et al*. (2012) did not detect feldsparic minerals in any of the WMF rock samples tested, however trace amounts were detected in the mineralogical analysis of Gad *et al*. (1968).

There are numerous geochemical differences between Alum shale and Mulgrave shale members and individual units (Gad *et al*., 1968). There are enriched concentrations of Mn and S in Jet rock (Mn 420-550 ppm, S 3.64-5.84 %) compared to the other shale units (Mn 160-270 ppm, S 1.55-3.48 %), but Jet rock is depleted in aluminium oxide (13-18 % compared to 21-25 % in other shales). Cement shales and some Alum shale samples tested were enriched in Zr (210-280 ppm compared to 110-180 ppm), while both Jet rock and Bituminous shales were enriched in Sr (average 538 ppm, compared to 164 ppm) and calcium carbonates (average 8.09 % compared to 2.1 %).

4.1.4 Coastal erosion and cliff recession on the North Yorkshire coastline

The geology of the North Yorkshire Jurassic coastline has been surveyed and studied since the 17th Century (Powell 2010) with notable reviews and guides produced over the last 200 years (Young and Bird, 1822; Fox-Strangways *et al*., 1915; Hemingway *et al*., 1968; Rawson *et al.,* 2000). Coastal erosion on the North Yorkshire coastline was beginning to be studied in the middle of the 20th century (Agar, 1960), when cliff recession was estimated to have been an average 16 feet (4.87 m) per century (0.05 m a^{-1}) across the whole coastline since the last glaciation 10,000 years ago.

Further work started to unveil possible erosive mechanisms that could drive this cliff recession including slaking (see Chapter 2) from intermittent wetting, abrasion by fine grained particles from foreshore beaches and wave quarrying (Robinson, 1977a, 1997b and 1997c). More recently, new technology and techniques (including digital photogrammetry and laser scanning) have been used to accurately quantify rates of erosion across cliff surfaces (Lim *et al*., 2005, Rosser *et al*., 2005). These have been used in conjunction with environmental monitoring and physical modelling to determine which processes drive cliff erosion at numerous studied sites on the North Yorkshire coastline (Lim *et al.*, 2010; Rosser *et al*., 2013; Vann Jones *et al*., 2015).

The primary finding of these studies is that cliff erosion is not defined by sporadic, large erosive events, but rather a continuum of erosive loss across the magnitude-frequency spectrum has an interconnected effect on shaping the rock face. They show that the average size of rock falls from shale lithology within the studied cliffs was 0.018 m^3, with volumetric loss ranging between 0.0001 and 350 m^3 (Lim *et al.,* 2010). Furthermore, they suggest that erosive losses propagate up the cliff face, with smaller volumetric losses preceding larger blocks being lost (Lim *et al*., 2005; Rosser *et al*., 2013). Correlational analysis of micro-seismic motions (offshore, nearshore and at-cliff) indicated that marine influence had the strongest relationship with total volume and size of rockfalls. Although marine influence is strongest at the cliff toe, it had indirect effects across the whole cliff face (Vann Jones *et al*., 2015).

Together, these studies demonstrate that erosion of smaller shale fragments play an important part of the total erosive processes within cliffs on the North Yorkshire coastline. The mechanisms which result in the formation of these smaller fragments and their loosening from the main rock body are therefore of central interest to understanding the erosion of the cliff face as a whole.

4.2 Field sites

4.3.1 Introduction and maps

In order to determine the role of microbes in shale weathering within cliff environments, rock samples from weathered shale outcrops were obtained for

culturing and further microbiological work. Several cliff toe locations accessible by foot from the foreshore were chosen as study sites. Sample collection from above the cliff toe was deemed unfeasible due to the dangers involved of an eroding, unstable cliff face.

North Yorkshire has had an extensive industrial history that has either extracted resources from shale (Alum for cloth dyeing, calcareous concretions for cement and Jet for jewellery) or cut though shale bedrock as part of a mining tunnel network (e.g. Boulby Alum Works) (Bax *et al.,* 2015; Jecock, 2009; Morris and Whitlock, 2005; Howarth, 1962; Pybus D., personal communication 2017). Industrial sites within the cliff faces are sheltered from marine erosive processes, while other industrial sites are either at the cliff top or within the mainland away from the coast (and therefore away from marine erosive processes). The lack of erosion and removal of eroded rock has allowed the rock at these locations to become heavily weathered and become coated in a range of secondary mineral deposits. These sites therefore provide proxy sampling sites for inaccessible cliff face locations.

Samples were taken from nine field sites across North Yorkshire, eight from coastal locations (including both natural cliffs and disused industrial sites) and one from an inland disused mine. A list of these sites and further information about them can be found in tables 4.1a and 4.1b. Maps showing the locations of these sites can be found in figures 4.3, 4.4, 4.10, 4.23 and 4.31. All maps have been produced using the Ordinance Survey online mapping facilities.

The North Yorkshire coastline was chosen as a study area for this thesis for numerous reasons. Firstly, the project funding for this doctoral work was provided by Israeli Chemicals Limited, who own Cleveland Potash Limited and their mining operation at Boulby, Yorkshire. These companies have a specific interest in the erosive processes that impact the North Yorkshire coast, so both geomicrobiological and rock samples were taken from sites along this coastline. Based upon previous findings (Lim *et al.*, 2010), shale strata are the most rapidly eroding sections of hard rock cliffs of the coastline, so sampling focused on these lithologies. Specific sampling sites were chosen by the industrial supervisor (Mr David Pybus), based upon the degree of weathering at the rock surface and accessibility for study.

Table 4.1a¦ Sample site information including site industrial history, dates visited and references.

Site no.	Site name	Associated industry	Map	Sample use in thesis	Collection dates (mn/yr)	Reference
1	Hole Wyke adit	Boulby Alum Works	Figure 4.3	Chapters 6 and 7	01/14 (C6) and 04/14 (C7)	Morris and Whitlock, 2005.
2	Cliffs by Hole Wyke adit	N/A	Figure 4.3	Chapter 5	08/15	N/A
3	Tellgreen/Loop Wyke mines	Jet mining	Figure 4.4	Chapter 5	08/15	Pybus D., personal communication 2017; Howarth, 1962
4	Cliffs by Keldhowe Steel	N/A	Figure 4.4	Chapter 5	08/15	N/A
5	Deepgrove quarry	Mulgrave Estate Alum Works	Figure 4.4	Chapter 5	08/15	Jecock, 2009; Bax *et al*., 2015
6	Sandsend Ness quarry	Mulgrave Estate Alum Works	Figure 4.4	Chapters 5 and 7	04/14 (C7) and 08/15 (C5)	Jecock 2009; Bax *et al*., 2015
7	Gaytress quarry	Mulgrave Estate Alum Works	Figure 4.4	Chapters 5 and 8	08/15 (C5 and C8)	Jecock 2009; Bax *et al*., 2015
8	Assholm wood (inland) mines	Cement stone mining	Figure 4.5	Chapters 5 and 8	08/15 (C5 and C8), 08/16 (C8)	Pybus D., personal communication 2017
9	Cliffs at Saltwick Bay	N/A	Figure 4.6	Chapters 5 and 8	08/15 (C5 and C8)	N/A

Table 4.1b¦ Sample site information including geology, weathered surface pH measurements, sample descriptions and experimental use of collected samples.

Site	Geology	pH of weathered surface (data from chapter 5)	Collected sample description	Experimental use
Hole Wyke adit	Pyritous shale, Redcar Mudstone Formation.	N/A	Shale rock chips knocked from adit wall and large blocks of rock taken from a ceiling collapse.	Blocks crushed to powder for leaching experiments (chapter 7) and rock chips inoculated into enrichment cultures (chapter 6).
Cliffs by Hole Wyke adit	Pyritous shale, Redcar Mudstone Formation.	7.65 (cliff), 6.50 (hole in cliff)	Shale rock chips knocked from cliff surface.	Use in phenotypic plate assay (chapter 5).
Tellgreen/Loop Wyke mines	Mulgrave shale, Whitby Mudstone Formation.	8.07	Chips of shale rock and carbonate precipitate knocked from mine wall	Use in phenotypic plate assay (chapter 5).
Cliffs by Keldhowe Steel	Mulgrave shale, Whitby Mudstone Formation.	5.79	Shale rock chips knocked from cliff surface.	Use in phenotypic plate assay (chapter 5).
Deepgrove quarry	Mulgrave shale, Whitby Mudstone Formation.	7.46	Water from stream flowing through the quarry.	Use in phenotypic plate assay (chapter 5).

Table 4.1b (continued)¦ Sample site information including geology, weathered surface pH measurements, sample descriptions and experimental use of collected samples.

Site	Geology	pH of weathered surface (data from chapter 5)	Collected sample description	Experimental use
Sandsend Ness quarry	Mulgrave shale, Whitby Mudstone Formation.	2.81	Shale scree collected from slope.	Inoculated into enrichment cultures (chapter 7), leaching experiments (chapter 7) and use in phenotypic plate assay (chapter 5).
Gaytress quarry	Alum shale, Whitby Mudstone Formation.	2.59	Shale scree collected from slope.	Inoculated into enrichment cultures (chapter 8) and use in phenotypic plate assay (chapter 5).
Assholm wood (inland) mines	Alum shale, Whitby Mudstone Formation.	5.19	Shale rock chips knocked from mine wall. *In situ* mesocosms buried in the scree coating the mine floor.	Inoculated into enrichment cultures (chapter 8), *in situ* mesocosms buried in floor scree (chapter 8) and use in phenotypic plate assay (chapter 5).
Cliffs at Saltwick Bay	Mulgrave shale, Whitby Mudstone Formation.	2.59	Shale rock chips knocked from cliff surface.	Inoculated into enrichment cultures (chapter 8) and use in phenotypic plate assay (chapter 5).

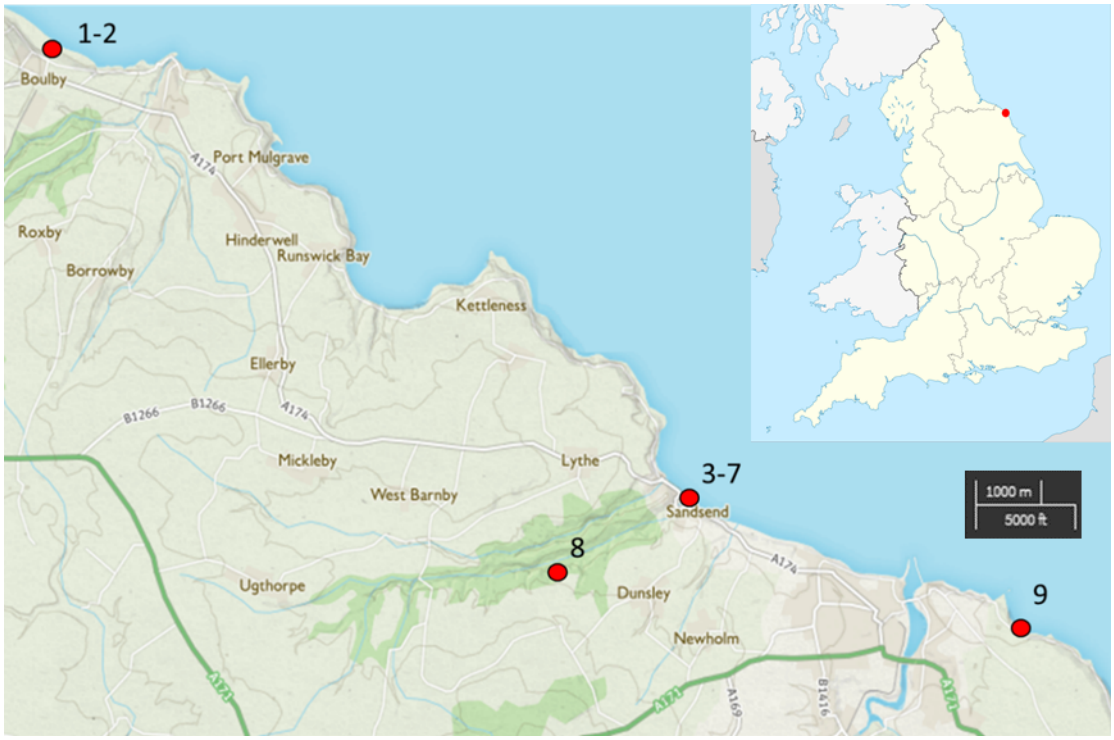

Figure 4.3¦ An overview map of the field sites sampled in North Yorkshire, see table 4.1a for site descriptions corresponding to the numbers labelled. The inset image in the top right shows a map of England, UK, with the location of the study area highlighted (red circle).

4.3.2 Hole Wyke – adit

The Boulby Alum Works operated on the cliff top by the village of Boulby, produced crystallised alum as a dye fixative for the dyeing industry. Alum shale rock was piled up into heaps and burnt, producing sulfuric acid which initiated mineral dissolution and elemental release from the rock. The burnt shale would then be steeped in water, the resultant liquor mixed with seaweed and urine before being boiled to concentrate the alum solution. Heating was continued until the alum crystallised out of the solution (Morris and Whitlock, 2005; Jecock, 2009).

A mine adit was cut down through the bedrock and then across to the cliff toe, with an artificial harbour cut into the foreshore at Hole Wyke. Ships brought coal to the Alum works for heating the boiling pans, and then subsequently took alum products to other ports in the British Isles and continental Europe (Morris and Whitlock, 2005).

The entrances to the Hole Wyke adits (Fig. 4.5) can be accessed from the foreshore west of 2km west of Staithes village and Cowbar Nab. Only one entrance is now open, the other being covered by shale eroded from higher up the cliff face (Morris and Whitlock, 2005). The adit is cut through the Redcar Mudstone Formation, specifically within the Ironstone shale unit.

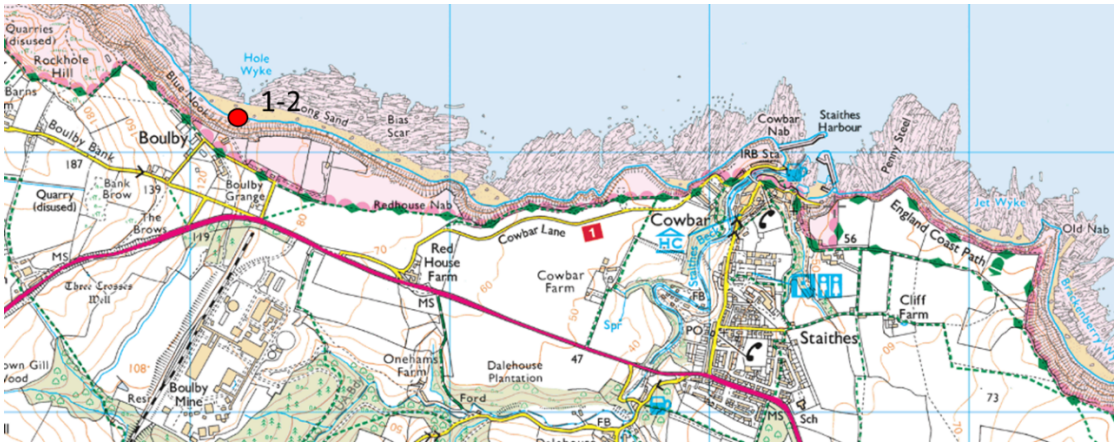

Figure 4.4¦ Sampling locations at the adit (1) and the cliff toe face on Long Sand beach (2) at Hole Wyke. 1:25,000 OS map, blue line squares are 1 km^2.

Figure 4.5¦ Cliffs at Hole Wyke, with the entrance to the Boulby alum works mine adit to the right-hand side of the image (see arrow). The entrance is roughly 1.5 m across in width.

Figure 4.6¦ Inside wall of Hole Wyke mine adit. Secondary mineral deposits (white crystals and red/brown coatings) cover the rock. The rock itself, although fractured, is largely intact and did not appear to be extensively slaked (rock chip formation). The image represents an area ~75 cm in width.

Inside the adit, secondary mineral formations were tentatively identified as fine gypsum crystals (Fig. 4.6) and ferromanganese deposits (primarily comprised of iron and manganese (hydro)oxides) (Fig. 4.7). The shale rock, although highly fractured, was not as slaked as other weathered shale environments sampled. This possibly suggests that the humidity level within the adit is relatively constant, meaning that hydration and desiccation cycling is less severe than at other locations.

Figure 4.7¦ Ferromanganese deposits (putative identification) on the ceiling of Hole Wyke mine adit. Thin crusts of iron (red/brown) and manganese (purple/black) oxides were found coating the rock. The image represents an area ~1 m in width.

Use of samples from this location in thesis: For Chapter 6, rock samples were used as inoculum for enrichment cultures in which *Variovorax paradoxus* was isolated. Rock material was also collected for crushing and use as a growth substrate. For Chapter 7, rock samples were used both as an inoculum for enrichment cultures and as a source of crushed rock for leaching experiments.

4.3.3 Hole Wyke – Cliffs

Samples were also taken from the cliff faces near to the adit entrances. These cliffs near their base are also of the Redcar Mudstone Formation, specifically from the Pyritous shale and Ironstone shale units. Cliff rock surfaces were also extensively covered in ferromanganese deposits (Fig. 4.8 and 4.9). A sterilised rock hammer was used to chip away ferromanganese coated rock samples into sterile Whirlpak© bags (samples taken from pyritous shales). White crystals were not found on the cliff rock surfaces, suggesting that the weathering environment either did not support their formation, or that any crystals formed are dissolved by either marine or meteoric waters.

Figure 4.8¦ Cliffs at Hole Wyke (upwards view). Ferromanganese deposits (putative identification) coated patches of the cliff surfaces, with areas subjected to recent erosion revealing fresh bedrock. The image represents an area ~2 m in width in the foreground.

Figure 4.9¦ Sample extraction at Hole Wyke cliffs. A sterilised rock hammer was used to chip rock coated in manganese oxides (putative identification) into a Whirlpak© bag. Scratchings made by the rock hammer can be seen in the centre of the image. The image represents an area ~50 cm in width.

Use of samples from this location in thesis: For chapter 5, collected samples were suspended in phosphate buffered saline (PBS) and suspended and plated onto phenotypic assay agar plates.

4.3.4 Tellgreen Hill – Jet Mine level

Four mine entrances are dug into the cliff face below Tellgreen Hill and by Loop Wyke (Fig. 4.11), which was mined for Jet in the 19th century with mining leases from the Mulgrave estate (Pybus, D. personal communication 2017). The mines are dug through the Jet rock unit of the Mulgrave shale member.

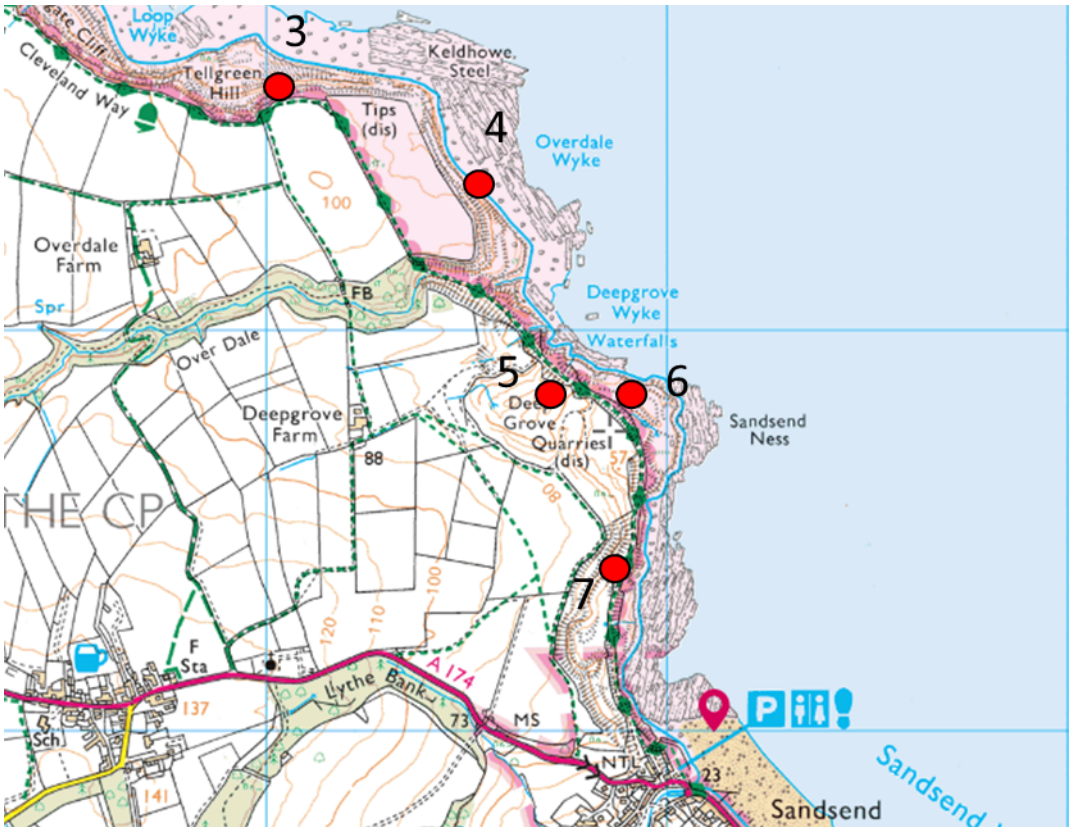

Figure 4.10¦ Sampling sites located near Sandsend. Tellgreen Hill jet mines (3) and the cliffs by Keldhowe Steel (4) are accessible from the foreshore, while Deepgrove quarry (5), Sandsend Ness quarry (6) and Gaytress quarry (7) are accessible from the Cleveland Way public footpath. 1:25,000 OS map, blue line squares are 1 km^2.

Figure 4.11¦ Entrances to Tellgreen Jet mine. The left-most entrance is ~2m in width

Inside the mines, the walls are heavy encrusted with what has been tentatively identified as carbonate speleothems, from calcite that has leached out of the Jet rock and subsequently precipitated on the mine walls (Fig. 4.12). The carbonate deposits and the shale bedrock are encrusted with ferromanganese deposits (Fig. 4.12 and 4.13).

Figure 4.12¦ Mineral deposits on the wall of Tellgreen jet mine. The white (tentatively identified as precipitated carbonates) mineral crust was roughly 1 cm thick, and formed a hard coating on the shale rock. An area where this crust has broken away can be seen to the left of the image.

.

Figure 4.13¦ Within Tellgreen jet mine. The walls are highly weathered, with extensive coatings of weathered mineral deposits. Putative mineralogy includes leached carbonates which have precipitated at the surface (white), iron (hydr)oxides (orange/red), manganese oxides (dark purple/black) and gypsum (white crystals). Right, the author collecting samples within the mine, using a sterilised rock hammer to collect manganese oxide coated samples into the Whirlpak© bag. The left image represents an area ~1 m in width.

Use of samples from this location in thesis: For chapter 5, collected samples were suspended in PBS and suspended and plated onto phenotypic assay agar plates.

4.3.5 Keldhowe Steel – Cliffs

Cliff surfaces by Keldhowe Steel, located roughly 2 km north along the foreshore from Sansend village. The stratigraphy at the cliff toe is the Jet rock unit of the Mulgrave shale member, samples of which were collected (Fig. 4.14 and 4.15). Cliff rock surfaces were thinly coated in iron (hydr)oxides and were relatively intact at the sampling site, with minimal slaking degradation or weathering deposit accumulation.

Figure 4.14¦ Cliff surface at Keldhowe Steel. Above the rock hammer the area where rock was chipped away for sample collection is visible. A thin coating of iron (hydr)oxides (putative identification) cover the rock surface.

Figure 4.15¦ Cliffs at Keldhowe Steel. Eroded rock chips from the cliff surface collect at the bottom of the cliff. These chips are largely unweathered, which suggests that the rock is eroding at a rate that limits the extent to which weathering can take place.

Use of samples from this location in thesis: For chapter 5, collected samples were suspended in PBS and suspended and plated onto phenotypic assay agar plates.

4.3.6 Deepgrove – Quarry

Deepgrove quarry was part of the Sandsend Alum Works active in the 18th century (Jecock, 2009). A deep pit was dug down through the bituminous shale unit of the Mulgrave shale member (the wall of this pit can be seen in figure 4.16) to house a steeping tank for the alum shale quarried further back into the quarry (Bax *et al.*, 2015).

Figure 4.16¦ Stream running down the quarry wall at Deepgrove. The wall is coated in iron (hydr)oxide ochreous material.

A small stream now runs down the quarry wall, with iron (hydr)oxides thickly coating the rock wall behind the stream (Fig. 4.16). The water within this stream and

the pool that collects at its base contains large amounts of ochreous material (Fig. 4.17).

Figure 4.17¦ Closer images of ochreous material at Deepgrove quarry. Both water and ochreous material deposited on the quarry wall were collected for the work in Chapter 5.

Both solid ochreous material from the stream rock wall and liquid samples from the pool at the rock wall base were collected in Whirlpak© bags or in 50 mL Falcon tubes.

Use of samples from this location in thesis: For chapter 5, collected samples were suspended in PBS and suspended and plated onto phenotypic assay agar plates.

4.3.7 Sandsend Ness – Quarry

Figure 4.18¦ An outcrop of Hard shales within the Alum shale member on the top of Sandsend Ness.

Sandsend Ness was an alum quarry supplying the Sandsend Alum Works (Jecock, 2009). An outcrop of the Hard shale unit within the Alum shale member stands on top of Sandsend Ness, with the shale rock being heavily slaked (very loose shale fragments from the rock surface) and weathered (Fig. 4.18).

Figure 4.19¦ Weathered mineral deposits and crusts on the rock outcrop on Sandsend Ness. To the left, a tentatively identified crust of gypsum crystals with interspersed iron (hydr)oxides loosely adheres to the surface of the rock. To the right, iron (hydr)oxides form a thin coating on the rock surface which is highly slaked. Both images represent an area ~20 cm across.

Thick layers of gypsum crystals (putative identification) coat the rock surface along with ferromanganese deposits (Fig. 4.19).

Figure 4.20¦ Weathered shale scree on the top of Sandsend Ness. This was collected using a sterilised trowel and scooped into Whirlpak© bags and sterile Duran bottles.

Weathered shale scree from the bituminous shale unit of the Mulgrave shale member below the alum shale member on Sandsend Ness was collected in large volumes for the simulated weathering experiment detailed in chapter 7 (Fig. 4.20).

Use of samples from this location in thesis: For Chapter 7, slaked rock chips (saprolites) were collected in sterile Whirlpak© bags (Fig. 4.20), for use as both an inoculum for enrichment cultures and as rock material for leaching experiments. For the work in chapter 5 samples were taken from a small outcrop (Fig. 4.19), for the plating out of suspended rock samples onto phenotypic assay agar plates.

4.3.8 Gaytress – Quarry

Gaytress quarry supplied the Sandsend Alum Works, being a source of the Main alum and Cement shale units within the Alum shale member (Jecock, 2009). A large body of highly weathered scree has formed a slope below the Main alum shale unit (centre of the image in Fig. 4.21).

Figure 4.21¦ Gaytres quarry, as visible from the Cleveland way public footpath. The Alum Shale Member and Peak Mudstone Members (grey rock) can be seen in the distance above the heather (Rawson and Wright, 2000). The image represents an area ~1m across in the foreground.

Figure 4.22 provides an indication of the depth that this slope has formed. Weathered scree material was collected using a trowel into a sterile Whirlpak© bag.

Figure 4.22¦ Alum Shale scree at Gaytres quarry. A trowel has been used to dig down roughly 15-30 cm into the scree. Roots from surrounding vegetation extended into the scree.

Use of samples from this location in thesis: For chapter 5, collected samples were suspended in PBS and suspended and plated onto phenotypic assay agar plates. For Chapter 8, collected rock samples were used as an inoculum for enrichment cultures.

4.3.9 Assholm – Mine level

Calcareous concretions (cement stones) within the Cement shale unit of the Alum shale member were mined and used for making hydraulic cement in North Yorkshire between 1860 and 1935 (Howarth, 1962). Mines within Mulgrave Woods at a location called Assholm (Fig. 4.24) are known to be a relic of this cement stone mining industry (Pybus, D. personal communication 2017).

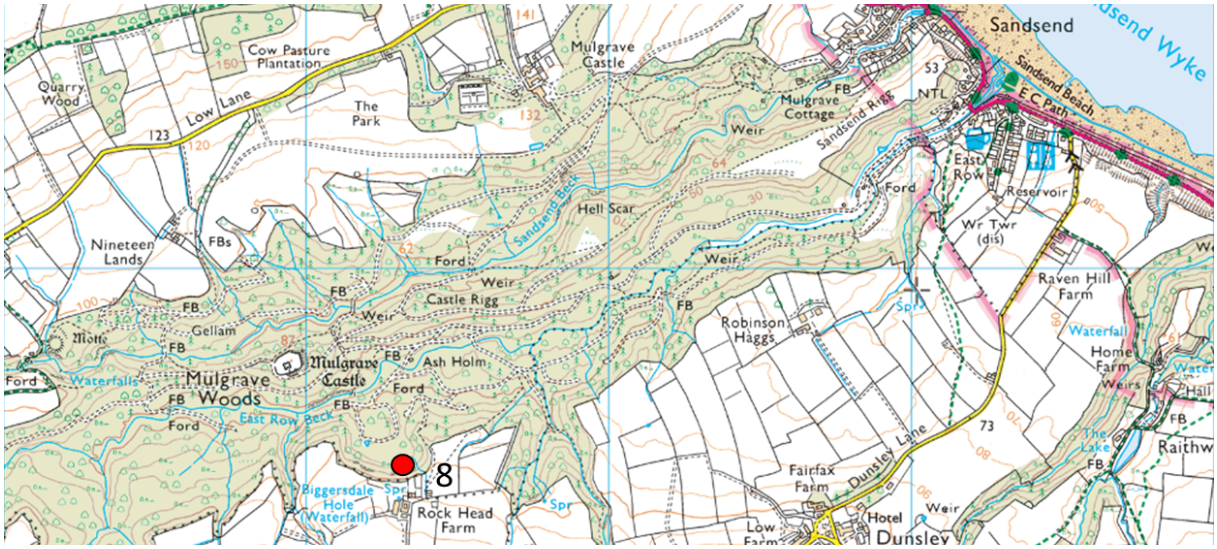

Figure 4.23¦ The location of Assholm mine network (8) within Mulgrave woods South-West of Sandsend. 1:25,000 OS map, blue line squares are 1 km^2.

Figure 4.24¦ Entrance to one of the Assholm mine levels. Vegetation surrounds the entrance and grows within the first few metres of the level.

The inside of the mine is heavily coated in secondary mineral deposits and crusts, including ferromanganese deposits and extensive deposits of white crystals (Fig. 4.25-4.29). These crystals are larger than crystals found at other weathered shale

locations, indicating that crystal formation has been supported for a longer, undisturbed period of time.

Figure 4.25¦ Inside of Assholm mine level. The walls were completely coated in weathered mineral deposits including (putative identification) iron (hydr)oxides (red/orange), manganese oxides (purple/black), jarosite (yellow) and gypsum (white crystals). The image represents an area ~ 1 m in width.

Figure 4.26¦ A close up image of black/purple weathered deposits (tentatively identified as manganese oxides) within Assholm mine level. The deposit resides of the surface of the rock, possibly on top of the surrounding red/orange coloured crust. Although mainly black in colour, a distinctive purple hue can be seen under the right lighting conditions. The image represents an area ~ 15 cm in width.

Figure 4.27¦ Close up image of white crystals (tentatively identified as gypsum), displaying extensive crystal growth (crystals ~2-5mm in length). The image represents an area ~ 5 cm in width.

Figure 4.28¦ White crystal deposits extensively coated some areas of the mine level, often on top of other weathered mineral deposits that coated the underlying shale. The image represents an area ~ 1m in width.

Due to the stable environment that the mine provides, with no removal of eroded shale fragments (that have accumulated to form the mine floor), a location within the mine was chosen to bury mineral mesocosms (Chapter 8).

Figure 4.29¦ Further close up images of a thick layer (~5mm) of white crystals that is peeling away from the rock surface, revealing that the crystal layer is on top of the iron (hydr)oxide crust (putative identification) on the rock surface. These iron (hydr)oxides can be seen to also coat the under-surface of the white crystal layer. The image represents an area ~10 cm across in width.

Figure 4.30¦ Burial site of the field microcosm mineral samples (Chapter 8). Brown Nalgene© 8 mL bottles can be seen in the centre of the image (red circle), which have been excavated using a sterilised rock hammer (right). The bottles were buried several centimetres below the surface of the shale scree forming the floor of the mine level. The wall behind the scree is wet (glistening rock, centre) due to a seep further up that flowed down into the scree below, where the bottles were buried.

The burial location of the mesocosms was near a seep in the mine wall, allowing water to flow through the scree below and through the mescososm bottles. This was intended to encourage microbial colonization of mineral surfaces within the mescososms over the one year burial period (Fig. 4.30).

Use of samples from this location in thesis: For chapter 5, collected samples were suspended in PBS and suspended and plated onto phenotypic assay agar plates. For the work in Chapter 8, rock samples were collected and used for enrichment culturing, and mineral samples were buried in the floor scree (Fig. 4.30).

4.3.10 Saltwick Bay – Cliffs

Figure 4.31¦ The location of Saltwick Bay (9) sampling site at the cliffs roughly ½ km West of Black Nab.

The cliffs at Saltwick Bay provide some of the most extensive exposure of the Whitby Mudstone Formation, with both the Mulgrave and Alum shale members being accessible from the cliff toe (Fig. 4.32 and 4.33). Samples were taken from the bituminous shale and main alum shale units using a sterilised rock hammer/trowel and Whirlpak © bags.

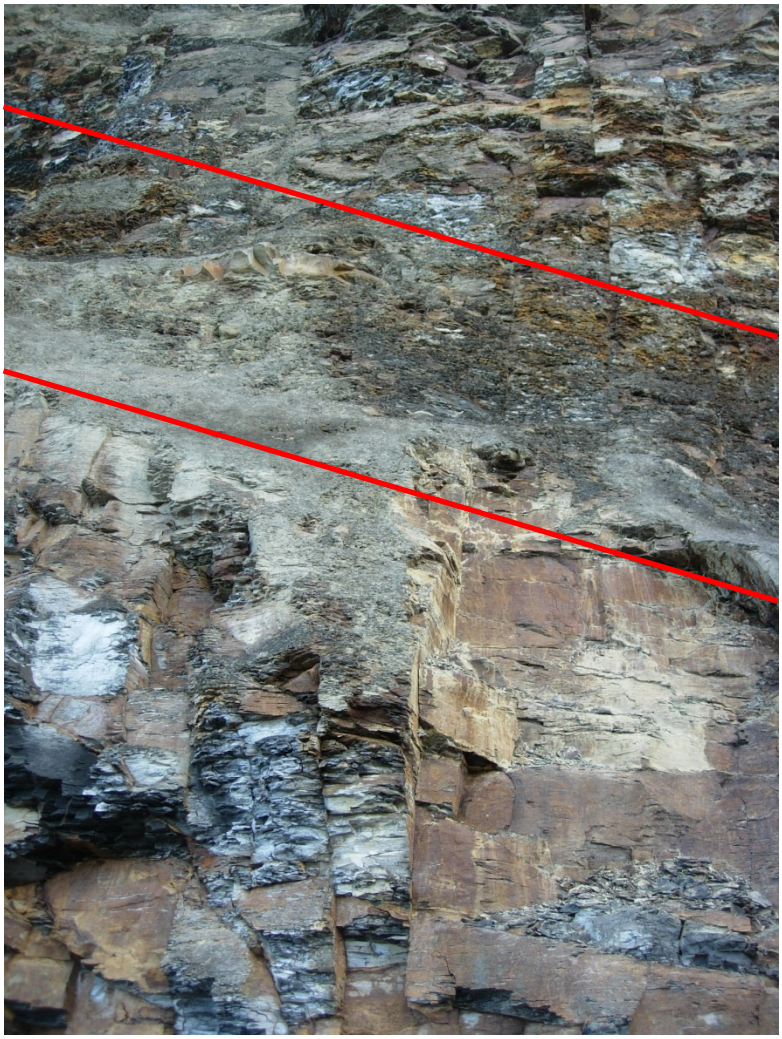

Figure 4.32¦ Cliffs at Saltwick Bay. The degree of weathering is noticeably different along the vertical cliff profile, corresponding to the different strata present. The Mulgrave shale member (Jet shale and Bituminous shale units) forms the bottom stratum in this image, the rock of a blocky morphology which is highly fractured, coated with white, yellow and red/orange weathered mineral crusts. The stratum above this is the Alum shales member, highly weathered and broken down from slaking into a scree slope. The top stratum above this is the Peak mudstone member, with a similar geomorphology to the Jet rock formation (Powell, 1984; Rawson and Wright, 2000). Red lines roughly denote strata boundaries. The image represents an area ~3 m across in the foreground.

Figure 4.33¦ Closer images of the cliff surface of the Jet Rock Formation at Saltwick Bay. Weathered mineral deposits coat the rock extensively, likely formed from a variety of different minerals. Based on the colouring of the deposits and the known mineralogy of the shale, minerals such as jarosite (yellow) and iron (hydr)oxides (orange/red/brown) are believed to be present.

Use of samples from this location in thesis: For chapter 5, collected samples were suspended in PBS and suspended and plated onto phenotypic assay agar plates. For Chapter 8, collected rock samples were used as an inoculum for enrichment cultures.

Chapter 5 - Isolation of rock weathering bacteria from shale ferromanganese deposits

5.1 Introduction

5.1.1. Background

Microbes are abundant in almost every environment on Earth, in terms of both species diversity and total population. Rocky environments are no exception, with a vast multitude of microbial species having specialised rock-specific adaptations to utilise limited resources (Gorbushina, 2007). The conditions within rocky habitats pose challenges to microbes, including toxicity from heavy metals and physical stresses such as desiccation. However, rocks also provide a rich habitat for life to survive and grow. Minerals can be used for redox reactions that can power microbial metabolisms, such as iron within pyrite. Other minerals can act as sources of nutrients to support growth, such as the phosphorus contained within apatite (Uroz *et al*., 2009).

In order to access energy and nutrients, or to cope with stressors, microbes often alter their geochemical and physical environment. Processes that microbes use to alter their rocky habitat can be collectively termed rock weathering (Gorbushina, 2007; Ehrlich *et al.,* 2015). However, not all microorganisms that live within rocky environments are able to alter that environment. Numerous studies have isolated microbial strains from weathering environments, and found that only a subset of these culturable microbes have rock weathering capabilities (Palmer *et al.,* 1991; Farbiszewska-kiczma and Farbiszewska, 2005; Cockell *et al.,* 2009; Matlakowska and Sklodowska, 2009; Frey *et al.,* 2010). Quantifying the distribution and abundance of weathering-capable organisms across environments is therefore vital to understand the relative contribution microbial activity can have in rock weathering processes.

In this chapter, data covering the abundance and distribution in shale ferromanganese deposits of the following five weathering mechanisms is presented:

- Iron oxidation
- Manganese oxidation
- Acid production
- Siderophore production
- Phosphatase production

Ferromanganese deposits (also called crusts or coatings) are weathered mineral products that can coat the surface of a weathering rock body (Post, 1999; Carmichael *et al.,* 2013). Primarily comprised of iron and manganese oxides minerals such as goethite (α-FeO(OH)), lithiophorite ($(Al,Li)Mn^{4+}O_2(OH)_2$) and todorokite ($(Mn,Ca,Mg)Mn^{4+}{}_3O_7 \bullet H_2O$), they can also contain aluminium hydroxides, clay and phosphate minerals (Northup *et al*., 2003). These minerals complex with and accumulate trace metals (e.g. As, Ba, Ni and Zn) to several orders of magnitude in concentration above the crustal average concentration (Manceau *et al*., 2007). Studies of weathered shale profiles have documented the coating of weathered shale with ferromanganese deposits, often in conjunction with efflorescent salt crusts (Joeckel *et al*., 2005; Tuttle and Breit 2009; Cockell *et al*., 2011).

The activity of rock weathering microbes within ferromanganese deposits has been indicated in several studies (Northup *et al*., 2000; Northup *et al*., 2003; Spilde *et al*., 2005; Carmichael *et al*., 2013). Iron and manganese oxidizing microbes such as *Leptothrix* sp. and *Pedomicrobium manganicum* are found abundantly within these environments (Carmichael *et al*., 2013; Northup *et al*., 2003). These microbes form part of diverse microbial communities with members associated with a range of rock weathering activities including organic acid production (e.g. *Lactobacilli*) and siderophore production (e.g. *Pseudomonas*) (Northup *et al*., 2003).

In this chapter, the abundance and distribution of microbial strains with rock weathering capabilities in shale ferromanganese deposits has been investigated.

Microbial sulfur oxidation, although an important rock weathering process in shale (Joeckel *et al*., 2005; Li *et al*., 2014), will not be covered in this work. This is due to the lack of developed agar plate assays for the detection of sulfur oxidisers. Although sulfur oxidizing bacteria can be grown on agar (Vupputuri *et al*., 2015), there is not a visual test that allows for the positive identification of sulfur oxidizing microbes.

A detailed overview of microbial shale weathering mechanisms has been presented in Chapter 2. Therefore, in the following sections only information specifically referring to the phenotypes tested in this work is included.

5.1.2. Iron and manganese oxidisers

Iron and manganese are common constituents of shale, and in most cases are the most abundant heavy metals present within the rock (Coveney *et al*., 1987; Gad *et al*., 1968). The oxidation of both metals can be actively or passively facilitated by microbial activity and growth (Gadd, 2010). Minerals that are comprised of reduced metals such as pyrite (FeS_2) and rhodochrosite ($MnCO_3$) found in shale can be dissolved by biogeochemical or geochemical processes (Matlakowska *et al*., 2012). This liberates the metal from the mineral, making it available for microbial oxidation (Tuttle and Breit, 2009; Tuttle *et al*., 2009). Within shale, ferrous iron (II) is oxidised to ferric iron (III) forming minerals such as lepidochrocite (γ-FeO(OH)) or jarosite ($KFe_3(SO_4)_2(OH)_6$). Reduced manganese (II) can become oxidised to either (III) or (IV) oxidative states, forming manganese oxide minerals such as birnessite ($(Na_{0.3}Ca_{0.1}K_{0.1})(Mn^{4+},Mn^{3+})_2O_4 \bullet 1.5\ H_2O$) (Grote and Krumbein, 1992; Ghiorse, 1984).

The oxidation of iron and manganese, and the formation of their oxide minerals, has multiple effects on the rock they reside in. Highly crystalline primary minerals (e.g. pyrite) that are dissolved are replaced with secondary minerals (e.g. ferrihydrite) that are poorly crystalline. This effect, in combination with the volumetric expansion associated with secondary mineral formation in pyrite oxidation (Pye and Miller, 1990) weathers the rock and introduces structural weakness (Anderson, 2008). In the case of metal sulfides such as pyrite, the dissolution of the mineral also liberates sulfur which can become oxidised to sulfuric acid. Acid-driven dissolution of

minerals, such as calcite and feldspars within shale, also contributes to overall rock weathering processes (Tasa *et al.,* 1997; Li *et al.,* 2014).

Manganese oxidizing organisms have been previously identified in ferromanganese deposits within carbonate caves systems (Northup *et al*., 2000; Carmichael *et al*., 2013). At Carlsbad Cavern (Guadalupe), the well-known manganese oxidizing species *Leptothrix* sp. and *Pedomicrobium manganicum* were isolated (Northup *et al.,* 2000). Additional species that have been indicated in manganese oxididation and were isolated from this site included *Variovorax paradoxus* (Northup *et al*., 2000), *Stenotrophomonas* sp. (Northup *et al.,* 2003), *Bacillus* sp. and *Alcaligenes* sp. (Spilde *et al.,* 2005). Carmichael *et al.* (2013) isolated a range of manganese oxidizing bacteria from ferromanganese deposits in Appalachian cave systems, including *Pseudomonas* sp., *Leptothrix* sp., *Flavobacterium* sp., *Arthrobacter* sp., *Acinetobacter* sp. and *Janthinobacterium* sp. (Carmichael *et al.,* 2013).

Known iron oxidisers isolated from ferromanganese deposits in the above studies include *Leptothrix* sp., *Pedomicrobium* sp., *Leptospirillum ferrooxidans* and *Alcaligenes* sp. *Acidiferrobacter thiooxydans* was the only known iron oxidizing organism identified within the iron oxide crusts coating weathered shale in Hole Wyke mine adit (Chapter 4; Cockell *et al.,* 2011). It is worth noting that several species can perform redox reactions with more than one element, such as *Leptothrix sp.* which can oxidise both iron and managanese (Ghiorse, 1984).

5.1.3. Organic acid and siderophore producers

The production of organic acids has a dual effect on rock weathering. Firstly, it can act as a source of protons and directly reduce pH that enhances mineral dissolution. Secondly, organic acids can also act as cationic ligands, complexing with metals and enabling their release from the crystal structure of minerals. The relative contributions of these two effects are not necessarily equal, with some studies suggesting that the role of organic acids as acids (Anjum *et al.,* 2010) has a greater impact on rock dissolution, with the opposite being found in other studies (Palmer *et al*., 1991; Frey *et al.,* 2010). A well-known example of microbial acid weathering in a geomicrobiological environment is within the mouth, where bacteria such as

Streptococcus and *Lactobacillus* acidify their environment and enhance the dissolution of hydroxylapatite, releasing calcium and phosphorus from tooth enamel and causing dental caries (Uroz *et al.,* 2009). The acid production of fungi in association with algae in lichens is another notable example of microbial rock and mineral weathering (Banfield *et al.,* 1999). Microbial organic acid production has been indicated as an important driver of shale weathering. Production of organic acids by the fungi *Aspergillus niger* (Anjum *et al.,* 2010) and *Penicillium notatum* (Anjum *et al*., 2009), and by the bacterial genera *Pseudomonas*, *Bacillus*, *Microbacterium* and *Acinetobacter* (Włodarczyk *et al.,* 2015) contributed to increased leaching of numerous metals from black shale.

Another type of metal binding ligand produced by microbes are siderophores, a group of low molecular weight compounds that chelate with high affinity to ferric iron. Siderophores also bind less specifically to a range of other metal cations including Cu^{2+}, Ni^{2+}, Zn^{2+}, Mn^{3+}, Co^{3+} and Al^{3+} (Ahmed and Holmström, 2014). These effects are used by bacteria and fungi in two ways; firstly to increase the bioavailability of metals for cellular uptake, and secondly to reduce its mobility in the environment and so reduce its toxic effects (e.g. As). When triggered by iron limitation or heavy metal toxicity response, cells release siderophores extracellularly allowing them to chelate available metal ions. In the case of iron limitation in bacteria, receptors on the cell wall bind to the siderophore complex and transport it into the periplasm, and subsequently into the cytoplasm through ABC transporters. Over 500 different biologically produced siderophores have been identified, which can be separated into multiple structural groups (Hider and Kong, 2009). Microbial siderophore production has been implicated as an important mechanism in black shale weathering, enhancing the release of numerous metals including As (Matlakowska *et al.,* 2008), Co, Cu and Ni (Włodarczyk *et al*., 2015), Cu (Rajpert *et al*., 2013), Fe (Matlakowska and Sklodowska, 2009) and U (Kalinowski *et al.,* 2006).

5.1.4. Phosphatase producers

Phosphate is often a limiting nutrient for microbial populations in the environment (Bryce *et al.,* 2016) and as such is one of the best studied microbial weathering mechanisms, particularly in relation to microbes increasing phosphate availability to

plants within the rhizosphere (Uroz *et al.,* 2009). Although specific microbial species will weather minerals or whole rocks for elements to use for specific purposes (such as the liberation of Fe^{2+} for iron oxidation), all microbes require phosphorus for synthesizing nucleic acids. The rock bound sources of phosphorus include minerals that have phosphate inclusions (not part of the mineral matrix) such as potassium feldspars (e.g. albite) and also minerals with phosphorus directly incorporated into the mineral matrix (e.g. apatite) (London, 1992). In the case of shale and mudstones, phosphorus can also be bound to organic material predominantly in the form of P-esters (Kolowith and Berner, 2002).

Phosphorus can be solubilised by microbes via numerous mechanisms, including the production of extracellular phosphatases (Hirsch *et al.,* 1995) and the production of gluconic acid (Haameda *et al.,* 2006). Bacterial strains of *Bacillus*, *Pseudomonas* and *Microbacterium* isolated from black shale waste at Lubin copper mine, Poland, demonstrated alkaline phosphatase and naphthol phosphohydrolase activity (Matlakowska and Sklowdowska,2009). Furthermore, the activity of these organisms enhanced the release of phosphorus from a medium containing crushed black shale (Matlakowska *et al.,* 2012). Other studies have shown that microbial activity can have significant impact on the weathering of shale organic material (Petsch *et al.,* 2001a; Petsch *et al.,* 2005; Farbiszewska-Kiczma and Farbiszewska, 2005; Matlakowska *et al.,* 2010a) which could also contribute to the release of phosphorus.

5.1.5 Knowledge gap

The importance of mechanisms in microbial shale weathering has been well established *in vitro*, but with the exception of iron oxidation, the abundance of organisms with these weathering capabilities *in situ* has not been investigated. Studies such as Li *et al.* (2014) and Cockell *et al.* (2011) have used culture independent approaches to characterise microbial shale weathering communities. Li *et al*. (2014) demonstrated that pH, Fe and S were important factors controlling microbial community composition within a black shale weathering profile. Dominant phyla included *Proteobacteria, Actinobacteria and Firmcutes,* with the bacterial genera *Acidithiobacillus*, *Sulfobacillus*, *Thiobacillus*, *Ferrimicrobium* and *Ferrithrix* presented as potential active iron and sulfur oxidisers (Li *et al.*, 2014). In contrast,

Cockell *et al*. (2011) identified only one species (*Acidiferrobacter thiooxydans)* previously associated with microbial iron oxidation (Hallberg *et al*., 2011), but highlighted the presence of numerous bacterial and archaeal genera known to be active in nitrogen cycling, heterotrophy and methanotrophy (Cockell *et al*., 2011). These studies demonstrate the heterogeneity of microbial community composition in analogous environments. Importantly, these studies do not directly identify microbial weathering phenotypes in the organisms and metabolisms highlighted.

This chapter asks the following central questions:

- What is the abundance of microbial isolates with differing rock weathering capabilities in samples of weathered shale?
- Are different rock weathering phenotypes found ubiquitously across shale weathering sites? If not, do particular phenotypes co-associate?
- Which microbial taxa have rock weathering potential within the weathered shale environments sampled?

To address these questions, phenotypic plate assays and subsequent sequencing has been used to isolate microbial strains with rock weathering capabilities. Further analysis has determined the pattern of their distribution across shale weathering environments. Geochemical analysis (SEM-EDS and Raman spectroscopy) have been used to further analyse colonies of putative iron and manganese oxidisers.

5.2 Methodology

5.2.1. Rock sample collection and pH measurements

Samples were collected from the following field sites described in Chapter 4: Saltwick Bay cliffs (A), Keldhowe Steel cliffs (B), Hole Wyke cliffs (two sites, C and D), Assholm cement stone mine wall (E), Tellgreen Hill jet mine wall (F), Deepgrove quarry ochreous stream (G), Sandsend Ness quarry rock chips (H) and Gaytress quarry scree (I). The lettering of these site names will be used throughout

this chapter. Numerous samples were taken from each site (2-5 samples per site) with a total of 25 samples taken from across all sites. The exact number of samples taken from each site is as follows: A (3), B (2), C (3), D (2), E (5), F (4), G (2), H (2) and I (2).

Sample collection was carried using the following protocol. A ethanol and flame sterilised rock hammer or garden trowel was used to knock/scrap chips of rock from the cliff face, mine wall or scree slope and placed into Sterilin (20 mL) screw top tubes which were fully sealed. These were then kept at ambient temperature until return to the laboratory where they stored at 4^{o} C until use.

pH measurements of ferromanganese crusts on the weathered shale rock samples were obtained using the following method. Crusts were scraped from the rock surface using a scalpel until 50 mg of material had been collected. Scrapings were suspended in 2 mL of Milli-Q filtered water and allowed to equilibrate for 30 minutes. Triplicate pH measurements were taken of single suspensions using a Jenway 3510 advanced bench pH meter. Measurements were automatically compensated for temperature (25 ^{o}C).

5.2.2 Phenotypic plate assays – Media

The following media types were prepared to make agar plates. All chemicals were obtained from Sigma-Aldrich unless otherwise specified. The black shale rock powder was obtained by collection and subsequent crushing of (<0.5 mm size fractionated) slabs of black shale from the bituminous shale strata at Saltwick Bay. Addition of rock powder to media to stimulate the growth of rock weathering organisms was demonstrated in Puente *et al.* (2004). Defined mediums often lack all of the required nutrients required to support the growth of environmental isolates, so the addition of rock powder can help to culture those strains that will not grow in standard laboratory medium. All media recipes below are for 1 L preparations made with Milli-Q UV- purified and filtered (0.22 µm) water, and autoclaved at 121^{o} C for 20 minutes unless otherwise specified. The bracketed description after each media name indicates the microbial metabolism/phenotype targeted on that media type.

Nutrient agar (neutrotolerant heterotrophs): Used primarily to culture neutrotolerant heterotrophs. Ingredients: 28 g nutrient agar powder, 2 g of black shale rock powder were mixed in 1 L of water and sterilised.

Acidotolerant nutrient agar (acidotolerant heterotrophs): Used to culture acidotolerant heterotrophs. Ingredients: 28 g of nutrient broth powder and 2 g of black shale rock powder were mixed in 750 mL of water which was then adjusted to pH 3 with sulfuric acid. This solution was autoclaved. Seven grams of agarose was mixed in 1 L of water and stirred for 30 minutes to allow agarose hydration. The agarose was then allowed to settle, and 750 mL of the water removed. The remaining 250 mL containing the hydrated agarose was then autoclaved. After autoclaving, the two molten agar solutions were mixed under sterile conditions. This medium was adapted from a recipe within Johnson (1995).

Milk agar (acid production): Used to test for microbial isolates that can produce organic or inorganic acids. Produced acid disrupts the colloids within the milk powder and causes a clear halo to appear around the colony. Ingredients: 15 g agar, 5 g dried skimmed milk powder (Sainsbury's Supermarket, UK) and 2 g of black shale rock powder were mixed in 1 L of water. This solution was autoclaved. Adapted from Frazier and Rupp (1928) and Grube *et al.* (2009).

Chrome Azurol S (CAS) blue agar (siderophore production): Used to test for microbial isolates that produce siderophores. Secreted siderophores surrounding a colony displace iron (III) chloride from CAS turning the agar from blue to orange, producing an orange halo around the colony. The following solutions were prepared A) 0.324 g $FeCl_3 \bullet 6H_2O$ is mixed in a 100 mL aqueous solution of 0.01 M HCl, B) 60.5 mg of CAS powder in 50 mL of water and C) 72.9 mg of hexadecyltrimethylammonium bromide (HDTMA) in 40 mL of water. Ten millilitres of solution A was mixed with all of solution B, which was then mixed with solution C. This final solution was autoclaved.

Two hundred millilitres of 5x M9 salts (34 g Na_2HPO_4, 15 g KH_2PO_4, 2.5 g NaCl and 5.0 g NH_4CL in 1 L water - autoclaved), 15 g agar, 30.25 g piperazine-N,N-bis(2-ethanesulfonic acid) (PIPES) and 2 g of black shale rock powder were mixed in 650 mL of water and adjusted to pH 6.8 with NaOH. This solution was autoclaved.

After autoclaving, the solution was cooled to 50 ^{o}C in a water bath before being added to the CAS solution (above) with thorough stirring under sterile conditions. Adapted from Schwyn and Neilands (1987) and Rossbach *et al.* (2000).

Phenolphthalein phosphate agar (PPA) (phosphatase production): Used to test for the production of phosphatase producers. Phosphatases secreted into the agar liberate the phenolphthalein from the phosphate, and following the addition of an alkali phenolphthalein turns pink, producing pink colonies for those microbes positive for phosphatase production. Ingredients: 15 g of PPA and 2 g of black shale rock powder was mixed in 1 L of water before autoclaving. This protocol was adapted from Hirsch *et al.* (1995). Note that agar is present within the PPA powder purchased from Sigma Aldrich.

Manganese oxidizing agar (manganese oxidisers): Used to test for the oxidation of reduced (II) manganese. Microbial colonies that oxidise the reduced manganese (manganese sulfate) produce manganese oxide products, which alters the Leucoberberlin blue (LBB) dye from light blue to dark blue. Ingredients: 2 g Peptone, 0.5 g yeast extract, 1 mg $FeSO_4 \bullet 7H_2O$, 150 mg $MnSO_4 \bullet H_2O$, 2.38 g of 4-(2-hydroxyethyl)-1-piperazineethanesulfonic acid (HEPES), 8 mg LBB and 15 g agar were added to 1 L and adjusted to pH 7.4 using NaOH/HCl. Adapted from Cerrato *et al.* (2010) and Krumbein and Altmann (1973).

Washed Agarose - Yeast Extract (WAYE) agar (iron oxidisers): Used to test for the oxidation of reduced (II) iron. Microbial colonies that can oxidise the reduced iron (ferrous sulfate) will produce ferric hydroxide or oxide products, which are visibly an orange/rust colour. A basal salts solution (1 L - autoclaved) was prepared by the addition of 0.5 g $MgSO_4 \cdot .7H_2O$, 1.5 g $(NH4)_2SO_4$, 1 g KCl and 0.1 g of $Ca(NO_3)_2 \bullet 4H_2O$. Solution A) 100 mL of basal solution is added to 650 mL of water, with 0.2 g of yeast extract powder and 2 g of black shale rock powder added. This solution is then adjusted to pH 3 with sulfuric acid before autoclaving. Solution B) 7 g agarose was mixed in 1 L of water and stirred for 30 minutes to allow agarose hydration. The agarose was then allowed to settle, and 750 mL of the water removed. The remaining 250 mL containing the hydrated agarose is then autoclaved. Solution C) 800 mM $FeSO_4.7H_2O$, adjusted to pH 3 with sulfuric acid before filter

sterilization (0.22 μm filter) was prepared. When hot, solutions A and B are mixed (ensuring agar is fully molten) along with 5 mL of solution C under sterile conditions. Adapted from Johnson *et al.* (1995) and Joe *et al.* (2007).

5.2.3 Phenotype plate assays – procedure

One gram aliquots of field samples were suspended in 5 mL of 1x PBS (8 g NaCl, 0.2 g KCl, 1.44 g Na_2HPO_4 and 0.24 g KH_2PO_4, 1 L water - adjusted to pH 7 with HCl) in 50 mL Falcon tubes and hand inverted for 5 minutes to ensure thorough mixing. Suspensions were then serially diluted in phosphate buffered saline (PBS) and plated out onto each of the seven agar types in triplicate. This created a total of 75 plates (triplicate plates for 25 samples) for each of the agar types. Plates were wrapped in parafilm to prevent the plates from drying out and then incubated at room temperature (~23 ^{o}C) for one month.

After incubation, the plates were opened and the number of positive colonies recorded. Values were calculated for the number of colony forming units (with the assumption that one cell grows to one colony) per gram of rock sample (CFU/g). Example descriptions and images of positive colonies for each agar type are shown below.

Nutrient agar: All colonies were counted as neutrotolerant heterotrophs.

Acidotolerant nutrient agar: All colonies were counted as acidotolerant heterotrophs.

Milk agar: All colonies with a clear halo surrounding the colony edge were counted as positive for acid production. Organic acids mediate a drop in pH within the agar, destabilising the milk colloids which eliminates the opaqueness of the agar in that region (Fig. 5.1).

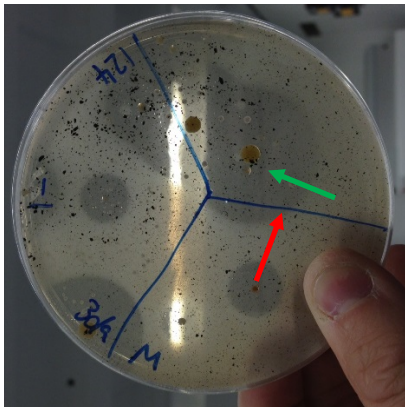

Figure 5.1¦ Positive test results on milk agar. Clear halos (red arrow indicates halo edge) surround colonies (green arrow) that have produced acid. The size of these halos varies between colonies, indicating that the level of acid production varies between colony type and size.

CAS blue agar: All colonies with an orange halo (secreted siderophores have displaced ferric iron from the CAS/HDTMA complex, causing the ferric iron to be visible) surrounding the colony edge were counted as positive for siderophore production (Fig. 5.2).

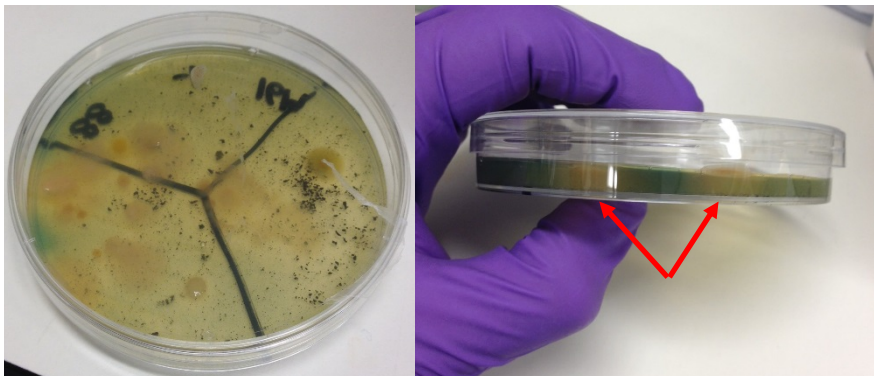

Figure 5.2¦ Positive test results on CAS blue agar. Orange halos surround colonies that have produced siderophores. The left image shows that produced siderophores scavenged iron from most of the agar. The difference between unaltered agar (blue/green) and agar with secreted siderophores (orange) can be more easily recognised when the plate is seen side on (right image – red arrows indicate areas of iron scavenged orange agar).

PPA: After incubation, several drops of NH_4OH were placed inside the lid of the inverted agar plates, allowing evaporative gas from the fluid to reach the agar.

Colonies that turned pink were positive for alkaline phosphatase production. Under alkaline conditions, phenolphthalein dye is colourless when bound to phosphate, but turns pink when the phosphorus is liberated.

Manganese oxidizing agar: Colonies that were dark blue were counted as positive for manganese oxidation. LBB dye changes colour from light blue to deep, dark blue when it reacts with manganese (III, IV) oxides. No distinction could be made between active metabolism (direct) and passive (indirect) manganese oxidation (Fig. 5.3).

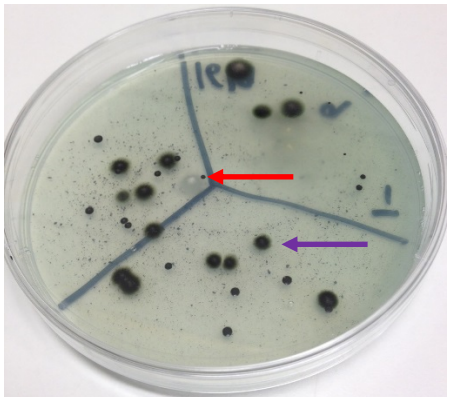

Figure 5.3¦ Dark blue colonies positive for manganese oxide production on manganese oxidizing agar (purple arrow). Notice white colonies near the centre of the plate that were negative for this test (red arrow).

WAYE agar: Colonies that were distinctly rust coloured were counted as positive for iron oxidation. Iron oxides/hydroxides are visibly rust coloured when produced within the agar, so iron oxidizing colonies acquired this colour if actively oxidizing iron. No distinction could be made between active metabolism (direct) and passive (indirect) iron oxidation (Fig. 5.4).

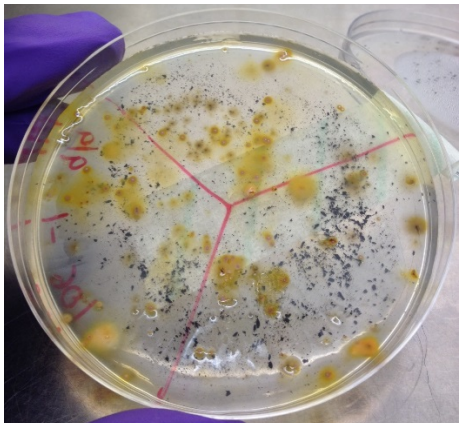

Figure 5.4¦ Rust coloured colonies positive for iron oxide production on WAYE agar.

5.2.4. Phylogenetic identification of isolates

Numerous colonies from the phenotypic assay agar plates were picked for phylogenetic identification. This was carried out through a colony PCR (cPCR) step which amplified the 16S rDNA region of the isolates genome, followed by the amplicons being sequenced (Sanger).

Individual colonies were picked and suspended in 50 µL of molecular grade water. One microlitre of this solution was used as the DNA template for the PCR reaction. Each 25 µL reaction included a 12.5 µL PCR Mastermix, 1 µL of both the forward and reverse primer solutions and 10.5 µL of molecular grade water. PCR Mastermix (New England Biolabs) contained *Taq.* DNA Polymerase, deoxynucleoside triphosphates (200 µM) and buffer ($MgCl_2$ – 1.5 mM). Primer concentration was 0.4 µM in the final PCR reaction volume.

The forward primer used was 27F (5'-AGAGTTTGATCCTGGCTCAG-3') and the reverse primer used was 1389R (5'-ACGGGCGGTGTGTACAAG-3'). The PCR procedure started with a 10 minute denaturation step at 96° C for 10 minutes, followed by 30 cycles of denaturation at 95° C for 1 minute, annealing at 60° C for 1 minute and extension at 72° C for 1 minute, with a final step of extension at 72° C for 10 minutes. A negative control lacking added DNA template was also carried out to rule out false positive results from reagent contamination.

PCR products were analysed using gel electrophoresis. Five microlitre of amplicon was mixed with 5 µL of 10x loading buffer, and loaded into wells of a 0.8 % TAE agarose gel submerged in TAE solution within an electrophoresis tank. The gel contained a 10,000 fold dilution of SYBR Green for DNA staining. Gels were run for 45-60 minutes at 100 mV before removal and imaging using ultraviolet transillumination (Syngene G-Box, Syngene, Cambridge, UK). All gels were run with a 1 kb ladder (New England Biolabs) to assess the size of the amplified product to confirm it as the 16S rDNA gene.

Successfully amplified products were then processed using a DNA purification kit (Qiagen) according to the manufacturer's instructions. DNA concentration was assessed through the use of a NanoDrop instrument (Thermofisher).

Purified DNA was then added to a total volume of 6 µL containing 25-40 ng of DNA. Separate preparations were made with the forward and reverse primers (same as used in the PCR reaction), each preparation containing template DNA, 1.3 µM primer and molecular grade water. These preparations were then sent to Edinburgh Genomics for Sanger sequencing and subsequent read processing.

For more information on Sanger sequencing, see Chapter 3.

Colony PCR was unsuccessful for iron and manganese oxidizing colonies. DNA extraction using a Qiagen DNA extraction kit was successful for some of the chosen colonies. The 16S rDNA was then successfully amplified from the extracted DNA, using the same PCR protocol as used in the colony PCR. However, the PCR products were not successfully sequenced. As a result, no phylogenetic data is available for any of the chosen iron or manganese oxidizing colonies.

5.2.5. Colony analysis via SEM-EDS

SEM-EDS (Chapter 3) was used to visualise colonies for biosignatures of microbial iron oxidation, and to determine elemental concentration of colony material. Iron and manganese oxidizing microbial colonies were embedded within the agar, so "scoops" of agar containing one colony was taken and air dried on a glass microscope slide.

Samples were gold coated and imaged in a Carl Zeiss SIGMA HD VP Field emission SEM with Oxford AZtec EDS System, with an accelerating voltage of 20 kV. For further information on SEM-EDS, see Chapter 3.

5.2.6. Colony analysis via Raman Spectroscopy

Raman spectroscopy was used to identify mineral products within the iron and manganese oxidizing colonies. The samples prepared for SEM-EDS were also used for Raman spectroscopy. For further information on the technical details and settings of the Raman instrument used, see Chapter 3.

5.3 Results

5.3.1 All five weathering phenotypes identified, but with variable distributions

Neutrotolerant heterotrophs were isolated from all nine sites sampled, with CFU/g abundances varying by less than 2 orders of magnitude (~10^4-10^6). These high numbers of viable cells suggests that biomass was sufficiently preserved between sample extraction and processing in the lab (Fig. 5.5). The presence/absence of acidotolerant heterotrophs largely matched with the pH of the weathered crust scrapings, with three of the four sites where acidotolerant heterotrophs were identified being below pH 3 (Fig. 5.5).

All five phenotypes screened for (iron oxidation, manganese oxidation, siderophore production, acid production and phosphatase production) were identified in samples taken from at least one site (Fig. 5.6).

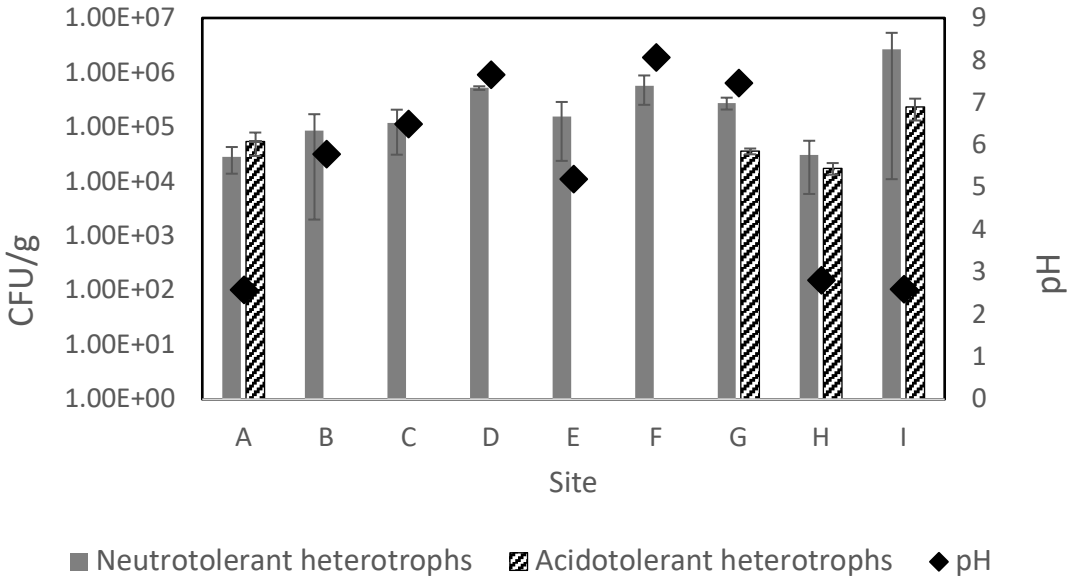

Figure 5.5¦ Abundance of microbes (CFU/g) that were neutrotolerant and acidotolerant isolated from each site (A-I, see methods section 5.2.1.). The pH values of ferromanganese deposit scrapings from each site are also displayed. N = 6-15 dependent on site (see 5.2.1 and 5.2.3) and error bars are standard error of the mean average.

Phosphatase production was the most widely distributed being found at all nine sites, with abundance ranging across two orders of magnitude ($5 \times 10^3 – 5 \times 10^5$ CFU/g). Both acid production (C, E and H) and manganese oxidation (A, H and I) were the least distributed, being only found at three of the sites. Sites E (Assholm cement stone mine wall) and H (Sandsend Ness quarry rock chips) had the greatest number of phenotypes present, with four out of five phenotypes present at each site (manganese oxidation isolates absent from site E, siderophore producing isolates absent from site H).

Abundance of isolates of particular phenotypes varied, with iron oxidiser abundance varying by two orders of magnitude ($10^3 – 10^5$ CFU/g) across four sites, while manganese oxidiser abundance varied by less than one order of magnitude ($3 \times 10^4 – 2 \times 10^5$ CFU/g).

The pH of the nine sites also widely varied, with highly acidic sites A, H and I (pH 2.6 – 2.8) being separated by over 5 pH units from the moderately alkaline

environments at sites D, F and G (pH 7.5 – 8). Manganese oxidisers were isolated exclusively from the three acidic (< pH 3) sites (A, H and I). Iron oxidisers were isolated from the three acidic sites and also from a mildly acidic site E (pH 5.2). Of the three sites where siderophore producers were isolated, two of them were moderately alkaline (F and G) (Fig. 5.6).

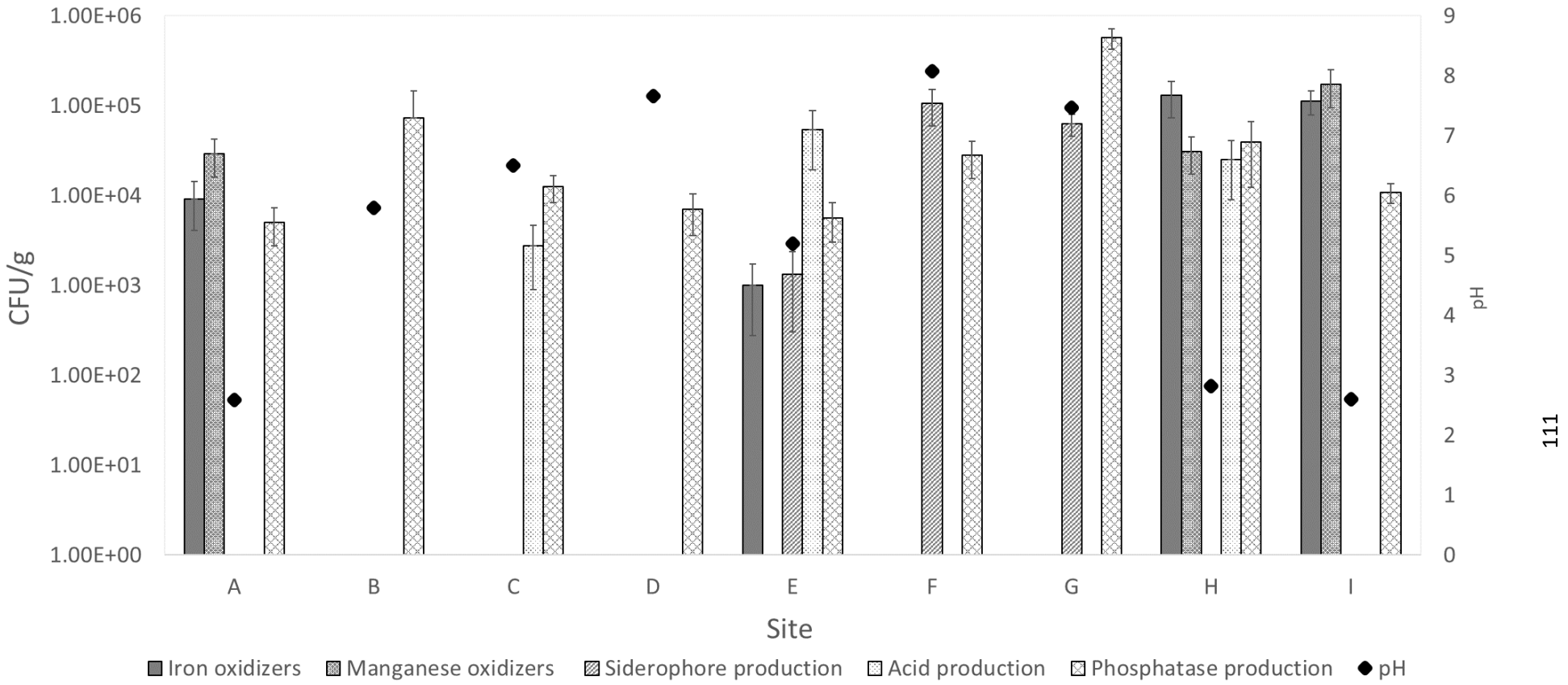

Figure 5.6¦ Abundance of microbes (CFU/g) that possessed the phenotypes selected for at each site (A-I, see methods section 5.2.1.). The pH values of ferromanganese deposit scrapings from each site are also displayed. N = 6-15 dependent on site (see 5.2.1 and 5.2.3) and error bars are standard error of the mean average.

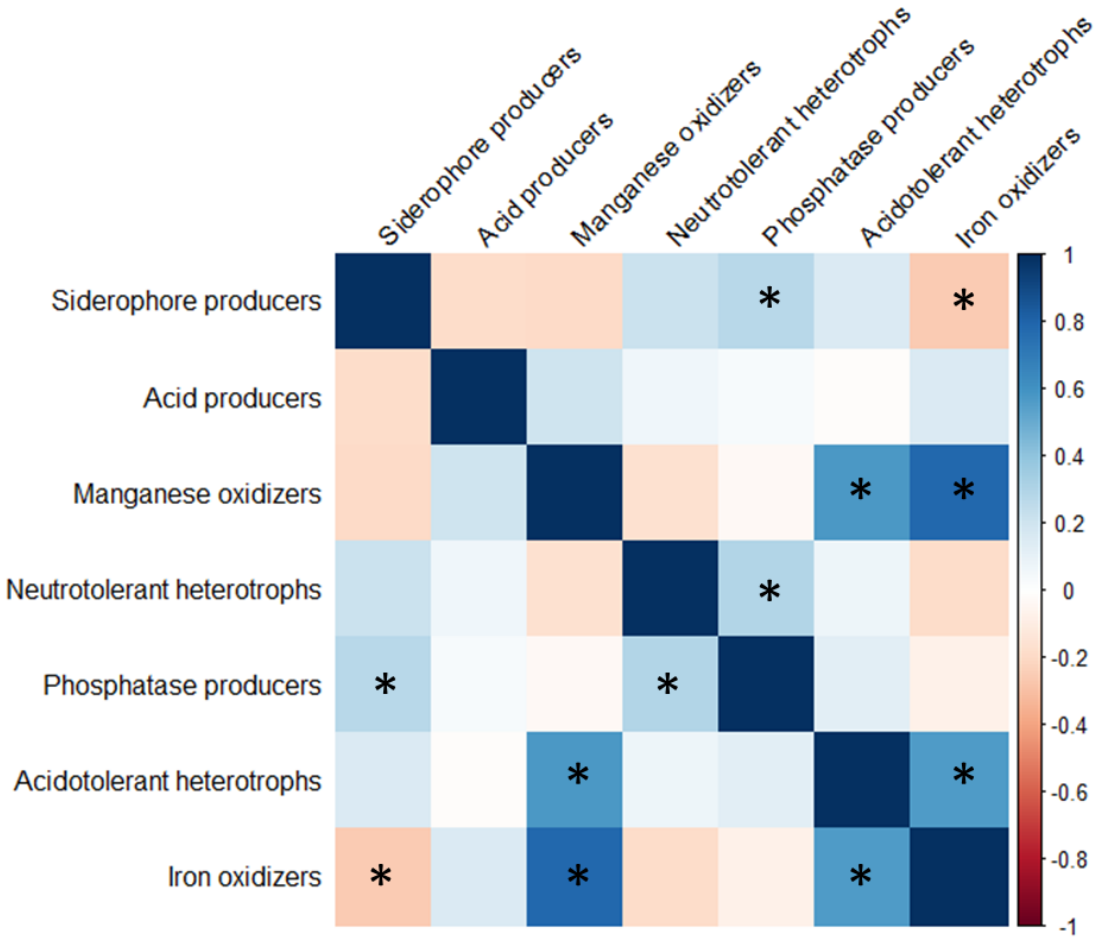

Figure 5.7¦ Spearman's rank-order correlation coefficient heat map, presenting associations in the abundances of bacterial isolates with rock weathering phenotypes cultured from collected weathered shale samples (N=75). The abundance (CFU/g) of different metabolisms/phenotypes isolated in samples collected from different sampling sites is presented in Figures 5.5 and 5.6. Stars indicate the correlation values that are statistically significant ($p > 0.05$).

Histograms of the CFU/g data for each phenotype was analysed visually for normality and was shown in all cases to be not normal (data not shown). Therefore, the data was used in a Spearman's rank-order correlation analysis (non-parametric test) to test for associations between the seven groups (Fig. 5.7). Large positive correlations were found between iron oxidisers and manganese oxidisers ($r = 0.78$, $p<0.05$), and acidotolerant heterotrophs with iron oxidisers ($r = 0.56$, $p < 0.05$) and manganese oxidisers ($r = 0.57$, $p < 0.05$). When these results are taken into account with the site pH data, it can be concluded that iron oxidisers, manganese oxidisers

and acidotolerant heterotrophs were all preferentially isolated from acidic environments and as such co-associated in their distributions (Fig. 5.6 and 5.7).

Weaker positive correlations, although still statistically significant, were also found between phosphatase producers with neutrotolerant heterotrophs ($r = 0.29$, $p < 0.05$) and siderophore producers ($r = 0.27$, $p < 0.05$). The only statistically significant negative correlation was between iron oxidisers and siderophore producers ($r = -0.25$, $p < 0.05$) (Fig. 5.7).

5.3.2 Numerous bacterial genera were identified with single or multiple phenotypic capabilities

Thirty four isolates were successfully sequenced and the genera of the organism identified (Table 5.1). The result of this analysis was the identification of 14 different generaacross three out of the five weathering phenotypes. Roughly equal numbers of isolates from each of the three weathering phenotypes processed for sequencing were identified: 11 siderophore producers, 10 organic acid producers and 13 alkaline phosphatase producers. No phylogenetic data for the iron and manganese oxidizing colonies could be obtained.

Several genera were identified within more than one phenotypic group including *Aeromonas* (S, P), *Pseudomonas* (S, P) and *Streptomyces* (A, P). Interestingly, of the 11 siderophore isolates successfully sequenced, nine of them belonged to the genus *Pseudomonas* (Table 5.1).

5.3.3. Microbial metal oxidizing structures identified in iron and manganese oxidizing colonies

cPCR of the iron and manganese oxidizing isolates was problematic, with numerous attempts required to obtain low concentrations of amplified DNA. However, the sequencing reactions of the successfully amplified isolates failed, resulting in no identification data being collected for these groups.

Table 5.1 Genera identified from phenotypic plate assays from different field sites. Letters correspond to the site they were isolated from, with the figure in brackets representing how many isolates were identified from that site.

Genus	Phyla	Siderophore (S)	Acid (A)	Phosphatase (P)	References – Genera previously identified in weathered shale environments
Aeromonas	γ-Proteobacteria	G (1)	-	G (1)	Farbiszewska-Kiczma and Farbiszewska, 2005
Arthrobacter	Actinobacteria	-	-	D (2)	Jiang *et al*., 2015; Włodarczyk and Matlakowska, 2017
Bacillus	Firmicutes	-	-	F (1), G (1)	Matlakowska and Sklodowska, 2009; Farbiszewska-Kiczma and Farbiszewska, 2005; Jiang *et al*., 2015; Włodarczyk and Matlakowska, 2017
Flavobacterium	Bacteroidetes	-	F (1) G (1)	-	Joeckel *et al*., 2005; Jiang *et al*., 2015
Microbacterium	Actinobacteria	-	F (1)	-	Matlakowska and Sklodowska, 2009; Włodarczyk and Matlakowska, 2017
Micromonospora	Actinobacteria	-	C (1), G (1)	-	None found
Moraxella	γ-Proteobacteria	-	-	C (1)	None found
Pseudomonas	γ-Proteobacteria	F (6), G (3)	-	A (1), F (2), G (1)	Matlakowska and Sklodowska, 2009; Farbiszewska-Kiczma and Farbiszewska, 2005; Jiang *et al*. 2015; Dziewit *et al*., 2015; Włodarczyk and Matlakowska, 2017
Rhizobium	α-Proteobacteria	F (1)	-	F (1)	Jiang *et al*., 2015; Włodarczyk and Matlakowska, 2017

Table 5.1 (continued)¦ Genera identified from phenotypic plate assays from different field sites. Letters correspond to the site they were isolated from, with the figure in brackets representing how many isolates were identified from that site.

Genus	Phyla	Siderophore (S)	Acid (A)	Phosphatase (P)	References – Genera previously identified in weathered shale environments
Sphinopyxis	*α-Proteobacteria*		F (1)		Jiang *et al*., 2015; Włodarczyk and Matlakowska, 2017
Stenotrophomonas	*γ-Proteobacteria*	-	G (2)	-	Jiang *et al*., 2015; Dziewit *et al*., 2015
Streptomyces	*Actinobacteria*	-	D (1)	G (1)	Włodarczyk and Matlakowska, 2017
Tetrasphaera	*Actinobacteria*	-	E (1)	-	None found

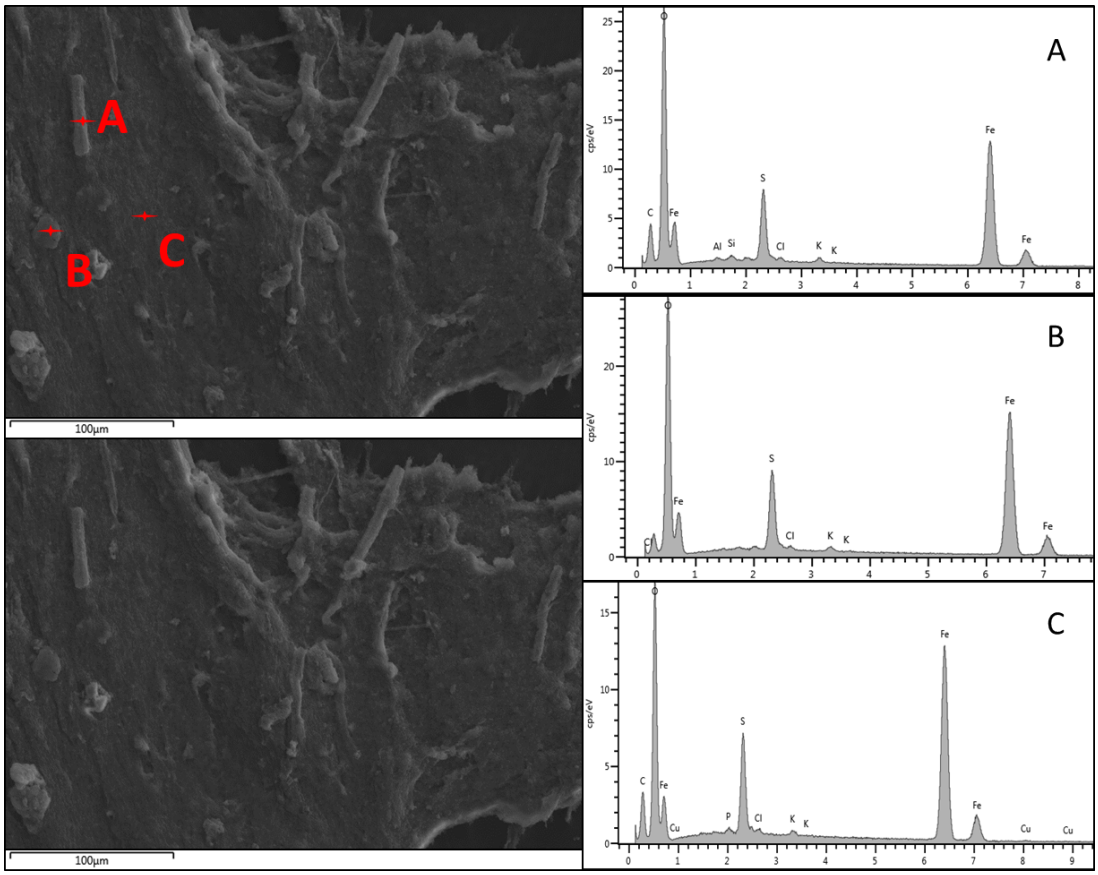

Figure 5.8¦ SEM images (left) and qualitative EDS spectra (right) of a desiccated rust-coloured microbial colony that grew on WAYE agar. Point spectra were taken of A) a sheath-like structure B) a rock particle and C) background material (dried agar medium).

To obtain some information about these colonies, SEM-EDS was used to look at surface and cellular morphology of dried iron and manganese oxidizing colonies (Fig. 5.8 and 5.9). The colonies analysed were picked from plates inoculated from samples taken from Saltwick Bay cliffs (sample site A). Raman spectroscopy was used to determine mineralogy of the colony content in dried iron oxidizing colonies (Fig. 5.10).

Three spectra were taken for both colonies analysed a) biological material (cell sheath/filaments), b) a rock particle from the agar and c) background material (dried agar).

For the iron oxidizing colony, there were multiple sheaths identified in the matrix of the agar (Fig. 5.8). These sheaths were between 50-75µm in length and 6-8µm in thickness. In the manganese oxidizing colony, cell shaped holes can be observed in the background media (green arrow). Furthermore, a huge volume of filamentous material was present on the dried colony surface (Fig. 5.9, point A).

Although the EDS measurements were not quantitative, so abundances of elements cannot be surmised, the presence or absence of particular elements could be assessed for each measurement. Note that the y-axis varies in scale between graphs. No large differences in elemental composition between the spectra taken from points A, B or C were identified for the iron oxidizing colonies (Fig. 5.8). Although some elements were identified by the EDS in the sheath analysed (Al, Si) which were not identified in either the rock particle or the background media, this result was not consistent (data not shown). The lack of detected Al and Si within the rock particles analysed suggests a) that these elements leached out of the rock beyond detection limit or b) that these rock particle like structures are artefacts of the drying process.

There were observed differences in the spectra taken from the manganese oxidizing colony (Fig. 5.9). A peak for manganese was detected in the filamentous material (A) that was not seen in the rock particle (B), and although manganese was detected in the background material (C), the sharp peak was not observed. Numerous elements were detected in the rock particle that were not observed in the filamentous material or the background material, including Al, Si, Fe, Ti and Mg (Fig. 5.9).

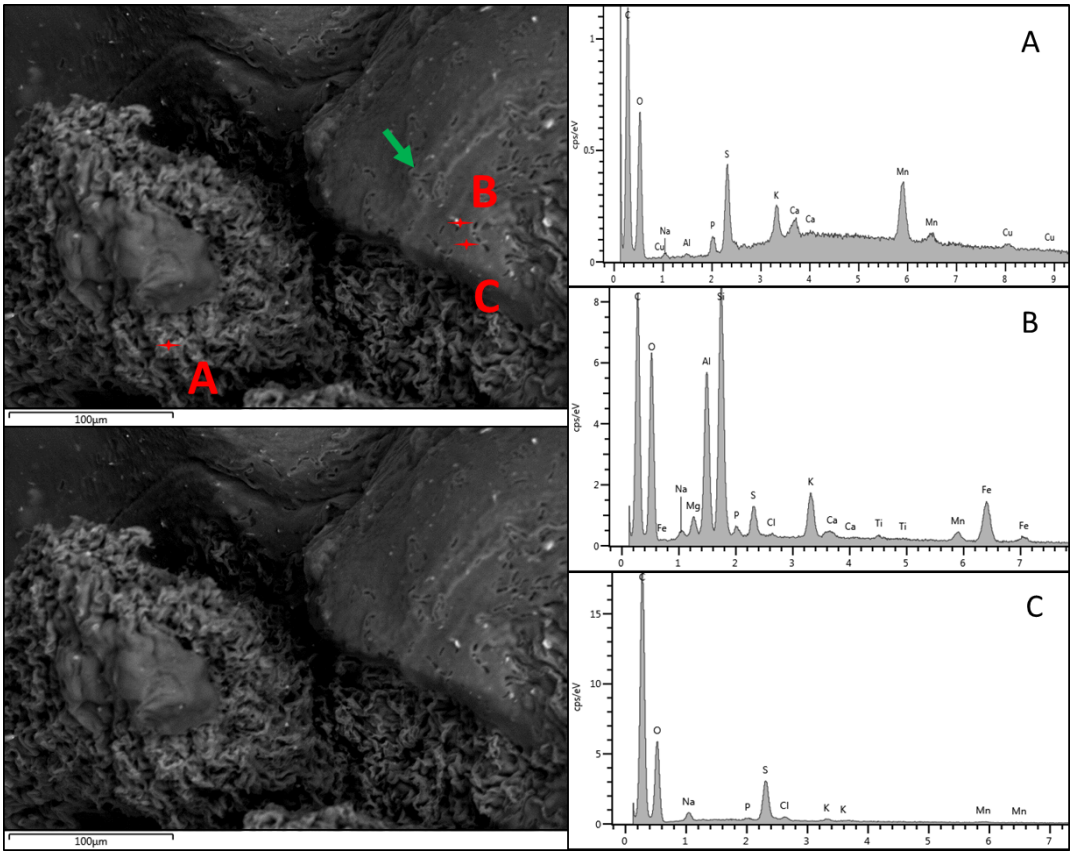

Figure 5.9 SEM images (left) and qualitative EDS spectra (right) of a desiccated manganese oxidizing microbial colony. Point spectra were taken of A) filamentous material B) a rock particle and C) background material (dried agar medium).

5.3.4 Putative identification of lepidocrocite iron oxidizing colonies

In addition to SEM-EDS, iron oxidizing colonies were analysed using Raman spectroscopy to determine if microbially produced oxide/hydroxide minerals could be distinguished. Background fluorescence in the Raman spectra of the manganese oxidizing colonies resulted in this data having to be removed from the analysis.

Spectra taken from iron oxidizing colonies A and B (isolated from samples taken from Saltwick Bay cliff) were similar with peak values at 138-139, 293, 354-356, 427-429, 554, 845 and 983 cm^{-1} (Fig. 5.10). Many of these peaks are matched by peaks within the sterile agar such as 354-356, 544, 845 and 983 cm^{-1}. However, distinctive peaks at 293 and 427-429 cm^{-1} in the iron oxidizing colonies were not clearly seen in the sterile agar (Fig. 5.10).

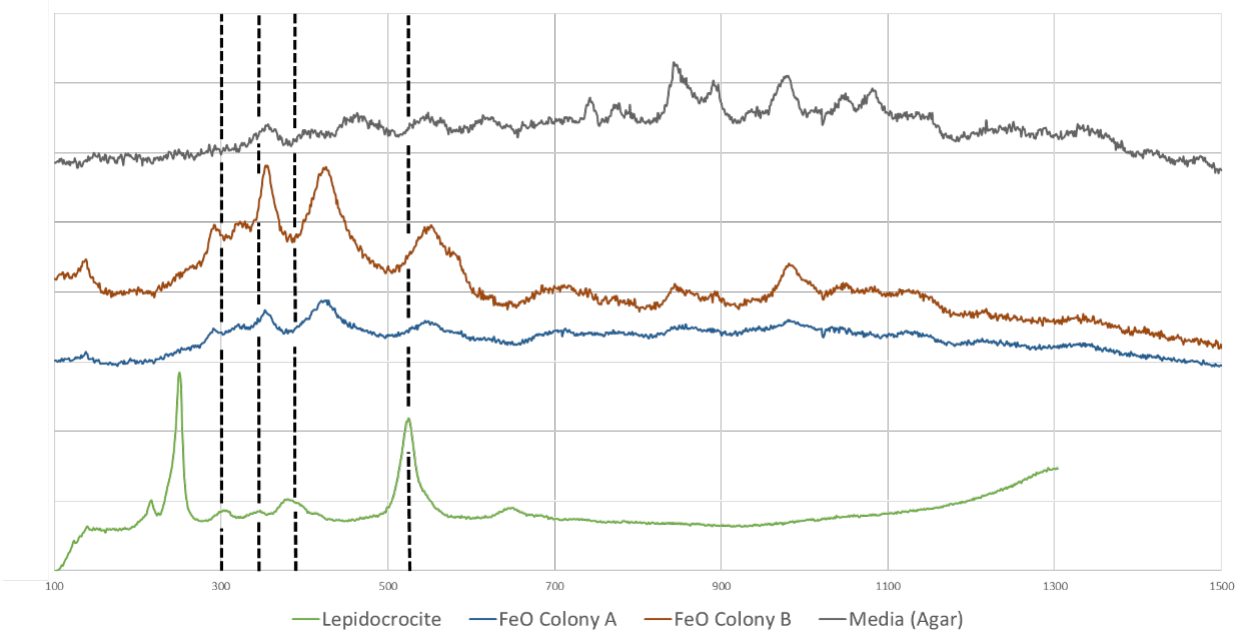

Figure 5.10¦ Raman spectra of two rust coloured colonies (FeO colonies A and B) isolated from a WAYE agar plate, and the sterile agar of a WAYE plate (Media (Agar)). The spectra of a standard sample of Lepidocrocite (FeO(OH)) (RRUFF 2016) is included. Dotted lines highlight similar peaks in the Lepidocrocite spectra with those found in iron oxidizing colonies A and B.

The spectra of various pure iron minerals were compared to the iron oxidizing colony spectra including ferrihydrite ($(Fe^{3+})_2O_3 \bullet 0.5H_2O$), lepidocrocite (FeO(OH)), goethite (FeO(OH)), pyrite (FeS_2), haematite (Fe_2O_3) and magnetite (Fe_3O_4). The spectra of lepidocrocite had the best match with the spectra of the iron oxidizing colonies (Fig. 5.10). Two of the seven peaks in the lepidocrocite match closely with peaks in the lepidocrocite (293 and 354-356 cm^{-1}), while another two roughly match (427-429 and 554 cm^{-1}). However, the large peak in the spectra of lepidocrocite at 250 cm^{-1} is missing from the colony spectra. As such, the exact mineralogy of the iron minerals in the microbial iron oxidizing colonies remains unclear (Fig. 5.10).

However, the samples analysed for the microbial iron oxidizing colonies are complex containing components of agar with constituent compounds, black shale rock powder, cellular biomass and iron minerals formed. It therefore is unsurprising that exact mineral spectra cannot be matched precisely to the spectra from the iron oxidizing colonies.

5.4 Discussion

5.4.1 Widespread isolation of rock weathering microorganisms

Microorganisms with at least one weathering phenotypic capability were isolated from weathered material taken from all of the nine sites sampled (Fig. 5.5). These environments were highly heterogeneous in numerous ways, from the extent of weathering of the rock structure was (relatively fresh rock chips at cliff surface compared to rock chips crumbling into soil at quarry screes), the surface pH and humidity. These details are explored more in Chapter 4.

Despite these differences, microbes potentially capable of weathering were found at every site and in significant numbers (10^3-10^6 CFU/g for each phenotype present). The total number of organisms within a sample is not known, as there is likely to be overlap in the numbers calculated from each phenotypic plate count i.e. species that can grow on multiple agar types. Cockell *et al.* (2011) estimated in their study that 4.2 x 10^4 cells/cm^2 covered the weathered surface of shale on the walls of Hole Wyke mine, which was a sampling site for the data presented in Chapter 6. This number fits within the range of microbial CFU/g presented in this chapter (Fig. 5.5).

The distribution of weathering phenotypes was highly variable. Samples from environments such as the Saltwick Bay cliff (A), the Assholm mine wall (E) Sandsend Ness (H) and the Gaytress quarries (I) yielded groups of isolates that possessed 3-4 of the phenotypes targeted. In contrast, other environments such as Keldhowe Steel cliffs (B), Hole Wyke cliff (C), Tellgreen Hill jet mine wall (F) and Deepgrove quarry ochreous stream (G) were sparse in weathering phenotypes (1-2)(Fig. 5.5). This suggests that not all of these phenotypes are important or even viable in all of these environments. Factors such as rock geochemistry and environmental conditions such as pH and humidity, are therefore likely to play a role in the distribution of weathering organisms.

Although the presence of particular organisms/phenotypes within an environment could be confirmed in this study, it cannot confirm the absence of them. The absence

of a particular organism/phenotype does not mean that they were not present at that site, but that the culturing methods used were not adequate to determine their presence/absence. It is known that only a small fraction of total microbes within an environment are culturable under laboratory conditions (Stewart, 2012). However, the use of culturing techniques as opposed to molecular techniques such as community 16S rDNA sequencing, allows this study to directly prove phenotypic capability of culturable organisms within these environments.

Twelve different genera were identified in this study, with each one attributed to one or two phenotypes (Table 5.1). The majority of these genera fell into two phyla, the *Actinobacteria* (six strains) and the *Proteobacteria* (six strains).

5.4.2 Iron and manganese oxidizing strains primarily isolated from acidic environments

The growth and presence of iron oxidisers, manganese oxidisers and acidotolerant heterotrophic isolates at particular sites seems to at least be partially controlled by pH. This can be deduced from their abundances in Figures 5.5 and 5.6, where all of these phenotypes were primarily isolated from sites with low pH values. This is further supported by the strong positive correlation coefficient values between these three phenotypes (iron oxidisers with manganese oxidisers, $r = 0.78$, manganese oxidisers with acidotolerant heterotrophs, $r = 0.57$ and iron oxidisers with acidotolerant heterotrophs, $r = 0.56$, all p values < 0.001) (Fig. 5.7). The grouping of acidotolerant heterotrophs at more acidic sites seems intuitive; organisms that can survive and proliferate in acidic environments will do so and will thrive due to reduced competition from neutrotolerant heterotrophs. The association of iron oxidisers with acidic environments is also relatively common. Aerobic iron oxidation (as selected for in this study) becomes energetically favourable within environments at pH 4 or less (Hedrich *et al.*, 2011). In more pH neutral or alkaline environments abiotic iron oxidative reactions are more prevalent, meaning that there is a lack of bioavailable ferrous iron to oxidise.

Microbial manganese oxidation by *Leptothrix discophora* however, has been found to be most favourable in pH neutral conditions (7.3-7.5) (Adams and Ghiorse 1987,

Zhang *et al.,* 2002). The positive result on the manganese oxidizing agar plates requires the presence of Mn (III) or Mn (IV) to interact with the dye Leucoberbelin Blue (Fig. 5.3 and 5.6), turning it from a light aqua blue to a dark blue (Krumbein and Altmann 1973). This does not distinguish how the oxidised manganese was produced.

Although manganese oxidation for chemoautolithic growth is thermodynamically favourable, there is no substantial evidence that any group of manganese oxidizing organisms use this process for energy acquisition (Tebo *et al.,* 2005). This however, does not mean that microbial manganese oxidation does not provide adaptive advantage to microbial cells. Manganese oxides are hypothesised to provide protection from radiation and act as a store of manganese oxide for microbial manganese reduction (Tebo *et al.,* 1997). Active microbial manganese oxidation has been shown to be mediated by multi-copper oxidases in manganese oxidizing bacteria (Tebo *et al.,* 2005). Alternatively, microbial manganese oxidation is believed to also be a passive process in certain cases (Ghiorse 1984) e.g. on the surface of *Bacillus* sp. SG-1 spores (Tebo *et al.,* 2005).

These facts have three possible implications for the results presented in this chapter. Firstly, the manganese oxidizing microbes isolated here are not active oxidisers of manganese, but passively oxidise manganese when manganese is present in growth media. Secondly, these microbes are active manganese oxidisers but do not use this ability in the environment from which they were isolated . Potentially their ability to oxidise manganese is a by-product of their ability to oxidise other metals in that environment. Finally, these organisms are active cyclers of manganese in acidic environments. Further physiological studies on these isolates would be required to confirm the validity of these hypotheses.

These conclusions can also be applied to iron oxidizing isolates in this study. Of the four sites where iron oxidisers were isolated, three of them were acidic (<pH 3) whilst one was only mildly acidic (Assholm Mine – pH 5.2) (Fig 5.6). The pH of Assholm mine is above what is considered energetically favourable for aerobic iron oxidisers (Hedrich *et al.*, 2011), suggesting that the same hypotheses for the

manganese oxidisers above could be true for the strains isolated from this site (Fig. 5.6).

In this study, although not classified as manganese oxidisers, species of *Pseudomonas*, *Stenotrophomonas* sp. and *Bacillus* sp. were identified for having rock weathering phenotypes (Table 5.1). They have beenfound to be manganese oxidisers in ferromanganese deposits in other studies (Northup *et al.,* 2003; Spilde *et al.,* 2005; Carmichael *et al.,* 2013). Additional genera identified in this study with rock weathering capabilities include *Aeromonas, Flavobacterium and Streptomyces*; strains of these organisms have been found capable of manganese oxidation (Ghiorse 1984). Bacterial phylogenetic analysis of aluminium coatings on weathered schist in Swedish Lapland revealed the presence of *Tetrasphaera*, that demonstrated manganese oxidizing capabilities (Marnocha and Dixon 2013). Furthermore, *Actinobacteria* and *Firmicutes* were identified within the various rock coatings analysed in this study (Fe-Mn crusts, aluminium crusts and sulfate crusts); these two phyla include seven out of the twelve genera identified (Table 5.1).

Pseudomonas sp. and *Micrococcus* sp. are bacterial isolates identified in this study that have been previously associated with microbial iron oxidation (Konhauser 1998; Sudek *et al.,* 2009; Hedrich *et al.,* 2011). As far as the author is aware, this iron oxidation can be considered passive as it is enabled by positive iron cations non-specifically precipitating on the cell wall of these organisms (Konhauser 1998). *Micrococcus* sp. was another organism identified in this study that has been previously associated with ferromanganese deposits, but not linked to any specific metal cycling capabilities (Northup *et al.,* 2003).

Variovorax paradoxus, along with other species including *Pseudomonas* sp., were also identified from enrichment cultures inoculated with ferromanganese deposit material as described in Chapter 6. *Variovorax* sp. was identified as a manganese oxidiser by Northup *et al.* (2000), but was also found in other ferromanganese deposits (Northup *et al.,* 2000; Northup *et al.,* 2003; Carmichael *et al.,* 2013). The identification of *Alcaligenes* as a manganese oxidiser by Spilde *et al.* (2005) is interesting due to its close genetic relatedness with *Variovorax* (Willems *et al.,*

1991). The potential importance of *Variovorax* sp. in ferromanganese deposits is explored more in Chapter 6.

5.4.3 SEM-EDS and Raman spectroscopy evidence for microbial iron and manganese oxidation

The lack of taxonomically identified iron or manganese oxidisers from this study makes it difficult to resolve the hypotheses made about the active/passive role of iron and manganese oxidisers in the previous section. SEM-EDS and Raman spectroscopy of iron and manganese oxidizing microbial colonies isolated from samples taken from Saltwick Bay cliffs has provided evidence to confirm the microbial phenotypes identified (Fig. 5.3, 5.4 and 5.6).

The identification of sheaths in the SEM images of the iron oxidizing colony is strong evidence for microbial iron oxidation. Numerous sheaths can be seen in Figure 5.8, roughly 5µm in diameter and 50-80µm in length. Hollow sheaths are commonly formed by the four known species of *Leptothrix* and *Sphaerotilus natans* (Konhauser 1998; Chan *et al.,* 2009; Hedrich *et al.,* 2011). However, the size and shape of the sheaths seen in the SEM images more likely supports the putative identification of a strain of *Leptothrix*. Cells of *Leptothrix* sp. are 0.6-0.8µm in diameter and 1.5-12µm in length (Spring *et al.,* 1996), with longer *Leptothrix*-like sheaths (80-300µm) have been reported in iron and manganese rich wetlands (Johnson *et al.,* 2012). Although the sheath diameter was greater than that of *Leptothrix* cells, sheaths can be several diameters in thickness around the cell exterior (Konhauser, 1998). *Leptothrix* and *Sphaerotilus* species are normally obligatory neutrophiles (Spring *et al*., 1996), however acidophilic sheath forming organisms are believed to be closely related to these species that have been identified (Johnson *et al.,* 1992).

Pits morphologically similar in size and shape to bacterial cells were found embedded in the background material of the manganese microbial colony (Fig. 5.9). These holes were possibly formed from the growth of a bacterial species, which upon drying and then gold coating either burst or became dislodged. Evidence to support thatactive biological manganese oxidation occurred in within the colony comes from the filamentous material found surrounding the background material (Fig. 5.9),

which looks analogous to the iron oxyhydroxide stalks produced by organisms such as *Mariprofundus ferrooxydans* and *Gallionella ferruginea* (Emerson *et al.,* 2010). Stalked or budding manganese oxidizing bacterial genera such as *Hyphomicrobium* or *Caulobacter* could be responsible for formation of these filaments (Ghiorse, 1984). However, the stalks of these species are not analogous in morphology to that of filaments seen in the manganese oxidizing colony. Filamentous material has been found ferromanganese deposits (Spilde *et al*., 2005), although the nature of this material remains unknown.

The Raman spectra obtained of the iron oxidizing microbial colonies best matched with the spectra of lepidocrocite (FeO(OH)), although only a subset of the peaks matched with the colonies spectral peaks (Fig. 5.10). Comparison of the colony spectra with other iron oxides/oxyhydroxides did not reveal any matches with other iron minerals (data not shown). The lack of well-defined iron oxide, hydroxide or oxyhydroxide minerals can likely be attributed to the complex nature of the samples analysed containing cells, iron complexes (crystalline and non-crystalline), agar with supplemented compounds and rock powder. It is likely that other iron-bearing material is within these colonies, but in a poorly crystalline or completely amorphous form. The Raman spectral analysis of weathered shale material from Hole Wyke mine adit also revealed only partial matches with the iron minerals haematite and goethite (Cockell *et al.,* 2011). Lepidocrocite has been identified in ferromanganese deposits in the Guadalupe caves (Northup *et al*., 2003; Spilde *et al*., 2005), suggesting that the identification of this mineral within the colonies analysed is plausible.

5.4.4. *Pseudomonas* strains are the dominant producers of siderophores in shale ferromanganese deposits

Of the eleven identified siderophore-producing bacterial isolates, nine of them were from the genera *Pseudomonas* (Table 5.1). These organisms were identified at two sites, along with single isolates of siderophore-producing *Aeromonas* and *Rhizobium*, which were isolated from Tellgreen Hill jet mine wall and Deepgrove quarry ochreous stream both of which were pH neutral sites (Fig. 5.6).

The isolation of these organisms in pH neutral environments fits with the negative correlation ($R= -0.25$, $p < 0.05$) between the distribution of siderophore producers and iron oxidisers (Fig. 5.7). Ferric iron is much less soluble at pH values above 4 (Kalinowski *et al.,* 2006), so the production of siderophores in pH neutral environments to increase iron bioavailability is advantageous to capable organisms. In contrast, aerobic iron oxidation is not energetically favourable at neutral pH, so the growth of iron oxidisers is inhibited (Hedrich *et al*., 2011). Of additional interest is the lack of genera that demonstrated both siderophore and acid producing phenotypes, suggesting that the organic acids produced by those strains were not iron chelators (Table 5.1). However, no positive or negative correlation between these two phenotypes was found in this study (Fig. 5.7).

The important role of *Pseudomonas* species in the production of siderophores in shale ferromanganese environments is highlighted in this work. Although the results of culture based work will not represent all of the siderophore producing organisms (non-culturable organisms not represented), the genera *Pseudomonas* dominates the culturable siderophore producers within the shale weathering environments studied.

Siderophore production has been reported in the genera *Aeromonas* and *Rhizobium* previously, but not in the context of mineral or rock weathering. *Aeromonas* species such as *A. salmonicida* and *A. hydrophila* are known for producing siderophores which act as virulence factors in fish and amphibian hosts (Hirst *et al.,* 1991). *Aeromonas* was found associated with a community that contributed to the biodeterioration of peridotite and other constructional materials in a church, although this activity is associated with acid production and not siderophores (Herrera *et al*., 2004). *Rhizobium* species are generally plant-associated bacteria that inhibit the growth of plant pathogens through the extracellular release of siderophores (Arora *et al.,* 2001; Saha *et al.,* 2013). Zhao *et al.* (2013) show that *Rhizobium* sp. *Q32* can significantly increase the dissolution of feldspar and biotite minerals by 1.2-4.7 and 1.2-1.5 fold-increase for Si and K leaching in comparison to sterile controls. They find that the *Rhizobium* strain only moderately acidifies its environment (6.0-6.5 pH), but produced siderophores and exopolysaccharides which is what they attribute to the enhanced mineral dissolution (Zhao *et al.,* 2013).

Siderophore and secondary metabolite producing *Pseudomonas* have been highlighted in numerous studies as important weathering organisms of shale (Matlakowska *et al.,* 2008; Włodarczyk *et al.,* 2015; Matlakowska and Sklodowska 2009, Kalinowski *et al*., 2006). *Pseudomonas* in these studies are often associated with heavy metal tolerance, which is partially due to their extensive production of siderophores that can immobilise toxic metal cations (Matlakowska *et al.,* 2008). Although *Pseudomonas* produced siderophores have been primarily associated with sequestering iron, they have also been implicated in sequestering a range of heavy metals including Co, Cu, Fe, Ni, U and Zn (Gadd, 2004; Kalinowski *et al.,* 2006). The production of siderophores of a mixed community of eight species, five of which were *Pseudomonads*, increased the release of Mn (280 %), Fe (200 %) and Co (180 %) (Włodarczyk *et al.,* 2015). This wide spread release of metals from shale by siderophores is likely to be a driver in shale mineral dissolution and rock degradation.

5.4.5. Acid producers are phylogenetically diverse and are ubiquitous in shale ferromanganese deposits

Six different genera across three phylogenetic divisions were shown to produce acid on milk agar plates (Fig. 5.6 and Table 5.1). Four of these six genera all belong to the phylum Actinobacteria (*Microbacterium*, *Micromonospora*, *Streptomyces* and *Tetrasphaera*).

A strain of *Microbacterium* is part of the microbial consortium that has been used in a series of studies to investigate the role of microbes in shale weathering and metal bioleaching (Matlakowska and Sklowdowska, 2009; Matlakowska *et al*., 2010a; Włodarczyk *et al*., 2015). They demonstrate that this group of bacteria produce low molecular weight organic acids including aliphatic and aromatic carboxylic acids, which increase metal leaching out of black shale (Matlakowska *et al.,* 2014).

Micromonospora was shown to produce both acetic and propionic acid as products of glucose and cellulose fermentation (Hungate, 1946). Further studies have demonstrated that both *M. saelicesensis* can also produce acid when grown on glucose substrate (Trujillo *et al.,* 2007). *Streptomyces* sp. strains have been

demonstrated to produce organic acids in the rhizosphere of pine trees, including the release of pyruvic, α-ketoglutaric, lactic, malic, citric, succinic and oxalic acids (Rózycki and Strezelczyk, 1986). The production of these organic acids was suspected to contribute to the increased dissolution of hornblende, which in combination with the production of siderophores resulted in a 5-fold increase of Fe leaching from this mineral (Liermann *et al*., 2000). Both *Streptomyces* and *Micromonospora* (along with other *Actinobacteria*) were isolated from the indoor air of a stone (limestone) church, and subsequent testing of the isolated strains revealed production of a wide range of different organic acids. The incubation of isolates *Micromonospora carbonacea* and *Streptomyces diastaticus* with discs of granite revealed that the activity of these organisms could reduce disc mass by >4 % and 2-3 % respectively, driven by acidic dissolution of the limestone (Abdulla *et al.,* 2008).

Genome analysis of numerous species of *Tetrasphaera* reveal that some of them have the capability to produce lactic acid as a fermentation product (Kristiansen *et al.,* 2013). More recent work has indicated the genera's importance in fermentation processes in lactic acid formation from 16S rDNA community sequencing, but not from direct quantification of acid production (Liang *et al.,* 2015). *Tetrasphaera* was enriched in a sulfur oxidizing enrichment from samples of Alpine dolomite, in which the microbial community caused 34 % increased leaching of Mg from the rock compared to the sterile control (Sonnleitner *et al*., 2011).

The taxonomic article defining the genera *Stenotrophomonas* identifies it as capable of producing acid through the digestion of starch (Palleroni and Bradbury, 1993), yet no further studies have been undertaken to investigate this acid production . *Stenotrophomonas* has been associated with mineral weathering communities in the rhizosphere of beech and spruce trees, but was not identified as increasing Fe leaching from biotite (Collignon *et al.,* 2011).

Both *Stenotrophomonas* and *Tetrasphaera* strains have been associated with phosphorus cycling, particularly with the degradation of polyphosphate and other inorganic phosphorus sources in geological environments (Xiao *et al.,* 2009; Kristiansen *et al.,* 2013). However, neither of these strains have been linked to phosphatase production in this study (Table 5.1).

A limited number of *Flavobacterium* strains have been identified as producers of organic acids (Hayes, 1963; Vandamme *et al.,* 1994), with most species studied not having the ability to produce acid. Of significance was the isolation of *Flavobacterium* from sulfate mineral crusts formed on weathered shale (with clear evidence of pyrite weathering) in the Dakota formation and Graneros shale (Joeckel *et al.,* 2005), although the activity of this organism within this environment is unknown. Considering the similarity in the environment that *Flavobacterium* was isolated from in this study (ferromanganese deposits on the wall of Tellgreen jet mine wall), it can be postulated that this organism may be well adapted for survival and activity within weathered shale crusts. *Flavobacterium* has also been identified in other microbial mineral/rock weathering communities (Collignon *et al.,* 2011; Skidmore *et al.,* 2005).

5.4.6. Numerous phosphatase producers isolated from shale ferromanganese deposits

Five different genera across three distinct phyla were isolated for their ability to produce phosphatases on phenolphthalein phosphate agar (Table 5.1). Three of these genera were also identified in one of the other phenotypic assays: *Aeromonas*, *Pseudomona*s (both siderophore production) and *Streptomyces* (acid production). Other phosphatase producing genera isolated were *Bacillus*, which was also identified as an acidotolerant heterotroph, and *Rhodococcus*, which was not identified from any of the other assays (Table 5.1).

Phosphatase producers were positively associated with both neutrotolerant heterotrophs ($r = 0.29$, $p < 0.05$) and siderophore producers ($r = 0.27$, $p < 0.05$). Neutrotolerant heterotrophs and siderophore producers did not significantly correlate ($p = 0.0699$), but did have a similar rho value ($r = 0.21$). A likely explanation for these associations is that phosphatase (and possibly siderophore) producers identified in this study are also neutrotolerant heterotrophs. It is additionally possible that isolates cultured in this study had multiple rock weathering capabilities (i.e. isolates that could produce both phosphatases and siderophores). This is supported by the phylogenetic analysis carried out, where isolates from the genera *Aeromonas*,

Pseudomonas, *Rhizobium* and *Streptomyces* were all identified for both phosphatase and siderophore production.

Strains of *Aeromonas*, *Pseudomonas* and *Streptomyces* that produce phosphatases under environmental conditions have been identified in previous studies (Lim *et al.,* 1996; Richardson and Hadobas 1997; Li and Strohl 1996). In the case of *Pseudomonas*, the phosphatase production enabled the metabolism of inositol phosphates (poly-phosphates) and in *Streptomyces* the action of phosphatase enzymes were necessary forthe production of anti-microbial compounds (Majumdar and Majumdar, 1971). The production of phosphatases in *Aeromonas* has not been previously linked with rock weathering capabilities.

Arthrobacter sp. are well known members of rock weathering microbial communities (Gorbushina, 2007; Frey *et al*., 2010; Cockell *et al*., 2013) and strains of this genera have been demonstrated to enhance the dissolution of hornblende via the release of organic acids and siderophores (Kalinowski *et al*., 2000; Brantley *et al*., 2001). In this study, *Arthrobacter* was isolated for the production of alkaline phosphatase and contrarily was not associated with organic acid or siderophore production (Table 5.1). No previous studies have associated *Arthrobacter* with phosphate solubilisation. The identification of *Arthrobacter* sp. within weathered shale is of interest, as it has been previously identified through culture independent community analysis of weathered shale profiles within an oil shale (Jiang *et al*., 2015) and black shale copper mine (Włodarczyk and Matlakowska, 2017). *Arthrobacter* could therefore be an important member of rock weathering communities within weathered shale.

The work of Puente *et al.* (2004) tested *Pseudomonas* and *Bacillus* strains isolated from the rhizoplane of cacti for their ability to weather igneous rock by comparing particle size before and after microbial incubation. After microbial activity, there was a greater number of smaller particles (0.1-2µm) and a smaller number of larger particles (7µm). The weathering capabilities of these organisms was believed to be partially caused by their ability to solubilise insoluble phosphate compounds such as $Ca_{10}(OH)_2(PO_4)_6$ and $FePO_4.2H_2O$. Strains of *Bacillus* in this study were also found to enhance the dissolution of marble and limestone, associated with the production of acid (Puente *et al.,* 2004).

Streptomyces has also been identified as important in phosphate solubilisation in geological environments. *Actinobacteria* strains were isolated from an insoluble rock phosphate (hydroxyapatite) mine for their ability to solubilise phosphate; seven isolates of *Streptomyces* and one of *Micromonospora* were identified. The isolates were found to be capable of using the insoluble rock phosphate as the sole source of phosphorus. The production of siderophores by these strains was believed to be the primary driver of mineral dissolution by chelating calcium, although the production of phosphatases was not tested (Hamdali *et al.,* 2008).

Another organism isolated for phosphatase production was *Rhodococcus*, an organism which has been investigated across numerous studies for its production of surfactants in oil shale (Lee *et al*., 1991; Ivshina *et al*., 1998; Haddadin *et al*., 2009). First identified in the anoxic zone of an oil shale leachate column, it was highlighted as a degrader of pyridine, a toxic by-product of many industrial activities (Lee *et al.,* 1991). Later, its ability to remove oil from oil shale cuttings and oil polluted sands was investigated and the production of surfactants was found to be central for this ability (Ivshina *et al.,* 1998; Haddadin *et al.,* 2009). It is worth noting that *Rhodococcus* was also identified along with *Variovorax* to grow in extreme low nutrient enrichment cultures inoculated with weathered shale from Hole Wyke mine adit, as detailed in Chapter 6. The importance of *Rhodococcus sp.* in rock weathering is further demonstrated by its identified ability to contribute to granite dissolution, and from its identification in a volcanic rock weathering microbial community (Frey *et al.,* 2010; Cockell *et al*., 2013).

5.4.7. Conclusions

This chapter has identified numerous bacterial genera with one or more mineral/rock weathering capabilities (Table 5.1), and demonstrated that such organisms are present in significant numbers at a diverse range of shale weathering sites (Fig. 5.6). Through an extensive search of the literature it has been established that the majority of the genera found have been previously identified as active rock weathering microbes including *Pseudomonas*, *Streptomyces*, *Rhizobium, Microbacterium, Tetrasphaera* and *Micromonospora*.

An important point to re-iterate is that although these organisms have been isolated from shale weathering profiles and have been characterised for rock weathering capabilities, neither *in vitro* nor *in situ* demonstration of microbial rock weathering has been presented here. Experimental data exploring these points will be presented in Chapters 7 and 8. However, the significance of the data presented here still stands. Rock weathering organisms have been found to be ubiquitous in ferromanganese deposits coating weathered shale, with many such organisms having multiple rock weathering capabilities such as *Pseudomonas* (siderophores and phosphatase production) and *Streptomyces* (organic acid and phosphatase production) (Table 5.1).

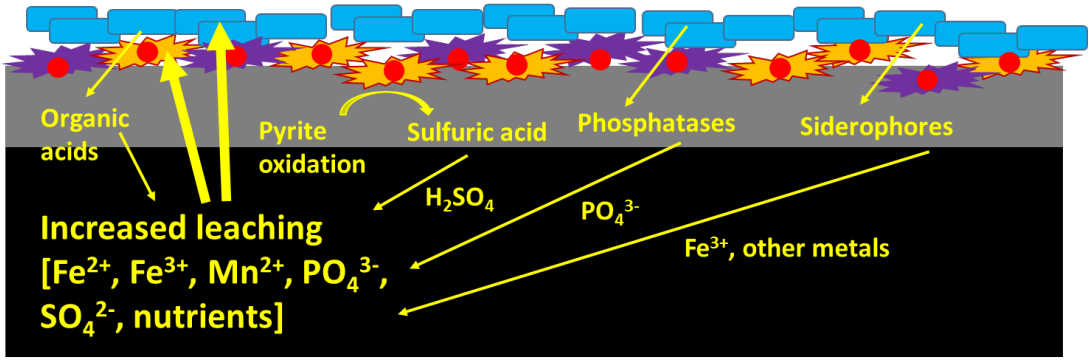

Figure 5.11¦ Diverse microbial communities drive positive feedback in the rock weathering cycle of ferromanganese deposits on the surface of weathered shale. The release of rock weathering products (siderophores, organics acids, phosphatases, *etc*.) by heterotrophic microbes (blue rectangles) weathers minerals and the rock as a whole, releasing metals and nutrients to the microbial community above. This further stimulates the growth of the heterotrophs and autolithotrophic iron and manganese oxidizing microbes (red circles), which produce iron and manganese hydroxy/oxides which form the ferromanganese crust (orange and purple explosions). The dissolution of pyrite (FeS_2) by iron oxidizing microbes (with aid of sulfur oxidizing bacterial activity – not shown) produces sulfuric acid, which further weathers the rocks releasing metals and nutrients.

Although taxonomic identification of the iron and manganese oxidizing isolates was not possible, SEM analysis of the colony morphology revealed well-known signatures of metal oxidizing microbes (putative *Leptothrix* sheaths and metal oxide stalk material) (Fig. 5.8 and 9).The identification of the iron hydroxyoxide mineral

Lepidocrocite in iron oxidizing colonies (Fig. 5.10), further supports that active iron oxidizing microbes have been isolated from ferromanganese deposits on weathered shale.

The importance of finding diverse microbial communities with multiple rock weathering capabilities is demonstrated in Figure 5.11 below, which has been adapted from a figure in Northup *et al.* (2000) that shows microbial rock weathering in ferromanganese deposits on calcite/dolomite cave walls (Northup *et al.,* 2000).

The inter-related activities of differing microbial metabolisms and activities helps to further feed rock weathering processes. An example of one such metabolism that has not been explored in this chapter is microbial sulfur oxidation. Upon the dissolution of pyrite by iron oxidizing bacteria, sulfur is released which can be subsequently oxidised to sulfuric acid (Pye and Miller, 1990). Although the ability of the isolates to oxidise sulfur has not been investigated directly, *Tetrasphaera* (organic acid producer) was identified in a sulfur-oxidizing enrichment medium that enhanced the dissolution of dolomite (Sonnleitner *et al*., 2011).Furthermore, *Flavobacterium* (organic acid producer) was a dominant organism in the pyrite-weathering produced gypsum crusts ($FeSO_4$) on weathered shale, indicating its potential involvement with the formation of the gypsum crust (Joeckel *et al*., 2005). The isolation and study of sulfur oxidizing organisms from the field sites sampled in this study would be a logical direction for future work.

The use of geochemical modelling, via software such as Geochemists workbench, is one way that future work could be focused. By combining geochemical and environmental data from sampling locations, the availability of nutrients and other growth parameters could be determined. This information would provide constraints on where best to isolate particular taxa (e.g. *Leptothrix*) or microbial functional groups (e.g. siderophore producers).

Chapter 6 - Ecophysiology of the shale ferromanganese deposit isolate *Variovorax paradoxus* YC1

6.1 Introduction

From a geomicrobiological perspective, shale can be considered to be comprised of three major constituent groups. The first is the mineral assemblage which is primarily formed from quartz, clays, feldspars and minor reactive minerals such as pyrite and calcite. The second is the organic material found within the rock matrix; 95 % of sedimentary organic matter (OM) is in the form of kerogen, large, recalcitrant macromolecular (>1 kDa) structures. The final group is the metal content of the shale, which is found both within mineral crystal structures and bound up with organic ligands such as porphyrins. Microbes interact with all three groups, and the focus of the following two chapters will be on microbe-metal (Chapter 7) and microbe-mineral interactions (Chapter 8). This chapter will focus on the isolation of an extreme low nutrient isolate, and how it grows and behaves under different carbon source regimes, including sedimentary OM.

Weathering of shale and other sedimentary OM has been extensively studied from a range of industrial and environmental standpoints. Aerobic degradation of OM releases CO_2, and so can act as a source for the global carbon cycle. With over 10^{20} mols of carbon locked in sedimentary rocks, it is one of the largest reservoirs of organic carbon on Earth, with a capacity greater than that of the planets oceans, soils or biomass. When OM is degraded anaerobically, methane and other low weight, volatile organic gases are released. This is the source of shale gas, which has huge commercial value and has been of increasing global interest in the 21st century as conventional fossil fuel sources continue to decline. Microbial activity is believed to accelerate the degradation of OM under both aerobic and anaerobic conditions. This activity has also been specifically indicated in another concern related to OM weathering, the release

of toxic organic compounds and heavy metals that can pollute the surrounding land and ground water.

The percentage content of OM within unweathered shale rock can vary from around 1 %percent to above 20 % (Petsch *et al*., 2001a), which has serious implications for the impact that OM weathering can have on shale rock structure and strength. Natural weathering of a Lias shale (the same stratigraphy of shale as sampled in the work of this thesis) outcrop in Germany resulted in 14 % mass loss of OM from the rock. Comparative analysis of the weathered and un-weathered rock revealed that weathering increased pore size and pore volume within the shale (Littke *et al.,* 1991). Weathering of OM in Marcellus shale in the USA was directly linked to this increase in porosity volume, with shales comprised of a higher OM content weathering more quickly than less organic rich rocks (Jin *et al.,* 2013).

Higher porosity in rocks is generally associated with decreased physical hardness and resistance to compression. The increase in pore number and volume assists in the propagation of stress-induced microfractures, increasing the opportunity for shale degradation and erosion (Koncagul *,* 1998). Bhattarai *et al*. (2006) studied the role of physical weathering on the slope stability of a mudstone outcrop. The authors make a direct link between physical weathering which increases porosity, and reduced shear strength properties of the rock and a reduction in slope stability (Bhattarai *et al.,* 2006). Although the role of chemical or biological weathering were not confirmed in this study, it is plausible that other mechanisms that also increase porosity would likely have a similar effect.

Chemical weathering of shale can reduce OM mass by 10-90 %, which has a significant impact on the rock's physical structure and strength (Matlakowska and Sklowdowska*,* 2010). It has been reported that chemical weathering of shale increases its external surface area, through the formation of macropores from the dissolution of OM (Fisher and Gaupp, 2005). Enhanced surface area has been identified in other shale weathering studies and promotes other weathering mechanisms, such as mineral dissolution and alteration (Jin *et al.,* 2013).

The extent of biological activity in shale OM weathering is poorly constrained, but numerous studies over the past 15 years have increasingly identified microbes as contributors (Petsch *et al.,* 2001b; Petsch *et al*., 2005; Wengel *et al*., 2006; Farbiszewska *et al.,* 2006; Haddadin *et al*., 2009; Matlakowska and Sklowdowska*,* 2010; Matlakowska and Sklowdowska 2011; Berlendis *et al*., 2014). The work of Petsch *et al*. (2001a) demonstrated for the first time that a microbial community grown on shale rock powder could assimilate carbon from rock bound kerogen. ^{14}C ratio analysis of phospholipid fatty acids identified that the microbial assimilated carbon came from a highly depleted C^{14} source, of which the rock-bound kerogen was the only possible source (Petsch *et al.,* 2001b).

The method by which microorganisms obtain carbon from shale derived kerogen remains poorly understood, although certain mechanisms that help to break small compounds off the macromolecule and others that increase the kerogen solubility have been indicated. The ability to catabolise polycyclic aromatic hydrocarbons (PAHs) has been cited as an important contributor to kerogen degradation (Matlakowska and Sklowdowska, 2011 ; Berlendis *et al*., 2014). Aromatic groups comprise part of the kerogenous structure and, if available to enzyme action at the surface of the molecule, can be cleaved by enzymes such as naphthalene dioxygenase (Vandenbrouke, 2003; Berlendis *et al*., 2014). Matlakowska *et al*. across several papers indicate that metal-binding porphyrin degradation is responsible for the release of copper, nickel and other transition metals in the biodegradation of black shale organic matter (Matlakowska and Sklowdowska, 2010;Matlakowska and Sklowdowska, 2011 ; Rajpert *et al*., 2013). The wood-rotting basidiomycete fungus *Schizophyllum commune* increased the release of metals from black shale through degradation of OM. The authors relate this degradation of shale OM as analogous with its ability to degrade wood through the release of exoenzymes such as peroxidases and laccases (Wengel *et al*., 2006). Biosurfactant production by *Rhodococcus* sp. grown on oil shale increased the amount of oil extracted combined with hydrogen peroxide pre-treatment of the rock by 26 % (Hadaddin *et al*., 2009). By reducing the surface tension between the rock and aqueous interface, the biosurfactants enable OM to become solubilised and available for

degradation. These identified mechanisms enable certain specialised microbial species to utilise kerogen, a non-hydrolysable, insoluble macromolecular structure that is highly recalcitrant.

The result of this biological action has a physical impact on the structure of shale derived kerogen. Microbial activity that degraded OM in Polish black shale resulted in qualitatively assessed increase in rock surface area with the surface morphology observed to become more open and fluffy (Matlakowska and Sklowdowksa, 2010). An increase in surface area has been associated with other chemical and physical weathering mechanisms, as previously highlighted (Fisher and Gaupp, 2005; Jin *et al*., 2013). Overall, this evidence suggests that microbes play an active role in the degradation shale OM, which in turn contributes to weathering and erosive processes in shale rock.

As stated in Chapter 1 (Section 1.4), previous work identified that heterotrophic organisms dominated the microbial community in weathered shale on the North Yorkshire coastline (Cockell *et al*., 2011). The results presented in Chapter 5 revealed 15 heterotrophic bacterial genera with rock weathering capabilities inhabited weathered shale from a range of sampled locations. Chapters 7 and 8 have attempted to quantify the mineral and rock weathering capacity of shale-inhabiting microbial communities both *in vitro* and *in situ*.

In this chapter, the adaptations of heterotrophic microbes to geological environments has been investigated. To fully comprehend the capacity of microbial weathering processes to contribute to rock weathering and erosion, an understanding of how microbes colonise rock surfaces, access nutrients and cope with environmental stress is required. Studies focusing on these points will enable geomicrobiologists to constrain factors limiting growth and activity in geological environments, and therefore provide upper and lower bounds on microbial weathering potential. The work presented here has characterised the ecophysiology of a single heterotrophic organism isolated from weathered shale, *Variovorax paradoxus* (strain name Yorkshire Coast 1, or YC1).

V. paradoxus YC1 was isolated from a low nutrient enrichment culture inoculated with weathered shale. A series of enrichment cultures were established, all lacking a easily accessible organic carbon source, but supplemented with crushed rock powder containing sedimentary organic matter. The aim of this enrichment work was to isolate organisms that could catabolise sedimentary organic matter from shale and other sedimentary rock types (section 6.2.2). When this process failed due to continued microbial growth in negative control cultures lacking added rock powder, individual isolates were identified using phylogenetic analysis (section 6.2.4). *V. paradoxus* was one of the organisms isolated, and was chosen for further study due to its known ability to catabolise a diverse array of recalcitrant organic compounds (Satola *et al.*, 2013). As a low nutrient isolate, it was expected that *V. paradoxus* would have numerous adaptations to survive in low nutrient geological environments, making it a suitable candidate for further experimentation.

The following central questions are addressed in this Chapter:

- What adaptations does *V. paradoxus* YC1have to access carbon in an organic carbon depleted environment?
- What stress responses does *V. paradoxus* YC1 use to cope with toxic geological materials?
- What factors influence the colonization of geological materials by *V. paradoxus* YC1?
- What nutritional and geological factors influence motility in *V. paradoxus* YC1?

6.2 Isolation of *Variovorax paradoxus* YC1– Methodology and Results

6.2.1 Field work and sampling

Samples were collected from a Hole Wyke mine adit which is dug into the cliff face near Boulby Head, roughly 1 km West along the foreshore from Staithes. The adit is part of a 17th – 19th century former alum working complex. For more details of this field site, see Chapter 4. Samples of ferromanganese crusts coating the shale walls and ceiling of the adit were collected using a sterilised rock hammer, with chips being collected in sterile whirlpak bags. These were kept at ambient temperature until they were taken to the lab, where they were stored at 4^{o} C for 2 months until use.

6.2.2 Sequential enrichment cultures – rock powder transfers

A volume of 5 mL of rock chips was suspended in 20 mL of minimal M9 medium (see Chapter 3 for media recipe) in 50 mL Falcon tubes and were incubated for 2 weeks at room temperature in a lit room under aerobic conditions. M9 medium (without glucose) was chosen because it lacked both a carbon and iron source, with the aim of enriching microorganisms that could utilise sources of these two nutrients from the material in the rock chips.

A set of enrichments were inoculated from this original enrichment, with various types of rock highly enriched in kerogens as the solid medium. Each rock type used (Table 6.1) contained differing types of kerogen (types I-IV, see section 2.1.3). The sedimentary organic matter contained in Redcar mudstone is kerogen type II, so the extent of type II and other kerogen type rocks could stimulate growth was the focus of this work.

Transfer enrichments (called transfers from hereon) contained 6 mL of minimal M9 medium, 400 mg of rock powder and 6 µL of inoculum from the enrichment culture. Cultures were grown in 15 mL glass vials with metal lids containing a rubber seal, and were incubated at room temperature in the dark. The different rock powders used in

these transfers are shown in Table 1 6.1. For more details on the lithology of these rock types and their kerogen content, see Chapter 2. A minimal M9 medium negative control (lacking rock) and sterile controls were run alongside the rock powder transfers. All conditions were set up in biological triplicate. After two weeks of culturing, growth was assessed via CFU/mL determination on nutrient agar.

Table 6.1¦ Characteristics of the rock types used in the cultures of transfer sets 1-6. Further information on kerogens can be found in Chapter 2. Vitrinite reflection (VRo %) is an index of thermal maturation of the rock during diagenesis.

Rock type	Sampling location	Kerogen Type	Total Organic Carbon (TOC) %	Extractable Organic Matter (EOM) %	Vitrinite reflectance (VRo %)
Mudstone (Redcar)	Hole Wyke mine adit, Boulby Cliff, Yorkshire	Type II	N/A	N/A	N/A
Lacustrine Shale	Port Edgar, West Lothian	Type I	13.43	0.08 %	0.9
Marine Shale	Monmouth Beach, Dorset	Type II	8.14	Below detection limit	0.6
Bituminous Coal	Daw Mill, Warwickshire	Type III	56.4	0.6	0.6

Growth in the M9 cultures lacking rock powder transfers were found to match those in the rock powder enrichments. This was surprising as M9 medium lacks both a carbon and iron source, so heterotrophic growth should not have been sustained. It was hypothesised that growth was being sustained by shale rock material from the inocula being carried over into the transfers. Shale readily breaks down to form sediment when immersed in water, so this sediment would have been transferred from the initial Redcar mudstone enrichment into the following rock enrichments.

In an attempt to enrich for microbial communities that could utilise the nutrients (primarily the carbon source) from the rock powders in Table 6.1, 10 µL aliquots of each transfer culture was used to inoculate fresh medium with the same set up (400 mg of the same rock powder, 6 mL M9). These transfers were then incubated under the same conditions for 2-4 weeks before the CFU/mL of the cultures were calculated and each of these transfers was subsequently used to inoculate a new set of transfers. This process was repeated four more times (six transfer sets in total). This whole experiment is displayed diagrammatically in Figure 6.1.

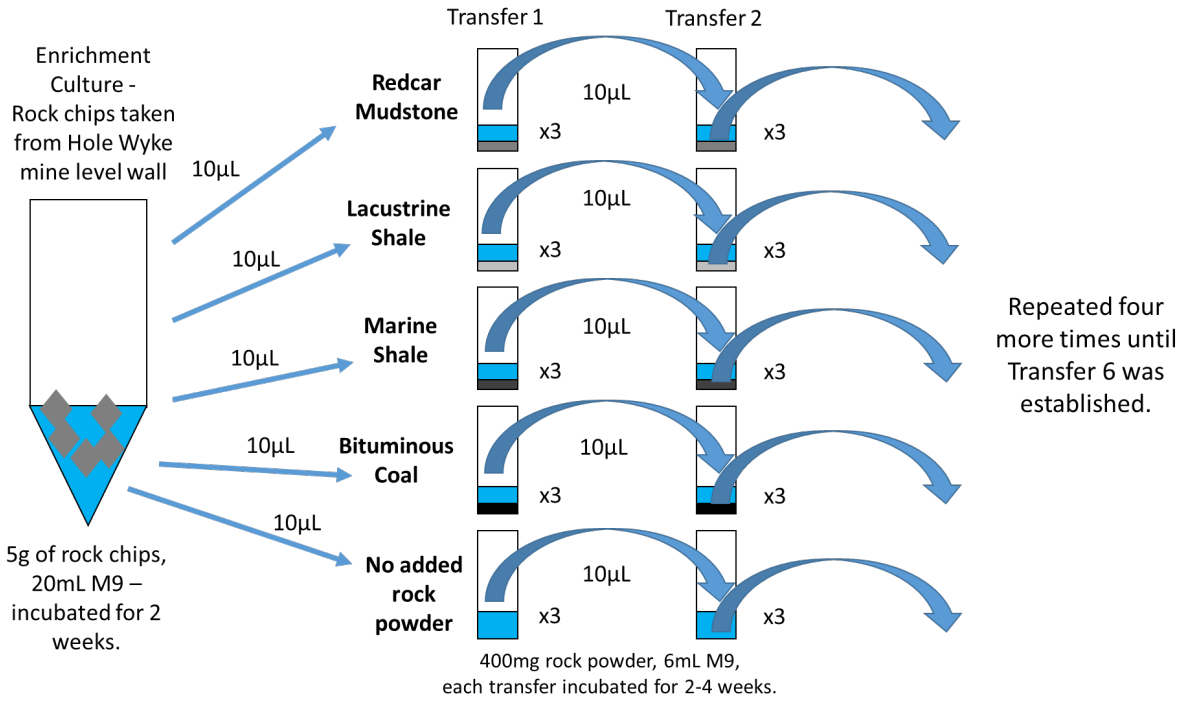

Figure 6.1¦ Establishment of a sequential series of transfer sets containing different rock powder types, from a weathered shale environmental enrichment culture. An enrichment culture of M9 medium with weathered rock chips was incubated for two weeks at room temperature and then used to inoculate transfer set 1. Transfer set one contained triplicate cultures of M9 (6 mL) and 400 mg of the following rock types: Redcar mudstone, lacustrine shale, marine shale and bituminous coal. These cultures were incubated for 2-4 weeks before being used to inoculate transfer set 2, identical in set up to transfer set 1 with transfer 1 cultures being used to inoculate corresponding transfer 2 cultures. This process was repeated until 6 transfer sets were completed.

By the end of these transfers, the original inoculum from the Hole Wyke enrichment culture had been diluted by 2.14 x 10^{-17}, yet CFU/mL numbers were still sustained in the negative control cultures. In the final transfer after two weeks of incubation, community growth reached 5 x 10^6 - 1 x 10^7 CFU/mL in the rock cultures and 6 x 10^6 CFU/mL in the M9 media lacking rock powder. This suggested that the microbial species present in these transfers were capable of growth in extremely nutrient limiting environments. Cultures from transfer set 4 were imaged using fluorescence microscopy (acridine orange staining) to determine if cells were growing on the rock surface (Fig. 6.2).

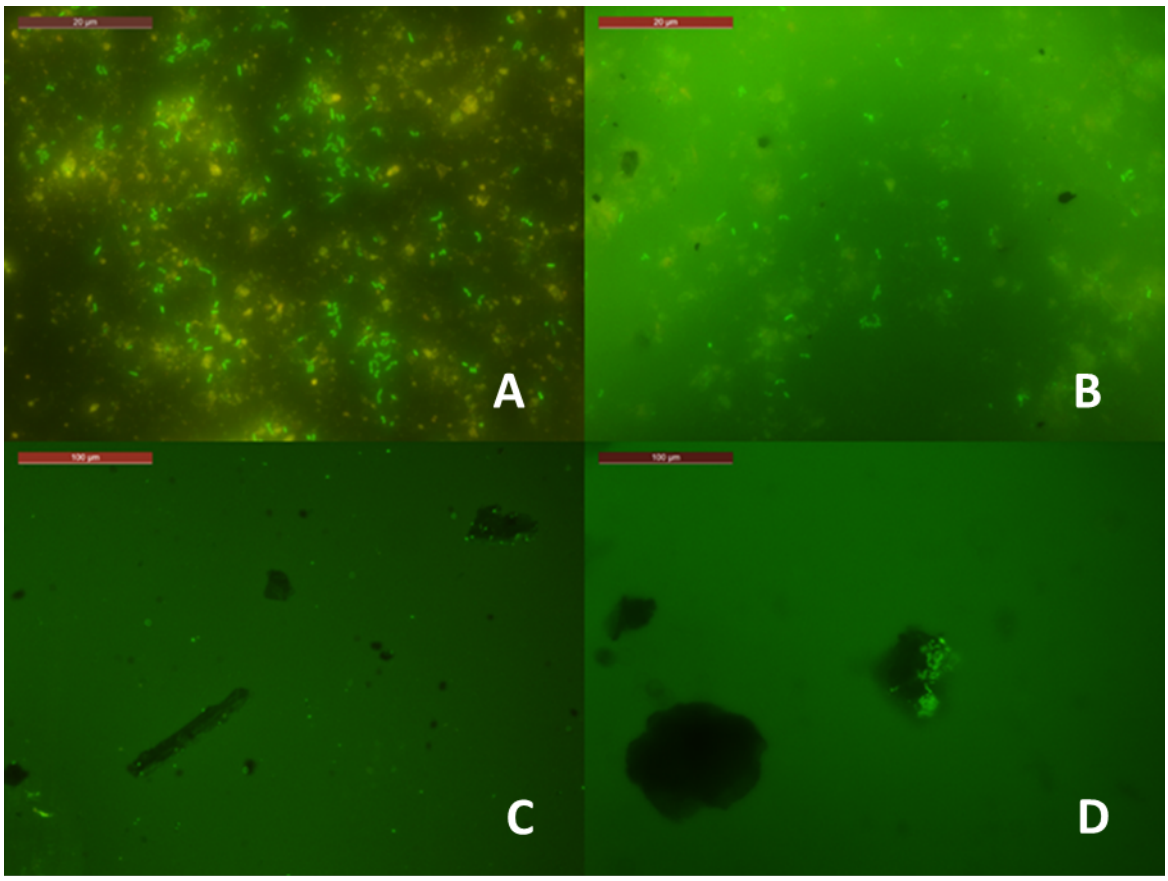

Figure 6.2¦ Photomicrographs of enrichment cultures on Redcar mudstone (A), lacustrine shale (B) and bituminous coal (C, D). Staining with acridine orange (0.1 mg/mL) for 2 hours. Scale bar is 20 µm for A and B, 100 µm for C and D.

Microscopy of the Redcar mudstone and the lacustrine and marine shales proved difficult due to high levels of non-specific binding and background fluorescence of the

dye. Other dyes were tried, including SYBR green, SYBR gold and DAPI, but none were an improvement on acridine orange. Cells growing in the Redcar mudstone and lacustrine shale cultures appeared to clump into small collections of cells (4-8 cells), with many other cells found in pairs connected at the polar ends. These singular, pairs or groups of cells were not found to attach to rock particles from the images obtained (Fig.6.2).

However, in bituminous coal there was clear evidence of preferential microbial attachment to the coal particle surfaces. Image D (Fig. 6.2) shows the attachment of a large collection of cells that have formed a microcolony on the surface of the coal particle. This indicates that the surface of these particles stimulates the growth of at least some of the species in this community. It is difficult however to infer a specific causation of this growth enhancement, as multiple factors could enhance the growth of specific species, including attachment to surfaces (Tuson and Weibel 2013). As such, the ability of the organisms to obtain nutrients, carbon or energy from the rock particles cannot be deduced from these images.

6.2.3 Attempt to determine carbon contamination in rock powder transfers

The sterile controls of each transfer set were all determined to be sterile by CFU/mL and microscopy cell count quantification, indicating that the growth found in the M9 without rock powder (putative negative control) had come from the inocula transferred between each new transfer set. This continued microbial growth suggested that the organisms were sustaining their growth by utilizing a carbon source that was contaminating the cultures. Dissolved carbon dioxide from the air in the culture vessel could be forming bicarbonate ions in the media, providing a carbon source if the organisms were autotrophic.

The only autotrophic metabolism possible under the conditions (chemical constituents of the M9 and the conditions of the incubation) was ammonium oxidation. When establishing transfer set 6, triplicate sets of transfer cultures were set up with M9 media containing either NH_4Cl, a mixture of NH_4Cl and $NaNO_3$, or $NaNO_3$ as nitrogen

sources. CFU/mL quantification of each these three sets revealed no difference in growth (data not presented) after 2 weeks of growth. This was taken as a lack of evidence for the autotrophic growth of the microbial community.

Organic carbon contamination of the cultures was hypothesised to be the only alternate possibility for carbon input into the cultures. In an attempt to eliminate this source of contamination, the following steps were taken in the next set of transfer cultures:

- Total organic carbon (TOC) free water, and new chemical reagents (Sigma-Aldrich) were bought at 99.9 % purity or higher and were used to prepare M9 media.
- All glassware, metal spatulas and tinfoil used to prepare media and establish cultures were baked at 500^{o} C for 5 hours to purge them of organic contamination.
- Plastic was used only where necessary such as plastic lids on Duran bottles for media storage and plastic pipette tips when aliquoting solutions.

6.2.4 Sequential enrichment cultures – blank media transfers

Following the organics contamination control procedures outlined in the section above, a new transfer set of cultures was established using one of the M9 medium without rock powder cultures from transfer set 6 as an inoculum. This new transfer set was comprised of the three following medium types: M9 + glucose (0.4 %), M9 and water. All three conditions lacked rock powder. Transfer set 7 and subsequent transfer sets (9-11) were conducted in the same manner as transfer sets 1-6 (Fig. 6.1).

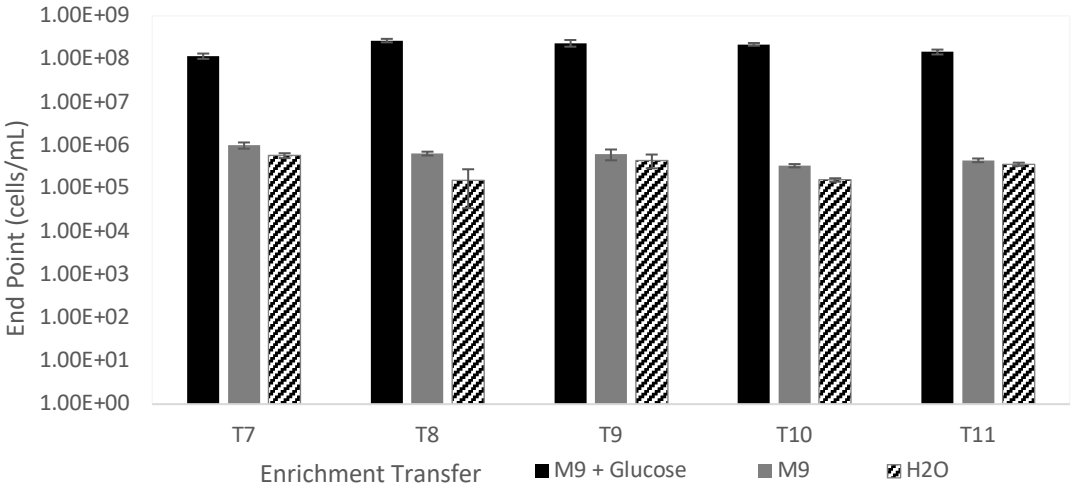

Figure 6.3¦ Mean growth (cells/mL) of microbial communities in the final five transfer enrichments (T9-T13) in three different medium types (M9+glucose, M9 and water) without rock powder. Biological replicates (N=3) were used for all conditions. Error bars represent standard error of the mean average.

The aim of this culturing work was to establish a reliable negative control, where growth would be observed in the M9 + glucose cultures, but would be absent in the M9 and water cultures.

The CFU/mL quantification of each of these transfer sets (7-11) can be seen in Figure 6.3. The growth supported in each of the transfers was consistent for each of the three medium types, with growth in the M9 + glucose cultures ($1 \times 10^8 – 5 \times 10^8$) being 2-3 orders of magnitude higher than growth in the M9 medium ($5 \times 10^5 – 1 \times 10^6$) and the water medium ($1 \times 10^5 – 5 \times 10^5$). These results suggest that in the M9 and water cultures sufficient organics were available for the microbial community to grow consistently in each transfer, meaning that a true negative control was not attained. Contamination of organic material into the liquid medium has therefore come from a source not previously accounted for.

The microbial species present in the M9 and water cultures were demonstrated to utilise nutrients, and specifically a carbon source, from an incredibly extreme nutrient poor environment (growth was sustained in TOC free water with no added nutrients). This capability is likely to be an adaptive advantage in the environment the organisms

were isolated from (weathered shale rock), where bioavailable carbon is likely to be limited.

To determine what bacterial genera were present in these extreme nutrient limited communities, the M9 and water cultures from transfer set 11 were plated out onto nutrient agar. A selection of colonies that grew were processed through colony PCR to amplify the 16S rDNA. The same cPCR protocol used in Chapter 5 was used in this investigation. Successfully amplified and sequenced 16S rDNA sequences were put through BlastN search to identify their similarity with published sequences. All isolates that sequenced with >97 % similarity with a published sequence can be seen in Table 6.2.

Table 6.2¦ Bacterial isolates identified by cPCR and subsequent 16S rDNA sequencing from enrichment cultures grown on M9 and water medium lacking rock powder.

M9 isolates	Water isolates
Microbacterium sp.	*Rhodococcus sp.*
Phyllobacterium sp.	*Variovorax sp.*
Pseudomonas sp.	
Rhodococcus sp.	

The isolation of *Microbacterium* sp., *Pseudomonas* sp. and *Rhodococcus* sp. were all genera identified from the phenotypic plate screening of weathered shale ferromanganese deposits carried out in Chapter 5. Finding them in the M9 cultures of the transfer set 11 indicates that these organisms have the ability to survive and grow in low nutrient environments, along with the additional characteristics previously identified (*Microbacterium* – Acid production, *Pseudomonas* – siderophore and phosphatase production, *Rhodococcus* – phosphatase production) (Chapter 5 Results).

However, of additional interest was the isolation of only two organisms from the water cultures of transfer set 11, *Rhodococcus* sp. and *Variovorax* sp. These organisms demonstrated survival and growth in an extremely nutrient limiting environment. Literature research revealed that both *Variovorax* sp. (Northup *et al*., 2000; Frey *et al*.,

2010; Collignon *et al.,* 2011; Sonnleitner *et al.,* 2011; Carmichael *et al.,* 2013) and *Rhodococcus* sp. (Haddadin *et al.,* 2009; Frey *et al.,* 2010; Cockell *et al*., 2013) have been previously associated with mineral and rock weathering environments. Both organisms also have been extensively studied for their abilities to utilise a wide array of organic carbon compounds in their metabolisms (Larkin *et al.,* 2005; Satola *et al.,* 2013).

It was decided to choose one isolate for further study. *Variovorax* was chosen due to its additional association with heavy metal contaminated environments (Belimov *et al*., 2005; Abou-Shanab *et al*., 2007), manganese oxidizing (Noguiera *et al.,* 2007; Yang *et al.,* 2013) and arsenic oxidizing (Macur *et al.,* 2004; Battaglia-Brunet *et al.,* 2006) communities. This indicated *Variovorax* as a possibly active metal cycling organism in weathered shale. Furthermore, from a practical standpoint, *V. paradoxus* colonies of the strain isolated have an iridescent sheen that makes them easy to identify on agar plates. The sequence analysis of the *Variovorax* isolates identified had up to 99 % similarity with the specific species, *Variovorax paradoxus*. Therefore, the strain of *Variovorax* identified in the study was designated *V. paradoxus* YC1 (Yorkshire Coast 1).

In the remainder of this chapter, physiological studies of *Variovorax paradoxus* YC1 will be presented and evidence for its adaptation to its geological environment explored.

6.3 *Variovorax paradoxus* YC1 experiments - Methodology

6.3.1 Basic physiology of *Variovorax paradoxus* YC1

6.3.1.1 Colony description

Variovorax paradoxus was identified under its current taxonomic classification in Willems *et al.* (1991). This paper also contains a description of *V. paradoxus* colony morphology and other information on the type strain.

Colonies of *V. paradoxus* YC1 were primarily cultured on nutrient agar (Sigma-Aldrich), where colony size was sufficient for CFU counting after 36-48 hours (~1 mm diameter). M9 agar containing 0.4 % glucose was also occasionally used to culture *V. paradoxus* (including motility plate assays); colonies grew at the same rate as those grown on nutrient agar.

Colony morphology varied between colonies cultured from the same liquid culture, plated onto the same agar plate. Colony types could be broadly characterised into two categories:

A) Golden-yellow, circular, convex, 0.8 - 1.5 mm diameter, slightly mucoid. The colony edge is either smooth at the base of the convex dome, or a flat "skirt" (~0.1 - 0.2 mm) protrudes from the convex dome base. The skirt edge is circular and smooth but could be slightly irregular. The skirt appears iridescent (like the colourful sheen seen on petrol) in colour when the colony is held up to the light, and can also display a slightly wrinkled texture.

B) Transparent, circular, flat, smooth edge, slightly irregular, 1 mm diameter, slightly wrinkled. The whole colony has an iridescent sheen. This colony looks like the skirt of colony type A, but for the whole colony surface.

Images of these colony types can be seen in Figure 6.4 in the results section 6.4.1.

6.3.1.2 Growth curves in M9+glucose, M9 and water media

A colony of *V. paradoxus* YC1 was suspended in 1 mL of sterile water and mixed until no lumps were present.

CFU/mL growth curves

A 50 µL aliquot of this solution was used as an inoculum for each 6 mL culture in 25 mL glass vials with tin foil lids (tin foil scrunched over the opening of the vial). All glassware and tinfoil used to set up the experiment was baked at 500^{o} C for 5 hours.

Triplicate cultures of three different medium types (M9 + glucose (0.4 %), M9 and water) were established. Each medium type was prepared with TOC free water and new stocks of the purest chemical reagents (99.9 % purity or as close to).

Cultures were incubated aerobically at 30° C. At 24 hour intervals each culture was plated out onto nutrient agar and the CFU/mL calculated for a total of seven days.

Optical density (OD 600) growth curves

A 50 µL aliquot was used as an inocula to inoculate separate 6 mL cultures of M9 + glucose (0.4 %), M9, and water.

These solutions were then aliquoted into a 96 well microtitre plate (180 µL aliquots), with three replicate wells. These plates were incubated without shaking at 30° C in a warm room, with OD 600 measured in a plate reader every 24 hours for four days. The plates were wrapped in parafilm during incubation to reduce evaporation.

6.3.1.3 Swimming and swarming motility

An overnight culture of *V. paradoxus* in M9 + glucose (0.4 %) media was grown and used as an inoculum for the following experiment.

Triplicate 30 mL solid medium plates were prepared with agarose of differing concentrations (0.3, 0.4, 0.5, 0.6, 0.7, 0.8. 0.9 and 1.0 %) in M9 + glucose medium. This set up was duplicated, with one set also being supplemented with 0.1 % casamino acids (CAA) and the other set lacking CAA. Plates were poured on an even surface and allowed to air dry until set. Care was taken not to over-dry the plates; as soon as the agarose had set the lids were placed on the plates.

A single five microlitre drop of inoculum culture was spotted into the centre of each plate and allowed to air dry. Plates were incubated face up at 30° C and the motile colony diameter measured after 72 hours. A distinction was made between the colony edge and the surfactant edge, as described in Jamieson *et al*. (2009). The plates were then incubated for a further 3 days before photographing.

6.3.1.4 Growth under extreme nutrient limitation – utilization of rubber

A culture of *V. paradoxus* YC1 was prepared in 50 mL of M9 media, with a 5 µL inoculation from a 25 % glycerol stock and incubated for 1 week. A higher dilution (1:10,000) was chosen to reduce the amount of organic material (glycerol) that would be transferred to the experimental cultures.

This culture was used to inoculate the experimental cultures (1:1000). The same basic protocol outlined in 6.3.1.2. was followed. Four different conditions were established in the three medium types (M9 + glucose, M9 and water):

- Chunk of butyl rubber (¼ of a lid seal) added to the vial, capped with a metal lid containing a rubber seal – Rubber Lid, Rubber Chunk (RL-R).
- Butyl rubber chunk not added, capped with metal lid with rubber seal (RL-NR).
- Butyl rubber chunk added, capped with a scrunched tin foil lid (TFL-R).
- Butyl rubber chunk not added, capped with a scrunched tin foil lid (TFL-NR).

All conditions were carried out in triplicate, with samples incubated at 30°C for 7 days. Cultures were plated onto nutrient agar after 1, 2, 5 and 7 days to determine CFU/mL at those time points.

6.3.1.5 Growth under extreme nutrient limitation – polyhydroxyalkanoate storage

Polyhydroxyalkanoates (PHA) are a group of organic polymers that can be used by bacteria for intracellular carbon storage. PHA is usually stored in granules, which can be visualised by fluorescence staining and microscopy (Lee *et al*., 1991). A 1µg/mL Nile Red dye dissolved in ethanol was used to stain an aliquot of the *V. paradoxus* YC1 inoculum culture used in section 6.3.1.3. (final Nile Red concentration – 0.1 µg/mL). A series of culture dilutions into PBS were carried out to obtain optimal cell density; these dilutions were stained in the same manner. All cell solutions were allowed to stain for 30 minutes in the dark. Cells were observed under fluorescence microscopy with the I3 filter (450-490 nm excitation wavelengths).

6.3.1.6 Growth curves of *V. paradoxus* on M9 medium containing Naphthalene

A 25 % glycerol stock of *V. paradoxus* YC1 was used to inoculate a water medium culture (1:1000), which was grown for 3 days at 30° C. An aliquot of this culture was then used to inoculate a fresh water culture (1:1000), which was incubated for a further 3 days. This second water culture was then used to inoculate the main experiment. This

was done to starve the cells, with the aim of reducing the amount of intracellularly stored PHAs that could alter the use of carbon by cells in the main experiment.

The basic set up outlined in 6.3.1.3. was followed, but the experiment was only conducted in M9 + glucose and M9 media. Three conditions in each media type were established: Media supplemented to contain 0, 100 or 1000 µg/L Naphthalene. Each condition was established in triplicate and incubated at 30^{o} C for 4 days.

Cultures were plated onto nutrient agar at 24 hours intervals to determine CFU/mL at those time points.

6.3.2 Ecophysiology of *Variovorax paradoxus* YC1 in geological environments

6.3.2.1 Growth on Redcar mudstone powder

Crushed Redcar mudstone was size fractionated to 250-500 µm. Four hundred milligrams of rock powder was added to 3 mL of water, which was then autoclaved at 121 ^{o}C for 20 minutes. This formed a hydrothermal extract of the rock powder. Three millilitres of a 2x M9 media solution was then added to the hydrothermal extracts to produce a 6 mL M9 medium.

This was carried out in triplicate, with an additional triplicate control M9 samples that were not hydrothermal extracts and did not contain rock powder.

These cultures were inoculated with a water culture prepared in the same manner as described in 6.3.1.6. (2nd water culture). The basic set up of the experiment (baked glass vials with tin foil) described in section 6.3.1.3. was used for this experiment.

Cultures were incubated at 30^{o} C for 5 days and were plated onto nutrient agar after 1, 2, 3 and 5 days to determine CFU/mL.

6.3.2.2 Mineral and rock colonization

Samples of the following minerals/rocks were prepared: albite, calcite, jet, muscovite, pyrite and quartz as detailed inChapter 3. . Two sample cubes of each rock/mineral type were inundated in 10 mL of M9+glucose, but at an altered glucose concentration

of (0.004 %). A 10 µL inoculum was added to each tube; the inoculum culture was an overnight M9+glucose culture of *V. paradoxus* YC1 grown from an M9+glucose glycerol stock. Lids were loosely screwed onto the tubes and were wrapped in parafilm to allow gaseous exchange, but to reduce evaporation. The cultures were incubated for 5 weeks at 30^{o} C. After this period, cubes were removed from the culture and washed twice in PBS, before being fixed in a 2.5 % glutaraldehyde PBS solution and stored at 4^{o} C until analysis.

One of the duplicate samples was removed from the glutaraldehyde solution and washed in PBS. They were stained with 10 µg/mL acridine orange for 10 minutes before imaging with the use of a Leica microscope using an I3 filter (450-490 nm excitation wavelengths). Counts were done manually for the quartz, whereas counts for the jet were done manually and by using the "Analyze Particles" function in ImageJ.

The other sample was prepared for SEM analysis by removal from the glutaraldehyde solution and then put through a chemical drying process. See Chapter 3 for more details on chemical drying and use of the SEM.

6.3.2.3 Growth of *Variovorax paradoxus* YC1 in liquid medium with shale and coal powder

A *V. paradoxus* YC1 water culture (2nd culture, as described in section 6.3.1.6.) was set up to use as an inoculant for this experiment. The basic set up of the cultures in this experiment is outlined in section 6.3.1.3.

For cultures containing rock powder in this experiment, the protocol described in section 6.3.2.1 was followed but only 150 mg of rock powder was used per 6 mL total volume culture. For cultures containing rock treated medium (referred to by TM), aqueous hydrothermal solutions were filtered (0.22 µm) and mixed with 2x M9 media to make the final growth medium (50:50 mix of 2x M9 media and rock treated medium). The following conditions were set up in triplicate: shale rock with M9+glucose, shale rock with M9, coal with M9+glucose, coal with M9, shale rock TM with M9+glucose, shale rock TM with M9, coal TM with M9+glucose, coal TM with M9, M9+glucose and M9.

Cultures were incubated for 4 days, with CFU/mL data being collected daily by plating onto nutrient agar. Plates were incubated for 48 hours and colonies counted, distinguishing between colony morphology types and recording the frequency of each type. Fluorescence microscopy imaging of coal cultures was obtained by staining with 10 µg/mL acridine orange and the use of a Leica microscope using an I3 filter (450-490 nm excitation wavelengths).

The experiment described in the above section was duplicated without a biological inocula, but otherwise treated the same and incubated for 4 days at 30° C. Both the inoculated and sterile medium ± rock powder preparations were filter sterilised (0.22 µm) after 4 days. Emulsions were prepared from the filtered supernatant, with 3 mL of hexadecane mixed with 3 mL of the supernatant in 15 mL Falcon tubes by vortexing for 1 minute. The mixtures were then assessed for emulsion formation (bubbles at the oil-water interface) after 30 minutes and 24 hours.

An aliquot of filtered supernatant was also analysed using a pendant drop tensiometer, allowing the interfacial surface tension (IFT mN/m^2) to be calculated for culture supernatants that produced emulsions. Further details of the methodology used in this analysis can be found in Chapter 3.

6.3.2.3 Growth and motility of *Variovorax paradoxus* YC1 on agarose plates with varying media and rock powder composition

A 25 % glycerol culture was inoculated 1:1000 into M9+glucose media and incubated for 2 days at 30° C. This culture was used to inoculate the main experiment.

The following agar types were prepared in both M9+glucose and M9 media: no rock powder, added shale rock powder, and added coal rock powder.

Shale and coal solutions of 0.1 g/30 mL of water were prepared and pH adjusted to pH 6.9-7.1 using NaOH and HCl, before being autoclaved. A large aqueous solution of 1.4 % agarose was also autoclaved. Both autoclaved solutions and a 5x M9 stock solution were warmed in a water bath to 60° C. These components along with $MgSO_4$ and $CaCl_2$ solutions (with or without glucose added) were mixed to produce a 0.01 g/L rock powder, 1x M9, 0.7 % agarose solution (and 0.4 % glucose if added). These were

poured to a total volume of 25 mL in petri dishes on a flat surface and were air dried until the agarose had set.

Plates were inoculated with single 5 µL spots of culture in the centre of the plate and allowed to air dry. Plates were sealed with parafilm to reduce evaporation and incubated face down at 30^{o} C on a flat surface for three days where upon colony diameter was measured. Plates were photographed after another 2 days of incubation.

6.4 *Variovorax paradoxus* YC1 experiments – Results and Discussion

6.4.1 Basic physiology of *Variovorax paradoxus* YC1

Liquid culture of *V. paradoxus* YC1 was plated and grown on nutrient agar to discern colony morphology (Fig. 6.4). Colonies could be broadly split into two categories, those that had smooth edges (A) and those that had a protruding flat outer skirt from the main colony edge (B). Three distinct forms of colony type B were also identified. Description of these four colony types (A, B1, B2 and B3) can be found below. Colony size is given as a mean average with standard error). A) 1.25±0.08 mm, golden yellow, opaque, round, smooth edge and convex, B1) 0.85±0.06 mm, golden yellow, central convex peak surrounded by a thin, flat outer skirt, convex peak opaque; flat skirt transparent, round, irregular edge, B2) 1.8±0.09 mm, larger than type A but morphologically similar to B1 but with an incomplete skirt surrounding the colony, skirt more of a bleb from the colony, B3) 1.1±0.06 mm, colourless, transparent, flat, round, irregular edge.

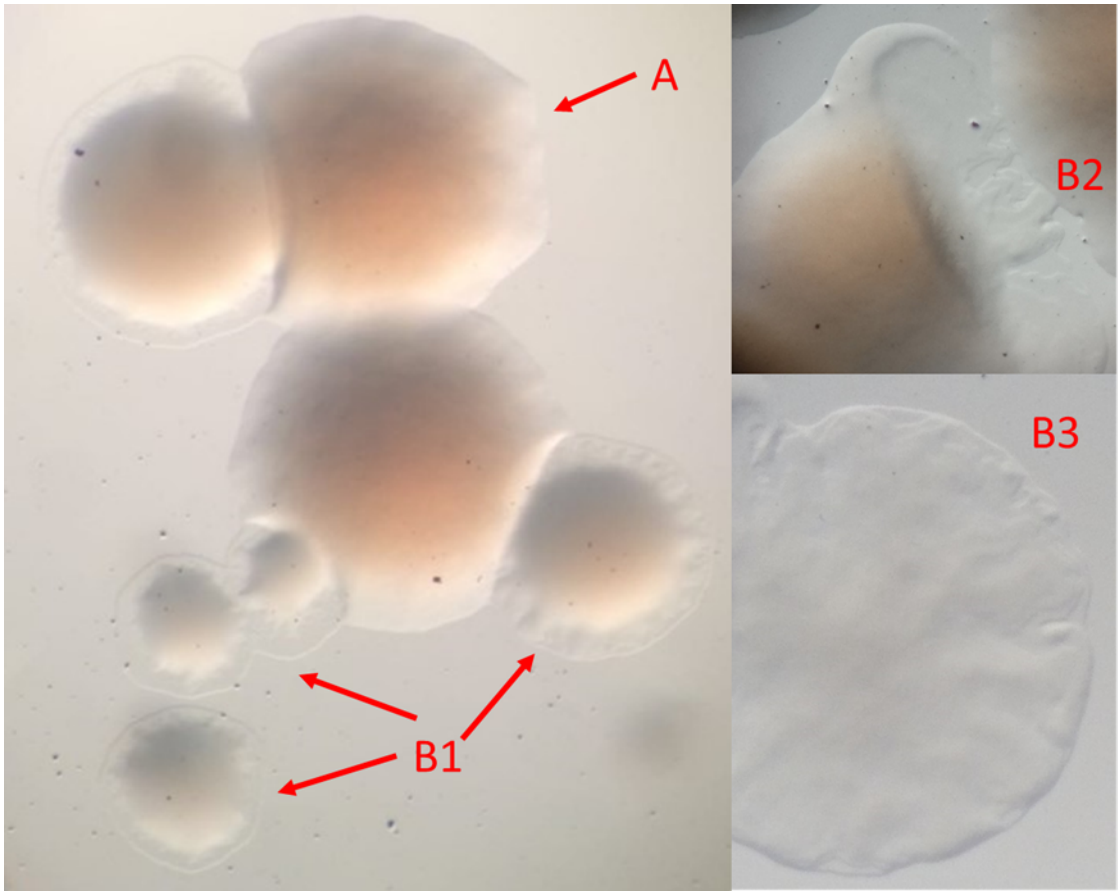

Figure 6.4¦ Colonies of *V. paradoxus* YC1 on nutrient agar with differing morphologies after 2 days of growth on the agar (red labels A-D). The average size of these colonies were 1.25±0.07mm for A, 0.85±0.06mm for B1, 1.8±0.09mm for B2 and 1.1±0.06mm for B3.

6.4.1.1 Growth curves in M9+glucose, M9 and water media

Growth curves of V. paradoxus YC1 in water, a minimal medium both with (M9 + glucose) and without (M9) an organic source was determined.

The CFU/mL and OD600 growth curves of *V. paradoxus* YC1 over 7 and 4 day periods respectively can be seen respectively in Figures 6.5 and 6.6.

The optical density measurements for the M9 + glucose cultures did not produce a reliable growth curve, with growth after 4 days producing an OD600 value above 0.025 (Fig. 6.6), however the absorbance values were much lower than that of commonly used laboratory organisms. Optical density absorbance did not work for the M9 and water cultures, where reliable OD values above those of the sterile control

media was not recorded (Fig. 6.6). The low optical density of *V. paradoxus* strains has been observed previously, with growth of an arsenic transforming strain on R2A media after 36 hours producing a medium OD600 value of 0.03 (Macur *et al*., 2004).

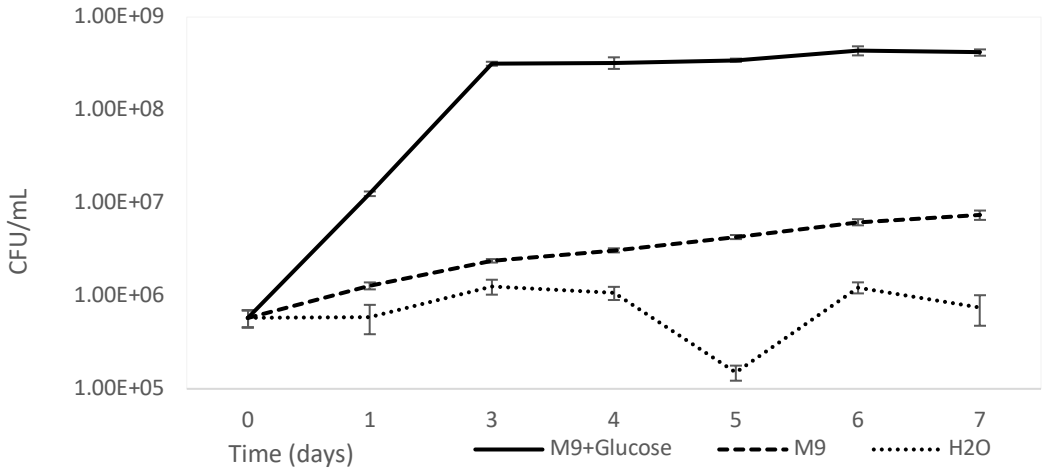

Figure 6.5¦ Growth curves (CFU/mL) of *Variovorax paradoxus* YC1 in M9+glucose, M9 and water media.Biological replicates (N=3) were used for all conditions. Error bars represent standard error of the mean average.

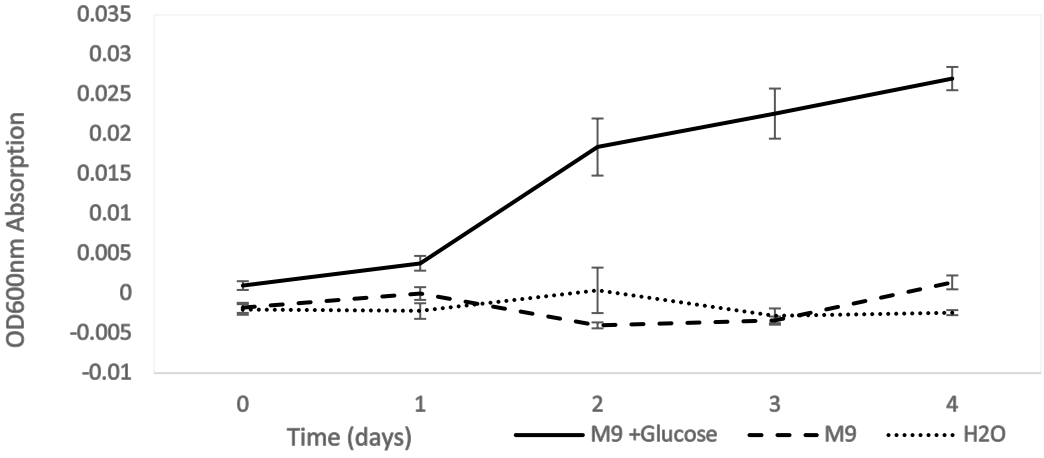

Figure 6.6¦ Growth curves (OD 600) of *Variovorax paradoxus* YC1 in M9+glucose, M9 and water media. Biological replicates (N=5) were used for all conditions. Error bars represent standard error of the mean average.

The growth of *V. paradoxus* YC1 in M9 was observed in the CFU/mL calculations (Fig. 6.5), but was not seen in the OD600 measurements (Fig. 6.6). This suggests that

for media that induces only slow growth in *V. paradoxus* YC1, optical density is not an accurate method for growth quantification.

Estimation of growth in both methods identified that *V. paradoxus* YC1 grew more readily in the M9 + glucose media, reaching ~5 x 10^8 CFU/mL by the time the culture had reached stationary phase (Fig. 6.5). Analysis of both the CFU/mL and the OD600 growth curves reveals that the exponential phase of *V. paradoxus* YC1 growth is between 1-3 days, which is supported by the growth curves of experiments described later in this chapter, where the exponential phase appears between 24-48 hours (Fig. 6.10, 6.12, 6.26).

Growth of *V. paradoxus* YC1 in M9 media did not appear to have a distinctive sigmoidal growth curve, with growth being steadily maintained across the 7-day incubation period. Growth in water was not observed in this experiment, with the CFU/mL values being stable across the incubation period (Fig. 6.5). The lack of a distinct sigmoidal growth curve was also observed by Macur *et al*. (2004), with growth in a minimal medium (R2A) also producing a steady rate of growth between 5 and 36 hours of incubation (Macur *et al*., 2004).

6.4.1.2 Swimming and swarming motility

The motility of *V. paradoxus* strains has been investigated in two previous studies (Jamieson *et al*., 2009; Pehl *et al*., 2012). Its ability to swarm on the surface of agar was characterised, and genetic factors that enable this capability identified. Casamino (CAA) acids is a common constituent of swarming motility agar recipes (Caiazza *et al*.. 2005), and is included in the agar recipes used in the cited *V. paradoxus* motility studies. Amino acids are normally required to induce swarming in motile species, and as such CAA (an undefined mixture of amino acids) is often used to supply this need (Köhler *et al*., 2000).

Agar or agarose concentration is also well known to control the mode of motility in species that can swim and swarm. Swimming motility is where single cells swim through liquid filled connected pore spaces within the agar. Swarming motility is where specialised cells (elongated, hyperflagellated and cells aggregated in rafts) move across the surface of the agar. Optimal agar/agarose concentrations for swarming

motility varying between 0.5-0.8 % depending on species (Harshey and Matsuyama, 1994), whereas swimming motility typically occurs at lower concentrations (<0.4 %) (Köhler *et al*., 2000).

In this experiment, the effect of agarose concentration and the addition of CAA to the solid medium on the motility of *V. paradoxus* YC1 was investigated.

Increasing agarose concentration in the solid medium proportionally reduced colony size after 72 hours in the absence of CAA (Fig. 6.7). Colony diameter was reduced by over 4 fold (>20 mm to <5 mm) between 0.3 and 1.0 % agarose concentration. This is in stark contrast to the solid media with 0.1 % CAA added. Reduction of agarose concentration from 1% did not increase colony diameter; colony diameter remained ~5 mm regardless of agarose concentration in the presence of 0.1 % CAA.

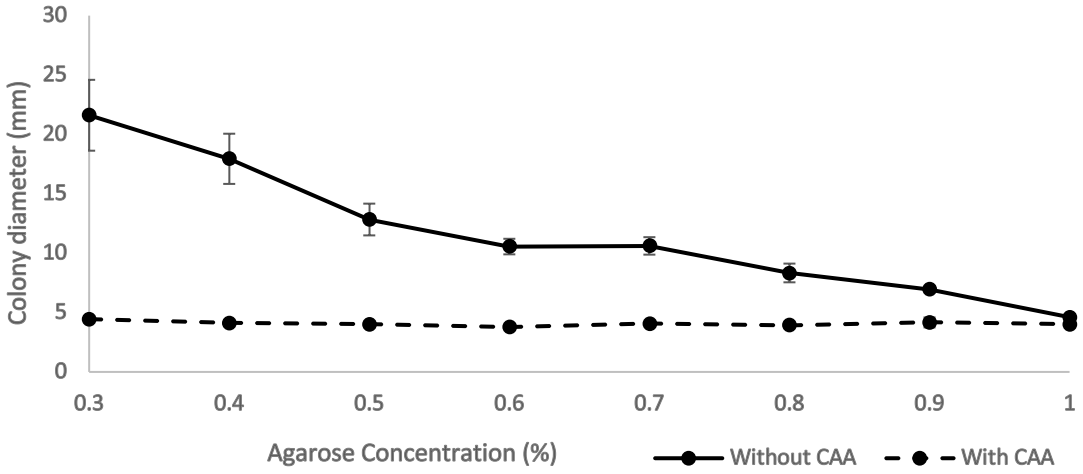

Figure 6.7¦ Colony diameter of *V. paradoxus* YC1 swarming and swimming colonies after 72 hours of growth (from a 10 µL spot in the centre) on M9+glucose agarose gel plates at varying agarose concentration (0.3-1.0 %). The dash line is for gel plates amended with 0.1 % casamino acids (CAA), whereas the solid is without amendment. Biological replicates (N=3) were used for all conditions. Error bars represent standard error of the mean average. Error bars are present for all data points, but are small enough to be hidden at some points.

Photographs of the colonies after 6 days revealed that at lower agarose concentrations (0.3-0.5 %) the cells were swimming through pores in the agarose, whereas at higher concentrations (0.6-1.0 %) they were swarming over the surface (Fig. 6.8, images A

and B). Swimming colonies were determined by two observations a) clearer agarose lacking turbidity, an indication of biomass absence, in the centre of the plates (Fig. 6.8A), and b) the lack of visible colony edge on the surface of the agarose, indicating that the biomass is not on the surface. Swarming colonies in contrast lacked this central clear zone and displayed visible surface texture and a colony edge on the surface (Fig. 6.8B). The insert image on Figure 6.8B shows the outline of the colony edge more clearly. The reduction in colony size by the presence of 0.1% CAA can be seen clearly between images B and C in Figure 6.8.

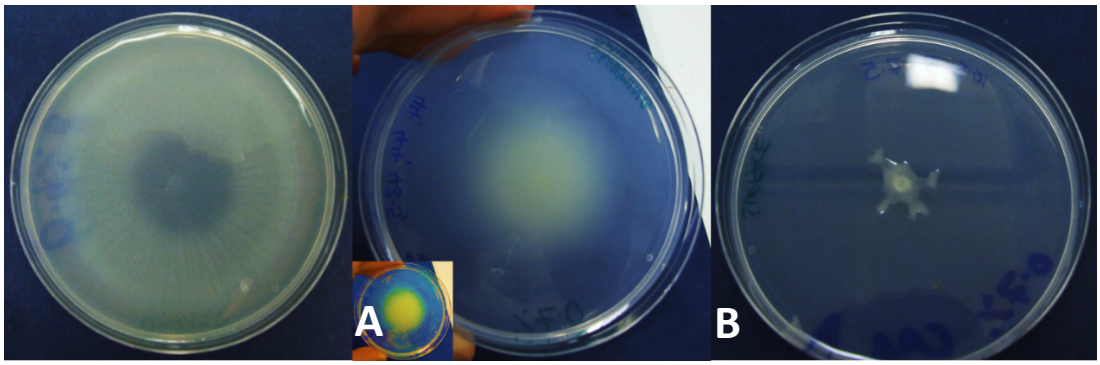

Figure 6.8¦ Images of *V. paradoxus* colonies (from Fig. 6.5) after 6 days of growth. A) is 0.4 % agarose without CAA, B) is 0.7 % agarose without CAA and, C) is 0.7% agarose with CAA (0.1 %). The insert on image B is a smaller copy of image B, with the colours inverted to make the colony outer edge clearer.

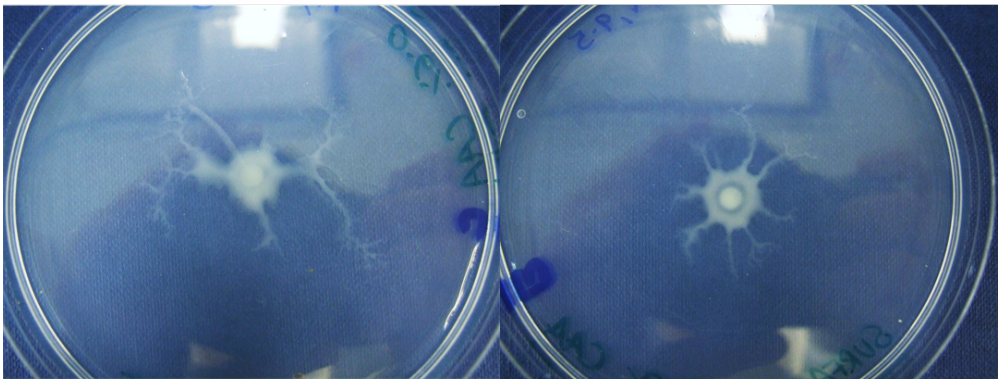

Figure 6.9¦ Images of dendritic *V. paradoxus* colonies (from Fig. 6.5) after 6 days of growth. Both images are from agarose gel (0.6 %) plates amended with CAA (0.1 %).

The presence of 0.1 % CAA in the solid media had a marked impact on colony morphology (Fig. 6.9). Colonies had a central spot of dense growth where the

inoculum spot had dried, surrounded by a small ring of growth with dendritic tendrils radiating from the colony in numerous directions.

These results indicate that the addition of CAA to both agarose medium had a significant impact on *V. paradoxus* YC1 growth and behaviour. The presence of growth on the surface of the plates at all agarose concentrations indicates that CAA inhibited swimming motility, and stimulated a swarming phenotype (Fig. 6.9). Jamieson *et al*. (2009) identified that CAA was the most important component of their swarming medium to induce swarming behaviour in *V. paradoxus* EPS. They observed the use of CAA as a carbon source on M9 swarming media resulted in greater colony diameter after 24 hours compared to other carbon sources (including glucose, succinate and malic acid). The addition of different single amino acids to swarming media as the sole nitrogen source (rather than a mix of amino acids in CAA) induced differing swarming patterns and extents of colony size in *V. paradoxus* YC1 (Jamieson *et al*., 2009). This is in stark contrast to the results presented in this chapter for *V. paradoxus* YC1, where the addition of CAA significantly reduced colony size after 72 hours (Fig. 6.7).

The source environment for these two strains could explain this difference in behaviour. *V. paradoxus* EPS was isolated from a plant root rhizosphere environment, where amino acid rich exudates are released by the plant (Jamieson *et al*., 2009). The authors suggest it is this environmental stimuli which could trigger swarming motility. *V. paradoxus* YC1 in contrast was isolated from a rocky environment that is likely to be relatively nutrient poor. If motility is considered as an adaptive behaviour to seek more nutrient rich environments than where the organism currently finds itself (either direct chemotaxis or induced motility) (Kearns, 2010), then CAA may act as a repressor of motility in *V. paradoxus* YC1. The detection of amino acids, which can act both as a carbon and nitrogen source, might indicate to *V. paradoxus* YC1 that it should remain in its nutrient rich environment.

Swarming has been identified as a social behaviour in other bacterial species, a phenomena often linked to biofilm formation and virulence in pathogenic species which can be stimulated by quorum sensing molecules such as N-acylhomoserine lactone (AHL) molecules (Daniels *et al*., 2006). CAA enhanced biofilm formation

more than nine other carbon sources tested in *V. paradoxus* EPS, suggesting that CAA likely induces multiple responses in *V. paradoxus* behaviour dependent upon cell state (planktonic/surface attached, motile/non-motile) (Jamieson *et al*., 2009).

6.4.1.3 Growth under extreme nutrient limitation – utilization of rubber and PHA storage

The ability of *V. paradoxus* YC1 to grow in an extreme nutrient limiting environment (TOC free M9 in organics purged glassware – Fig. 6.5) suggests that this organism is obtaining carbon from an unconventional source to enable its growth. It was hypothesised that the butyl rubber in the seal of the metal lid used to cap the glass vials used in previous experiments could be a source of carbon. An experiment investigating the effect of butyl rubber on *V. paradoxus* YC1 growth was therefore carried out (Fig. 6.10).

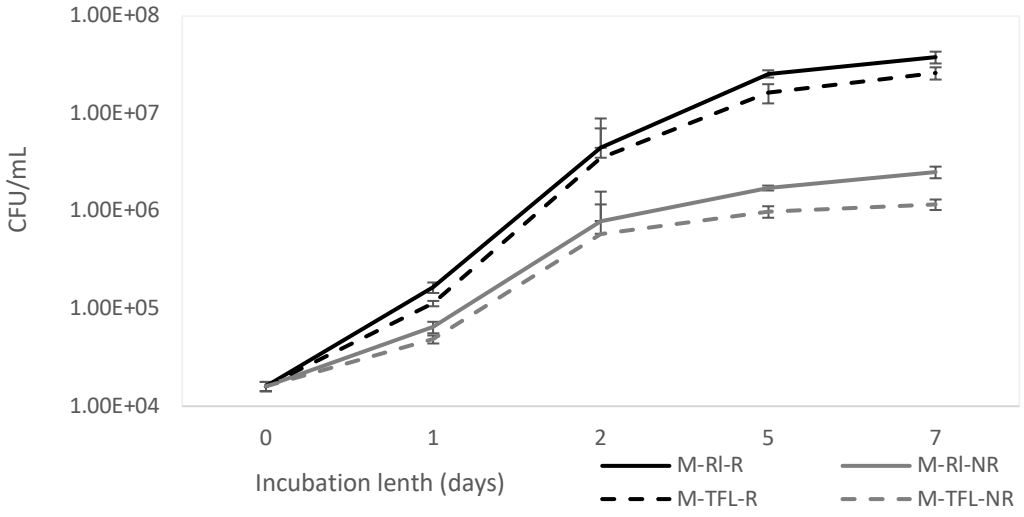

Figure 6.10¦ Growth curves (CFU/mL) of *V. paradoxus* YC1 grown in M9 medium in 15 mL serum vials covered either with a metal lid with a rubber seal (Rl) (solid line) or with a tin foil lid (TFL) (dashed line). This experiment was duplicated, with a quartered rubber seal either added to the liquid medium (R) (black lines) or not added (NR) (grey lines). Biological replicates (N=3) were used for all conditions. Error bars represent standard error of the mean average.

Growth of *V. paradoxus* YC1 was significantly enhanced by the addition of a rubber chunk (R) to the M9 liquid medium by over an order of magnitude (Fig. 6.10). This

was true for cultures capped with both a metal lid with a rubber seal (RL) and a tin foil scrunched lid (TFL).

Although not as pronounced, the capping of the culture vials with a metal lid containing a rubber seal increased the growth of *V. paradoxus* YC1 in both the presence and absence of an added rubber chunk. However, this result was only statistically significant in the absence of the rubber chunk (day 7, Mann-Whitney U test, Z=3.31, P=0.0009).

Definite growth in the M9 cultures with a tin foil lid lacking an added rubber chunk indicates that *V. paradoxus* YC1 grew in the absence of any added carbon source in M9 medium (Fig. 6.10). This suggests that although rubber may be supporting some of the growth in the cultures in this experiment, and in previous experiments, it is not the sole source of carbon for these cultures. No previous studies have identified that any strain of *V. paradoxus* can utilise butyl rubber. However, Zaitsev *et al*. (2007) identified that *V. paradoxus* CL-8 could degrade methyl tert-butyl ether ($(CH_3)_3COCH_3$), a compound that is structurally similar to the butyl rubber monomer isobutene ($C_2C(CH_3)_2$) (Zaitsev *et al*., 2007).

A potential source of carbon in these cultures, not taken into account in the methodology used in this experiment, is from the air within the laboratory environment that these cultures were established and incubated in. Carbon exists as fine particulate aerosols in the air of Northern Europe, being produced from a range of processes including transportation, industry and natural sources. This carbon can be found in elemental forms such as graphite and in organic forms such as oxalate. Graphite or black carbon is primarily formed from fossil fuel combustion, and so is most prevalent in urban environments. Organic molecules such as oxalate and levoglusan can come from a variety of sources including fossil fuel combustion, but also from biomass burning and biogenic sources; these two organic molecules were found at 0.088 and 0.064 $\mu g/m^3$ respectively in the air of Helsinki, Finland (Saarikoski *et al*., 2008).

Cell carbon mass is highly dependent on cell volume and species, but it is commonly accepted that 50 % of microbial dry biomass is carbon. If we take the cell biomass of *Escherichia coli* which has similar cellular dimensions to *V. paradoxus* (E. coli – 0.5 x 2 μm, *V. paradoxus* - 0.5 x 1.2-3 μm) (Willems *et al*., 1991), then each cell has 0.35

pg of carbon. In this experiment, 6.9 x 10^6 cells were grown (CFU taken as 1 cell here) in the M9 culture lacking rubber with a tin foil lid over 7 days, which would have required 2.4 µg of carbon just for the biomass (additional carbon would be required for energy). To provide this amount of organic carbon from oxalate and levoglusan from would require all of the organic molecules from 15.8 m^3 of air (Helsinki air) to dissolve in each culture. The head space in the glass culturing vials used is 9 cm^3, suggesting that although organic carbon from the air might sustain some growth of *V. paradoxus* YC1 in these experiments, it seems unlikely that this solely explains the growth observed in the absence of an added carbon source.

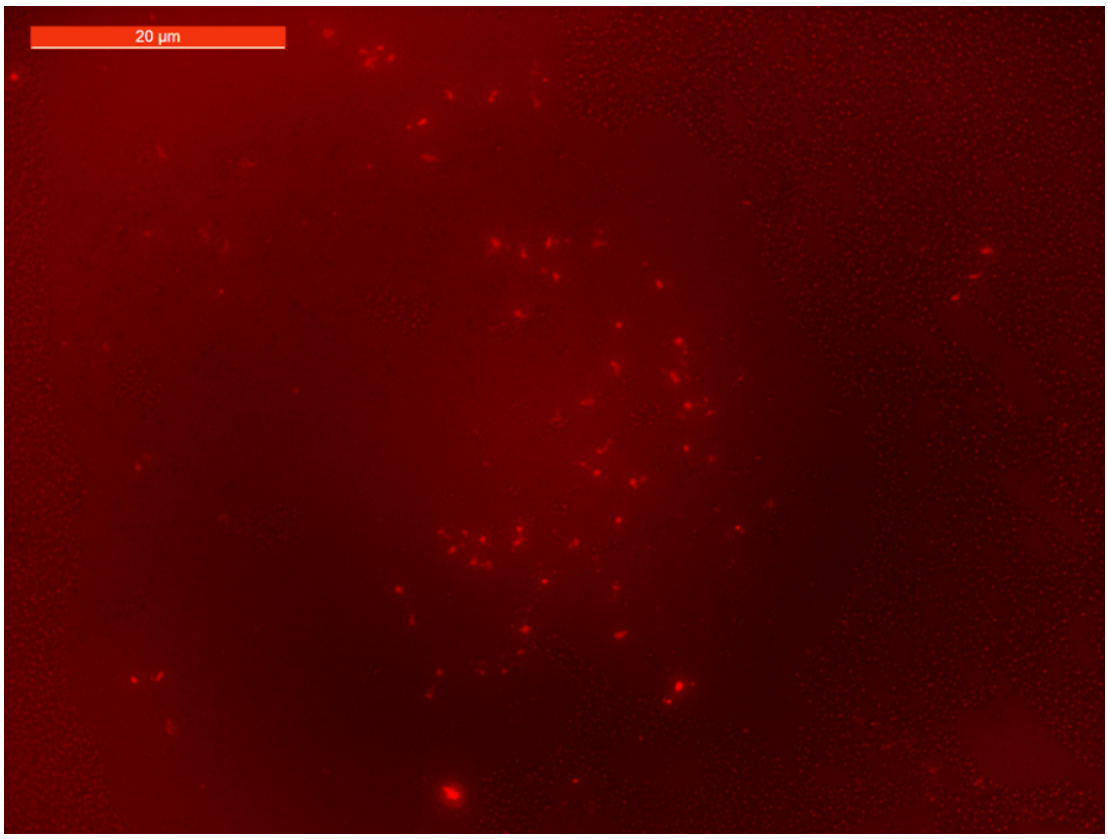

Figure 6.11¦ *V. paradoxus* YC1 cells grown in M9+glucose for 7 days, stained with Nile Red (0.1 µg/mL). Fluorescing cells are those that are storing polyhydroxyalkanoates (PHA).

Polyhydroxyalkanoates (PHAs) are carbon storage compounds stored in intracellular granules within certain species (Reddy *et al*., 2003). Organisms store this carbon source when nutrient supply is abundant, and then break down the stored PHA when

carbon is scarce. Nile Red staining can used to determine if cells are storing PHA (Jendrossek *et al.,* 2007)

Cells of *V. paradoxus* YC1 were positively stained in Nile Red dye, indicating that PHA or PHA-like substances such as waxy esters are stored either intracellularly or within the cell membrane (Fig. 6.11). Other strains of *V. paradoxus* have also been reported to store PHA ; *V. paradoxus* DSM 4058 was grown on sodium benzoate and stored the PHA molecule polyhydroxybutyrate (PHB) (Maskow and Babel, 2001). The storage of PHA by *V. paradoxus* YC1 would support the results obtained in previous experiments (Fig. 6.5 and 6.10), where cell growth was observed in culture medium lacking a carbon source. Both of these experiments were established from cells that had been grown in nutrient rich conditions (colony suspension from growth on nutrient agar and an M9 + glucose medium glycerol). As PHA storing cells accumulate PHA when in carbon rich conditions (Lee 1996), this would mean the cells inoculated into these experiments would have had PHA reserves. These reserves could then have been used to support growth in the experiment in media lacking an added carbon source.

The mechanism of carbon acquirement by *V. paradoxus* YC1 in M9 medium lacking an added carbon source has not been fully elucidated here, however enhanced growth in the presence of rubber and the storage of PHA has been demonstrated. These both have likely provided sources of carbon for the sustained growth of *V. paradoxus* YC1, but further experimentation is required to gain a comprehensive understanding of carbon acquirement and how to establish an effective negative control (no growth unless a carbon source is added).

6.4.2 Ecophysiology of *Variovorax paradoxus* YC1 in geological environments

6.4.2.1 Growth on Redcar mudstone powder

V. paradoxus YC1 was isolated from a ferromanganese crust that coated weathered Redcar mudstone, a shale lithology found within Hole Wyke mine adit. To determine if this basal rock could stimulate the growth of *V. paradoxus* YC1, it was crushed into a powder and added to liquid M9 to form a growth medium.

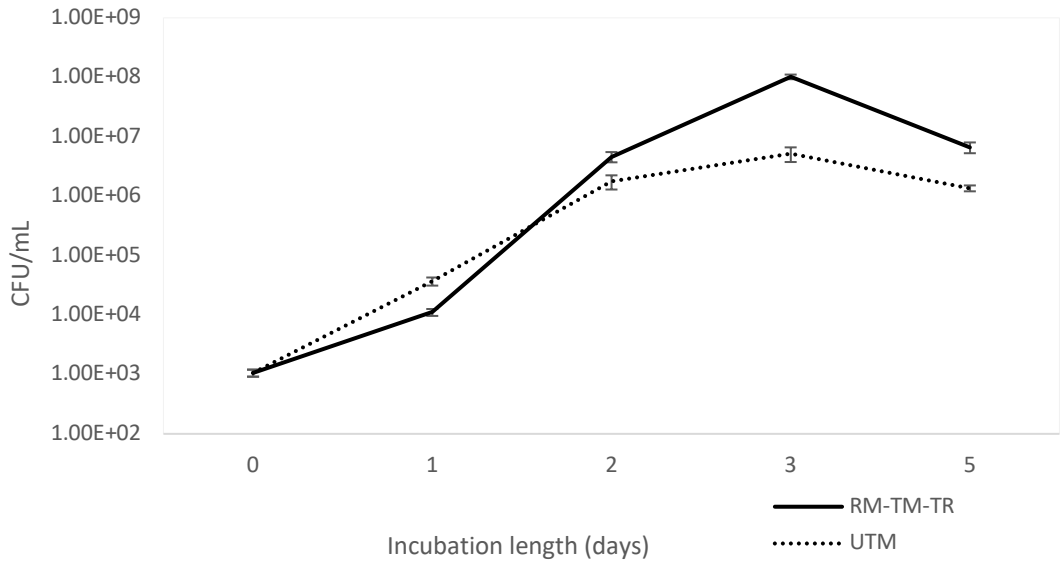

Figure 6.12¦Growth curves (CFU/mL) of *V. paradoxus* YC1 grown in either untreated M9 (UTM, dashed line) or in a hydrothermal extract (rock powder autoclaved in liquid medium) of Redcar mudstone in M9 (RM-TM-TR, solid line). Biological replicates (N=3) were used for all conditions. Error bars represent standard error of the mean average.

The results of this experiment clearly demonstrated that Redcar mudstone rock powder does stimulate the growth of *V. paradoxus* YC1, with growth overtaking that of the control after 2 days, then peaking at a higher total population at day 3 (Fig. 6.12). This increase in the total supported population at day 3 is over an order of magnitude, and was statistically significant (Mann-Whitney U test, $Z=4.64$, $P<0.0001$). This growth enhancement indicates that *V. paradoxus* YC1 is well adapted for survival and growth in the geological environment from which it was isolated..

However, what this experiment does not discern is which aspects of the rock powder stimulated growth. This can be broken down into two components, the chemical and physical stimulatory effects. Chemical stimulation could come from the rock leaching elemental micronutrients such as metals (Fe, Cu, *etc*.) that were not present in the M9 medium, or from the kerogenous organic matter bound within the rock (Matlakowska and Sklodowska, 2010). Physical stimulation occurs because microbes often grow better when attached to surfaces, reaching higher cell densities than when in a

planktonic state of growth. This is because on a surface cells can aggregate to form biofilm, a multicellular layered population held together by extracellular polymeric substances (EPS). Existence in a biofilm provides a range of advantages to microbial survival and growth, including enhanced resistance to pH fluxes and other environmental stresses (Davey and O'Toole 2000).

To better understand these differing stimulatory effects on the growth of *V. paradoxus* YC1, the attachment of cells to shale-comprising mineral surfaces (6.4.2.2) and the growth of this organism in the hydrothermal extracts of shale and coal (6.4.2.4) was investigated.

6.4.2.2 Mineral and rock colonization

Redcar mudstone was shown to have a positive impact on the growth of *V. paradoxus* YC1 (Fig. 6.12). The following analysis questioned which components of the Redcar mudstone provided the most favourable habitat for this organism. Representative minerals from the XRD analysis of Redcar mudstone in Chapter 4 were chosen and Whitby jet was used as a proxy for the kerogenous material within the mineral matrix of the shale. Surface images of some of these mineral/rock types can be seen in Figure 6.13.

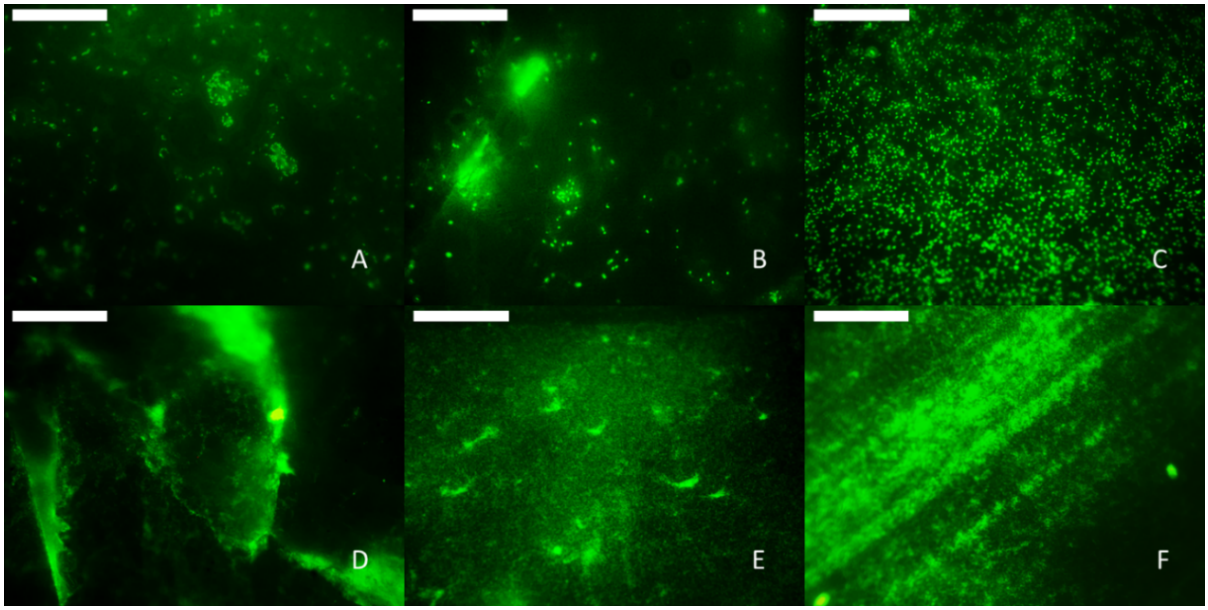

Figure 6.13 Fluorescent photomicrographs of *V. paradoxus* YC1 on polished mineral/rock surfaces (quantitative data in Fig. 6.14). Staining with acridine orange (0.1 mg/mL) for at least 30 minutes. A-C: 1000x magnification images of mineral surfaces for the quantification of colonization (cells mm^{-2}) A) albite, B) calcite, C) muscovite. D-E: images taken at a lower magnification (200x mag.) to capture aspects of non-even colonization D) albite, cells concentrated around a macro pit edge, E) muscovite, numerous microcolonies present and F) Whitby jet, cells concentrated in linear etches. Scale bars for A, B and C are 20µm and for D, E and F are 100µm.

The top three images (A-C) are at 1000x magnification, and such images were used for cell counts to quantify levels of colonization (cells mm^{-2}). The bottom three images represent features of non-even surface colonization on a larger scale (200x mag.). In images D-F, the tendency of *V. paradoxus* YC1 to colonise edges and rough surface topography can be seen. On muscovite (D), cells appears to be forming dense microcolonies within pits on the surface (Fig. 6.13). This can be seen at a finer scale on the surface of albite (A), where small groups of cells are seen aggregated around macro pits.

Bacterial colonization of a surface can be broken into two distinct stages, initial reversible attachment followed by irreversible adherence. Both the surface properties of the bacteria and the surface it is to attach/adhere to can affect these processes. The hydrophobicity and surface charges of the bacterium and the surface cause attraction,

with intermolecular forces such as Van der Waals and hydrogen bonding instigating initial attachment. Covalent bonds and specific bacterial attachment factors such as pili and flagella can then facilitate permanent adherence. Other surface properties such as chemical composition, roughness and configuration can also affect the success of attachment and adherence (An and Friedman 1998; Ohmura *et al*., 1993; Hori and Matsumoto 2010).

Bacterial properties were controlled within this experiment, as only one organism is being investigated. The degree of surface smoothness was qualitatively assessed from SEM imaging of the mineral/rock surface. Each mineral/rock type was polished using the same method, and this produced an evenly smooth surface for albite, calcite, pyrite and quartz, with the exception of macro scale pits in the albite and pyrite. When surface imaging for cell counts, areas with these macro scale pits were avoided. The freshly cleaved planes of muscovite used were also of the same smoothness, with no obvious signs of rough topography on the micron scale. Whitby jet was the only mineral/rock type with a distinctly more roughened surface, with etch lines running across the surface which may affect cellular surface adherence.

This leaves the remaining mineral surface properties (hydrophobicity, charge, chemical composition and configuration) as the primary factors behind differential surface adhesion. Each of these can be split into environment dependant (charge, hydrophobicity) and independent factors (chemical composition, configuration). A combination of these factors produced differing levels of surface colonization by *V. paradoxus* YC1 on the mineral/rock types tested (Fig. 6.13 and 6.14).

The surface characteristics of Gram negative bacteria is primarily defined by the outer membrane and secreted EPS, which make them negatively charged due to the polysaccharide and protein components. Bacterial membranes can range significantly in their hydrophobicity/hydrophilicity dependent upon the composition of the outer layer (which can vary even between strains of the same species). If both of these factors influence attachment, then an ideal attachment surface would be positively charged and also hydrophobic. Hydrophobicity enables attachment of bacteria to the surface, rather than remaining suspended in an aqueous solution. All of the minerals tested (excluding Whitby jet) have been identified as being negatively charged and

hydrophobic to differing extents across numerous studies (Fletcher and Loeb, 1979; Stenström, 1989; Scholl *et al*., 1990; Ohmura *et al*., 1993; Sharma and Rao, 2003; Botero *et al*., 2008; Hong *et al*., 2012). The environmental conditions around the mineral such as the ionic strength of the surrounding solution can affect these surface properties (Mills *et al*., 1994).

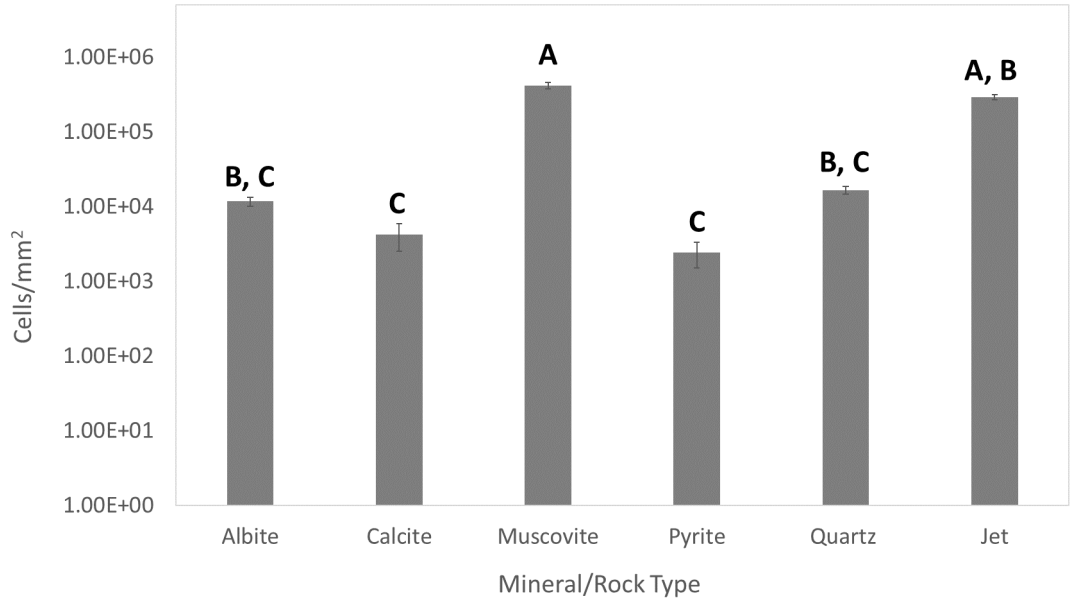

Figure 6.14 Colonization (cells/mm^2) of polished mineral and rock surfaces by *V. paradoxus* YC1 after 5 weeks of incubation in M9 +glucose (0.02 % glucose) media. A Kruskal-Wallis test was used to determine statistical differences in colonization between minerals. Letters represent significance groups, where minerals within the same groups are not significantly difference (Dunn's post-hoc test, P<0.05). Data is derived from single biological replicates, with multiple measurements (10-20 cell counts). Error bars represent the standard error of the mean average of the cell counts.

A Kruskal-Wallis test determined that there were significant differences in levels of colonization between minerals (Kruskal-Wallis chi-squared = 68.533, df = 5, p < 0.001). Further Dunn's post-hoc pairwise tests with Bonferroni corrections for multiple testing revealed colonization level differences between specific minerals. Three non-significance groups, no significance difference in colonization level between minerals within the same group, were identified (groups A-C, Fig. 6.14). Muscovite was the most colonised mineral/rock type (4.1 x 10^5), having over two orders of magnitude more cells/mm^2 than pyrite (least colonised – 2.4 x 10^3).

Muscovite was significantly more colonised than all other minerals tested, but was not significantly different from jet (Dunn-test, Z=0.901, p=1.00) (group A). Rock/mineral colonization can be split into a further two non-significance groups, with jet being more significantly colonised than calcite and pyrite (group B). There was no significant difference in levels of colonization between albite, calcite, pyrite and quartz (group C). (Fig. 6.14). These results are qualitatively reflected in the fluorescence microscopy images taken of these mineral/rock surfaces (Fig. 6.12 A-C). The surfaces of albite (Fig. 6.13A) and calcite (Fig. 6.13B) are noticeably less colonised than that of muscovite (Fig. 6.13C).

The majority of characterised *V. paradoxus* strains obtain their energy from heterotrophy, with the only other identified energy metabolism for this species being hydrogen oxidation under anaerobic conditions (Davis *et al*., 1969). Previous experiments have not indicated that *V. paradoxus* YC1 is not autotrophic (e.g. ammonia or iron oxidation), so the only mineral/rock that should have a direct impact on energy metabolism should be Whitby jet, which potentially explains why it was the second most colonised mineral/rock type (3 x10^5 cells mm^{-2}) (Fig. 6.14). The rougher surface topography could also have played a factor in enhanced colonization of Whitby jet, with higher cell densities observed in linear etches (Fig. 6.13F).

Muscovite (and other micas) has been previously reported as being relatively hydrophilic and highly negatively charged, and found to be poorly microbially colonised compared to other minerals tested in these studies (Stenström, 1989; Scholl *et al*., 1990; Hong *et al*., 2012). In this study, muscovite was the most colonised mineral/rock type (4.1 x 10^5 cells mm^{-2}), and the reasons for this are unclear although two possible explanations can be put forward. Firstly, cells with highly hydrophilic surfaces will preferentially attach to more hydrophilic surfaces, even though hydrophilicity generally has an overall reducing effect on bacterial surface binding (Ofek *et al*., 1983). The surface properties of *V. paradoxus* have not been studied here, but if hydrophobicity/hydrophilicity is important for bacterial-mineral adherence, then this would indicate that the outer membrane of *V. paradoxus* YC1 is relatively hydrophilic. Secondly, the edges of muscovite planes accumulate positive charge (Maslova *et al*., 2003), which makes the flat surface in the interior of the planes highly anionic at neutral pH (-35 to -45mV) (Stenström, 1989; Hong *et al*., 2012) compared

to the surface charges of albite (-15mV) (Stenström, 1989), calcite (+10mV) (Botero *et al*., 2008), pyrite (-8 to 0mV) (Ohmura *et al*., 1993; Sharma and Rao, 2003) and quartz (-20 to -45mV) (Stenström, 1989; Hong *et al*., 2012). If electrokinetic forces are dominant in cellular adhesion to a surface, then the greater the charge difference (regardless of direction), the stronger the force of attraction for attachment. If the surface of *V. paradoxus* YC1 is only weakly anionic, then it may be more attracted to highly anionic surfaces such as those of muscovite.

If the surface properties of *V. paradoxus* YC1 are as described above (moderately hydrophilic and weakly anionic), then this could explain why colonization of pyrite (also weakly anionic, moderately-highly hydrophobic) was so low (Ohmura *et al*., 1993; Sharma and Rao, 2003). However, as the surface of calcite is cationic (+10mV) and hydrophilic, it would be expected to have a much higher level of colonization by *V. paradoxus* YC1 than observed (Fig. 6.14) (Botero *et al*., 2008). A potential explanation for the lack of adherence to calcite could be the increased alkalinity on the surface of the calcite compared to the buffered bulk solution, which could inhibit the growth of *V. paradoxus* YC1 on the calcite surface.

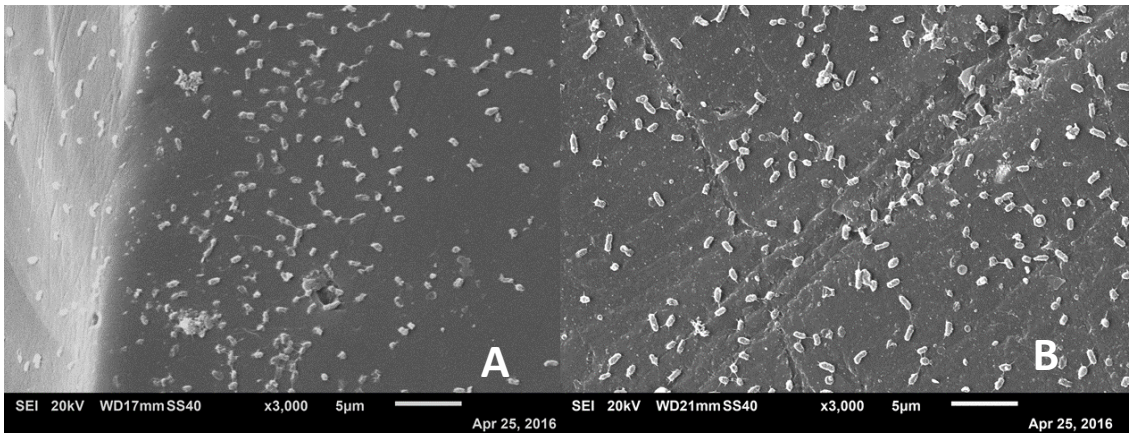

Figure 6.15¦ SEM images of *V. paradoxus* YC1 on polished mineral/rock surfaces (quantitative data in Fig. 6.14) of quartz (A) and Whitby jet (B). Scale bar is 5µm.

Cells with multiple pili were observed on the surfaces of quartz and Whitby jet (and to a lesser extent on albite), adhering them both to the geological surface and to other cells (Fig. 6.15). Type IV pili produced by Gram negative bacteria helps the cell to permanently adhere to the surface after initial attachment mediated by electrostatic and non-covalent forces (An and Friedman 1998). The presence of these features in the

adherence to quartz and Whitby jet indicates active processes by *V. paradoxus* to adhere to these geological surfaces.

6.4.2.3 Ecophysiological responses of *Variovorax paradoxus* YC1 to shale and coal - Introduction

V. paradoxus YC1 responded positively to the presence of Redcar mudstone and to organic-rich Whitby jet in terms of enhanced growth and surface colonization respectively. Both of these rocks are rich in ancient organic material (kerogen) that potentially could stimulate growth of *V. paradoxus* YC1 in a carbon limiting environment.

Redcar mudstone is a marine shale (with fossilised marine algae) and so is a source of type II kerogen, whereas Whitby jet is formed from fossilised terrestrial plants and is a source of type III kerogen. For more information on kerogen and its different types, refer back to Chapter 2. There are major differences in the chemical composition and structure of these two kerogen types, with type II kerogen being mainly comprised of aliphatic chains and type III kerogen being more oxidised and containing a range of aromatic groups (Vandenbroucke 2003).

Coal, another source of type III kerogen, appeared to act as a stimulant for growth in the coal enriched community in transfer sets 1-6, with biofilms forming over coal particles (Fig. 6.2). Although it is not known whether *Variovorax* sp. were members of the coal enriched community, it is plausible to assume that it could have been. *V. paradoxus* YC1 surface growth and attachment was stimulated by jet (Fig. 6.12-14), and strains of *Variovorax* have been isolated for their anthracene (a breakdown product of coal organic matter) degrading capabilities (Zhang *et al*., 2011).

In the following experiments the effect of two different kerogen rich rock types, shale (kerogen type I) and coal (kerogen type III), on the growth and activity of *V. paradoxus* YC1 is explored. Samples of these two rock types were provided by collaborators at Imperial College London. These rock types were chosen because of their extensive differences in kerogen composition and structure (see supplementary Figure 6.1). Type I is similar to type II kerogen in that it comes from an algal source, but for type I this comes from a lacustrine environment. It is even more highly aliphatic and reduced

(higher H:C ratio) than type II. Both samples have been chemically characterised using pyGC-MS techniques (Supplementary Figure 6.1). Type II kerogen is found within Redcar mudstone, the shale from which *V. paradoxus* YC1 was isolated, which is relatively similar to type I kerogen (see Chapter 2). Therefore, the results of this work have relevance to the interaction of *V. paradoxus* with the natural environment it was isolated from.

6.4.2.4 Growth of *V. paradoxus* YC1 in hydrothermal extract medium in the presence and absence of rock powder

V. paradoxus YC1 was cultured in both M9 + glucose and M9 media containing rock powder hydrothermal extract medium (HEM) with a) the powder still present (Fig. 6.16) or b) the powder removed by filtration (Fig. 6.18). This was carried out for both shale and coal rock powder and without rock powder as a control. CFU/mL values for each condition after 4 days of growth are presented in Figures 6.16 and 6.18.

In the presence of rock powder, shale stimulated growth in both the M9 + glucose and M9 medium compared to the medium lacking rock powder (Fig. 6.15). However, this enhancement was over an order of magnitude greater in the M9 medium lacking a carbon source (M9). A possible explanation for this greater enhancement of growth in M9 is that the *V. paradoxus* could use the kerogenous carbon from the shale to sustain greater growth of the population. However, it is also possible that the stimulatory effect of micronutrients such as heavy metals supplied by the shale simply had a greater effect when growth was already heavily limited in the absence of a carbon source.

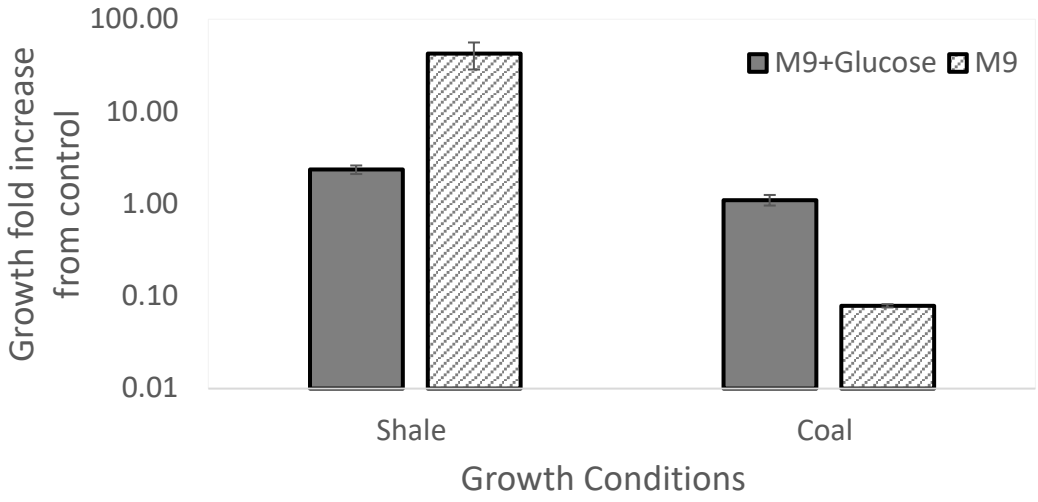

Figure 6.16¦ The relative growth (CFU/mL values, as a ratio of growth compared to untreated M9+glucose or M9) of *V. paradoxus* YC1 after 4 days of incubation in M9 liquid medium with and without glucose, with either 0.15 mg/mL shale or coal rock powder added. Standard error bars are present for all data points, but are small enough to be hidden at some points. Biological replicates (N=3) were used for all conditions. Error bars represent standard error of the mean average.

The coal HEM did not stimulate growth in the M9 + glucose medium, and actually reduced growth by an order of magnitude in the M9 medium. This potentially indicates that coal powder in the absence of a carbon source induces a toxicity effect in *V. paradoxus* YC1. Attachment of cells to coal powder was found in fluorescence microscopy imaging of the M9 + glucose cultures (Fig. 6.17), further supporting that the coal did not have a toxic effect on growth in the presence of a carbon source. Coal has been previously reported to be toxic due to the release of high concentrations of both heavy metals and toxic organic compounds such as PAHs and fatty acids (Francis and Dodge, 1989; Strąpoć*et al*., 2011). *V. paradoxus* YC1 cells growing without a carbon source are already under stress, so the addition of coal stressors seems to have had significant negative impact on growth. The lack of carbon might also have exacerbated coal toxicity, if the stress response mechanisms could not be activated due to the lack of available carbon or energy.

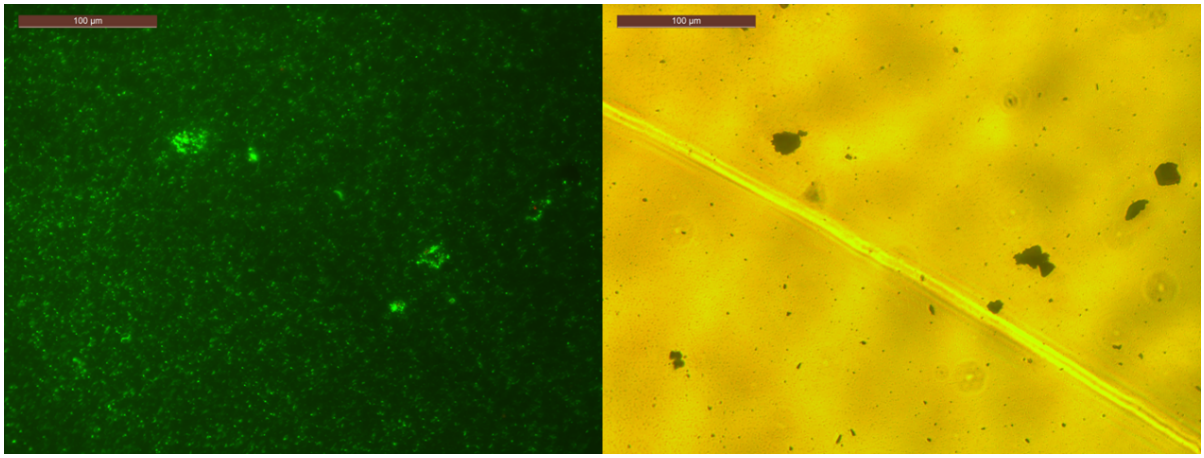

Figure 6.17¦ The attachment of *V. paradoxus* YC1 to coal particles in M9-glucose media from Figure 6.17; left, fluorescence microscopy image obtained with acridine orange (0.01 mg/mL) staining and right, a brightfield microscopy image. The scale bar is 100µm.

However, the lack of a toxicity effect in the presence of a carbon source suggests that *V. paradoxus* YC1 can tolerate the toxic components of the coal. The presence of *V. paradoxus* YC1 on the surface of the coal particles immersed in M9 + glucose indicates that the coal has at a minimum a non-toxic effect, but potentially could even provide nutrients for growth. However, no growth promotion in the presence of coal powder was seen (Fig. 6.16). Achten *et al*. (2011) found that coal PAH molecules were largely un-bioavailable and did not have a toxic effect on a soil microbial community (Achten *et al*., 2011), which would fit with the findings of this study. Other studies have found that certain microbial species can actively degrade coal and gain nutrients/energy from it, producing bi-products such as methane (Fakoussa and Hofrichter, 1999; Strąpoć *et al*., 2011).

The removal of rock powder from the HEM resulted in a significant change in the impact of these media on *V. paradoxus* YC1 growth (Fig. 6.18). Coal HEM no longer exhibited a toxicity effect in M9 medium, with growth promotion compared to the rock-free control being similar in both medium types (2.5-3 fold increase in growth). Shale HEM still enhanced growth in the M9 medium, but not as much compared to when the rock powder is still present (6-fold increase compared to 42-fold increase respectively). In the M9 + glucose medium, growth was reduced compared to the rock-free control (0.28-fold).

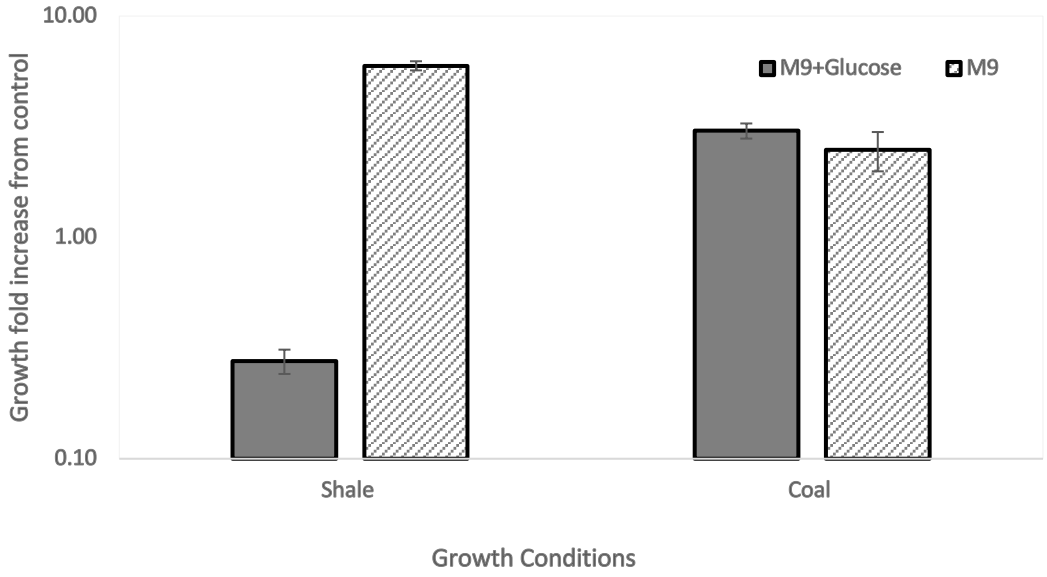

Figure 6.18¦ The relative growth (CFU/mL values, as a ratio of growth compared to untreated M9+glucose or M9) of *V. paradoxus* YC1 after 4 days of incubation in coal or shale rock treated water (with rock powder removed) supplemented with either M9+glucose or M9 medium. Biological replicates (N=3) were used for all conditions. Error bars represent standard error of the mean average.

The removal of coal rock powder from the HEM had a positive impact on growth promotion for *V. paradoxus* YC1 (Fig. 6.18). This has been previously observed in similar experiments carried out with hydrothermal extracts of carbonaceous chondrite (CC) meteorite material being used as growth substrates for the growth of *Pseudomonas maltophilia* (Mautner *et al*., 1995). Although originating from very different sources (i.e., fossilised biological material for coal, condensed interstellar medium for CC), the chemical structure and properties of coal and CC are analogous (Pizzarello *et al*., 2006).

Mautner *et al*. (1995) found that a hydrothermal extract of CC rock powder (125^{o}C, 15 minutes, rock powder still present) initially stimulated growth (1 day of incubation), but subsequently had a negative impact on *P. maltophilia* growth reducing CFU/mL numbers from ~10^6 (control) to ~10^4 (CC) after four days of incubation. After 7 days, the CC hydrothermal extract completely killed all remaining growth of *P. maltophilia*. However, when the CC rock powder was removed from the hydrothermal extract, growth of *P. maltophilia* in the CC medium

was at the same level as that in deionised water. Although chemical inhibition is provided as an explanation for the reduction in growth, no further analysis was carried out to confirm this. The authors also state that organic material from CC material could have directly contributed to *P. maltophilia* carbon acquisition, but this effect was overshadowed by the toxic effect of the rock powder. The experiment was duplicated with another organism, *Flavobacterium orzihabitans*, but neither the presence nor absence of CC rock powder in the hydrothermal extract had any impact on *F. orzihabitans* growth compared to the control (Mautner *et al*., 1995).

The results of the above study supports the response of *V. paradoxus* YC1 to coal rock powder, with strong growth promotion (2.5-3 fold increase compared to control) in the hydrothermal extract of coal with the rock powder removed (Fig. 6.18). The toxic effect of the coal in the presence of the rock powder (Fig. 6.15) could be caused by chemical inhibition as hypothesised by Mautner *et al*. (1995), but no further analysis was carried out to confirm this.

The reduction in growth of *V. paradoxus* YC1 in shale M9+glucose HEM in the absence of shale rock powder is difficult to explain, with shale HEM in all other conditions enhancing growth compared to the rock free control (Fig. 6.16 and 6.18). Further experiments are required to resolve this result.

Together, the results presented in this section paint a complex picture of growth promotion and inhibition by rock powder and HEM. The presence of the physical rock powder, rather than the leachate of coal acted as a growth repressor in M9 medium. The opposite was true for shale in M9 + glucose medium, where the extract medium without the powder had an inhibitory effect.

The growth promotion observed in the remaining conditions compared to the rock-free control suggests that overall growth promotion/reduction for each condition is a balance between growth enhancing and toxic effects of that particular condition. For example, the leachate of coal powder stimulates growth in M9 medium (Fig. 6.18), but when the rock powder is also present this growth promotion is overridden by the toxic effect of the physical presence of the rock powder (Fig. 6.16).

6.4.2.5 Coal and shale enhance colony morphology variation in M9 media

When plating out cultures from the experiments described in section 6.4.2.4, it was observed that colonies grown from particular cultures had markedly different frequencies of colony morphology variation (CMV). CMV was noticeably more prevalent in the plated cultures of rock powder M9 cultures compared to the rock-free M9 cultures. No colony variation was observed in M9 + glucose cultures, with all colonies being morphological identifiable with group A in section 6.3.2.3 (Methods).

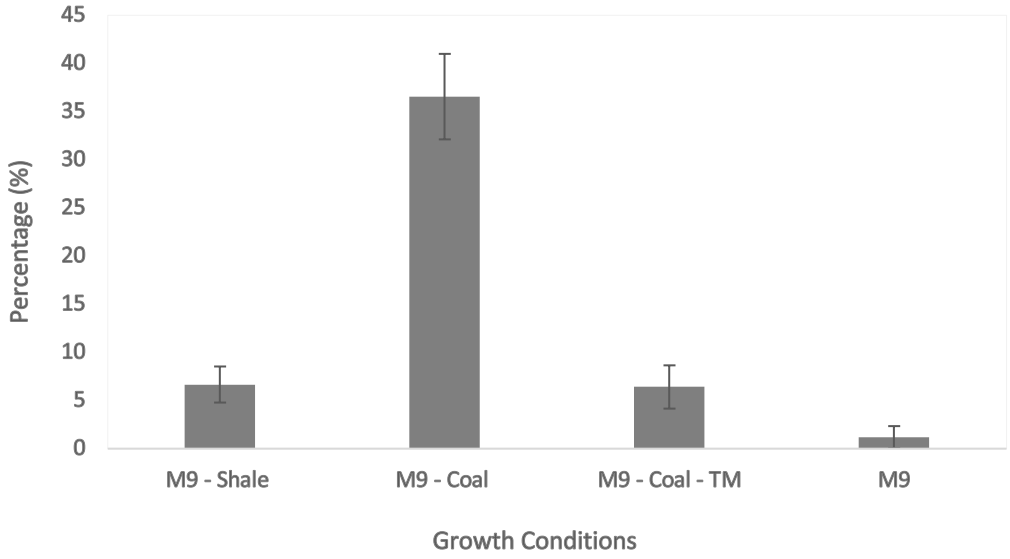

Figure 6.19 The percentage of colony counts with type B1, B2 or B3 morphologies from cultures after 4 days of incubation plated onto nutrient agar after 2 days of incubation. TM - treated medium lacking rock powder. Biological replicates (N=3) were used for all conditions. Error bars represent standard error of the mean average.

The percentage of colonies that were of a morphological variant (group B from section 6.2.1) for each condition is displayed in Figure 6.19. Images of these colony morphology variants (Group B from section 6.2.1 is split into three morphology types: B1, B2 and B3) can be seen in Figure 6.4. Culture conditions that are not present in this graph did not have any colonies with these variations when plated out.

The condition with the highest percentage of CMV was the M9 coal HEM with rock powder (36.5 %), which was statistically significantly greater than that of the M9 rock-free control (two sample t-test, $T=7.45$, $P<0.0001$) (Fig. 6.19).

The percentage of CMV in the plated cultures of M9 shale HEM with rock powder ($T=2.42$, $P=0.011$) and M9 coal HEM lacking rock powder ($T=2.00$, $P=0.027$) were also statistically significantly greater in the M9 rock-free control (Fig. 6.19).

These results are of interest as the condition with highest CMV frequency (M9 HEM with rock powder) also had significantly reduced growth compared to the rock-free cultures (Fig. 6.16). A hypothesis can be made that CMV is therefore related to toxicity effects of the growth medium as CMV formation is a known physiological stress response (Workentine *et al*., 2010). If the above hypothesis is correct, then in the conditions where CMV colonies were identified but growth in the liquid culture was not repressed (Coal TM M9, Shale M9 and to some extent M9) cells were still under some form of stress.

Colony morphology variation has previously been associated with stress adaptation, particularly with relation to the conditions within biofilms. *Vibrio cholera* O1 strain TSI-4 can display a rugose (raised, rugged surface), which was found to be associated with enhanced resistance to both osmotic (2.5M NaCl) and oxidative stress (20mM H_2O_2) that was caused by the increased production of amorphous exopolysaccharide (Wai *et al*., 1998). In another study, *Pseudomonas fluorescens* strain CHA19 was incubated in LB media with a range of molecules to determine which of them induced morphological variant appearance. SiO_3^{2-} (5mM), Ca^{2+} (0.5mM), Rb^{+} (25mM), F^{-} (20mM) and other molecules all caused a significant increase in morphological variant frequency compared to the control. They associate this frequency increase with morphological variants arising due to changes in metabolism that increase oxidative stress resistance, an adaptation to the oxidative stress the organisms were put under in the presence of these elements (Workentine *et al*., 2010).

The colony morphological variants of *V. paradoxus* YC1 either have an extended flat skirted edge (B and C) or have become entirely flat (D). These features are potentially indicative of exopolymeric substances being released by these cells,

lowering the surface tension of the agar and so allowing cellular growth to spread more easily across the plate surface (Fig. 6.19). To determine if *V. paradoxus* YC1 produces EPS that could convey these properties, the supernatant of the liquid cultures described in this section and section 6.4.2.4 had their interfacial surface tension (IFT) values measured, and were tested for their ability to form emulsions (see section 6.4.2.6).

6.4.2.6 Bioemulsification and reduction in interfacial surface tension in M9 + glucose medium

The previous results of this experiment demonstrated that *V. paradoxus* YC1 has both been stimulated and potentially put under stress by the physical powder and the leached compounds of shale and coal.

The organic components of coal have been previously identified as toxic to certain species of microbes (Brofft *et al*., 2002). Processed coal in the form of coal tar is an important environmental pollutant due to its release of toxic organic compounds and heavy metals. Organic pollutant compounds found in coal tar are commonly polycyclic aromatic hydrocarbons (PAHs) such as naphthalene and anthracene (Lors *et al*., 2010). It is likely that PAHs and other similar compounds leach out of the coal used in the above experiments, particularly as they are found in the pyGC-MS products of the coal used (Supplementary Figure 6.1). Such compounds could contribute to the toxicity affects observed.

V. paradoxus has been extensively studied for its ability to degrade a diverse range of pollutant organic compounds including anthracene, linuron and polychlorinated biphenyl (Satola *et al*., 2013). *V. paradoxus* and other microbial species are known to use a variety of methods to detoxify and breakdown these recalcitrant organic molecules. One such method involves the secretion of surfactant molecules which increase the solubility of surrounding organic compounds which are normally very hydrophobic. This actually performs two functions by firstly making the compound more bioavailable for cellular uptake and therefore degradation, and also increasing the surface area of concentrated sources of these organic compounds through emulsification.

This microbial mechanism has been previously studied in relation to the degradation of oil shale organic compounds by *Rhodococcus* sp. (Hadaddin *et al*., 2009). This organism optimally produced biosurfactants when naphthalene and diesel were used as a carbon sources for growth, with purified biosurfactant yield increasing oil extraction from the rock. The use of this mechanism in natural weathering environments has not been investigated, but *Rhodococcus* sp. has been isolated twice in the work of this thesis (Table 6.2 and Chapter 5).

Franzetti *et al*. (2012) investigated the production of bioemulsifiers by *V. paradoxus* in relation to reducing soil adsorption of organic pollutants (Franzetti *et al.,* 2012). The authors demonstrate that this organism produces primarily polysaccharide-based bioemulsifiers which enhanced the removal of crude oil from soil particles when washed. Of interest, they distinguish between surfactant and emulsifying properties. Surfactants lower the interfacial surface tension of the fluid they are present in, whereas emulsifiers enable the production of an emulsion when the aqueous solution they are present in is mixed with an oil. They identify that the molecules produced by *V. paradoxus* have emulsifying, but not surfactant properties (Franzetti *et al*., 2012).

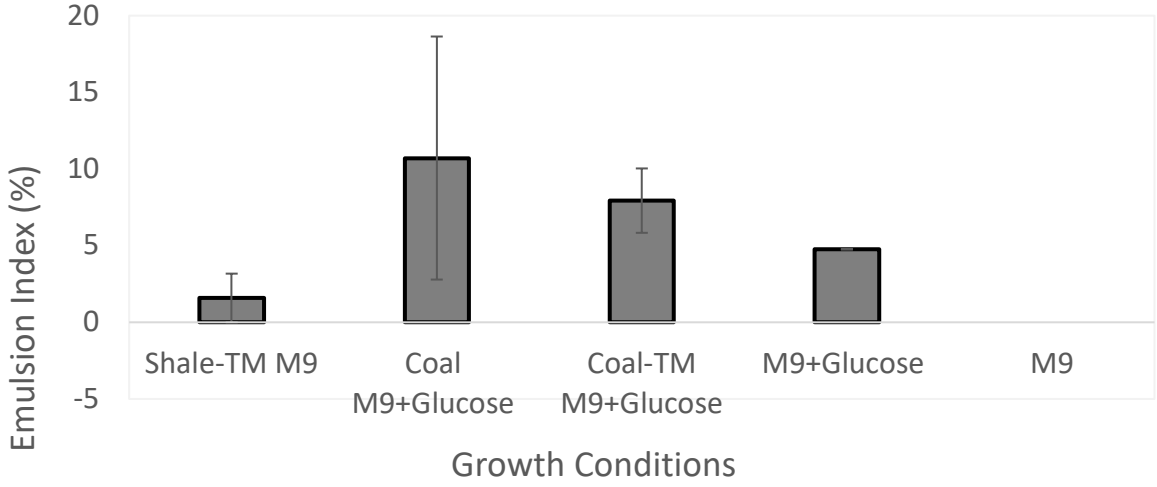

Figure 6.20a¦ Emulsification indices (percentage ratio of emulsion to total volume) of filtered (0.22µm) culture supernatant from cultures after 4 days of incubation, mixed with hexadecane. Biological replicates (N=3) were used for all conditions. Error bars represent standard error of the mean average. Standard error bars are present for all data points, but are small enough to be hidden at some points.

In this study, the supernatant of the experimental cultures after 4 days of incubation (CFU/mL of these cultures is presented in Figures 6.16 and 6.18) were filtered to remove the cells and rock powder if present. The filtered supernatant was then tested for its ability to form emulsions with hexadecane and its ability to lower the interfacial tension (IFT) in a drop tensiometer. For more information on drop tensiometry, see Chapter 3.

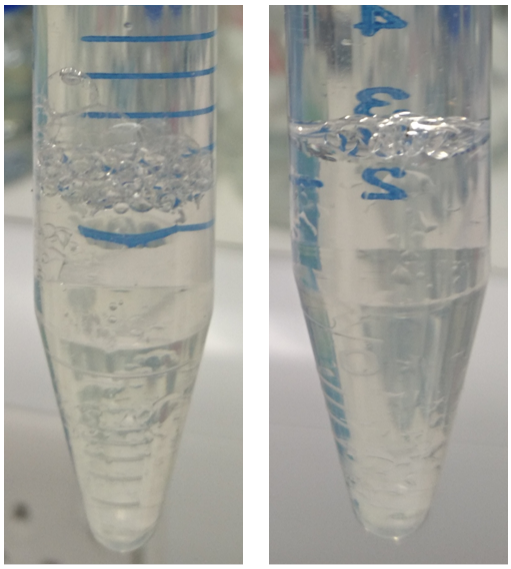

Figure 6.20b¦ Images of emulsions formed from supernatants obtained from M9-glucose cultures with coal added (left) or with no rock added (right).

Emulsions were successfully formed from the supernatants of M9 + glucose cultures containing coal HEM (both with and without rock powder present), in shale HEM lacking rock powder and in M9 + glucose rock-free culture (Fig. 6.20a). Representative images of these emulsions after 24 hours can be seen in Figure 6.20b. These emulsions remained stable for over seven days after initial formation (data not shown). Of interest, the formation of emulsions in the rock-free culture indicates that the emulsifying molecules produced by *V. paradoxus* are produced without recalcitrant organic or geological stimuli. The variability in emulsion formation within triplicate samples of each condition means that it cannot be deduced if some supernatants had stronger emulsifying properties compared to the rock free control.

None of the sterile condition media that were also incubated at 30 ºC for four days had emulsifying capabilities. Furthermore, emulsions were only formed from culture supernatants containing glucose, suggesting an abundant bioavailable carbon source is required for bioemulsifier production.

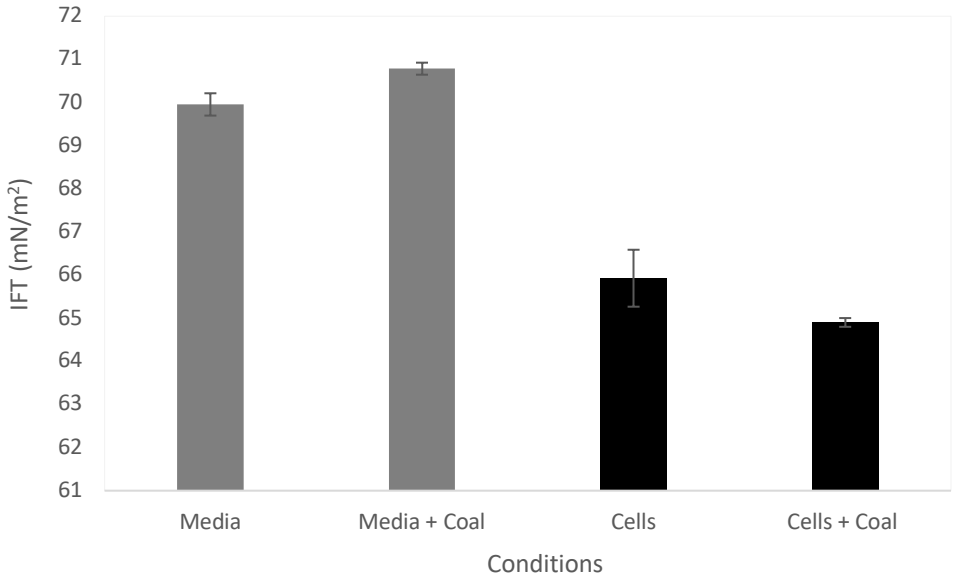

Figure 6.21¦ Interfacial tension (IFT - mN/m^2) values of cell-free liquid cultures, both blank media (grey bars) and *V. paradoxus* YC1 cultures grown for 4 days with the cells removed by filtration (black bars), for both M9+glucose media without (media) and with coal added (cells+coal). Biological replicates (N=3) were used for all conditions. Error bars represent standard error of the mean average.

Drop tensiometry of the sterile and biological media supernatants of rock-free and coal HEM media revealed that biological activity reduced the IFT of the medium (Fig. 6.21). This is an interesting result because as far as the author is aware, it is the first study to show that a *V. paradoxus* strain's biological activity lowers the IFT value of any growth medium. This indicates that the cells are releasing molecules that have either surfactant or surfactant-like properties. This is in contrast to the only published data on *V. paradoxus* in relation to surfactant production, which reported that although *V. paradoxus* supernatant did form emulsions, it did not lower the IFT and so the production of biosurfactants was ruled out (Franzetti *et al.*, 2012).

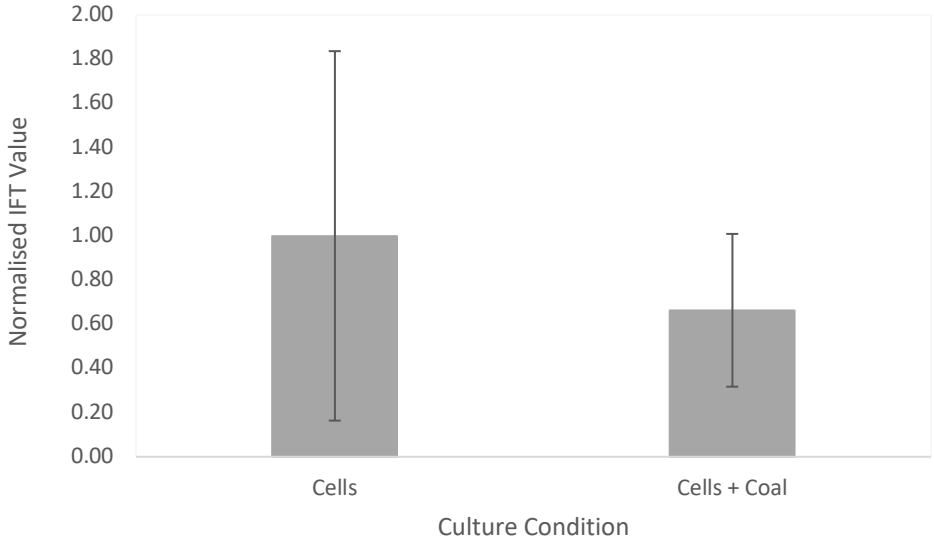

Figure 6.22¦ Normalised IFT values of both the M9+glucose without (cells) and with added coal powder (cells+coal) cultures of *V. paradoxus* YC1 grown for 4 days. Values have been normalised by IFT difference between culture and sterile media and CFU/mL number. Furthermore, both cultures have been normalised to the value of the M9+glucose medium, where M9+glucose has a normalised value of 1. Biological replicates (N=3) were used for all conditions. Error bars represent standard error of the mean average.

The actual difference in in IFT value between the biological and sterile medium was higher for the coal cultures (5.88 mN/m^2) compared to the rock-free cultures (4.03 mN/m^2). However, these differences do not take into account the number of cells that were present in the media to produce molecules that reduce IFT. When these difference values are normalised by cell number and adjusted to the IFT reduction in the rock-free medium, cells grown on coal HEM media did not significantly reduce the IFT more than the cells in the rock-free media (Fig. 6.22). However, the standard error range obtained for these values was very large, suggesting that more measurements would need to be taken to resolve these differences.

One particular contribution to this high error range is the differences in cell numbers (5.25×10^7 and 8.20×10^8 CFU/mL) between the duplicate M9+ glucose cultures analysed in this section. A third replicate of this condition had a CFU/mL of 1.04×10^8, although the supernatant of this culture was not analysed for bioemulsification or

IFT measurements. If the replicate with the highest CFU/mL is compared to the average of the two coal duplicates, then the cells grown on coal HEM in M9+glucose would have increased the normalised IFT to 4-fold above the M9+glucose control (data not shown). This highlights the need for this experiment to be repeated with a greater number of replicates analysed for IFT measurements and bioemulsification.

Overall, the data presented in this section demonstrates that *V. paradoxus* YC1 alters the media it is grown in, reducing its interfacial surface tension (Fig. 6.21) and enabling it to form emulsions with hexadecane (Fig. 6.21). These properties are likely conferred by the release of exopolysaccharides into the culture medium. Previous studies have quantified and analysed the release of exopolysaccharides by *V. paradoxus* strains and their contribution to bioemulsification, surface motility and biofilm formation (Jamieson *et al*., 2009; Pehl *et al*., 2012; Franzetti *et al*., 2012). However, coal and shale rock powder HEM did not appear to significantly affect the extent to which *V. paradoxus* YC1 released these putative active molecules or alter the supernatant's properties (Fig. 6.20 and 6.22).

6.4.2.7 Shale and coal enhance swarming motility

Numerous environmental factors are known to trigger and influence the level and mode of motility in bacterial species (Kearns, 2010). Chemotactic swimming motility towards environmental pollutants is well documented (Pandey and Jain 2002), but directed motility towards stimuli in swarming is less well understood. In swimming motility, the run and tumble mechanism allows for directional movement towards a chemical/physical gradient, but this is not possible in the fixed raft structure of swarming colonies (Kearns 2010). However, numerous studies have identified enhanced swarming toward stimuli. The polychlorinated biphenyl degrader *Pseudomonas* sp. strain B4 had enhanced swimming and swarming motility towards biphenyl and its chlorinated derivatives in capillary and swarm plate assays (Gordillo *et al*., 2007).

In the following swarm assays, the effect of adding shale and coal rock powder to M9 + glucose and M9 swarm plates is investigated.Fig. 6.23 shows diameter fold-

difference of the rock swarm plate to the rock-free control swarm plate after 72 hours of growth.

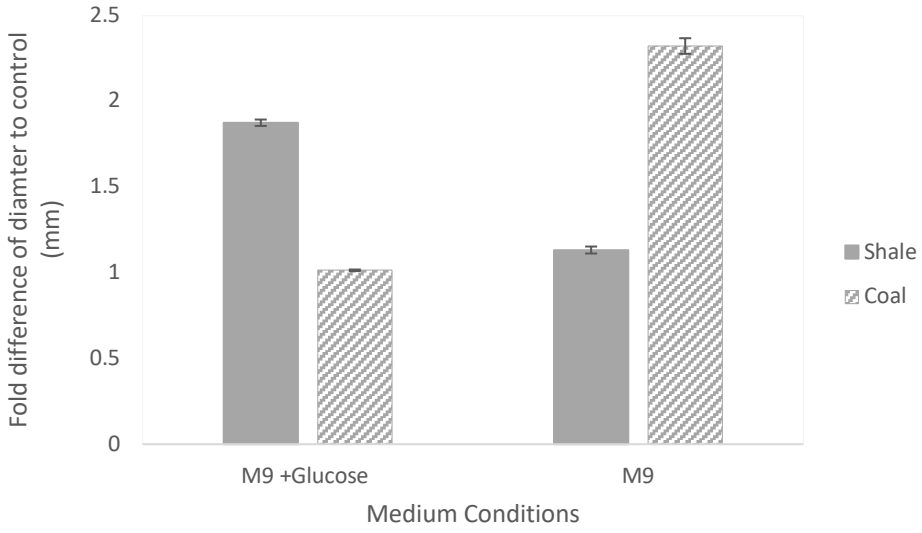

Figure 6.23¦ Diameter fold differences of *V. paradoxus* YC1 colonies on 0.7 % agarose, M9 (with or without glucose) gel plates with no rock, shale powder (2 g/L) or coal powder (2 g/L) added, recorded after 72 hours of incubation. Standard error bars are present for all data points, but are small enough to be hidden at some points. Biological replicates (N=3) were used for all conditions. Error bars represent standard error of the mean average.

Both shale and rock powder have a stimulatory effect on swarming motility (Fig. 6.23). However, there was a distinct difference between the results of the shale and the coal swarm plates. The addition of shale to the M9 + glucose swarm plates significantly increased the swarm diameter by 1.9 fold, but barely enhanced (1.1 fold) swarming on the M9 medium which lacked a readily bioavailable carbon source. In contrast, the addition of coal to the M9 swarm plates enhanced the swarm diameter (2.32 fold) whereas addition to the M9 + glucose swarm plates had little effect (1.01 fold).

This stark increase in the coal M9 swarm plate can be seen in Figure 6.24, where the appearance of the M9 coal colony is more similar to that of the M9 + glucose rock-free swarm plate than to the M9 rock-free swarm plate.

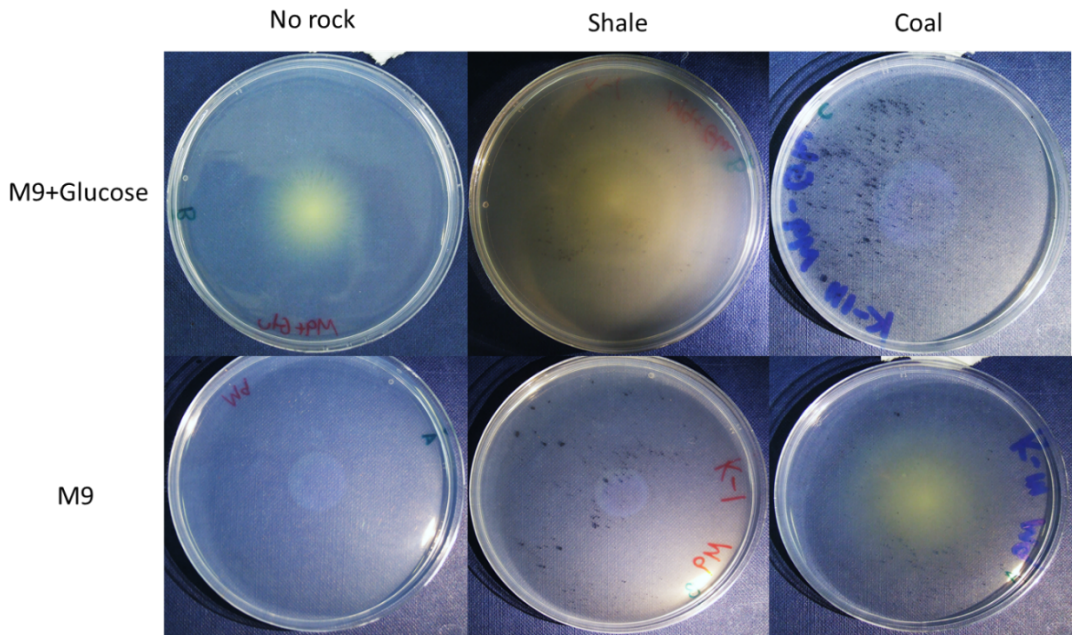

Figure 6.24¦ Photographs of the colonies presented in Figure 6.22 after 5 days of incubation.

Due to the differences in swarming motility enhancement dependent upon carbon and rock powder conditions, it can be concluded that shale and coal rock powder are affecting motility via different mechanisms.

The enhancement of swarming by shale rock powder only in the presence of glucose suggests that easily accessible carbon is the limiting factor in swarm diameter (Fig. 6.23). When glucose is absent shale does not enhance swarming, but when carbon is not a limiting factor shale rock likely provides a nutritional "fertilizing effect" that enhances swarming. Swarming motility is known to be nutritionally conditional; supplying different carbon sources to *Pseudomonas aeruginosa* had a significant impact on the extent and characteristics of this species swarming behaviour (Shrout *et al*., 2006). In the case of this study, as M9 is a very minimalist medium, numerous chemical components such as Fe and other trace nutrients of the shale could be causing swarming enhancement. This effect could be purely stimulatory i.e. that growth/activity limiting nutrients are now available, or cells may be directly chemotactically attracted to nutrient rich areas (Kearns, 2010).

Coal rock powder stimulated motility primarily in the absence of glucose, which suggests that a carbon source specific mechanism might be responsible for the

enhancement i.e. organic molecules that diffused into the agarose enhanced motility and increased swarm diameter (Fig. 6.23). Direct metabolism of specific organic components that leached out of the coal could account for the swarming enhancement, with those compounds acting as a carbon source for *V. paradoxus* YC1 in the absence of glucose. This is what was observed in the chemotaxis of *Pseudomonas* sp. strain B4 towards biphenyl, polychlorinated biphenyl and benzoate which were also directly utilised as carbon and energy sources (Gordillo *et al*., 2007). Chemotaxis in swim agar and capillary assays towards a range of plant derived and anthropogenic pollutant organic compounds have been identified in strains across multiple genera including *Pseudomonas*, *Azospirillum* and *Ralstonia* (Parales and Harwood 2002, Pandey and Jain 2002). One such compound is naphthalene, a primary constituent of coal tar and a common environmental pollutant. Grimm and Harwood (1997) reported that two strains of naphthalene degrading *Pseudomonas* displayed chemotactic induced motility towards a naphthalene source (Grimm and Harwood, 1997). Further studies indicated that motile wild type strains of *Pseudomonas* were better degraders of Naphthalene than motility mutants, suggesting that chemotaxis may enhance this compound's degradation (Marx and Aitkin 2000).

Naphthalene is one of the main constituents of the pyGC-MS products of the coal used in this study (Supplementary Figure 6.1), meaning that it or other related compounds could be responsible for the enhanced motility of *V. paradoxus* YC1 (Fig. 6.23). Motility experiments of *V. paradoxus* YC1 in the presence of specific organic compounds, including naphthalene, will be required to support this hypothesis.

6.4.2.8 Naphthalene does not stimulate growth in *Variovorax paradoxus* YC1

The colonization, growth and motility of *V. paradoxus* YC1 can be enhanced by coal rock powder or coal HEM (Fig. 6.16, 6.17 and 6.23). A likely contributory factor to this response is that *V. paradoxus* is either directly metabolizing or being stimulated by a chemical component leaching out of the coal. Naphthalene is one of the main

constituents of the pyGC-MS products of the coal used in this study (Supplementary Figure 6.1), and so the growth of *V. paradoxus* YC1 on this substrate was tested.

The addition of naphthalene, both at 100 and 1000 µg/L, to M9 + glucose or M9 media did not have a significant impact on the final CFU/mL at day 4 compared to the control cultures (Fig. 6.25). Naphthalene can therefore be deduced to not impart any toxicity effect on *V. paradoxus* YC1 growth, even at high concentration. However, the evidence presented here does not support the hypothesis that *V. paradoxus* YC1 can utilise naphthalene as a carbon source, having not increased the population size in media lacking any other additional carbon source (M9) compared to the control.

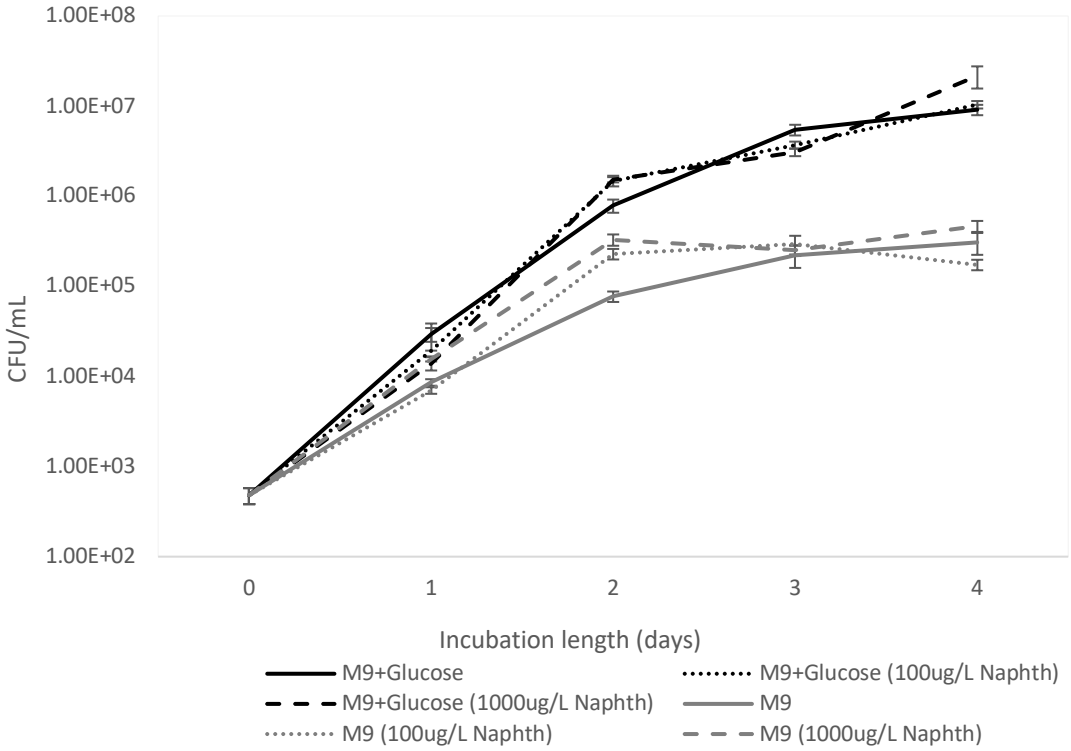

Figure 6.25¦ Growth curves (CFU/mL) of *V. paradoxus* YC1 grown in M9+glucose (black lines) and M9 media (grey lines). These media were either unamended (solid lines) or, amended with 100 µg/L (dotted lines) or 1000 µg/L (dashed lines) of naphthalene. Biological replicates (N=3) were used for all conditions. Error bars represent standard error of the mean average.

Although naphthalene did not stimulate growth in terms of population size, it appears to have had a stimulatory effect on growth rate in the exponential phase of growth (Fig.

6.25). This effect can be seen in the increased growth rate between days 1 and 2, for both concentrations of naphthalene and for both media types.

Statistical analysis revealed that this difference was only significant in the M9 medium, between the M9 lacking naphthalene and M9 with supplemented 1000 µg/L Naphthalene (two sample t-test, T=12.306, P<0.000). This indicates that this stimulatory effect is most effective in the absence of an added carbon source and at higher concentrations. The result of this stimulation is that in the M9 cultures, the addition of naphthalene causes the population maximum to be reached and stationary phase to be entered after two days instead of three (Fig. 6.26).

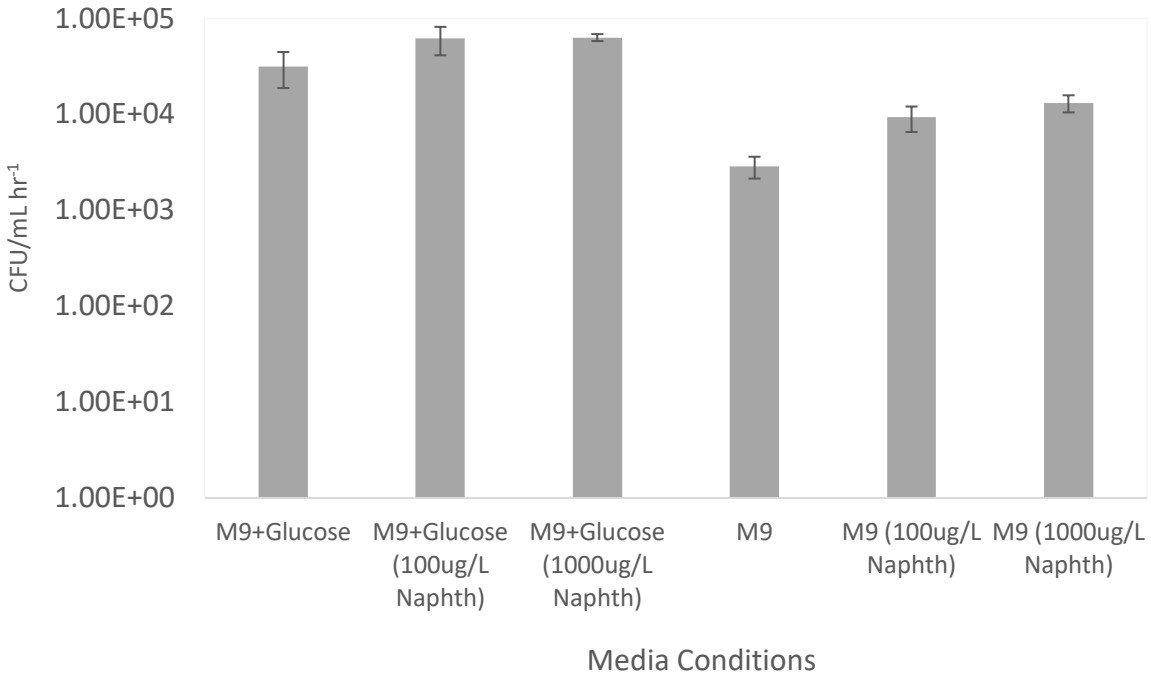

Figure 6.26¦ Growth rate (CFU/mL hr^{-1}) of *V. paradoxus* YC1 between 24 and 48 hours grown in M9 + glucose and M9 media supplemented with 100 and 1000 µg/L of naphthalene. Biological replicates (N=3) were used for all conditions. Error bars represent standard error of the mean average.

The lack of increased growth in the presence of naphthalene suggests that this compound is not actively metabolised for energy or carbon by *V. paradoxus* YC1, but that this organism can resist high concentrations of this toxic substance. This result is surprising, as previous studies have demonstrated that *V. paradoxus* has been identified in naphthalene contaminated environments and been shown to utilise

naphthalene metabolically. *V. paradoxus* was enriched in naphthalene amended culture (50µM) as part of a low diversity community from the naphthalene contaminated bottom layer of the Delaware estuary (Castle *et al*., 2006). This suggests that environmental strains of *V. paradoxus* can at a minimum survive in naphthalene contaminated environments (Castle *et al*., 2006). Furthermore, two wheat rhizosphere soil isolates of *Variovorax* had demonstrated capabilities to utilise naphthalene-2-sulfonate as a sole sulfur source (Schmalenberger *et al*., 2008). The ability of *V. paradoxus* to degrade naphthalene is further supported by three of the five genome sequences made of *V. paradoxus* strains (S110, EPS and B4) that all have genes for enzymes that can degrade naphthalene (Han *et al*., 2011; Han *et al*., 2013; Brandt *et al*., 2014). These enzymes include naphthalene 1,2-dioxygenase ferredoxin reductase (Vapar_5347 (S110), Varpa_2932 (EPS), VAPA_1c07020 (B4)) which can catabolise naphthalene and 2-methylnaphthalene and, S-(hydroxymethyl) glutathione dehydrogenase (Vapar_1703 (S110), Varpa_1874 (EPS), VAPA_1c17910 (B4)) which can catabolise 1-hydroxymethyl-napthalene and 2-hydroxymethyl-naphthalene (KEGG pathways - Kanehisa and Goto, 2000; Kanehisa *et al*., 2015).

However, despite there being no evidence for the direct metabolism of naphthalene which enhances growth, the addition of 1000 µg/L of this compound did significantly increase growth rate between 24 and 48 hours after inoculation (Fig. 6.26). This suggests that naphthalene acts as a stimulant to *V. paradoxus* YC1 growth rate during the exponential phase, but without being directly utilised as a carbon or energy source. Taking into account evidence from other studies, *V. paradoxus* YC1 might be capable of metabolizing naphthalene but did not in this experiment due to factors such as necessary nutrients or other environmental conditions.

6.5 Conclusions

V. paradoxus YC1 is an organism that can rapidly adapt to its surrounding environment, enabling it to survive and grow in a range of different substrates, conditions and stresses.

Having been isolated after being sub-cultured in growth medium only containing water, *V. paradoxus* YC1 demonstrated its capability to survive in extreme low

nutrient conditions (Fig. 6.3). Subsequent analysis of its growth in differing growth media revealed that it could be reliably cultured in a minimal salts medium lacking an added carbon source (Fig. 6.5). Although the exact mechanism for carbon and energy acquisition by *V. paradoxus* YC1 remains unknown, the storage of PHA as an intracellular reserve of carbon (Fig. 6.11) was demonstrated and the utilization of butyl rubber for carbon/energy indicated (Fig. 6.10).

The growth and activity of *V. paradoxus* YC1 was stimulated by geological substrates including Redcar mudstone, the rock type of the environment from which *V. paradoxus* YC1 was enriched (Fig. 6.12). Other shale rock types and bituminous coal also had an enhancing effect on *V. paradoxus* YC1's growth (Fig. 6.16 and 6.18). Shale-comprising minerals were shown to be suitable habitats for *V. paradoxus* YC1, with muscovite and sedimentary organic matter (Whitby jet) becoming particularly colonised (Fig. 6.13-6.15). This colonization was not just initial attachment to a surface, but an active process to colonise the surface through the production of pili to enable irreversible surface adherence (Fig. 6.15).

V. paradoxus YC1 is a motile organism capable of both swimming through an aqueous medium and swarming on a surface (Fig. 6.7). This motility is highly nutritionally dependent, with the addition of casamino acids to the minimal salts and agarose medium favouring surface growth and reduced motility but also increased swarming motility phenotypes such as a dendritic growth (Fig. 6.7 and 6.9). This behaviour could potentially enable *V. paradoxus* YC1 to remain in nutrient rich environments and to colonise the surrounding surfaces. Both shale and coal geological substrates enhanced swarming motility, with coal having a noticeable effect on swarm enhancement in the absence of a readily available carbon source (Fig. 6.23 and 6.24). This suggests that the activity of *V. paradoxus* YC1 maybe specifically altered by geologically sourced organic molecules. This is supported by the stimulation of *V. paradoxus* YC1 growth rate by the recalcitrant polycyclic aromatic hydrocarbon naphthalene (Fig. 6.26), a major constituent pyGC-MS product of coal (Supplementary Figure 6.1). *V. paradoxus* as a species is known to be able to catabolise a wide array of organic molecules (Satola *et al*., 2013), and future experimentation on strain YC1 could reveal what role this adaptive metabolism may play in geological environments.

However, survival in geological environments also comes with its drawbacks, and *V. paradoxus* YC1 was shown to be capable of tolerating and responding to toxic conditions. The presence of coal powder inhibited growth (Fig. 6.16), although hydrothermally extracted coal leachate enhanced growth (Fig. 6.18). The stress response of cells grown in the presence of coal rock powder was evident when they were plated onto nutrient agar, as they were much more likely to form a colony morphology variant (Fig. 6.4 and 6.19). This shift in colony phenotype is putatively believed to be caused by an increase in exopolysaccharide release (Jamieson *et al*., 2009; Pehl *et al*., 2012).

Exopolysaccharide molecules produced and released by *V. paradoxus* YC1 could be acting as biosurfactants, as previously suggested for other *V. paradoxus* strains (Pehl *et al*., 2012). This would support the evidence collected on how *V. paradoxus* YC1 growth reduces the interfacial surface tension of M9+ glucose media (Fig. 6.21), and enables the culture supernatant to form emulsions (Fig. 6.20a and 6.20b). However, this activity was not linked to cellular stress response and was identified under normal growth conditions as well as in cultures containing geological substrates (Fig. 6.22).

The work presented in this study highlights the ecophysiological adaptations of *V. paradoxus* YC1. It has been demonstrated that this organism has the capabilities to preferentially colonise suitable habitats and utilise recalcitrant resources that are biologically unavailable to most other microbes. It uses an array of mechanisms to help it survive when nutrients become depleted including making use of carbon stores and using its motility to seek more clement conditions. *V. paradoxus* YC1 can also respond to conditions toxic to its growth that have arisen from its geological environment by changing its behaviour (alteration of colony morphology), with the potential for other cellular activity (exopolysaccharide production) to contribute to these responses.

Future work on this organism should continue to investigate if *V. paradoxus* YC1 can utilise different carbon sources such as naphthalene that are primary constituents of the breakdown products of kerogen. This work would naturally lead on to determining what weathering capability *V. paradoxus* YC1 has on shale and other rocks containing sedimentary organic matter such as coal.

6.6 Supplementary Data

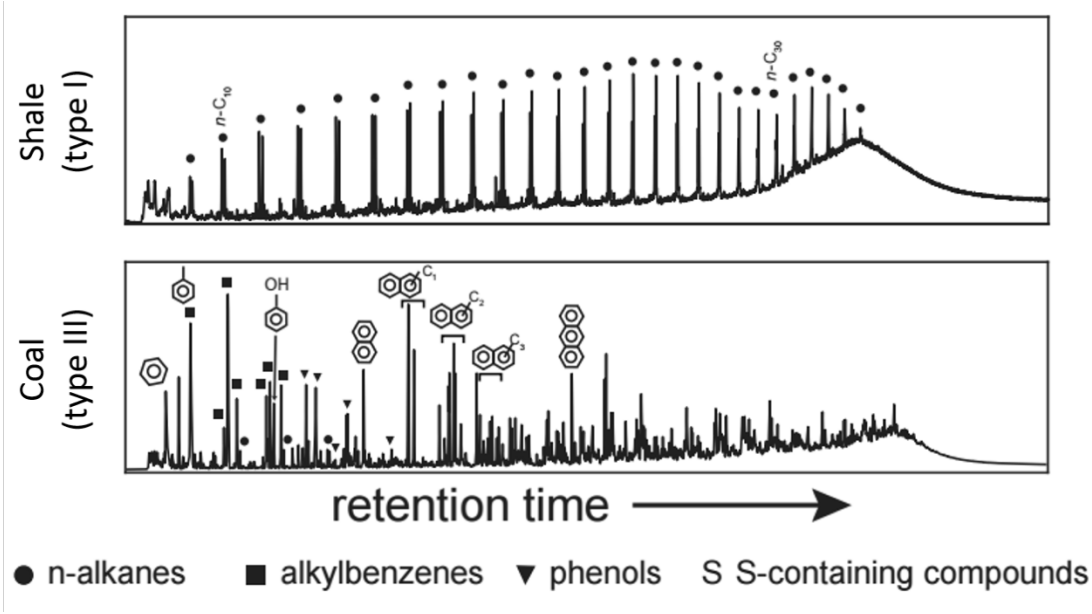

Supplementary Figure 6.1¦ py-GC-MS spectra of the Port Edgar shale (type I kerogen rich) and Daw Mill coal (type III kerogen rich).

Chapter 7 - Evidence for metal bioleaching and microbial iron oxidation from shale rock in batch flask cultures

7.1 Introduction

It is widely accepted that biological activity alters the geochemical environment of weathering shale (Joeckel *et al*., 2005; Tuttle and Breit, 2009; Li *et al*., 2014). An important process that microbes can contribute to is the enhancement of elemental leaching from a rock into surrounding fluid (Pye and Miller 1990; Tasa *et al.,* 1997; Wengel *et al.,* 2006; Grobelski *et al.,* 2007; Watling, 2015; Wlodarczyk *et al.,* 2015). Microbially catalysed oxidation of iron sulfides (e.g. pyrite) was a primary focus of early researchers studying microbial shale weathering due to the extensive impact of these reactions (Singer and Stumm, 1970; Grattan-Bellew and Eden, 1975; Taylor, 1988; Pye and Miller, 1990). The oxidation of the ferrous iron liberates sulfur which in turn is oxidised, producing sulfuric acid. The produced acid then contributes to calcareous mineral dissolution, acidolysis of metals within mineral matrices and enables other redox reactions to occur. Further details of these reactions and their specific impact on shale composition and structure can be found in Chapter 2.

However, in the last decade a growing body of evidence indicates that other microbial mechanisms could also play a significant role in shale weathering, or even be dominant weathering processes in environments that do not support pyrite oxidation. For example, numerous studies have shown that microbially produced complexes such as siderophores and organic ligands can displace ferric iron and other heavy metals such as Co, Cu, U, and Zn from the mineral matrices within the shale (Visca *et al.,* 1992; Kalinowski *et al.,* 2006; Matlakowska *et al*., 2014; Wlodarczyk *et al.,* 2015). Organic ligands are also often acidic, such as oxalic acid or citric acid, and as such also provide acidolytic action on metals in the same way as inorganic acids. Metals such as Cu, Co, Ni and V can also be released by enzymatic

action, which degrades metal-binding organic groups such as porphyrins within the organic carbon content of the shale, releasing the metal (Matlakowska and Sklowdowska, 2010; Matlakowska *et al.,* 2013). The isolation of bacterial and fungal strains from weathered shale environments that have some of these phenotypic capabilities is described in Chapter 5.

Enhanced knowledge of these additional weathering mechanisms means that it has become increasingly challenging to truly understand shale weathering systems, both in the laboratory and in the field. One method that has been widely adopted within the field of shale biogeochemistry is the use of induced coupled plasma (ICP) analytics, such as ICP-OES (optical emission spectroscopy). Although further details of this technique can be found in Chapter 3, it is sufficient to say here that it can be used to determine concentrations of any element within a solution. In batch culture of continuous flow experiments, aliquots of media can be removed at one or multiple time points of the experiment and elemental concentrations determined. By undertaking a widespread analysis of elemental content of the rock leachate, specific microbial activities can be deduced.

For example, in Matlakowska and Sklowdowska (2010) monitoring of the vanadium concentration in the shale rock leachate over 30 days allowed the authors to determine that its leaching was being enhanced under biological conditions compared to the control (Matlakowska and Sklowdowska,2010). However, care must be taken when interpreting either enhanced or reduced leaching of an element. Numerous complications or additional processes can occur within the geochemistry or biogeochemistry of the experiment that can complicate the results obtained. In the experiment just described, enhanced concentration of V in the rock leachate was observed, but the same observation was not made for Cu or Ni. This was initially surprising, as the expected mechanism for V release was through the degradation of porphyrins, which also bind to Cu and Ni. Further analysis revealed that leaching of Cu and Ni was bio-enhanced, but that these elements were up-taken into the microbial biomass, and so were not observed at enhanced concentrations in the leachate (Matlakowska and Sklowdowska*,* 2010).

Another complication includes bio-enhanced leaching of an element being hidden, due to the element being precipitated out of solution by authigenic mineral formation. In Matlakowska *et al.* (2012) the authors observe bio-reduced leaching of elements including Ca, Mg and S, and bio-enhanced leaching of elements including P, K and Cu (Matlakowska *et al.,* 2012). Further SEM analysis of the biologically weathered shale surfaces revealed the presence of both phosphate and sulfate salt crystals, and metal sulfides, that were not observed in the control samples. Such authigenic mineral formation (including gypsum, $CaSO_4$) probably obscured the bio-enhanced leaching of Ca, Mg and S.

A further obstacle arises when trying to apply knowledge obtained from laboratory experiments to understanding biogeochemical systems in the field (Pacheco and Alencoão, 2006; White and Brantley, 2003). Rates of weathering can be both over and underestimated in laboratory experiments in comparison to the environmental system they were designed to represent. Laboratory experiments by necessity have to be simplified versions of the environment in order to investigate the role of pre-specified factors while controlling others. A prime example of this in the field of shale biogeochemistry is the fluid to rock ratio. High ratio values mean that the fluid can remain unsaturated throughout the course of an experiment, maintaining high leaching rates out of the rock (Tasa *et al*., 1997). In the environment, the fluid to rock ratio would be expected to be much lower. Rocky surface outcrops are often not inundated with water, but are exposed to moisture and transient rainfall. Therefore it can be difficult to apply leaching rates calculated in the laboratory directly to the field. Another problem arises from the industrial focus of many studies on microbial shale weathering (Watling, 2015). Organisms isolated and used for shale leaching studies have been selected based on their suitability for use for biomining purposes (Matlakowska and Sklowdowska, 2009; Farbiszewska-kiczma *et al.,* 2004), not necessarily because they are environmentally significant drivers of rock weathering.

Despite these difficulties in data interpretation, the analysis of elemental bioleaching in shale weathering studies is of great importance. Biological activity that solubilises metals and whole minerals within a rock can result in significant mass loss (40 % in Meyer and Yen (1976) – laboratory experiment, 10 % in Pye and Miller (1990) – field analysis), meaning that bio-enhanced leaching can act as a major contributor to

shale weathering and erosion in the environment. Even moderate levels of mass loss will increase the porosity and potentially increase the permeability of the rock, providing increased surface area for further biogeochemical action and weakening the overall structure of the rock. In contrast, the formation of authigenic mineral crusts such as jarosite on the weathered surface of shale can also partially protect the rock from further chemical and physical weathering, and so counter the weakening effects of mass loss (Sethurajan *et al.,* 2012; Zhou *et al.,* 2009). Obtaining a holistic picture of these processes within experiments and in the field is crucial to fully understand microbial rock weathering of shale.

In this Chapter, the results of a series of batch culture experiments are presented. An initial experiment is described where crushed shale powder is incubated in a minimal salts medium for 28 days, with and without a biological inoculum. Further experiments use weathered chips taken from a shale weathering profile as a more natural surface for investigating biological weathering activity. Weathered chips were incubated under two different conditions: inundated in liquid media within an Erlenmeyer flask (liquid setup), or wetted with liquid media and suspended within a tube that allowed drainage of excess fluid (moist setup). The liquid set up experiment was replicated with three different media types: water, a minimal salts medium lacking a supplemented carbon source and a minimal salts medium with glucose added. All media types were pH adjusted to neutral (pH 7), but the water was unbuffered compared to the minimal salts medium (phosphate buffered). Weathered shale chips were incubated under both liquid and moist set ups for a total of 16 weeks, with analysis of sacrificial cultures being carried out every 4 weeks. In all experiments, growth of the heterotrophic microbial population (CFU/mL on nutrient agar), pH and elemental leaching via ICP-OES are analysed.

The chapter explores the following questions:

- How does biological weathering activity differ between an artificial (powdered rock) and a natural (weathered rock chips) rock surface?
- Does this activity also vary between an artificial (liquid inundated) and a more natural (moist set up) weathering environment?
- Does media type (water, minimal salts medium and, minimal salts medium with glucose) affect biological weathering activity?

Hypotheses from this last question include:

- The addition of inorganic nutrients (minimal salts medium) and carbon (minimal salts medium with glucose) will stimulate the growth of the heterotrophic population, potentially enhancing weathering activity.
- The addition of glucose will provide a readily available carbon source for oxidation, a by-product of this being the release of organic acids that could enhance bioleaching.
- The pH of the non-buffered media (water) will be more amenable to change than buffered (minimal salt media), which could alter the extent and types of biological weathering activity.

7.2 Methodology

7.2.1 Redcar Mudstone rock powder in M9 medium

7.2.1.1. Rock sample collection and preparation

Rock chips were collected from the walls and ceiling of Hole Wyke mine adit, located within the cliff face below Boulby Head and accessed via the foreshore, roughly 2 km West of Staithes village. See Chapter 4 for more details of the field site.

Surfaces covered in orange and black crusts (visually identified as ferromanganese deposits) were targeted for sampling. A previously flame sterilised rock hammer was used to break chips away from the rock surface into sterile Whirlpak bags. Large

chunks of mudstone rock were collected from a pile of rocks which appeared to come from a cave-in below a fault in the ceiling. Samples were kept at room temperature until they were returned to the laboratory, whereupon the rock chips were stored at 4° C until use.

The rock chunks were crushed in a mechanised rock crusher and the resultant powder size fractionated to below 500 μm.

7.2.1.2 Environmental enrichment culture in M9 medium

A 5 mL volume of rock chips was measured out in a 50 mL Falcon tube, and 20 mL of M9 medium was added. The lid was loosely screwed on before incubation at 27° C in a shaking incubator at 150 rpm in a lamp lit room for 17 days. This culture was used to inoculate the main experiment.

7.2.1.3 Experimental set up, sample processing and analysis

Five grams of Redcar mudstone powder (<500 μm) was added to 15 individual 100 mL Erlenmeyer flasks and autoclaved for sterilization. Three flasks were put to one side, for analysis of untreated rock (not incubated in either sterile or inoculated medium). The remaining 12 flasks were then filled with 20 mL of M9 media, to half of which 200 μL of the enrichment culture was also added (biotreated), with no addition to the other half (control treatment). These flasks were then incubated standing at room temperature in a lamp lit room. After 2 weeks, three biotreated treated flasks and three control treated flasks were thoroughly mixed and an aliquot of culture removed for plating onto nutrient agar for CFU/mL quantification of the heterotrophic population. Another aliquot was removed for pH measurements. The remaining powder-liquid suspension was filtered twice with 0.22 μm filter to remove powder and cells. The supernatant was poured into a 14 mL Falcon tube, 2 drops (~100 μL) of 70 % nitric acid was added before storage at 4° C until used for chemical analysis with ICP-OES. The powder was frozen at -18° C until it was ground down to a finer powder (~1 μm) for XRD analysis. This whole process was repeated after 4 weeks for the remaining cultures.

For the ICP-OES, the following elements with the wavelengths chosen for analysis were quantified: Al (396.153), Co (228.616), Cu (324.752), Fe (234.349), Fe (257.61), Ni (231.604), Pb (220.353), Ti (336.121), V (318.400) and Zn (206.200). The wavelengths chosen for analysis in each culture was based on qualitative assessment of its fit to the standard curves for that wavelength. From the selected wavelengths for each element that fit this criteria, the wavelength with the highest correlation coefficient values for that fit were chosen for the analysis, with wavelengths only chosen if the value was equal to or greater than 0.999. See chapter 3 for more details of the methodology for ICP-OES and XRD.

7.2.2 Mulgrave shale rock chips under both liquid inundated and moist conditions

7.2.2.1 Rock sample collection

Weathered rock chips were collected from a scree slope on Sandsend Ness beside the Cleveland Way National Trail near Sandsend village. See Chapter 4 for more details of the field site. A flame sterilised gardening trowel was used to scoop chips into sterile Whirlpak bags. Samples were kept at room temperature until they were returned to the laboratory, where upon the rock chips were stored for 1 month at 4^{o}C until use.

7.2.2.2 Environmental enrichment cultures

Two sterile 250 mL Erlenmeyer flasks were filled with 20 g of rock chips and 50 mL of either water or modified M9 medium. The M9 medium was modified to reduce the pH buffer capacity of the medium, allowing greater pH variation within the experiment. A modified recipe for M9 was used where the bi-sodium phosphate was replaced with additional mono-potassium phosphate. To prepare the 5x M9 salts, 34.15 g of KH_2PO_4, 2.5 g NaCl, 5.0 g NH_4Cl is dissolved in 1 L. This was diluted (200 mL in 1 L total) with the addition of 2 mL of 1M $MgSO_4$ and 100 µL of 1M $CaCl_2$, and then adjusted to pH 7 with HCl. This modified medium was used to slightly reduce the buffering capacity of the medium without reducing overall cation concentration. The Erlenmeyer flasks containing medium and rock were gently

mixed by hand and then were left standing at room temperature in a lamp lit room for 26 days.

7.2.2.3 Liquid experimental set up and analysis

Five gram aliquots of rock chips were autoclaved twice in 125 mL Erlenmeyer flasks. Twenty millilitres of either sterile water, modified M9 or modified M9 with glucose (0.02 %) was added to each flask, along with 1 mL of inoculum. All media was adjusted to pH 7 using HCl and NaOH. For both the M9 and M9+glucose cultures, the modified M9 enrichment culture was added and the water enrichment culture was used to inoculate the water cultures. CFU/mL quantification of both enrichment cultures was carried out prior to the experimental set up, with the enrichment cultures accordingly diluted so that they had equal CFU concentrations for the experimental inoculation.

The required number of flasks were prepared to allow triplicate sample analysis at four different time points for each condition. Flasks were incubated aerobically at room temperature without stirring, with sacrificial time points analysed after 21, 49, 84 and 112 days. At each time point, the sample analysis procedure as detailed in section 5.2.1.3 was carried out but without preparation for XRD.

For the ICP-OES of the water cultures, the following elements with the wavelengths chosen for analysis were quantified: Al (394.401), Ca (317.933) Co (230.786), Cu (327.393), Fe (393.562), Mg (285.213), Mn (259.372), Na (330.237), Ni (231.604), P (178.221), S (181.975), Si (252.851) Ti (337.279) and Zn (206.200). The following elements were not analysed for both of the M9 culture types: Al (396.153), Co (230.786), Cu (327.393), Fe (234.349), Mn (259.372), Ni (232.003), Si (252.851), Ti (334.940) and Zn (206.200). For the ICP-OES of the M9 and M9 with glucose cultures, the following elements with the wavelengths chosen for analysis: Al (396.153), Co (230.786), Cu (327.393), Fe (234.349), Mn (259.372), Ni (232.003), Si (252.851), Ti (334.940) and Zn (206.200). All elements present from the components of the M9 medium were not included in the analysis. See Chapter 3 for more details of the methodology for ICP-OES.

7.2.2.4 Moist experimental set up and analysis

Moist incubation vessels were made by combining two 50 mL Falcon tubes together, with the bottom of the top tube sitting inside the opening of the bottom tube and tape being used to hold the tubes together. A hole was drilled into bottom of the top tube, to allow drainage of excess fluid from the top tube into the bottom one. This preparation was made under sterile conditions, including the flame sterilization of the drill bit to make the holes.

The top tube of each dry incubation vessel was filled with 5 g of rock chips and 1 mL of inocula from the modified M9 enrichment culture. Excess fluid was allowed to drain through the hole in the top tube into the bottom tube, leaving the rock chips moistened but not inundated in liquid. The tubes were then sealed with screw tight lids, which were opened once a week under sterile conditions to allow fresh air into the tubes.

Vessels were incubated aerobically at room temperature without stirring, with sacrificial time points analysed after 21, 49, 85 and 110 days.

At each time point, the rock chips were transferred into a 50 mL Falcon tube into 10 mL of modified M9 and hand inverted for 5 minutes to thoroughly mix. The rock suspension was then incubated aerobically at room temperature without stirring for 24 hours. After the first hour of incubation, 2 mL of mixed suspension was removed for pH analysis. After the full 24 hours, the remaining liquid underwent preparation as detailed in section 5.2.1.3 but without preparation for XRD.

For the ICP-OES of the moist incubation extractions, the following elements with the wavelengths chosen for analysis were quantified: Al (394.401), Co (230.786), Cu (327.393), Fe (238.204), Mn (259.372), Ni (231.604), Si (288.158), Ti (334.940) and Zn (202.548). All elements present from the components of the M9 medium were not included in the analysis. See Chapter 3 for more details of the methodology for ICP-OES.

7.2.3 Statistical analysis

For the analysis of the ICP-OESresults, mean average concentrations with corresponding error bars were plotted onto bar graphs for comparison of elemental concentrations in the biotreated and control conditions. Error bars represent standard error of the mean average taken from single measurements of triplicated samples (i.e. three flasks were prepared and incubated for every condition tested). The error between ICP-OES measurements taken from a single sample was negligible. The normality and variance of data collected was initially assessed visually using normality and residuals plots. The Shapiro-Wilks test for normality and the Bartlett test for homogeneity of variance was then used to statistically determine normality and equal variance. For data sets with equal variance, 2-way analysis of variance (ANOVA) tests (T-W) were used to determine the effect of incubation time and treatment (biological or control) on elemental concentration. In cases where a parametric test could not be used, Kruskal-Wallis tests (K-W) were used to compare a single effect (e.g. treatment) on elemental concentration.

7.3 Results

7.3.1 Redcar Mudstone rock powder in M9 medium

In order to ascertain the level of microbial growth in the liquid-rock powder cultures, CFU/mL quantification was carried out for the heterotrophic population by plating the medium onto nutrient agar plates. Heterotrophic CFU/mL was taken as a proxy for the establishment and growth of the microbial community within these cultures. The majority of growth in the heterotrophic population occurred in the first 14 days (Fig. 7.1), with only a small increase in population size between days 14 and 28.

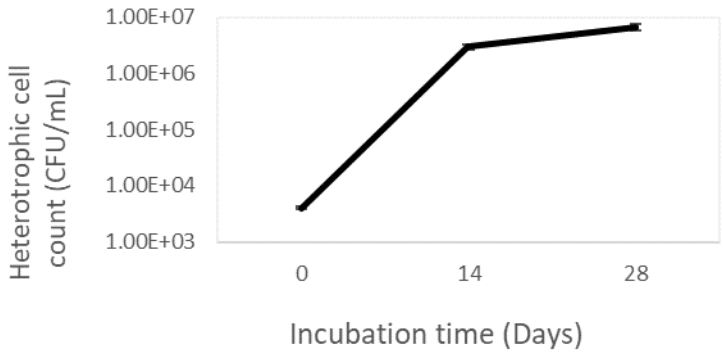

Figure 7.1¦ Heterotrophic CFU/mL quantification at inoculation (0 days) and after 14 and 28 days in the Redcar Mudstone rock powder in M9 medium experiment. Plotted values are mean average calculated from biological replicates (N=3). Error bars are for standard error of the mean, which are sufficiently low as to be obscured by the data points.

The pH for both the biotreated and control cultures remained the same throughout the experiment (pH 7.4), with no significant difference between the two conditions.

Elemental concentrations after 14 and 28 days of incubation did not reveal biologically enhanced leaching (Fig. 7.2). However, two-way ANOVA models did reveal that concentrations of Mn (T-W, effect of treatment on concentration, $F=5.42$, $p=0.0449$), Ni (T-W, effect of treatment on concentration, $F=17.36$, $p=0.0118$) and V (T-W, effect of treatment on concentration, $F=17.36$, $p=0.00876$) were significantly affected by treatment, demonstrating that microbial growth/activity reduced

concentrations of these elements in the leachate. Although no other significant differences were observed between biotreated and control conditions for the other six elements, the concentration of both Al for the first time point and Zn for both time points were lower in the biotreated samples compared to the control (Fig. 7.2).

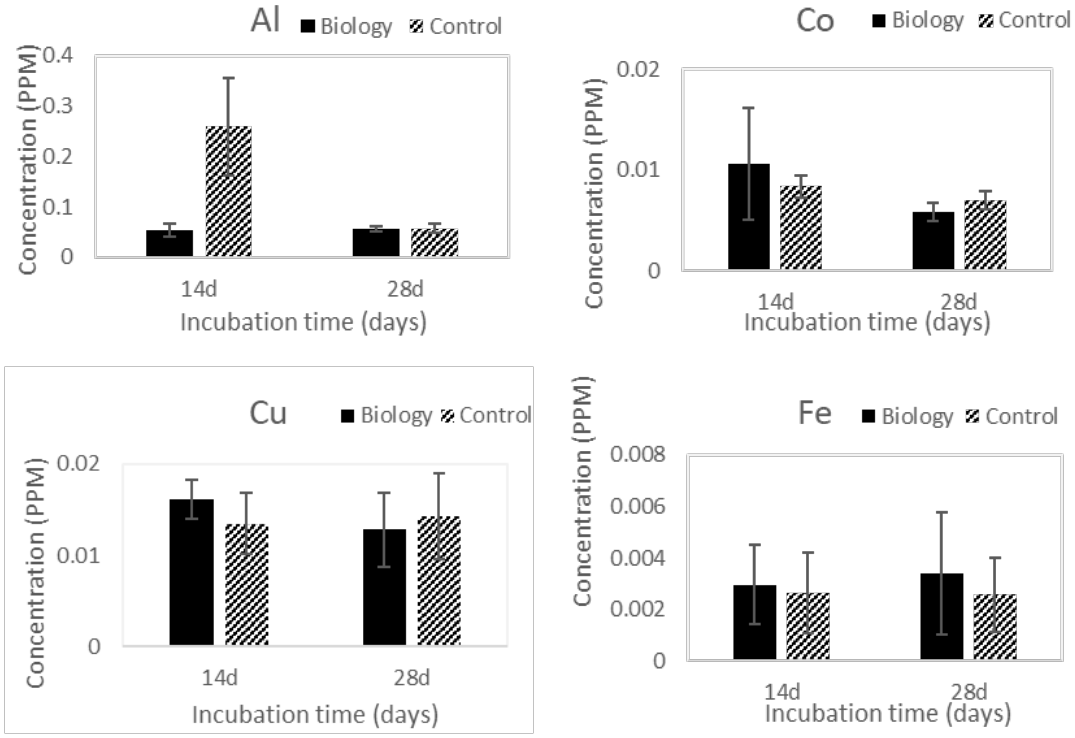

Figure 7.2¦ Elemental concentrations (PPM) in the culture medium after 2 weeks (14d) and 4 weeks (28d) from the Redcar Mudstone rock powder in M9 medium experiment. Plotted values are mean average calculated from biological replicates (N=3). Error bars represent standard error of the mean.

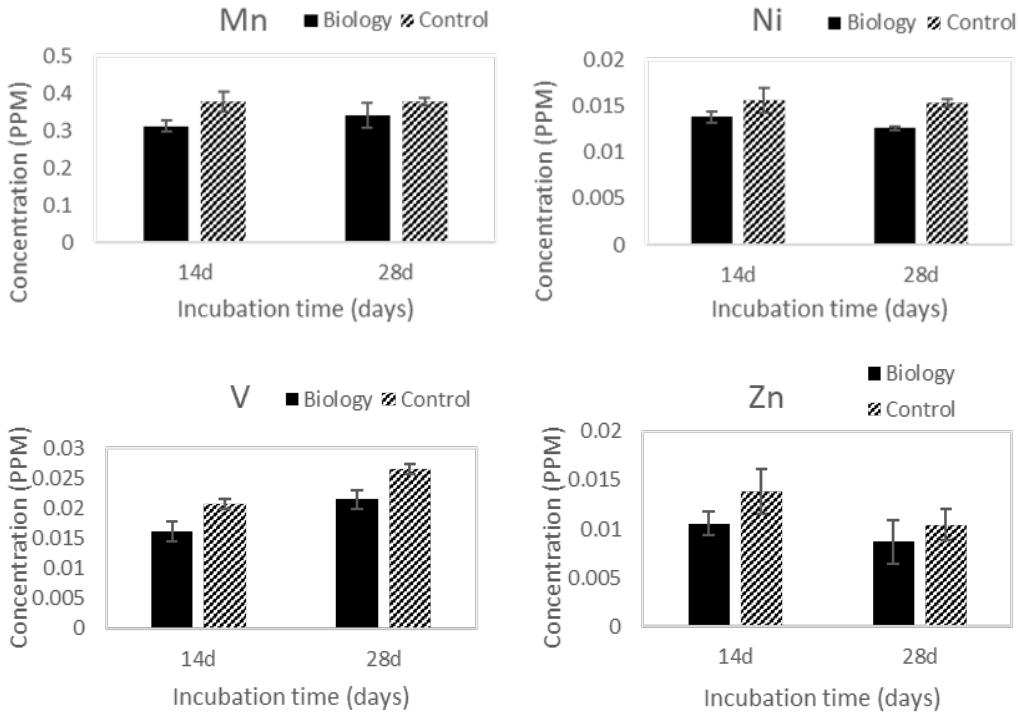

Figure 7.2 (continued)¦ Elemental concentrations (PPM) in the culture medium after 2 weeks (14d) and 4 weeks (28d) from the Redcar Mudstone rock powder in M9 medium experiment. Plotted values are mean average calculated from biological replicates (N=3). Error bars represent standard error of the mean.

XRD analysis of the Redcar mudstone revealed that several of the more reactive minerals were present at concentrations below the 1 % confidence limit, so their exact percentage composition cannot be determined accurately (Fig. 7.3). The major minerals identified were quartz (46 %), illite (13 %), albite (11 %) and kaolinite (8 %). In total, 26 % of the mudrock was comprised of clay. No evidence supporting secondary mineral formation, such as increased concentrations of secondary minerals from pyrite oxidation such as jarosite or gypsum were observed from the rock XRD analysis. There was no apparent difference between the mineralogical composition of the untreated shale and the control or biotreated shale after 14 days of incubation.

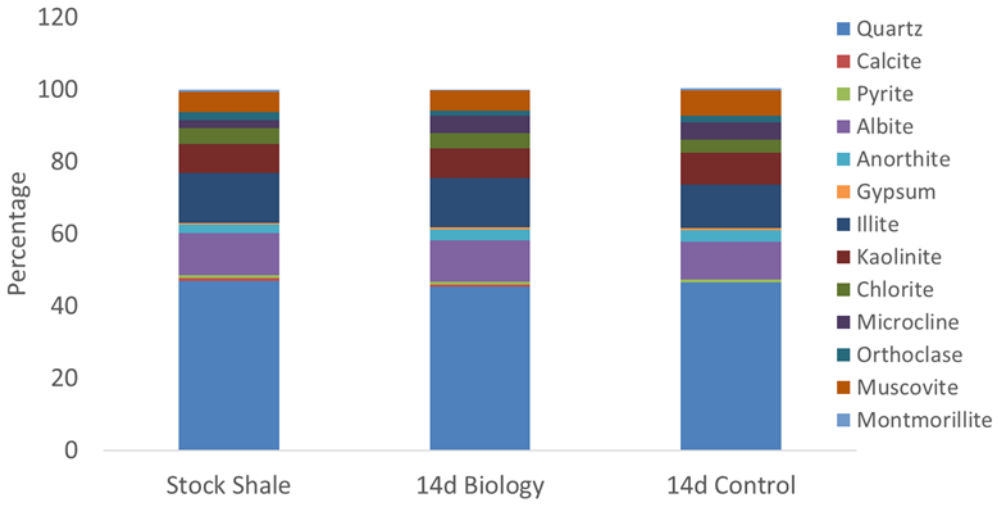

Figure 7.3¦ Mineralogy of the Redcar Mudstone rock powder without treatment (stock) and after 14 days of biotreated and control incubation in M9 medium as part of the Redcar Mudstone rock powder in M9 medium experiment. The minerals calcite, pyrite, gypsum and montmorillite were below the 1 % confidence limit, but their approximate percentage presence is presented here.

Overall there appears to have been little biological alteration of the geochemical conditions in this experiment, with the exception of reduced media concentrations of Mn after 2 weeks and Ni and vanadium after 4 weeks.

7.3.2. Mulgrave shale rock chips under both liquid inundated and moist conditions

7.3.2.1 Heterotrophic populations and pH

Following on from the lack of observable evidence for bioweathering of the Redcar Mudstone in M9 medium, the experiments described below attempted to replicate more natural, *in situ* conditions that might better reveal biogeochemical activity on shale rock.

Firstly, unaltered shale chips (other than sterilization via autoclaving) collected from the environment were used as the solid substrate for the experiment, rather than a refined rock powder. Although using unrefined material would likely introduce greater heterogeneity between samples, the benefits of a creating a more natural weathering environment was deemed justifiable. The experiment was also carried out

over a longer time period with more time points (110-112 days, 4 time points) to better resolve any potential biological activity over time.

The heterotrophic population in the samples were quantified at each time point, with significantly more growth in the liquid medium M9+glucose and M9 cultures compared to the water culture (1.5 orders of magnitude - Fig. 7.4). Despite the addition of a carbon source (0.02 % glucose) in the M9+glucose cultures, this did not significantly increase heterotrophic growth compared to the M9 cultures. Growth did not occur in the water cultures, but the inoculated microbial community slowly declined throughout the experiment. The heterotrophic population in the moist experiment significantly decreased between the experiment initiation and the first time point after 21 days (Fig. 7.4), and continued to decrease throughout the experiment by almost two orders of magnitude.

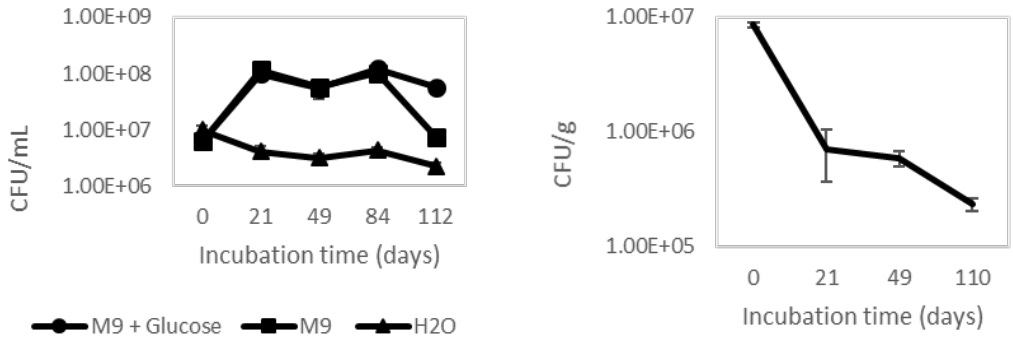

Figure 7.4¦ CFU/mL quantification on nutrient agar plates of the heterotrophic community in the biotreated cultures of the Mulgrave shale rock chips in liquid media (left) and under moist conditions (right). Plotted values are mean average calculated from biological replicates (N=3). Error bars represent standard error of the mean.

The pH in the liquid medium cultures remained relatively stable over the course of the experiment, with sample pH not varying more than 0.2-0.3 pH units (Fig. 7.5). The pH of the water culture was acidic at pH 3, while the pH of the M9 and M9+glucose cultures was only mildly acidic (~pH 4.7-5.1). The pH of the biotreated cultures was slightly lower than the control cultures for both the water and the M9+glucose cultures, but these differences were not consistently significant. The pH of the moist experiment remained stable at ~pH 5.5 throughout the experiment, with

no difference between the biotreated and control samples. All cultures, in both the liquid and moist experiments, had a significant drop in pH after 84-85 days, but with no difference between the biology and control (Fig.7.5).

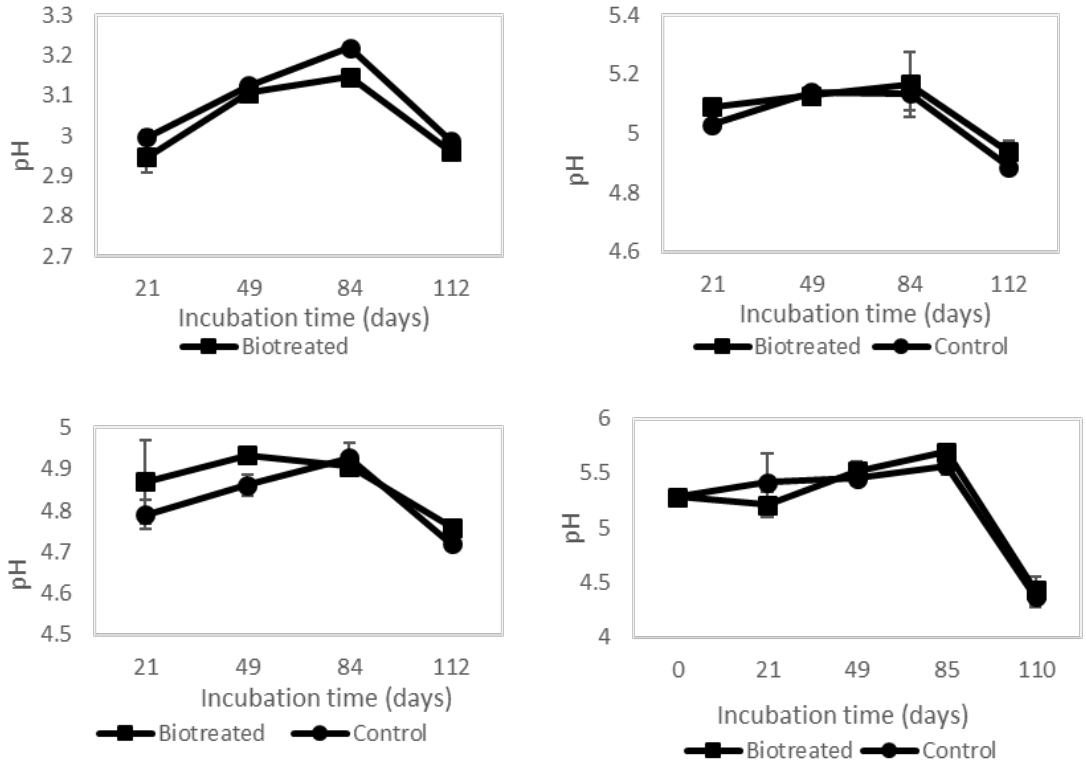

Figure 7.5 pH of the liquid medium (or liquid extract for the moist experiment) of the biotreated and control cultures in the Mulgrave shale rock chips in liquid medium (H2O - top left; M9 – top right; M9+Glucose – bottom left) and under moist conditions (bottom right). Plotted values are mean average calculated from biological replicates (N=3). Error bars represent standard error of the mean.

7.3.2.2 Water culture ICP-OES data

For the majority of elements analysed in this experiment, there was no discernible trend of either biologically enhanced or reduced leaching compared to the control (Fig. 7.6). Element concentration did not vary in a noticeable trend over time, but concentrations did vary between time points with biotreated cultures having greater elemental concentrations at 21 and 84 days, but lower concentrations at 49 and 112 days. The lack of coherent trend in these differences has therefore been attributed to

the heterogeneity of the geochemical composition of the rock chips used in this experiment.

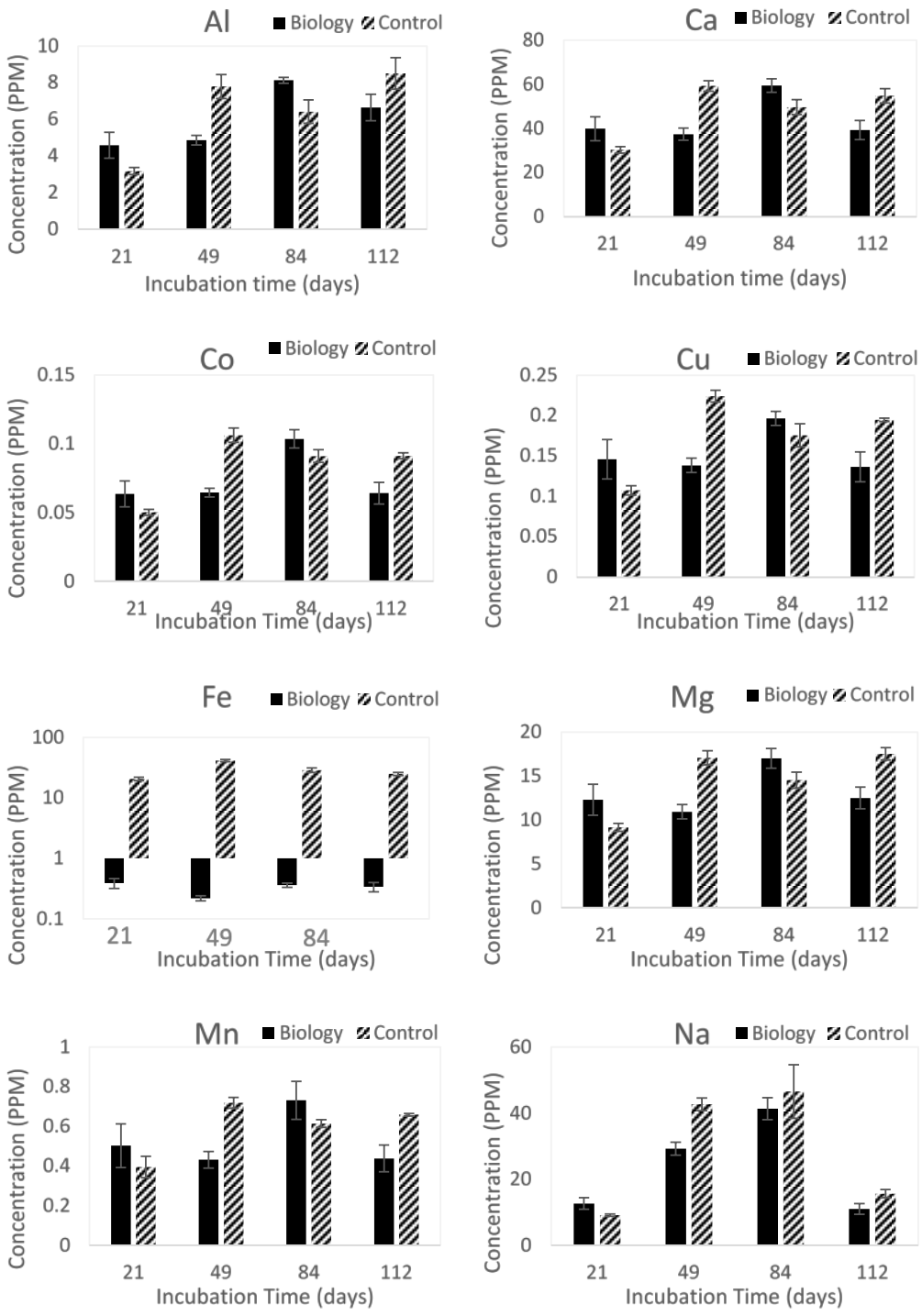

Figure 7.6¦ Elemental concentrations (PPM) in the biotreated culture and control mediums after 21, 49, 84 and 112 days of incubation from the Mulgrave shale rock

chips in liquid medium (H_2O) experiment. Plotted values are mean average calculated from biological replicates (N=3). Error bars represent standard error of the mean.

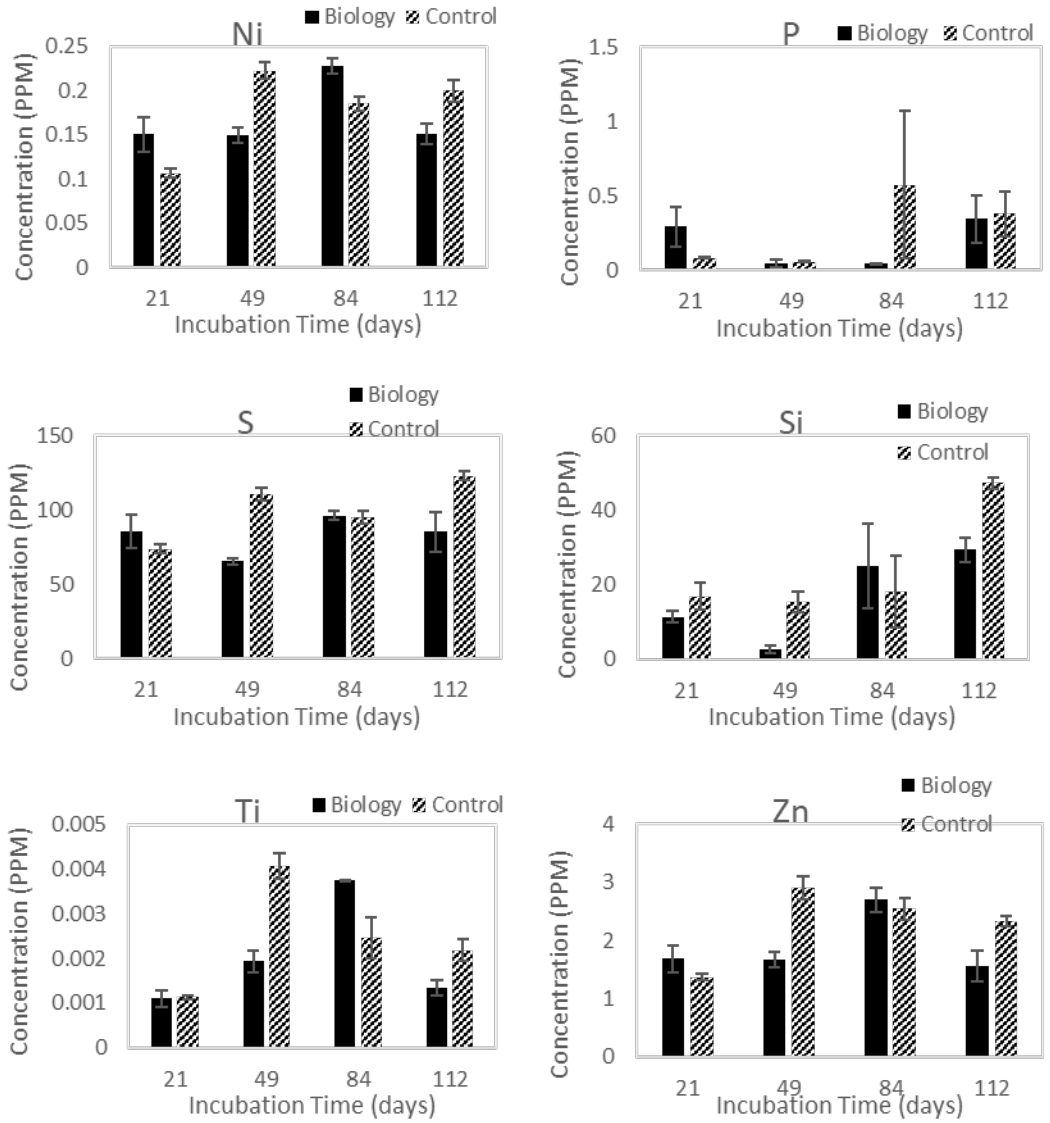

Figure 7.6 (continued)¦ Elemental concentrations (PPM) in the biotreated culture and control mediums after 21, 49, 84 and 112 days of incubation from the Mulgrave shale rock chips in liquid medium (H_2O) experiment. Plotted values are mean average calculated from biological replicates (N=3). Error bars represent standard error of the mean.

The exception to these results is the significantly lower concentration of iron in the biological culture medium compared to the control at all time points The exception to

these results is the significantly lower concentration of iron in the biological culture medium compared to the control (K-W, effect of treatment on concentration, X^2 = 17.28, $p<0.001$). The iron concentration of the liquid medium in the biotreated samples is around 0.5 ppm, two orders of magnitude below the control samples at around 50 ppm (Fig. 7.6). The same difference seen at all time points indicates that the trend is not only real, but that the biological activity causing it occurred early on (within the first 21 days) in the experiment.

7.3.2.3 M9 culture ICP-OES data

Compared to the results of the water culture experiment, the elemental concentrations in the liquid medium were overall much more stable (Fig. 7.7). However, elements did distinctly group into different trends.

For Cu, Fe and Mn (and to some extent Co) there was no difference in concentration between the biotreated and control samples at any of the four time points, but the concentration did rise in both sets of conditions over the course of the experiment. A second group can be separated by the stark differences in elemental concentrations at 21 and 112 days compared to 49 and 84 days (Al, Si and Ti). For Al and Ti, there were significantly higher concentrations for both the biology and control conditions at 49 and 84 days compared to 21 and 112 days. The inverse was true for Si (lower concentrations at 49 and 84, higher at 21 and 112).

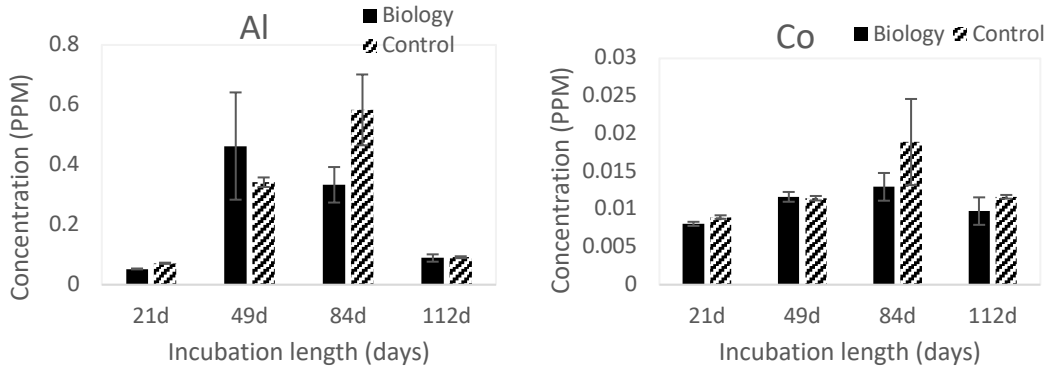

Figure 7.7 Elemental concentrations (PPM) in the biotreated culture and control mediums after 21, 49, 84 and 112 days of incubation from the Mulgrave shale rock chips in liquid medium (M9) experiment. Plotted values are mean average calculated from biological replicates (N=3). Error bars represent standard error of the mean.

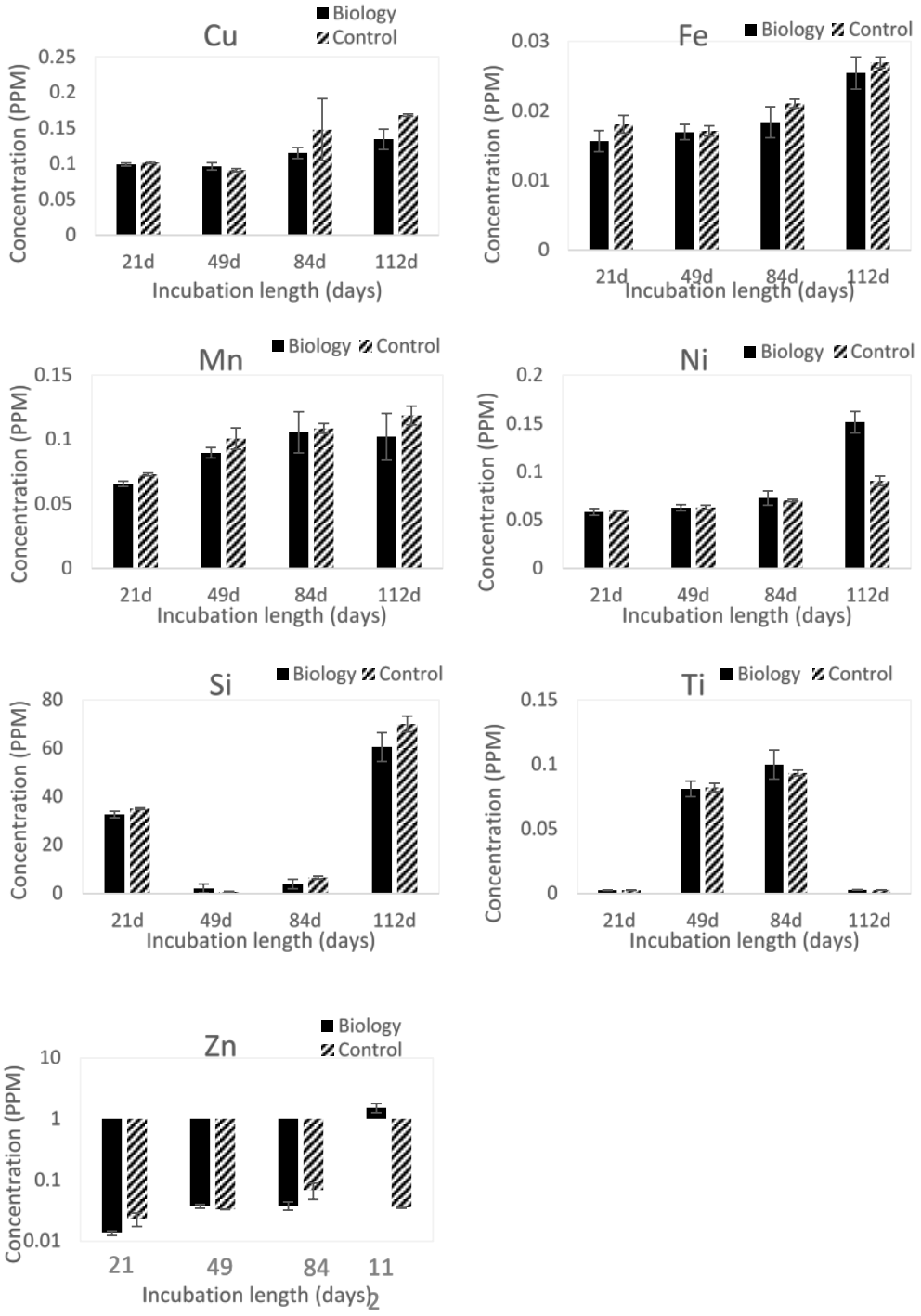

Figure 7.7 (continued)¦ Elemental concentrations (PPM) in the biotreated culture and control mediums after 21, 49, 84 and 112 days of incubation from the Mulgrave shale rock chips in liquid medium (M9) experiment. Plotted values are mean average

calculated from biological replicates (N=3). Error bars represent standard error of the mean.

A final group can be formed from Ni and Zn, where there is no difference between elemental concentration between 21 and 84 days, but at 112 days there is statistically significantly higher concentration in the medium of the biotreated samples compared to the control (Fig. 7.7). This is particularly prevalent in the case of Zn, where the concentration is over an order of magnitude greater. A Kruskal-Wallis test revealed a significant effect of incubation time on Zn concentration (K-W, effect of time on concentration, X^2=12.927, p=0.0047). A post-hoc Dunn's test on this analysis revealed a significant increase in zinc concentration (across treatments) between 21 and 84 days (Z=2.98, p=0.017), and 21 and 112 days (Z=3.18, p=0.008). However, the effect of treatment on Zn concentration across these incubation times was not shown to be statistically significant (K-W, effect of treatment on concentration, X^2=0.12, p=0.729).

7.3.2.4 M9+glucose culture ICP-OES data

The addition of 0.02 % glucose to the M9 medium, despite not increasing the heterotrophic CFU/mL compared to M9 alone (Fig. 7.4), did alter the pH of the medium (Fig. 7.5) and the pattern of elemental leaching for some elements (Fig. 7.8). One group that remained the same between the M9 and M9+glucose conditions is that of group two in section 7.3.2.3, the elements Al, Si and Ti. The same trend of increased concentration at 49 and 84 days for Al and Ti, with the inverse for Si, but without difference between the biotreated and control conditions was also observed in the M9+glucose cultures (Fig. 7.8).

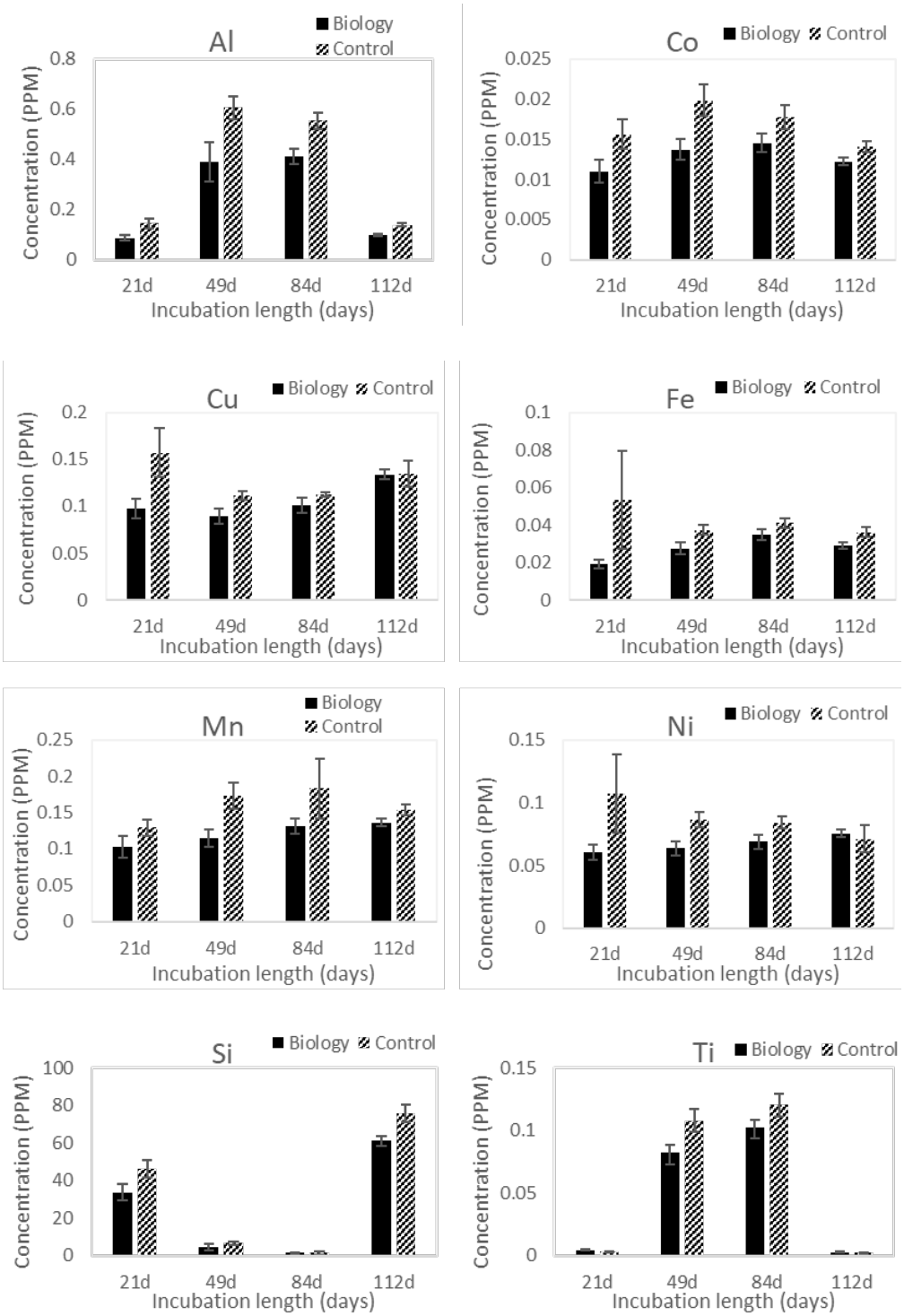

Figure 7.8¦ Elemental concentrations (PPM) in the biotreated culture and control mediums after 21, 49, 84 and 112 days of incubation from the Mulgrave shale rock chips in liquid medium (M9+glucose) experiment. Plotted values are mean average calculated from biological replicates (N=3). Error bars represent standard error of the mean.

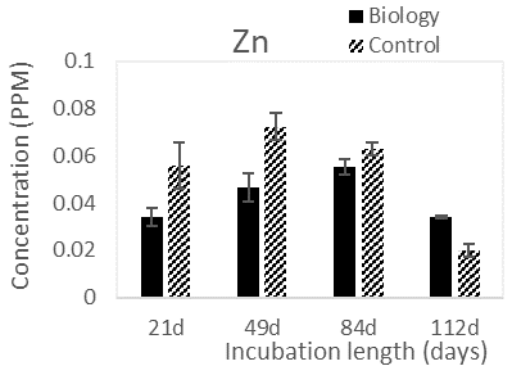

Figure 7.8 (continued)¦ Elemental concentrations (PPM) in the biotreated culture and control mediums after 21, 49, 84 and 112 days of incubation from the Mulgrave shale rock chips in liquid medium (M9+Glucose) experiment. Plotted values are mean average calculated from biological replicates (N=3). Error bars represent standard error of the mean.

However, for the group including Cu, Fe and Mn in section 7.3.2.3, the same trend is not seen in the M9+glucose medium (Fig. 7.8). Instead, an alternative group can be formed from the elements Co, Cu, Fe, Mn and Ni where there is a general trend of lower concentration of the element in the biotreated condition compared to the control. Statistical analyses showed that treatment had a significant effect on element concentration for Co (T-W, effect of treatment on concentration, $F=16.78$, $p= 0.000615$), Cu (T-W, effect of treatment on concentration, $F=6.206$, $p=0.0222$), Fe (K-W, effect of treatment on concentration, $X^2=9.01$, $p=0.0027$), Mn (K-W, effect of treatment on concentration, $X^2=8.33$, $p=0.0034$) and Ni (K-W, effect of treatment on concentration, $X^2=6.16$, $p=0.013$).

Zn forms a subgroup of this group, as it also has a significantly lower concentration in the biotreated condition compared to the control at 49 days, but then at 112 days the biotreated condition has a higher concentration compared to the control (Fig. 7.8). However, treatment did not have a significant effect on Zn concentration (KW, effect of treatment on concentration, $X^2=2.43$, $p=0.119$).

Despite this, the increased Zn concentration in the biotreated condition at 112 days is interesting, as it was also found in the M9 results (Fig. 7.7). The group containing

elements Al, Si and Ti, despite having their own trend, match with the group containing Co, Cu, Fe, Mn and Ni in having generally lower concentrations in the biotreated condition compared to the control (Fig. 7.8).

7.3.2.5 Moist experimental set up – extraction medium ICP-OES data

The results of this experiment are not directly comparable to those obtained in the liquid medium experiments, due to different experimental conditions. It is therefore unsurprising to note that the results of this experiment largely differed from that of the previous three experiments. For all of the elements analysed (Fig 7.9), there was for most time points no difference between the elemental concentration in the biotreated condition compared to the control. However, concentration change over time can be used to distinctly group certain elements.

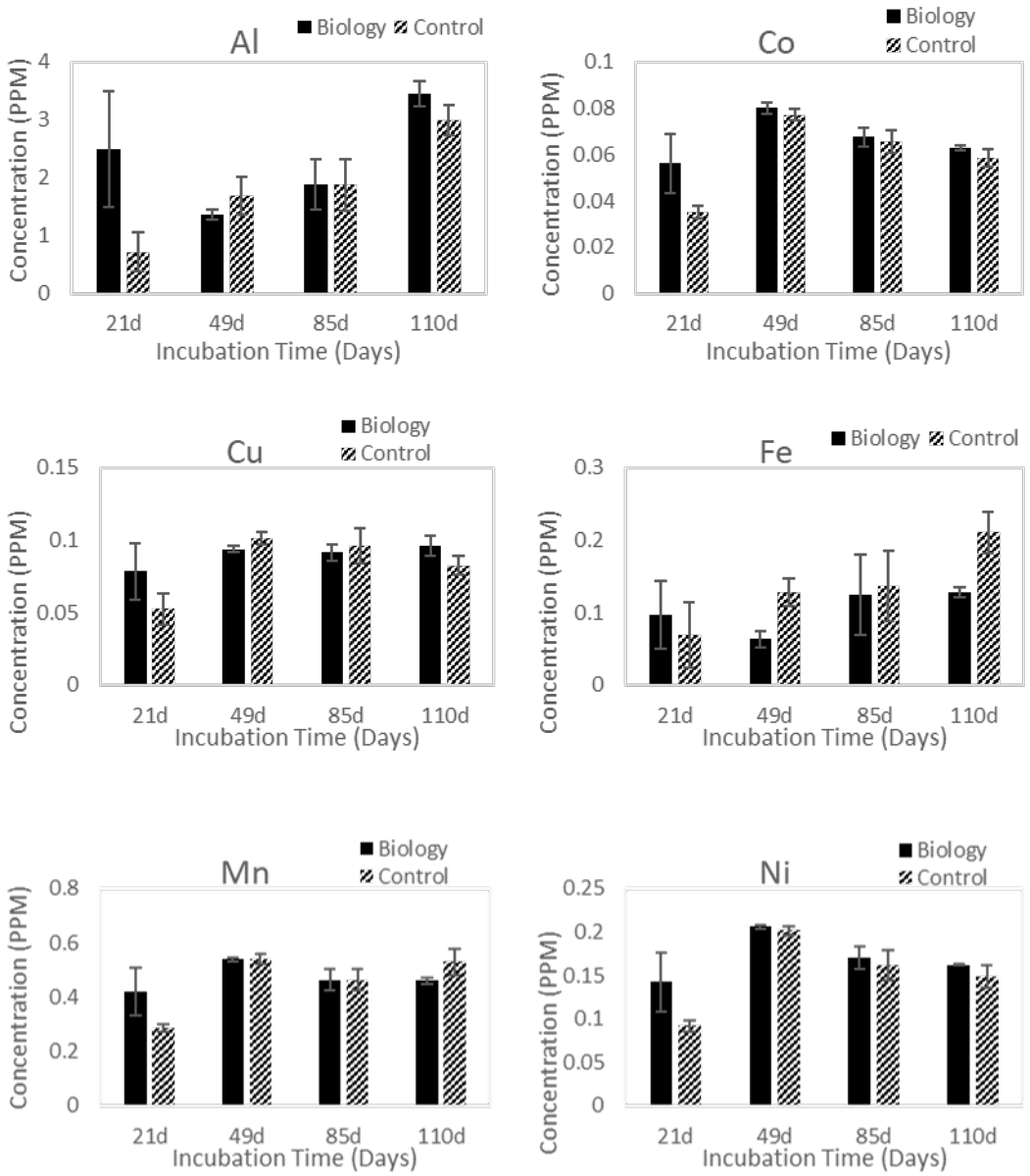

Figure 7.9¦ Elemental concentrations (PPM) in the extraction medium from the biotreated and control treated rock chips after 21, 49, 85 and 110 days of incubation from the Mulgrave shale rock chips under moist incubation experiment. Plotted values are mean average calculated from biological replicates (N=3). Error bars represent standard error of the mean.

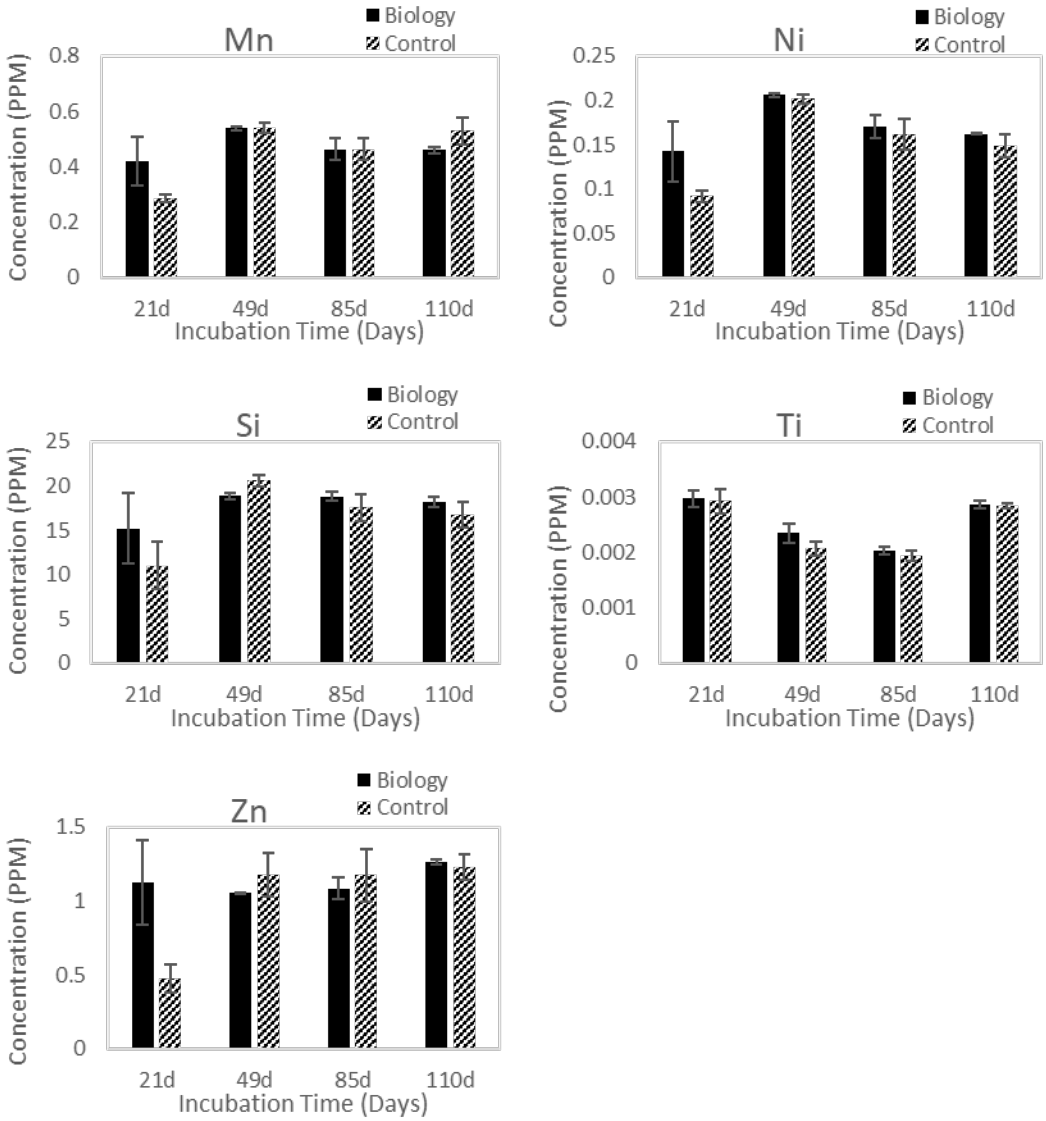

Figure 7.9 (continued)¦ Elemental concentrations (PPM) in the extraction medium from the biotreated and control treated rock chips after 21, 49, 85 and 110 days of incubation from the Mulgrave shale rock chips under moist incubation experiment. Plotted values are mean average calculated from biological replicates (N=3). Error bars represent standard error of the mean.

For the elements Al and Fe, there appears to be an increase in both the biotreated and control conditions over time (Fig. 7.9). Another group can be formed from Co, Mn, Ni and Si, where the concentration of elements in both conditions increases between 21 and 49 days, but then slowly decreases for the remaining two time points. A

subgroup of this can be formed from Cu and Zn, where concentration also increases between 21 and 49 days, but then remains stable for the remainder of the experiment.

Finally, Ti has an alternate trend of having an initially high concentration at 21 days that then drops until 85 days, whereupon it increases again at 110 days (Fig. 7.9).

An additional general trend is that at 21 days, there is a higher elemental concentration in the biotreated condition compared to the control (Fig. 7.9). This trend is particularly true for Al, Co, Mn, Ni and Zn. A final notable result is for Fe where at both 49 and 110 days, the elemental concentration in the biotreated condition is lower than that of the control, with the result being significant at 110 days (Fig. 7.9).

7.4 Discussion

7.4.1. Redcar Mudstone rock powder in M9 medium

An assessment of the results of the powdered shale experiment in section 7.3.1 reveals a lack of evidence for biotreated activity that could be associated with enhanced bioleaching or weathering of the shale. The medium supported a heterotrophic population which grew over time (Fig. 7.1), but growth of this or other metabolic populations in the cultures did not alter solution pH, which remained at roughly pH 7.4 throughout the experiment for both biotreated and control cultures.

The incubation of the shale in media, both under the control and the biotreated conditions after 14 days, did not alter the rock's mineralogical composition compared to the untreated rock as discerned by XRD analysis (Fig. 7.3). The main mineralogical constituents of the rock were quartz (46 %), albite (11.5 %), the clays illite, kaolinite and chlorite (total 26 %) and the mica muscovite (5.5 %). Pyrite was the only iron sulfide identified (0.7 %) and calcite the only carbonate (0.82 %), but both were below the 1 % confidence limit and so their exact abundances cannot be known with certainty. Gypsum ($CaSO_4$), a secondary mineral formed by pyrite-liberated iron reacting with calcite, was found at almost double the concentration in both the biotreated and control treated shale (0.68 %) compared to the untreated

shale (0.35 %). However as the abundance values are all below the confidence limit assumptions about underlying biogeochemical processes cannot be made.

The lack of biological weathering activity is further supported by the ICP-OES data, which revealed no evidence for biological enhanced leaching for any of the elements analysed (Fig. 7.2). However, biologically treatment resulted in decreased concentration of Mn (T-W, effect of treatment on concentration, T=5.42, p=0.0449), Ni (T-W, effect of treatment on concentration, T=17.36 p=0.0118) and V (T-W, effect of treatment on concentration, T=17.36, p=0.0087). Matlakowska and Sklowdowska, (2010) observed enhanced leaching of V, Cu and Co in their experiments, but only increased V concentration in the leachate with Cu and Co being up-taken by the microbial biomass (Matlakowska and Sklowdowska,2010). Vanadium, nickel and manganese are all utilised by both prokaryotes and eukaryotes for enzyme and other protein cofactors (Rehder, 2015; Crabb and Moore, 2010) so it is possible they have been selectively taken up the microbial community.

An alternative explanation include their sequestration from the leachate by secondary mineral formation (Matlakowska *et al*., 2012), but this would seem surprising as the concentration of Cu, an element that would be expected to form copper sulfides in the presence of sulfur (present in the M9 medium) was not reduced. Evidence that could support secondary mineral formation would be the biologically reduced concentration of Al at week 2 (Fig. 7.2) which, although not statistically significant, has been observed due to the formation of aluminium phosphate precipitation in other studies (Matlakowska *et al.,* 2012).

A further possibility is that of cationic metal absorption to the anionic surfaces of both live and dead cellular material and exopolymeric substances (EPS) (François *et al.,* 2012; Rajpert *et al.,* 2013). However, this then requires an explanation of why other cationic metals in the solution such as Cu, Co and Zn did not also have a reduced concentration in the biotreated leachate (Fig. 7.2).

7.4.2. Mulgrave shale rock chips under both liquid inundated and moist conditions

7.4.2.1 Microbial iron oxidation on rock chip surfaces in the acidic environment of the water cultures

Growth of the heterotrophic population was not significantly different over the course of the experiment between the M9 and M9+glucose conditions, however the heterotrophic population in the water culture did not grow but slowly declined throughout the experiment (Fig. 7.4). This suggests that there was insufficient nutrients to support a heterotrophic population in the absence of M9 nutrients, and that the addition of 0.02 % glucose did not provide a sufficiently abundant carbon source to support further growth.

The lack of growth in the heterotrophic population of the water culture could also have been pH controlled, with the pH of the water being more acidic (pH 2.9-3.2) than that of the M9 (pH 4.9-5.2) or M9+glucose (pH 4.7-4.9) (Fig. 7.5). No consistent significant differences were observed between the biotreated and control conditions for any of the media, suggesting that pH was defined by geochemical processes. The lower pH of the M9+glucose media compared to M9 indicates that abiotic oxidation of glucose to form organic acids could have occurred (Fig. 7.5).

The results of the ICP-OES elemental analysis for the water cultures provides a broad picture of fluctuating concentrations that is most readily explained by variation in the rock chips collected for the experiment (Fig. 7.6). The only consistent evidence for biological alteration of elemental concentration was for iron, where at every time point (from 4 weeks onwards) the Fe concentration was biologically reduced by 2 orders of magnitude (K-W, effect of treatment on concentration, $X^2 = 17.28$, $p<0.001$ - 0.5 ppm in biotreated conditions, 50 ppm in the control) (Fig. 7.6). It is likely that this level of reduction was primarily caused by microbial iron oxidation, although the results could be partially explained by the factors provided for biologically reduced concentration in section 7.4.1. The rock chips incubated under biotreated conditions in the water cultures had visibly extensive patches of orange/yellow colouration. The chips had already undergone environmental

weathering and had orange/yellow colourations when collected, but these patches appeared more extensive in the biological water cultures compared to the other conditions.

Microbial iron oxidation is known to be energetically favourable for microorganisms growing in aerobic conditions at pH 4 and below (Heidrich *et al.,* 2011), which would explain why this result was only obtained in the water cultures (Fig. 7.6). However, the source of reduced iron from the shale likely would have been an iron sulfide such as pyrite, meaning that if the pyrite underwent a redox reaction to become oxidised, then the sulfur it was previously complexed with would have been liberated. No trend of consistent biologically enhanced leaching of sulfur was observed (Fig. 7.6) suggesting that if microbial iron oxidation has occurred, then the concentration of sulfur in the medium has been regulated by abiotic, geochemical processes.

The observation of microbial iron oxidizing activity in this experiment fits with the isolation of iron oxidizing microbial strains from the results of Chapter 5, and from the ubiquitous presence of ferromanganese deposits identified in the field detailed in Chapter 4.

7.4.2.2 Possible bio-enhanced leaching of Ni and Zn from rock chips in M9 media

In the M9 medium experiments, although not statistically supported, there is evidence for bio-enhanced leaching of both Ni and Zn after 112 days (Fig. 7.7). Three possible explanations can be put forward to explain this result. Firstly, this result could be due to rock sample heterogeneity. If the rock samples used in the flasks for time point processing at 112 days were rich in Ni and Zn minerals (e.g. metal sulfides such as Sphalerite), then the enhanced concentration of these elements in the leachate could be explained. However, this does not explain why the results for Ni and Zn are not more variable across the whole experiment. The second explanation is that bioenhanced leaching of these elements was observed towards the end of the experiment (84 and 112 days) due to a distinct change in biological activity occurred between the start and end points of the experiment. A change in microbial community composition could provide an explanation for this change in

activity, with long generation time species/s accumulating in substantial numbers to have a significant contribution to shale leaching. However, if this change in community structure did occur, it was not reflected by a change in the abundance of culturable organisms (CFU/mL measurements – Fig. 7.4).

Another question that needs to be addressed is why enhanced leaching of Ni and Zn was observed, but not for other transition metals such as Fe, Mn, Cu or Co. Leachate concentrations of Ni and Zn in the M9 and the M9+glucose cultures were within a similar range (0.05-0.15ppm for Ni, 0.01-0.07ppm for Zn) (Fig. 7.7 and 7.8), if excluding the bio-enhanced leaching measurements, but these values are much lower compared to the water leachate concentrations (0.1-0.215ppm for Ni and 1.5-3ppm for Zn) (Fig. 7.6). The enhanced concentrations of Ni (0.15ppm) and Zn (1.5ppm) (Fig. 7.7) bring the concentrations within the range of the water leachate concentrations.

Numerous other studies have demonstrated biologically enhanced leaching of Zn and Ni (Farbiszewska-kiczma *et al.,* 2004; Farbiszewska *et al.,* 2003; Sethurajan *et al.,* 2012), with suggested mechanisms including primary mineral dissolution (Matlakowska *et al.,* 2012;), complexation with organic acids and/or siderophores and acidolysis from organic acid action (Matlakowska *et al.,* 2010; Matlakowska *et al.,* 2013; Matlakowska *et al.,* 2014; Wlodarczyk *et al.,* 2015; Anjum *et al.,* 2010; Anjum *et al.,* 2009). Common among these studies however is that the bio-enhanced leaching is normally for a wide group of elements (where analysed), not just Ni and Zn.

Although the exact metallurgy of the rock chips taken from this experiment was not analysed in this study, Gad *et al.* (1968) did a detailed analysis of the geochemistry of the sediments on the Whitby coast, including the strata (Mulgrave bituminous shales) that were sampled for this work (Gad *et al.,* 1968). The abundance of Zn (82-160ppm) and Ni (52-100ppm) are higher than that of Co (14-19ppm) and Cu (34-40ppm), but are lower than Mn (160-220ppm). This high abundance of Zn in the rock is reflected in its increased concentration in the water culture leachate, but the Zn concentration in the M9 and M9+glucose leachates is lower than that of other elements leachate concentrations, despite being more abundant in the rock. The same

is true for the leachate concentrations and rock abundances of Ni. This suggests that a geochemical process is either preventing leaching or precipitating out of solution the Ni and Zn in the M9 and M9+glucose cultures. It also indicates that whatever process has reduced the Ni and Zn concentrations in the M9 and M9+glucose compared to the water cultures could have been reversed by biological activity.

Ni, Zn, Co, Cu, Mn and Fe are primarily found in shales as metal sulfides (e.g. sphalerite for Zn, pyrite for Fe) (Anjum *et al.,* 2012) all with similar solubility product constants except for pyrite (Suzuki, 2001; Tributsch, 1999; Tributsch, 2001), indicating that geochemical solubilisation of Zn and Ni sulfides should have been similar to that for other metal sulfides. However, an additional source of metals can come from metal binding porphyrins and other organic matter (Szubert *et al*., 2006; Matlakowska and Sklowdoswka, 2010). Wlodarczyk *et al.* (2016) found that microbially produced complexing agents such as siderophores and organic acids complexed with both Cu and Zn from black shale leachate, suggesting that microbial activity had enhanced leaching of these two elements.

In contrast, microbial activity has also been shown to reduce element concentration in leachate, with suggested mechanisms including biologically mediated mineral precipitation (Matlakowksa *et al.,* 2012; Wlodarczyk *et al.,* 2016). Transmission electron microscopy imaging of microbial cells in cultures showed cells with outer membrane vesicles that appeared to be acting as nuclei for metal sulfide and phosphate mineral formation (Matlakowska *et al*., 2012). This observation is used to explain reduced concentrations in the biological leachate of various metallic elements and sulfur in their study. In the study presented here, magnesium sulfate is a constituent of the M9 medium, which could provide an abundant sulfur source for mineral formation and precipitation.

Metal adherence to live and/or dead biomass and EPS can also sequester metals from solution. The cationic charge of free dissolved ions of metals allows them to bind to anionic charges on biological material, such as proteins and polysaccharides (François *et al.* 2012). In Rajpert *et al.* (2013), Cu mobilised from black shale by the yeast *Rhodotorula mucilaginosa* bound to both live and dead biomass (Rajpert *et al.,*

2013). Similar results were found with Zn and Ni adhering to biomass and EPS (Drozdova *et al.,* 2014; Guibaud *et al.,* 2004)

Taking all of this information into account, there are three biological hypotheses to explain enhanced leaching of Ni and Zn: a) that selective microbial action bio-enhanced leaching of Ni and Zn, either through metal sulfide dissolution or extraction from metalloorganic complexes, b) that microbial presence/activity caused mineral precipitation of metal sulfides (or other minerals that complex these metals), but these processes excluded Ni and Zn or c) that a range of metals including Ni and Zn were precipitated by either biogeochemical or geochemical processes, but that microbial activity resulted in the redissolution of precipitated Ni and Zn minerals. Alternatively, these results could be explained by sample heterogeneity, meaning that no microbially enhanced leaching was detected.

Work in Chapter 5 isolated numerous microbial isolates of the same genera as isolated weathering organisms in other studies (Matlakowksa and Sklowdowska, 2009; Farbiszewska-Kiczma and Farbiszewska, 2004). Matlakowska and Sklowdowska(2009) isolated eight microbial strains including the genera *Pseudomonas*, *Microbacterium* and *Bacillus* with weathering capabilities such as siderophore production, porphyrin and polycyclic aromatic hydrocarbon degradation, organic acid production and phosphatase activity (Matlakowska and Sklowdowska, 2009). These 8 strains have been used in a series of studies by this group to investigate the various mechanisms of microbial activity that alter shale biogeochemistry as previously described in this Chapter including metalloporphyrin degradation (Matlakowska and Sklowdowska, 2010), organic acid production (Matlakowska *et al.,* 2014) and mineral precipitation inside the biofilm and outer membrane vesicles (Matlakowksa *et al.,* 2012; Wlodarczyk *et al.,* 2016). *Psuedomonas*, *Bacillus* and *Aeromonas* strains were also isolated by Farbiszewska-Kiczma and Farbiszewska (2005) for their ability to degrade organic compounds originating from shale mining waste tailings (Farbiszewska-Kiczma and Farbiszewska, 2005). These genera appear in multiple microbial shale weathering studies and are implicated as important contributors to rock and mineral weathering in the environment (Petsch *et al.,* 2005; Li *et al.,* 2014; Kalinowski *et al.,* 2006). All four genera (*Pseudomonas*, *Microbacterium*, *Bacillus* and *Aeromonas*) were

identified in Chapter 5 with weathering capabilities including siderophore production, acid production and phosphatase production.

The presence of such organisms within the shale weathering profiles sampled in this study suggests that the bio-enhanced leaching of Ni and Zn can likely be attributed to active microbial processes involved in shale weathering.

7.4.2.3 Transition metals sequestered from leachate by microbial community and possible biologically enhanced Zn leaching in M9+glucose media

Widespread statistically significant biologically reduced leaching of transition metals Co (T-W, effect of treatment on concentration, $F=16.78$, $p= 0.000615$), Cu (T-W, effect of treatment on concentration, $F=6.206$, $p=0.0222$), Fe (K-W, effect of treatment on concentration, $X^2=9.01$, $p=0.0027$), Mn (K-W, effect of treatment on concentration, $X^2=8.33$, $p=0.0034$) and Ni (K-W, effect of treatment on concentration, $X^2=6.16$, $p=0.013$) was observed in this experiment (Fig. 7.8). This provides evidence for biological activity having contributed to removal of metals from the leachate.

Referring back to the discussion in section 7.4.2.2., the potential explanations for such a result include biologically facilitated mineralization and precipitation of metal sulfides and/or other minerals (Matlakowska *et al.,* 2012), and metal adherence to live and/or dead biomass and EPS (Guibaud *et al.,* 2004). Either explanation, or more likely a combination of the two, are plausible to support the observed results. A question that needs to be addressed is why this widespread reduced concentration of metals in the leachate was observed in M9 media with supplemented glucose, but not in its absence. This is particularly curious as the addition of glucose did not stimulate further growth of the heterotrophic population (Fig. 7.4), although it did acidify the medium by roughly 0.2 pH (Fig. 7.5). A possible explanationis that, although glucose did not increase cell growth, it might have increased EPS production. The level of EPS production is known to be partially controlled by the availability of organic carbon in the environment (Hand *et al.,* 2008), so supplementing the medium with an available carbon source likely provided precursor molecules for EPS biosynthesis. The enhanced EPS production would provide a greater surface area for

metal adherence and mineral precipitation, explaining the reduced concentration of metals in the biological leachate (Fig. 7.8).

Another result from this experiment is the bio-enhanced leaching of Zn after 112 days (Fig. 7.8). This enhancement is not however as much as the increase in the M9 experiment (less than a one-fold increase)). As with the previous result in M9 medium (Fig. 7.7) both biological and sample heterogeneity can be proposed to explain this result. It should be noted however that the enhanced leaching of Ni seen in the M9 (Fig. 7.7) medium experiments was not found in the M9+glucose experiment (Fig. 7.8). If this result has been caused by biological activity, then it is possible that the same underlying mechanisms that enhanced leaching of Zn in the M9 experiment could have been active in the M9+glucose cultures.

7.4.2.4 Results of the moist set up experiment

Evidence was found for enhanced leaching of Zn at the first time point of this experiment (21 days) which further supports the importance of Zn leaching in the experiments presented in this Chapter. As with previous results, biological activity and sample heterogeneity can be put forward to explain these results. If the result is explained by biological activity, then it is worth noting that the enhancement in Zn leaching was at a different time point from its observation in the M9 and M9+glucose experiment (112 days).

The concentration of iron was biologically reduced after 110 days, but the result was isolated with no other elements demonstrating biologically reduced leaching.

7.4.3 Conclusions

The results of this Chapter provide a complex picture of microbial activity that has multiple influences on the geochemical environment of weathered shale. Broadly, these results can be summarised as the following: a) microbial iron oxidation that became metabolically favourable at an acidic pH (~pH 3) in the absence of inorganic nutrients or pH buffering components (Fig. 7.6), b) enhanced leaching of Zn and Ni in a slightly acidic (~pH 5), pH buffered solution with the addition of inorganic nutrients, both with (Fig. 7.8) and without (Fig. 7.7) supplemental glucose and c)

reduced concentrations of metals in the biological leachate of pH buffered solution with the addition of inorganic nutrients (Fig. 7.2), the effect of which was enhanced by the further addition of a carbon source (Fig. 7.8), suggesting that increased microbial biomass (EPS, rather than increased population size – Fig. 7.4) is responsible for this sequestration of metal cations.

The same microbial activity of metal sequestration was identified in an artificial (rock powder – Fig. 7.2) and more natural (weathered rock chips - Fig. 7.8) weathering system, but the results of this sequestration were stronger and more consistent in the more natural system. Furthermore, biological activity of enhanced elemental leaching was observed in the rock chip experiments but not in the rock powder experiment (Fig. 7.7). These results suggest that, despite greater sample variation in the composition of a natural weathered surface, it may provide more representative interpretations of microbial activity happening in the environment. Trying to extend this use of natural systems in the form of the moist experiment did not provide a platform for greater microbial activity (Fig. 7.9), suggesting that the controlling factors on the biological activity observed in these experiments may be more limiting in the actual environment.

The effect of different liquid medium composition had striking effects on the types and extent of microbial activity observed. Liquid water with no additional nutrients other than what leached out of the weathered shale provided an environment favourable to the growth of iron oxidizing microbes that had significantly altered the geochemistry of the environment within 3 weeks (Fig. 7.6). Such activity was not seen in the other two medium types, and can likely be attributed to the increased acidity of the water-rock medium (Fig. 7.5). The addition of inorganic nutrients did stimulate the growth of the heterotrophic population, but this was not further enhanced by the addition of 0.02 % glucose (Fig. 7.4).

Enhanced leaching of Ni and/or Zn was observed in biotreated cultures across 3 experiments (liquid M9, liquid M9+glucose, moist M9 set up) (Fig. 7.7, 7.8 and 7.9), but without further analysis a biological explanation for this result cannot be corroborated.

The results of this chapter demonstrate both the challenges, and the potential, of *in vitro* simulated weathering experiments to investigate microbial rock weathering processes. Within an *in vitro* experimental design as presented here, a broad array of environment (e.g. pH, oxygenation) and microbial growth parameters (e.g. nutrient availability, temperature) can be monitored and maintained. This allows for effect size of an investigated factor (e.g. nutrient limitation) to be maximised, by constraining confounding factors (e.g. liquid to rock mass ratio) that could influence the experimental outcome. In the case of the results presented in this chapter, greater control over factors such as liquid to rock surface ratio (use of uniform crushed powder, rather than weathered rock chips) could have enhanced the effect of results obtained (Fig. 7.7).

The use of geochemical models in this study could have provided insight into the potential effects and effect sizes of bioleaching activity. Software such as PHREEQC and Geochemists workbench can be used to model elemental leaching rates from bulk rock, based upon rock mineralogical composition and aqueous environment parameters including element saturation and temperature. By varying model parameters and exploring the resultant changes in predicted elemental leaching rates, the effect of abiotic leaching within the experimental design of the work this chapter could have been broadly defined. This could have led to an improved experimental design that could either enhance the effect size of biological leaching activity, or reduced the variability of abiotic leaching processes.

Chapter 8 - Surface colonization and weathering of shale-comprising minerals *in vitro* and *in situ*

8.1 Introduction

In order to understand how microbes interact with geological substrates, an investigation into how they colonise and potentially alter the different minerals within that substrate is crucial. In the case of shale, mineral grains compose the vast majority of the mass within the rock, and as such comprise the main available surfaces for microbes to interact with. Furthermore, due to the reducing conditions under which shale is formed, some shale-bound minerals are chemically reactive and therefore more liable to alteration by biological activity (Anjum *et al*., 2012).

Microbe-mineral interactions can be broadly thought about in terms of habitability i.e. how supportive a mineralogical environment is for the growth, activity, attachment and adherence of microbial cells to the mineral surface. Many microbial species will generally colonise surfaces where possible because it provides an adaptive advantage over planktonic growth, such as an enhanced resistance to stress (Hall-Stoodley *et al*., 2004). However, the habitability of any particular surface will be affected by a range of factors including surface roughness, physiochemical properties and whether the surface provides nutrients for microbial growth such as phosphorus or iron (Hori and Matsumoto, 2010; Bennett *et al*., 2001, Rogers and Bennett, 2004).

Any measure of habitability can be regarded at various scales or groupings of the minerals and organisms studied, such as a single species with a single mineral or a microbial community with a mineral assemblage (see Mielke *et al*., 2003 and Matlakowska *et al*., 2012 for examples). The scale at which microbe-mineral interactions are studied will affect the types of methods used to study them. These can be relatively straightforward such as direct cell counts of the colonised surface (McGuire *et al*., 2001), to more sophisticated methods that estimate colonised

biomass or try to assess species diversity (Cockell *et al*., 2011; Cowan *et al*., 2002, Edwards *et al*., 1999). The effect of microbial colonization on the mineral surface can also be investigated, as biological activity can act to alter surface chemistry or induce surface dissolution, producing characteristic biological footprints (Hiebert and Bennett, 1992; Mielke *et al*., 2003; Zhao *et al*., 2013).

In this study, I have focused on the microbe-mineral interactions of the following minerals: albite, calcite, muscovite, pyrite and quartz. The choice of these minerals was justified in Chapter 6, but essentially they are a representative collection of the mineralogy found within shale and mudrocks. Numerous studies of microbial interactions with these minerals have been undertaken, both with single species and with communities. The number of studies investigating pyrite, plagioclase feldspars and quartz are particularly high because quartz and plagioclase feldspars form the most abundant components of almost all rock types, and pyrite is significant in microbial iron oxidation and biogeochemical cycling (Gadd, 2010).

Microbial weathering of quartz has been demonstrated both under laboratory conditions, and within natural environments including aquafers, peat bogs, intertidal sediment and mountainous terrain (Bennett *et al*., 2001; Brehm *et al*., 2005). Microbial activity can produce acidity, resulting in proteolysis of Si-O-Si within the quartz mineral matrix, leading to surface dissolution. Numerous microbial mechanisms can produce this acidity including the release of organic acids and the production of acidic exopolysaccharides (Kinzler *et al.,* 2003). In some cases, microbially induced alkaline conditions can also cleave Si-O-Si bonds, having the same effect (Hiebert and Bennett, 1992). In both cases, direct microbial contact with the mineral surface or distal interaction of planktonic cells in the surrounding solution can weather quartz surfaces (Gadd 2010). The result of such weathering is normally identified on a polished surface by the occurrence of pits and linear etch marks that were not present in un-weathered controls (Hiebert and Bennett 1992; Bennett *et al.,* 2001, Brehm *et al*., 2005). As discussed in previous chapters, rates of weathering can be estimated by measuring the elemental release rate of rocks or minerals. Biological weathering rates of quartz vary widely in the literature, primarily dependent upon experimental set up and conditions, but are often relatively

low due to the strength of the atomic bonding within the mineral (Bennett *et al*., 2001)

An active discussion within the microbiological weathering community is to what extent we can consider microbes active agents of rock and mineral weathering (Uroz et al., 2009). Is microbial activity that contributes to weathering a by-product of their metabolism or is it an active, energetically expensive process which provides an adaptive advantage to those organisms? A primary argument put forward by those who are active proponents, is that microbes weather minerals to obtain growth limiting nutrients such as phosphorus (Uroz *et al*., 2009). Rogers *et al*. (1998) investigated different feldspar minerals as sources of nutrients for microbial growth in a freshwater aquafer, and found that those minerals with the highest phosphorus content were the most colonised (Rogers *et al*., 1998). For this reason, the rate of phosphorus release is often measured in microbial weathering studies of complex silicates (Rogers and Bennett, 2004).

Microbial weathering of complex silicates can be much faster than weathering of quartz, due to an additional mechanism available to the organisms. Metal cations present within aluminosilicate mineral matrices can be displaced by protons from microbially produced acidity, with these protons subsequently become oxidised to form water, which is then liberated to the surroundings. Theoverall result is the same as the other weathering mechanisms, the formation of gaps within the mineral matrix and dissolution of the mineral surface (Gadd 2010).

Non-silicate based minerals are weathered via different mechanisms, with mineral dissolution being just one outcome of overall weathering processes. Pyrite, like all metal sulphides, is weathered primarily by abiotic and biotically mediated redox reactions. Both iron and sulfur become oxidised, producing iron oxide/hydroxide minerals and sulfuric acid. The oxidation of iron within pyritic weathering is a multi-step process, with the rate of one intermediate step being increased by 10^6-fold by microbial activity (Mustin *et al*., 1992). Further details of these reactions can be found in Chapter 2, however overall these mechanisms result in dissolution of the mineral surface. The morphological effect of these processes has been extensively studied, with similar characteristic features being found between numerous studies

(Mustin *et al*., 1992; McGuire *et al*., 2001; Edwards *et al*., 2001; Mielke *et al*., 2003). They identify that microbial iron oxidation causes surface pitting, although the size and shape of these pits varied between studies and bacterial species used. These pits are often found to co-occur with secondary mineral deposits, formed from the products of the iron oxidation, surrounding the bacteria attached to the mineral surface (Edwards *et al*., 2001; Mielke *et al*., 2003). On a larger scale, these secondary deposits can extensively cover geological substrates that have undergone pyrite weathering (Joeckel *et al*., 2005).

In Chapter 5, I highlighted the various possible interactions that could occur between different microbial weathering mechanisms and found that they were performed by differing microbial groups. To understand the full extent of how microbial activity contributes to rock weathering, the total colonization of rock surfaces needs to be explored. In this chapter, the colonization of five representative shale comprising minerals was investigated both *in vitro* and *in situ*. An iron oxidizing enrichment community was chosen for the *in vitro* experiments, based on results obtained in Chapter 7 where iron oxidation was the dominant biological activity identified. In this chapter, three separate iron oxidizing communities isolated from different field sites were used to obtain a comprehensive understanding of mineral colonization in weathered shale environments.

In situ mineral mesocosms were established in the rock scree on the floor of Assholm mine (see Chapter 4 for images), and incubated for one year between August 2015 and August 2016. A suitable site for the mesocosms was chosen primarily based on site stability, where the buried samples would not be displaced by movement of the surrounding scree. The specific site was also chosen based on a seep from the mine wall that flowed into the burial area, hopefully facilitating sample colonization. The scree is composed of rock chips that have been eroded from the mine wall, which is heavily coated in secondary minerals including iron oxides/hydroxides. As such, it was hypothesised that the rock chips comprising the scree would harbour iron oxidizing microbes that would be able to colonise the buried mineral samples.

The questions addressed by the investigation are as follows:

- Are the selected minerals colonised to differing extents, and do these differences diverge between *in vitro* and *in situ* conditions?
- Do the microbial communities *in vitro* and *in situ* cause morphological alterations to the mineral surface that are indicative of weathering or deposition of secondary minerals?
- If so, are these signatures of weathering found more ubiquitously on some minerals compared to others?

Fluorescence microscopy and scanning electron microscopy were used to visually assess colonization and surface alteration of mineral samples, in order to address these questions.

8.2 Methodology

8.2.1 *In vitro* colonization of minerals in laboratory microcosms

Sample collection and iron-oxidizing enrichment cultures: In Chapter 5 section 5.2.1, details were provided of the collection of weathered shale samples. During this sample collection, additional samples from each site were directly inoculated into Sterilin screw top tubes (20 mL) containing sterile 10 mL Wakeman's iron-oxidizing liquid medium (Table 8.1 – adapted from Wakeman *et al*., 2008) with 0.5 g of crushed pyrite to each tube as an iron and an additional sulfur source. An iron-oxidizing enrichment was chosen based on the isolation of putative iron-oxidizing isolates in chapter 5 and the identification of microbial iron oxidizing activity in chapter 7. The specific liquid medium (Wakeman's) was chosen because it was used successfully to culture *Acidiferrobacter thiooxydans* in a previous study (Hallberg *et al*., 2011), the only iron oxidizing bacteria identified in the phylogenetic study of weathered shale carried out previously at Hole Wyke mine adit (Cockell *et al*., 2011). Further details of the field sites sampled can be found in Chapter 4.

Table 8.1¦ Adapted Wakeman's (iron-oxidizing) liquid medium recipe. Media preparations were adjusted to pH 3 using H_2SO_4.

Chemical	Concentration
Na_2SO_4	66.14 mg/L
$(NH_4)SO_4$	450 mg/L
KCl	50 mg/L
$MgSO_4$	25.15 g/L
KH_2PO_4	50 mg/L
$Ca(NO_3)_2.4H_2O$	14 mg/L
$K_2O_6S_4$	151 mg/L

Once inoculated, these enrichment cultures were incubated at room temperature for one month with natural daylight, with loosely screwed on lids to allow for gaseous exchange. At the end of this incubation period, three enrichment cultures were chosen for further work. The three enrichments chosen were inoculated from samples taken from three different site types: (A) Saltwick bay cliff (cliff surface), (B) Assholm mine (mine wall) and (C) Gaytres quarry (scree rock chips). Enrichments were also selected for those displaying signs of iron oxidation (orange colouration in the liquid medium and on the tube walls), but lacking signs of photoautotrophic growth (no green colouration).

Set up and inoculation of microcosms: Ten millilitres of each of the three chosen enrichment cultures was inoculated into 240 mL of fresh Wakeman's media (lacking pyrite), which was then split into two equal parts (125 mL). One part was sterilised by autoclaving the culture twice at 121°C for 20 minutes (control inoculum), the other was untreated (biology inoculum).

Three microcosm sets were established, each one being inoculated with a different enrichment culture (A-C). Each set had six 50 mL Falcon tubes, five tubes each containing two polished/smooth samples of one mineral type (albite, calcite, muscovite, pyrite and quartz) (single condition) and one tube that contained two samples of every mineral type (mixed condition – 10 mineral samples total). Mineral samples were roughly 2 cm^3 cubes, for more information see Chapter 3, section 3.5.

Each set was duplicated (12 tubes total), one group being inoculated with 18 mL of untreated inoculum (biology) and the other being inoculated with 18 mL of sterilised inoculum (control). All tubes were supplemented with 0.5 g of crushed pyrite as an iron and additional source surface, meaning that even single mineral conditions (i.e., albite single) had at least the test mineral type and pyrite present in the microcosm. However, colonization of the crushed pyrite was not analysed in this study. A summary of the experimental set up for the *in vitro* microcosms can be seen in Table 8.2.

Table 8.2¦ Experimental set up of the *in vitro* microcosm experiment.

		Number of mineral samples added per tube.	Number of tubes per microcosm set	Number of microcosm sets
Incubation conditions	Biological, single mineral.	2 mineral samples (~2 cm^3cubes) of one mineral type (e.g. albite).	5 tubes, 1 tube for each mineral type.	3 (A, B and C)
	Biological, mixed minerals.	10 mineral samples (~2 cm^3cubes), comprised of 2 samples of each mineral type.	1 tube.	3 (A, B and C)
	Sterile control, single mineral.	2 mineral samples (~2 cm^3cubes) of one mineral type (e.g. albite).	5 tubes, 1 tube for each mineral type.	3 (A, B and C)
	Sterile control, mixed minerals.	10 mineral samples (~2 cm^3cubes), comprised of 2 samples of each mineral type.	1 tube.	3 (A, B and C)

The microcosms sets were incubated at room temperature, with loosely screwed on lids to allow gaseous exchange, for five months. After this incubation period mineral

samples were removed from the liquid medium. The pH of the liquid medium for both biological and control microcosms was measured in triplicate after mineral sample removal.

Sample storage, preparation for microscopy and imaging: Upon removal from the liquid culture, mineral samples were fixed in 2.5 % glutaraldehyde in PBS solution and stored at 4^{o}C until imaging. As stated above, for each condition (five single, one mixed) there were two samples of each mineral, one that was imaged under fluorescence microscopy and the other under SEM.

Samples for fluorescence microscopy imaging were removed from the glutaraldehyde solution and washed in PBS, before being stained with 10 μg/mL acridine orange dye in PBS solution for at least 10 minutes. At least 20 images at 1000x magnification were taken at random of the polished/smooth mineral surface. Levels of microbial colonization were calculated by hand counting microbial cells in the images taken, with a minimum of five images being used for counting. Where cell density was high (approx. >200 cells), only a quarter of the image was used for counting. ImageJ software was used to optimise image contrast and brightness for counting.

Samples for SEM imaging were removed from the glutaraldehyde solution and were put through a chemical drying protocol. Details of this and of the SEM microscopy settings can be found in Chapter 3.

8.2.2 *In situ* colonization of mineral surfaces in field mesocosms buried for one year in Assholm mine

Following on from the successful colonization and weathering of shale-comprising minerals in the iron-oxidizing laboratory microcosms (8.2.1), *in situ* burial of these minerals within a shale weathering profile was carried out. Assholm mine was chosen as the site for mineral burial for a period of one year.

Sample preparation: Perforated 6 mL Nalgene bottles were used as containers for the mineral samples. Bottles were washed in 100 % ethanol to sterilise them, with remaining ethanol burnt off. Mineral samples were roughly 2 cm^3 cubes, for more information see Chapter 3, section 3.5.. Six different conditions were established;

five bottles with two samples of one mineral type from albite, calcite, muscovite, pyrite and quartz (single), and one bottle with two samples of each mineral type (mixed – 10 mineral samples in total per bottle). Sterile mineral samples were stored in the Nalgene bottles under sterile conditions, which were subsequently stored in sterile Whirlpak bags. A summary of the experimental set up can be seen in Table 8.3.

Table 8.3¦ Experimental set up of the *in situ* mesocosm experiment.

Mineral condition	Number of minerals per bottle	Number of bottles
Single mineral condition	2 samples (~2 cm^3 cubes).	5 bottles, 1 for each mineral type.
Mixed mineral condition	10 samples (~2 cm^3 cubes), 2 samples for each mineral type.	1 bottle.

Sample burial and collection: Samples were buried in the rock scree that comprises the floor of Assholm mine (for more information of the Assholm mine field site see Chapter 4). A flame sterilised trowel was used to dig roughly 10-15cm into the scree, where the sterile bottles containing the mineral samples were placed. The site for burial was chosen based on the wetness of the scree, as the hole was dug next to the mine wall below a seep in the wall. This would encourage liquid flow-through in the bottles and hence promote microbial colonization of the mineral surfaces. Samples were dug up one year later using a flame sterilised trowel, and the mineral samples of each bottle were tipped into 50 mL Falcon tubes containing 10 mL of 2.5 % glutaraldehyde in PBS. The Falcon tubes were stored in a cool box with freezer packs to keep them chilled under they were stored at 4 ^oC upon return to the laboratory.

Sample imaging: As there were two samples of each mineral in the conditions used, one was imaged under fluorescence microscopy (staining with acridine orange) and the other imaged under SEM. Details of the sample preparation and microscopy settings are detailed in section 8.2.1.

8.2.3 Statistical analyes

Data collected for the *in vitro* microcosms had three independent variables: inoculum type (A-C), mineral (albite, calcite, muscovite, pyrite and quartz) and treatment (single or mixed mineral condition), and one dependent variable: cells/mm^2. The *in situ* mesocosm experiment had only two independent variables, mineral type and treatment (single or mixed mineral condition). For both experiments (*in vitro* and *in situ*), a mixed effects linear model (e.g. MANOVA) should therefore be used to investigate the effect of these independent variables on the dependent variable. However, MANOVA assumes equal variance across the data set. This assumption was violated for both *in vitro* and *in situ* data sets, as determined by visual assessment of the residual vs fit plots and via tests for homogeneity of equal variance (Bartlett test). Attempts to transform the data via logarithmic and power (Boxcox) transformations did not successfully improve the homogeneity of variance of these data sets. As such, Kruskal-Wallis tests (K-W) were used to investigate the effect of individual independent factors (e.g. mineral type) on colonization. Post-hoc Dunn's tests were used to resolve specific effects (e.g. differences in colonization between two mineral types). For analysis of pH measurements in the in vitro experiment, MANOVA could be used due to equal variance across the data.

8.3 Results

8.3.1 *In vitro* colonization of minerals in laboratory microcosms

After five months of incubation at room temperature, the calcite and mixed microcosms of the sterile control and all of the biological microcosms displayed varying degrees of orange/rust colouration in all three microcosm sets (A-C) (Fig. 8.1a). All of the other sterile control microcosms mineral types (albite, muscovite, pyrite and quartz) did not display this colouration. In some but not all of the microcosms that displayed orange colouration, a distinctive yellow crust built up in a horizontal line that coated the tube interior (Fig. 8.1b).

The surface of pyrite samples incubated under biological conditions acquired an iridescent sheen which was not seen in samples incubated under sterile conditions (Fig. 8.1b – both single and mixed conditions).

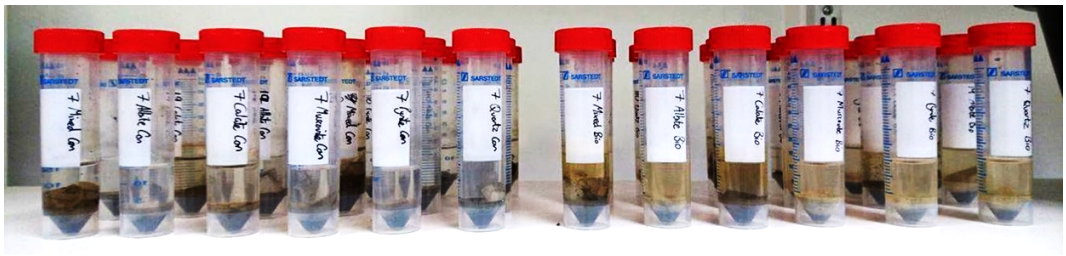

Figure 8.1a¦ Microcosm set A after five months of incubation, with the media in the control microcosms (six tubes, left) remain clear while the media in the biological microcosms (six tubes, right) were more orange coloured.

Figure 8.1b¦ Visual observations of biological activity. Above, (representative images from microcosm set A), pyrite incubated under biological conditions in both single (bottom left) and mixed (bottom right) mineralogical conditions acquired an iridescent sheen that was not observed on the pyrite incubated in single or mixed mineralogical control conditions (top). Below, (representative images from microcosm set B), yellow deposits accumulated on the tube walls of biological microcosms were not found in the control microcosms.

Upon mineral cube extraction and preparation, samples were imaged using fluorescence microscopy and SEM, the former of which was used for cell counting on the mineral surface in order to obtain a quantitative measure of colonization (cells/mm^2). The data from these counts can be seen in Figures 8.2a and

8.2b. For albite, muscovite and quartz the highest level of colonization was seen when the minerals were alone (single set) with an inoculum from the Saltwick Bay cliff iron-oxidizing enrichment (set A) (Fig. 8.2a). Pyrite was colonised to the same level when alone (single set) by all three inoculum types (A-C), at 5-7.5 x 10^5 cells/mm^2. Calcite was most colonised when alone with an inoculum from the Gaytres quarry enrichment, at 3 x 10^4 cells/mm^2 (Set C). Overall, for both single and mixed microcosm sets, minerals colonised by the community from the Saltwick Bay enrichment had higher cell numbers for all of the minerals tested (Fig. 8.2a).

The mean average values were calculated across all three microcosm sets for both the single and mixed microcosms Figure 8.2b). Presenting this data in this way allows a general assessment to the habitability of these different minerals for iron-oxidizing enrichment communities isolated from weathered shale.

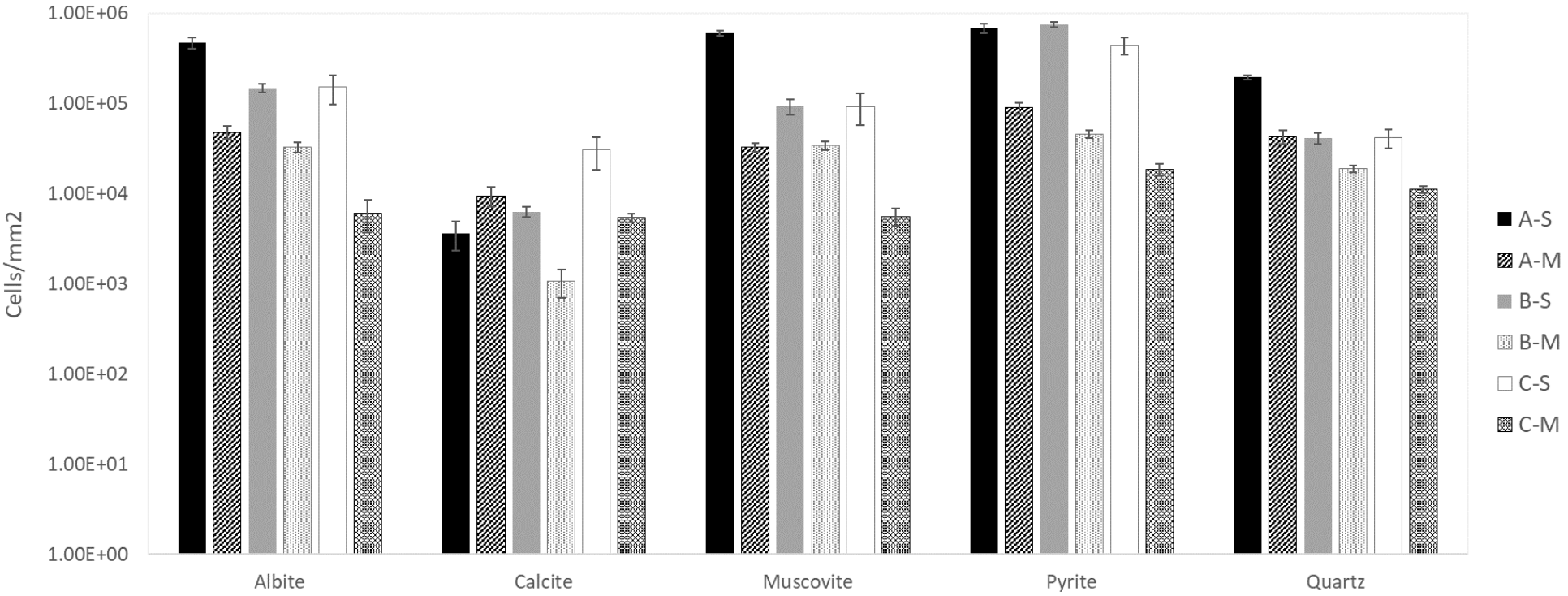

Figure 8.2a¦ *In vitro* colonization (mean average cells/mm^2) of shale-comprising minerals (albite, calcite, muscovite, pyrite and quartz) after five months of incubation in iron-oxidizing microcosms containing either only one mineral type (S) or containing all the mineral types mixed together (M). Data from three sets of iron oxidizing microcosms is presented, each inoculated from a different iron-oxidizing enrichment culture prepared from samples collected from Saltwick Bay cliffs (A-S/M), Assholm cement stone mine (B-S/M) and Gaytres Quarry C-S/M). Error bars are derived from the standard error of the mean from 5 replicate counts.

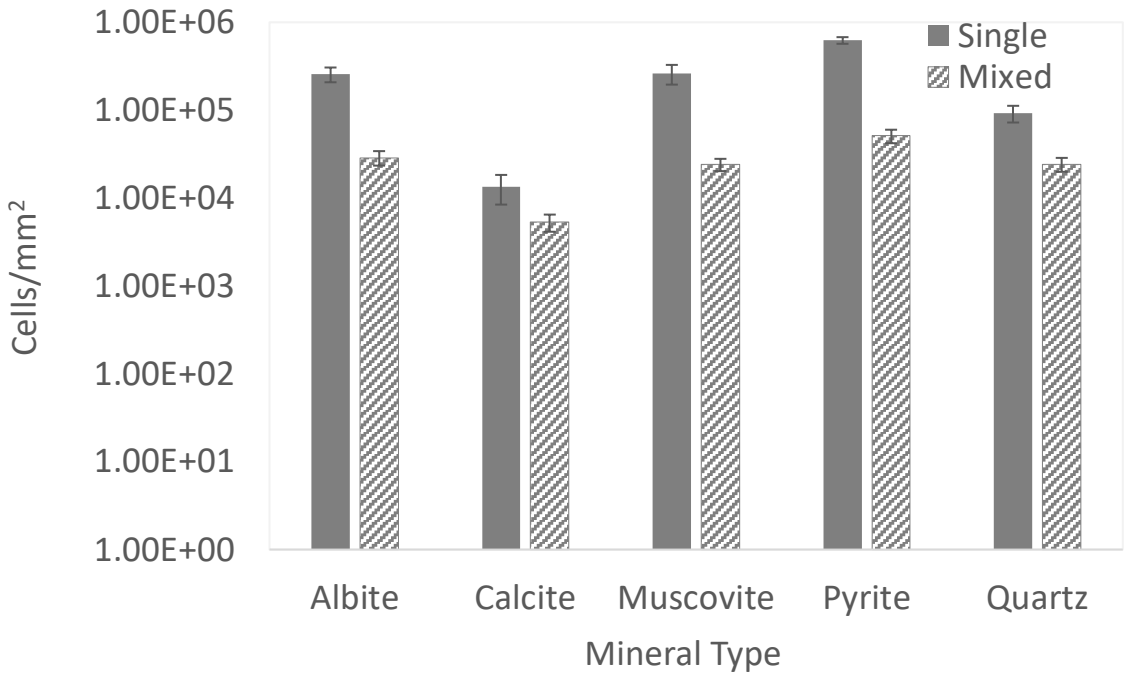

Figure 8.2b¦ Amalgamated mean average mineral colonization data (cells/mm^2) from all three microcosm sets (A-C) for both single and mixed microcosms, the data for which is presented in Figure 8.2a. Plotted values represent the mean average of 15 cell/mm^2 measurements (5 measurements per each of the three sets). Error bars represent standard error which was calculated from all 15 measurements.

The most and least colonised minerals in this analysis were pyrite when incubated alone at 6.24 x 10^5 cells/mm^2 and calcite when incubated in a mineral mixture with 5.31 x 10^3 cells/mm^2, respectively. This means that mineralogical conditions can affect surface colonization by almost two orders of magnitude.

Another trend that can be observed is that minerals were less colonised when in a mineral mixture compared to when they were incubated alone, although it should be noted that in all microcosms, whether under single or mixed conditions, granular pyrite is present as an iron source. Figures 8.2a and 8.2b demonstrate that colonization was markedly lower when minerals were incubated under mixed conditions compared to mixed conditions (K-W, across all microcosm sets (A-C), effect of condition on colonization, $Z=6.32$, $p<0.001$). Biological activity significantly reduced media pH compared to the abiotic control in the albite, muscovite, pyrite and quartz single microcosms, but this effect was not seen with

calcite nor in the mixed microcosms where calcite was present (Fig. 8.3). The data presented here is only for the pH values for the single and mixed microcosm for set A, but it is representative for both sets B and C. The pH of albite, muscovite, pyrite and quartz in the presence of a microbial community was ~pH 1.6, whereas the sterile control mediums for these microcosms was nearer to ~pH 2.4 (Fig. 8.3). Multivariate ANOVA (MANOVA) was used to analyse the effect of inoculum, mineral condition and treatment (biological test or sterile control) on the pH of the medium within microcosm sets A-C. A statistically significant effect of treatment (MANOVA, $F=106.5$, $p<0.001$) and mineral condition (MANOVA, $F=1542$, $p<0.001$) on pH was identified in this model.

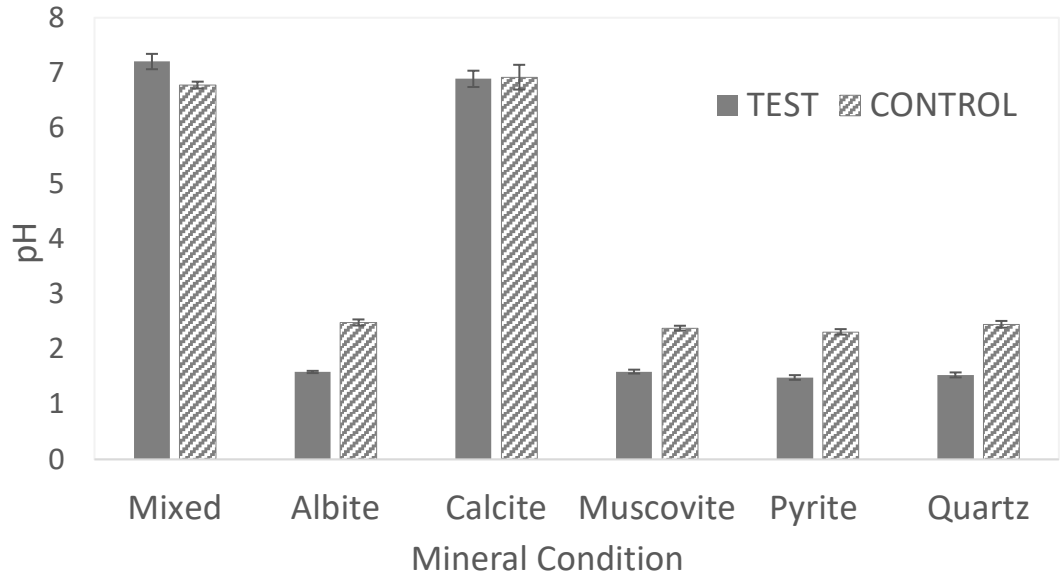

Figure 8.3 Mean average (N=3) pH measurements of the iron-oxidizing microcosm set A inoculated with a live (Test) and sterilised (Control) inoculum, after 5 months of incubation. Error bars are derived from 3 replicate measurements. The data presented here for the microcosm set A is also representative for the pH data obtained from microcosm sets B and C.

The pH of both the calcite and mixed biological microcosms for set A was significantly neutral, although the biological mixed microcosm was slightly more alkaline compared to the control. However, this slight alkaline increase was not observed for microcosms sets B and C (data not shown). These results indicate that calcite increases media pH (the unaltered WAYE liquid medium is pH 3) both when it is the only mineral and when it is in a mineral mixture (Fig. 8.3).

SEM imaging of the mineral surfaces was carried out to determine what effect microbial attachment, growth and activity had on mineral surface morphology. The most striking features were observed for the minerals pyrite (Fig. 8.4a-e) and muscovite (Fig. 8.5a-c).

After five months of incubation, the surface of pyrite that had been incubated individually (single) had become etched with a high density of rectangular pits (Fig. 8.4a – red arrow). These pits were not observed on the pyrite that had been incubated under sterile conditions (Fig. 8.4b) or in the pyrite that was incubated under mixed mineral conditions (data not shown). This suggests that the pits were formed due to biological activity that occurred only when the pyrite was not incubated with other mineral types.

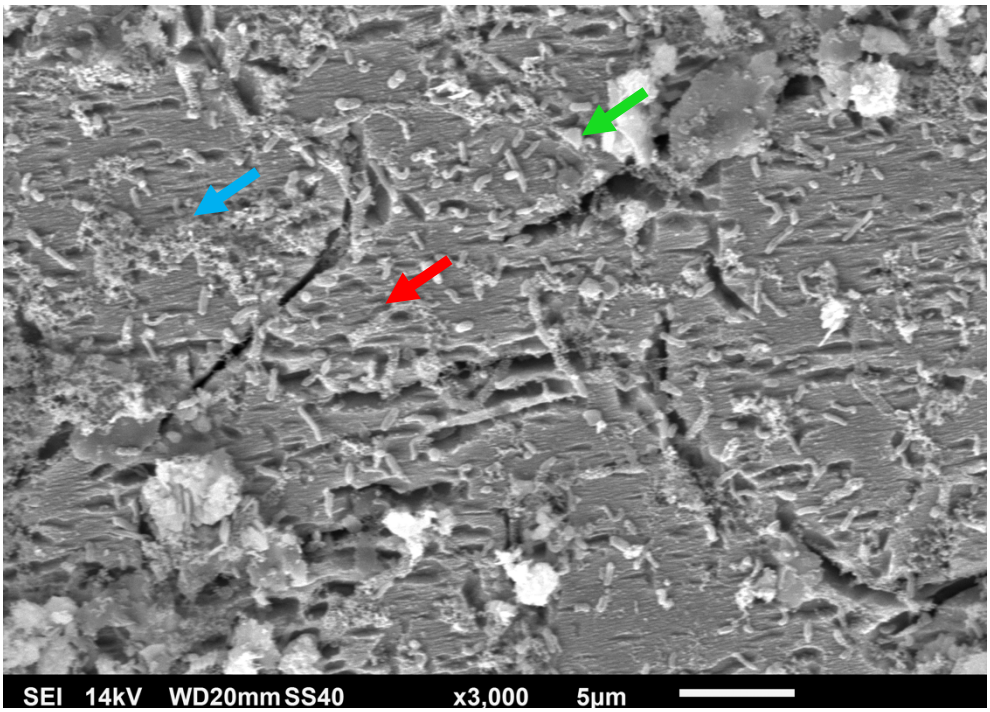

Figure 8.4a¦ SEM image of microbial colonization of pyrite (set A-S). Regular shallow to deep pits that are rectangular in shape are etched into the surface (red arrow). *Bacillus* shaped cells can also be seen adhered to the mineral surface (green arrow). Sections of the surface are also covered in a fine, crust-like coating (blue arrow).

The following Figures (Fig. 8.4a-e) show example images of these pits on the surface of pyrite incubated under single mineral conditions and inoculated with the

Saltwick bay cliff iron oxidizing enrichment community (set A), however these pits also formed when the pyrite was incubated with the other two enrichment cultures (sets B and C).

The cells attached to the surface of the pyrite varied in morphology, but rod cells predominated on the mineral surface (indicated by green arrow in Figure 8.4a). Another feature commonly found under these conditions was the presence of fine crusts that had a patchy distribution across the pyrite surface (blue arrow in Figure 8.4a).

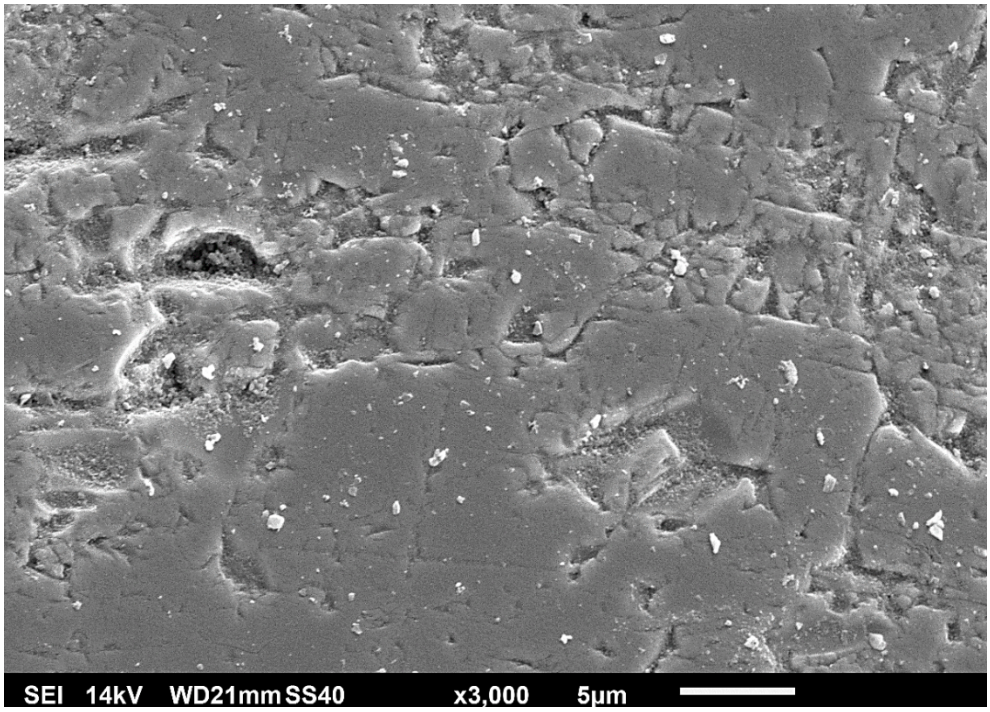

Figure 8.4b¦ SEM image of the surface of pyrite incubated in the sterile control. Although the surface is highly heterogeneous and pitted, it lacks the regular and conserved shape of the rectangular pits, or the crust coating observed in the biological test (Fig. 8.4a).

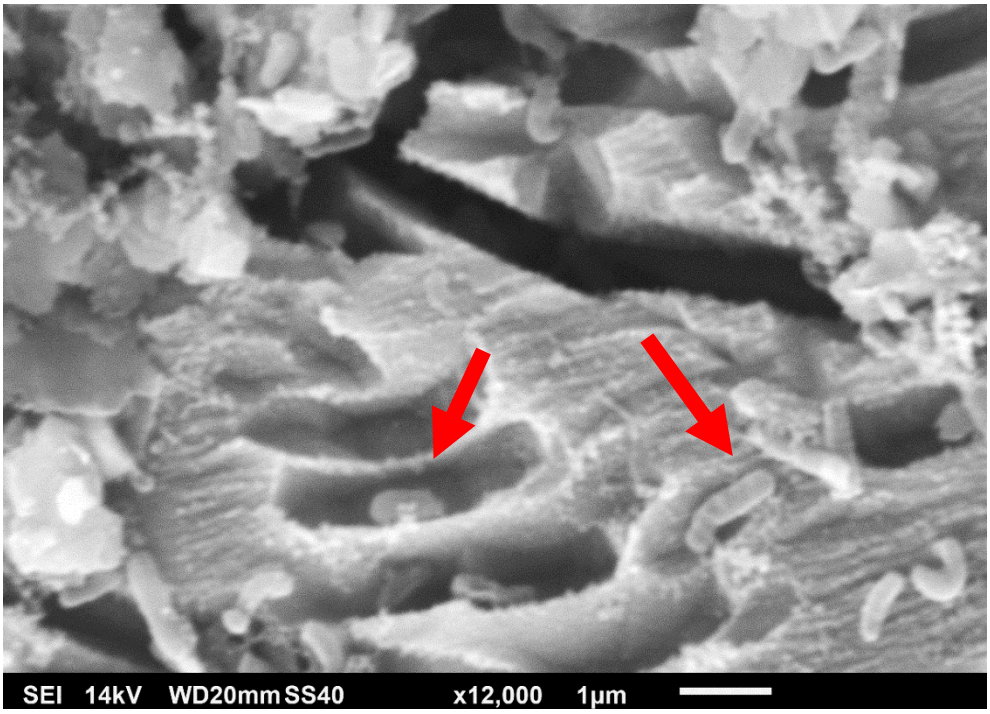

Figure 8.4c¦ A higher magnification SEM image of pyrite incubated in biological treated microcosm set A-S. The shape and size of the pits can be better assessed (2-3µm length, 0.5µm width). Red arrows indicate where microbial cells are present inside the pits.

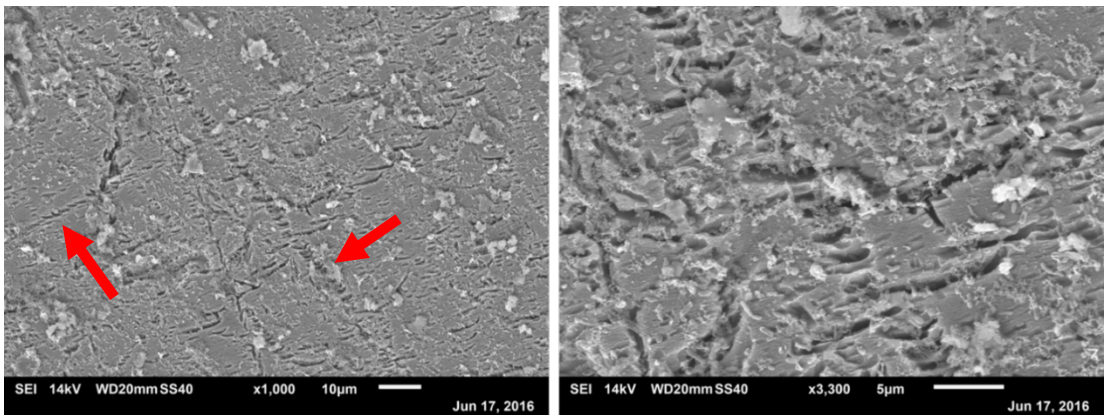

Figure 8.4d¦ SEM image of pits preferentially formed on an unidentified planar feature within the crystal, potentially a twin plane, on pyrite incubated in biological treated microcosm set A-S. Two of these lines can be seen in the lower magnification image (left – highlighted with arrows). A higher magnification of the line running from top left to bottom right is shown in the right-hand image, where pit density on the line is greater than the surrounding surface.

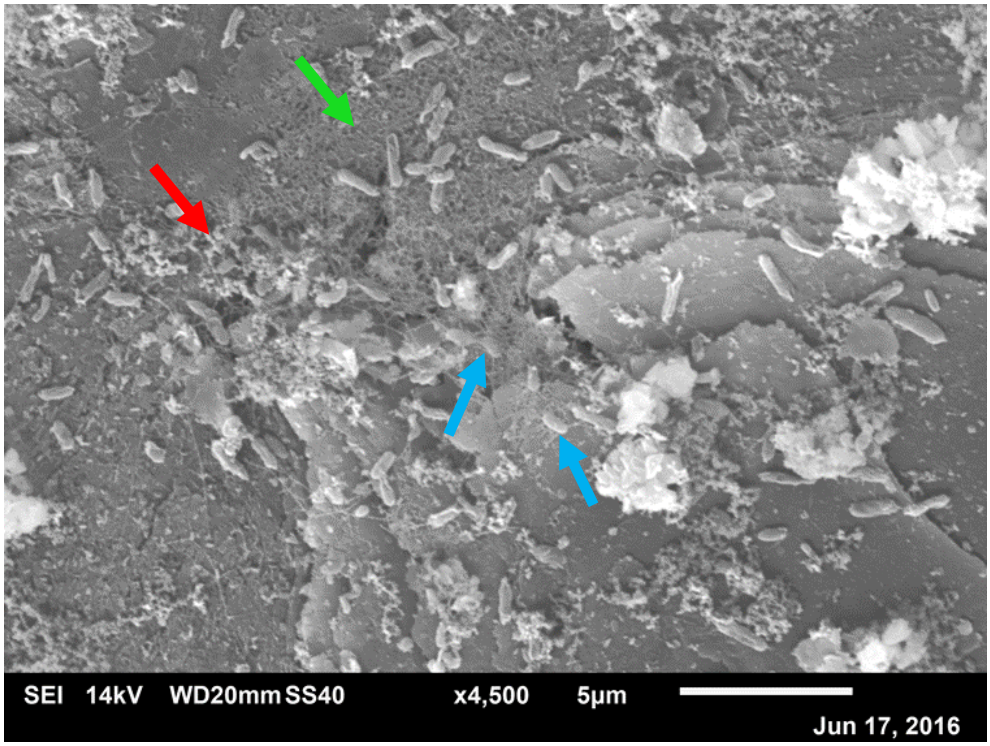

Figure 8.4e¦ SEM image of microbes adhered to the surface of pyrite (microcosm set A-S) are surrounded by a layer of filamentous material (green arrow) that appears to have been extruded by the cells (numerous cells are directly attached to multiple filaments – blue arrows). In places, crust material has formed on top of the filamentous material (red arrow).

Higher magnification SEM allowed a better approximation of both pit size and cell size, with the predominant rod cells being 1 x 0.5 µm and the pits being 2-3 x 0.5µm in size (Fig. 8.4c). In some cases, cells were found inside these pits (Fig. 8.4c – red arrows). Lower magnification imaging revealed that the etches were not entirely randomly distributed on the pyrite surface, but were found more densely on lines running across the mineral surface (Fig. 8.4d).

In addition to the fine crusts coating the pyrite surface (Fig. 8.4a), densely packed thin filaments (~30-40nm across) were adhered to the mineral surface and were often associated with microbial cells (Fig. 8.4e – green arrow). In some instances, the clear protrusion of these filaments from the microbial cell onto the mineral surface could be seen (blue arrows). Furthermore, small fragments of fine crust were identified lying over the top of the filamentous matrix (red arrow).

The colonised surface of the minerals albite, muscovite and quartz in the biological conditions of at least one of the microcosm sets were also encrusted as previously seen on the pyrite surfaces in Figures 8.4a and 8.4e. This is best exemplified in Figure 8.5a. The surface of the muscovite incubated under control conditions remained smooth after 5.5 months (Fig. 8.5b below). In stark contrast, the surface of biologically incubated muscovite was coated with a patchy distribution of fine crusts (Fig. 8.5a above). These crusts were also not observed in the biological incubation with mixed mineralogy (not shown). This pattern of crust occurrence is also true for quartz (images not shown) and albite (Fig. 8.5c). It can therefore be inferred that crust formation was precipitated through biological processes that only occurred in the absence of calcite, as the crusts did not form on any calcite samples and did not occur on minerals incubated in the presence of calcite (mixed conditions).

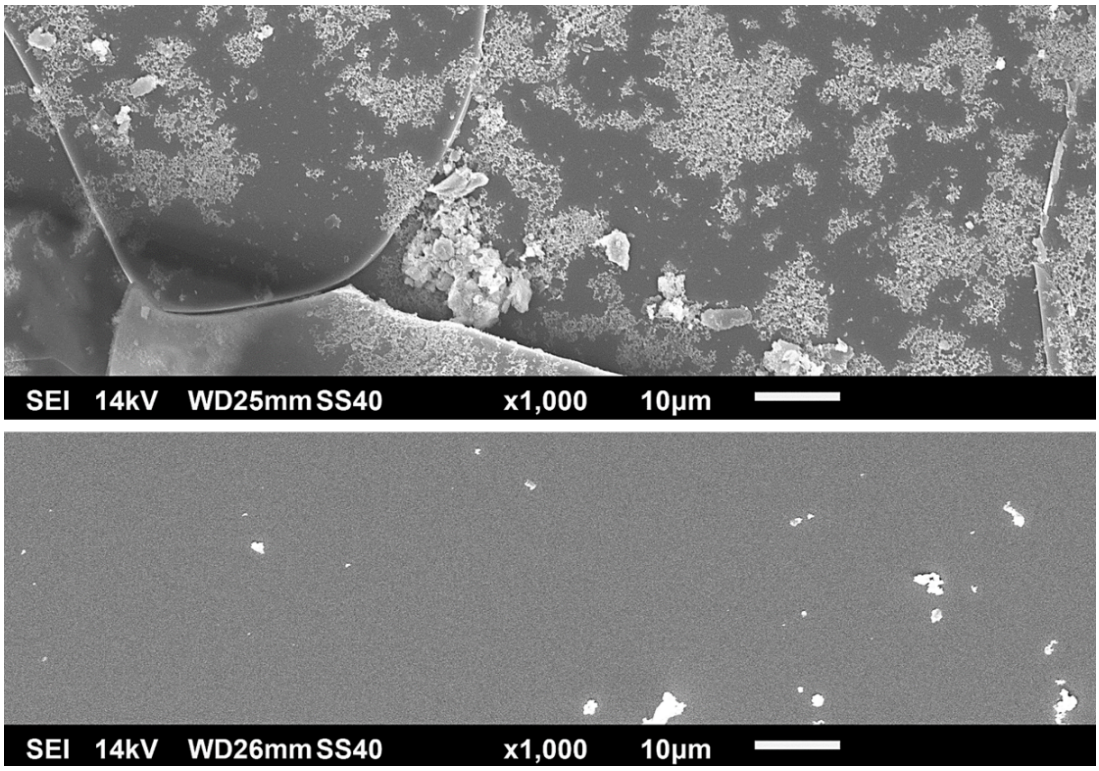

Figure 8.5a¦ SEM image of the surface of muscovite that has been incubated in iron-oxidizing medium for 5 months in the presence of a live (above) or sterilised (below) inoculum in microcosm set A-S.

Although microbial cells were primarily found to be distributed across the muscovite surface as single cells or in small groups, microcolonies and more extensive biofilms were also identified (Fig. 8.5b-d). The image of a microcolony in Figure 8.5b shows a high cell density in the centre of the colony with decreasing density at the colony edge and surrounding surface. The cells within the microcolony appear darker and cell edges are more difficult to distinguish (Fig. 8.5b). A more extensive biofilm of cells can be seen in Figure 8.5d. Cells can be seen in densely packed patches (red and green arrows) underneath a surface crust which covers most of the surface in this image. The crust can be seen in multiple locations to be directly coating the underlying cell layer (red arrows). The crust formations in image 8.5c are likely to be an intermediate phase of microbial surface alteration between images 8.5b and 8.5d.

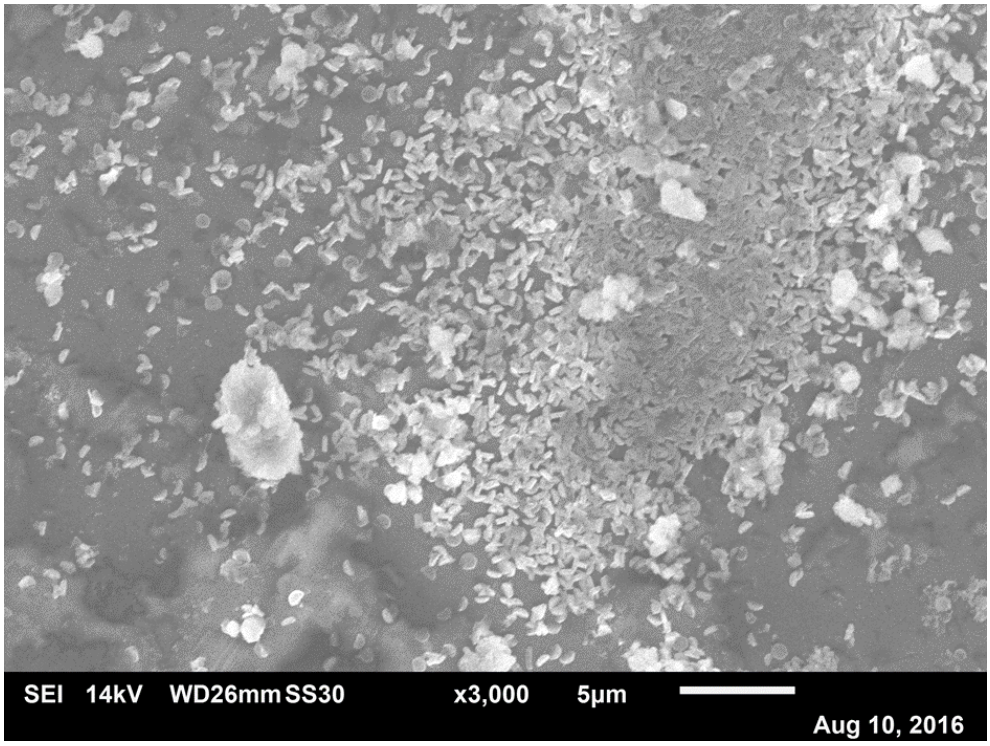

Figure 8.5b¦ SEM image of microbial colonization of the surface of muscovite in microcosm set A-S. A microcolony can be seen adhered to the surface, with cell density increasing nearer to the colony centre.

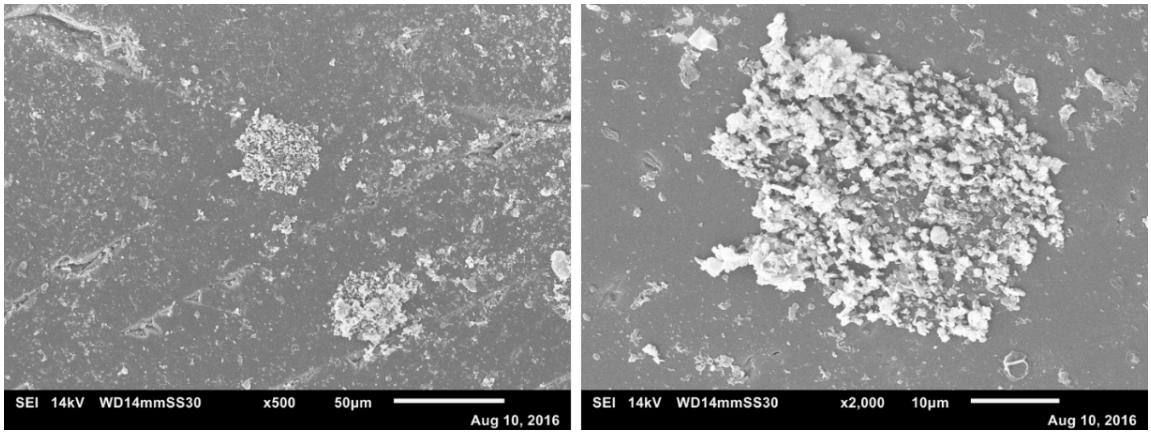

Figure 8.5c¦ SEM image of microbial colonization of the surface of albite in microcosm set B-S. The image on the left shows the mineral surface with two distinct, circular clusters of crust formation. The image on the right is a higher magnification image of the upper cluster; individual cells can be seen to be imbedded within the crust.

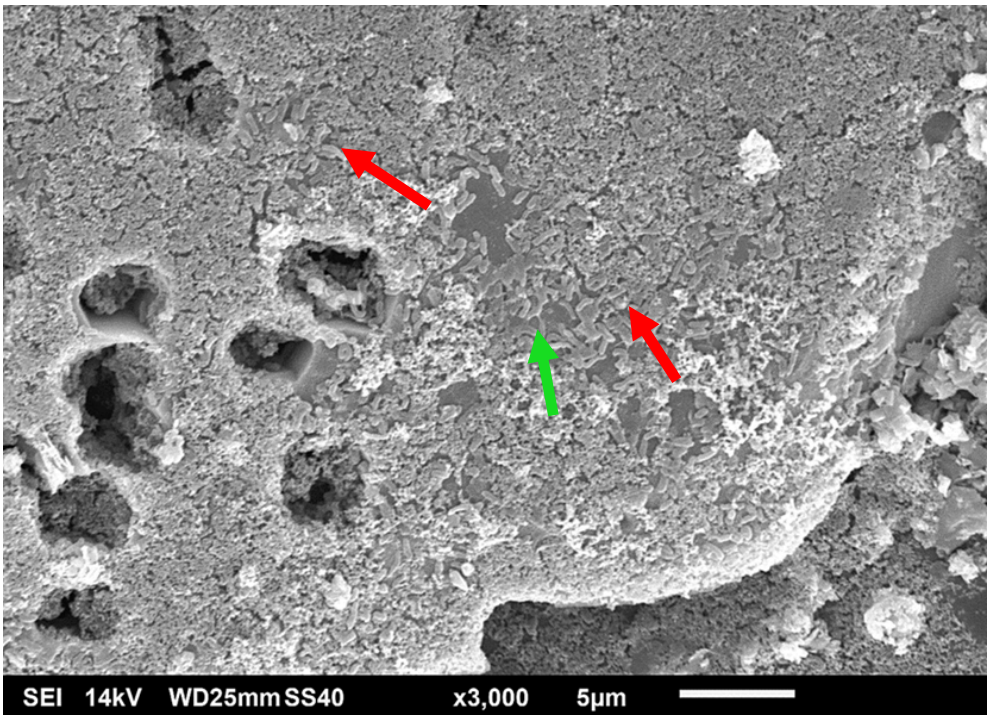

Figure 8.5d¦ SEM image of a microbial biofilm grown on the surface of muscovite with an overlying crust. A hole in the crust layer reveals the cells underneath (green arrow), but cells can be seen interspersed in the crust (red arrows).

SEM-EDS analysis of the surface crusts on pyrite and muscovite was carried out to compare the elemental composition of the crusts with the mineral surface (Fig. 8.6). The EDS spectra of the surface crust on pyrite revealed the presence of oxygen that was absent on the mineral surface (Fig. 8.6 images A and B). This indicates that the crusts are at least partially formed of iron or sulfur oxides. In the EDS analysis of muscovite, numerous elements were identified at low abundance in the surface crusts that were not present on the mineral surface including iron, carbon, calcium and potassium (Fig. 8.6 images C and D). All of these elements are present in the liquid medium that the muscovite was incubated in, suggesting that these elements became incorporated into the surface crust from this source.

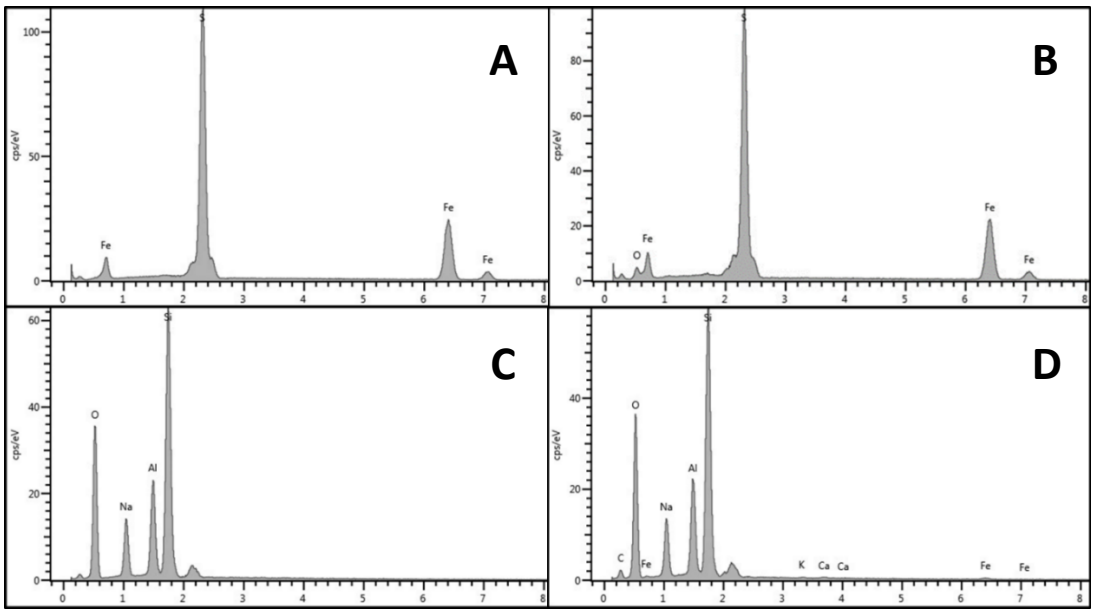

Figure 8.6 EDS spectra of the mineral surfaces (A and C) and the surface crusts (B and D) of pyrite (A and B) and muscovite (C and D) from microcosm set A-S.

8.3.2 *In situ* colonization of mineral surfaces in field mesocosms buried for one year in Assholm mine

Minerals either in isolation (single) or in the presence of other mineral types (mixed) were incubated in perforated bottles that were buried in scree in the base of Assholm mine for one year. Surrounding air and liquid could enter these bottles through the perforations, allowing microbes in the surrounding scree to enter the bottles and colonise the mineral surfaces. When extracted after incubation, many of the mineral

surfaces were found to be moist. Rock chips that surrounded the buried bottles were brought back to the lab for pH analysis, whereby they were immersed in water before triplicate pH measurements of the resulting solution were taken. The mean average of these measurements (N=3) was 5.24 (± SE 0.166). Fluorescence microscopy of the mineral surfaces allowed the level of colonization (cells/mm^2) to be calculated (Fig. 8.7).

Although levels of colonization did vary between minerals, such as between single calcite (7.7 x 10^3 cells/mm^2) and muscovite (6 x 10^4 cells/mm^2).the differences were not as extensive as those found in the laboratory microcosms (Fig. 8.2 and 8.7), with colonization variation spanning between ~10^4 and 10^5 cells/mm^2 (compared to ~10^3 to 10^6 in the laboratory microcosms – Fig. 8.2b).

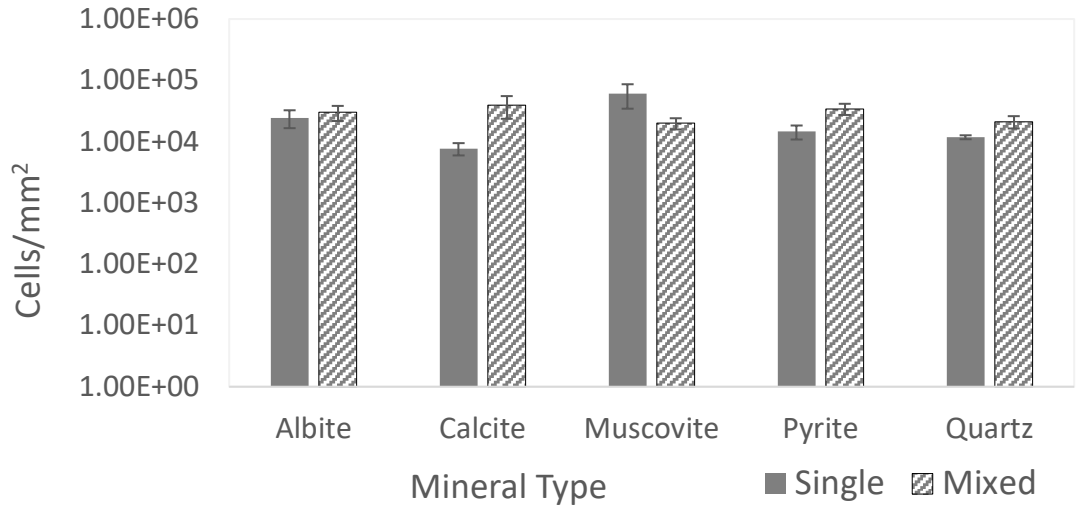

Figure 8.7¦ *In situ* colonization (mean average cells/mm^2) of single minerals alone in one mesocosm (single) or all mixed together in one mesocosm (mixed) after one year of burial within the scree at Assholm mine. Values presented are the mean average of 20 replicate cell/mm^2 counts from one sample. Error bars represent standard error of the mean.

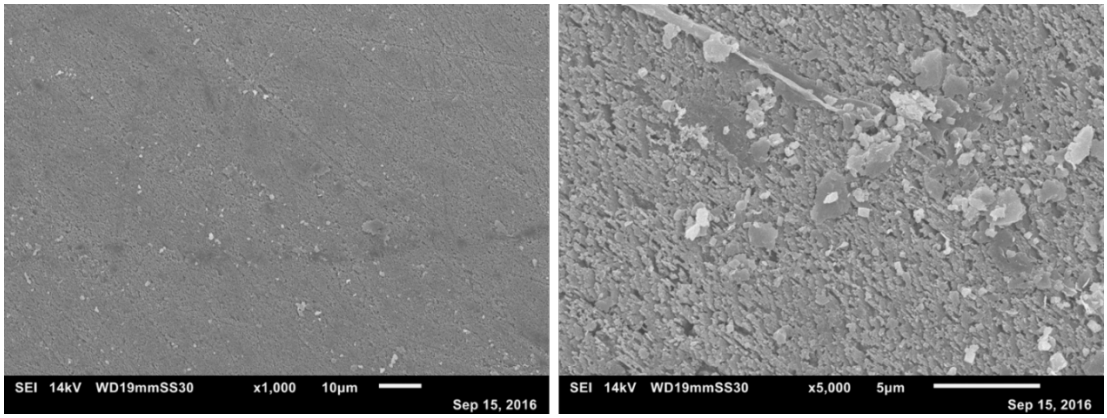

Figure 8.8¦ SEM image of the *in situ* weathering of calcite after one year (single). The surface has become roughened, leaving amalgamated elongated cleavage-parallel pits and upstanding remnants.

No consistent trend can be deduced from the differences in colonization between the single and mixed mineral incubations. Kruskal-Wallis tests determined that mineral type did not have a significant effect on levels of colonization (K-W, effect of mineral type on colonization, $X^2=4$, $p=0.4$), but incubation condition (single or mixed mineral condition in bottle) did (K-W, effect of incubation condition on colonization, $X^2=25.65$, $p<0.001$). However, there is no single consistent effect (e.g. minerals incubated under mixed mineral conditions are more colonised than those incubated under single conditions) across the data (Fig. 8.7).

The surface of calcite both from the single and mixed incubations showed extensive signs of weathering, with the smooth polished surface having become roughened (Fig. 8.8). Fine, acicular crystals (~1µm x 0.15µm) all orientated at the same angle (~315^o – bottom right to top left) cover the weathered surface in a loosely packed configuration. SEM imaging of the calcite surface failed to reveal microbial colonization, although the surface was shown to be colonised from fluorescence microscopy (data in Fig. 8.7).

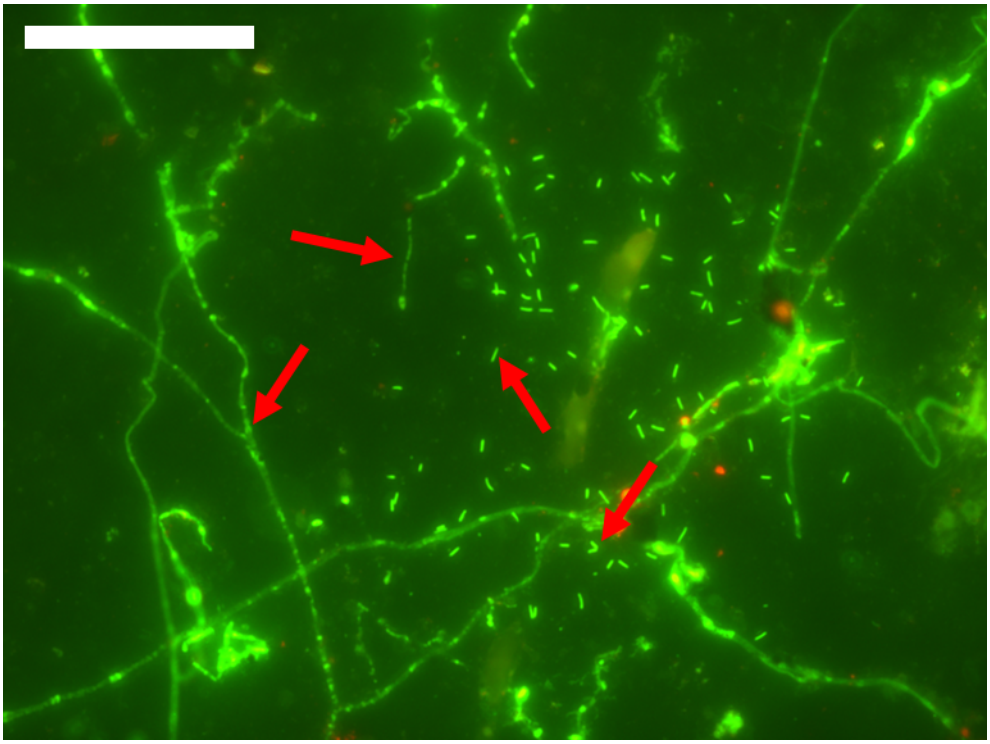

Figure 8.9a¦ Fluorescent microscopy image of the surface of pyrite (mixed) colonised by microbes ranging in cell type and structure after one year of *in situ* burial at Assholm mine. Arrows indicate some of the different cellular or cellular group morphologies present. Scale bar is 20µm.

If the surface of the calcite was already significantly weathered, the sample processing for SEM (see Chapter 3, section 3.7) may have dislodged cells adhered to the surface, explaining their absence.

Both SEM and fluorescence microscopy imaging of mineral surfaces revealed that a variety of microbial cell types had colonised mineral surfaces. Representative images of this can be seen in Figures 8.9a and 8.9b, with red arrows indicating a range of different cellular morphologies including bacilli, paired bacilli, streptobacilli, single teardrop shaped cells and filaments/hyphae.

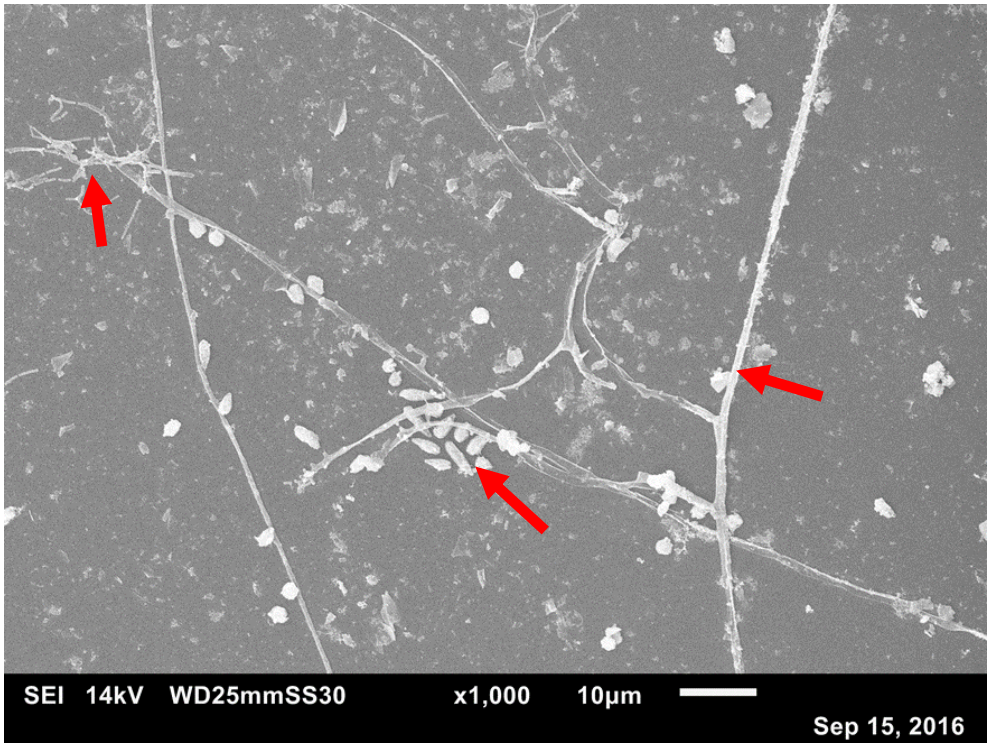

Figure 8.9b¦ SEM image of the surface of muscovite (single) colonised by microbes ranging in cell type and structure after one year of *in situ* burial at Assholm mine. Arrows indicate some of the different cellular or cellular group morphologies present.

This array of cellular morphologies suggests that a range of differing microbial species have colonised the mineral surfaces. It also seems likely that these species are not constrained to eubacteria, with the filaments possibly representing fungal hyphae. Clearer images of these filaments/hyphae can be seen in Figure 8.13.

A particular cellular morphology worthy of note was identified on the surface albite (Fig. 8.10). Large groups of twin bacilli cells joined at the poles were identified on the mineral surface both from fluorescence and electron microscopy. These cells were surrounded by a thick cellular sheath, which can be seen readily in the fluorescence microscopy image (Fig. 8.10 left – central bright green bacilli cell surrounded by a fainter but fluorescent sheath). The fluorescence of the sheath indicates that it also contains nucleic acids that would have bound to the acridine orange dye.

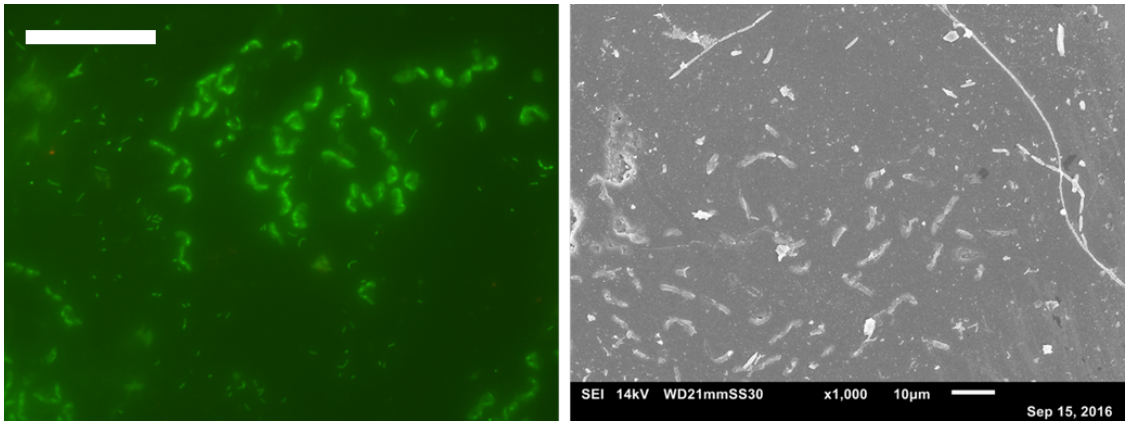

Figure 8.10¦ Fluorescence microscopy and SEM images of microbial colonization of the surface of albite (single) after *in situ* burial at Assholm mine. In the fluorescence microscopy image (left), bright green cells, often in pairs attached at the poles, are surrounded by a sheath which contains DNA (more faded green). This cellular morphology was also observed in the SEM images (right) of this sample type, although the sheath was not as well preserved. Scale bar for the left image is 20µm.

Numerous observations in relation to the filaments/hyphae present on the mineral surfaces were made, and are visually represented in Figures 8.11-8.13. Firstly, the filaments/hyphae that colonised the mineral surface acted as nucleation sites for the accretion of particulate material (Fig. 8.11). In the left-hand image of Figure 8.11, a fine crust similar to that observed coating pyrite and muscovite in the laboratory microcosms (Fig. 8.4e, 8.5a and 8.5c) can be seen coating the filament/hyphae. Larger particles can also be seen adhered to the filament/hyphae, with a clearer accretion of this material seen in the right-hand image with filaments/hyphae interspersed through the agglomerate (Fig. 8.11, right).

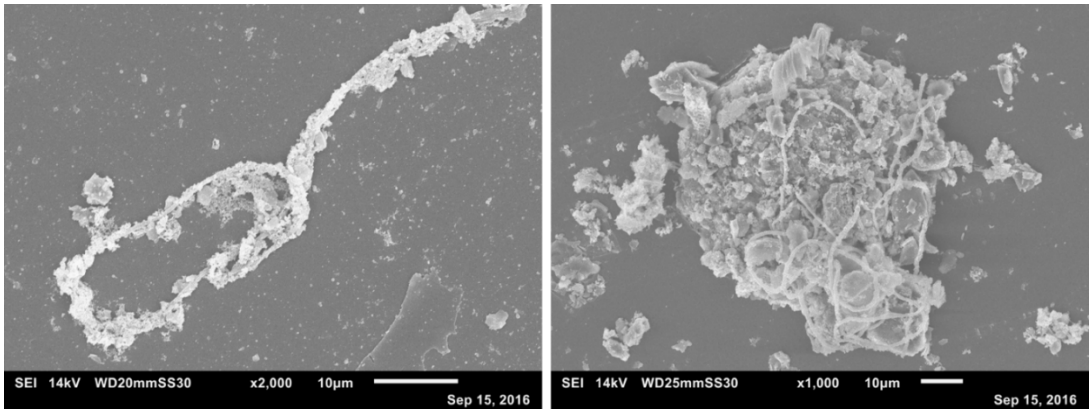

Figure 8.11¦ SEM image of filaments grown on the surface of quartz (single – left) and muscovite (mixed – right) after *in situ* burial at Assholm mine. The filaments have acted as nucleation sites for crust formation (left) and the accretion of fine particulates (right).

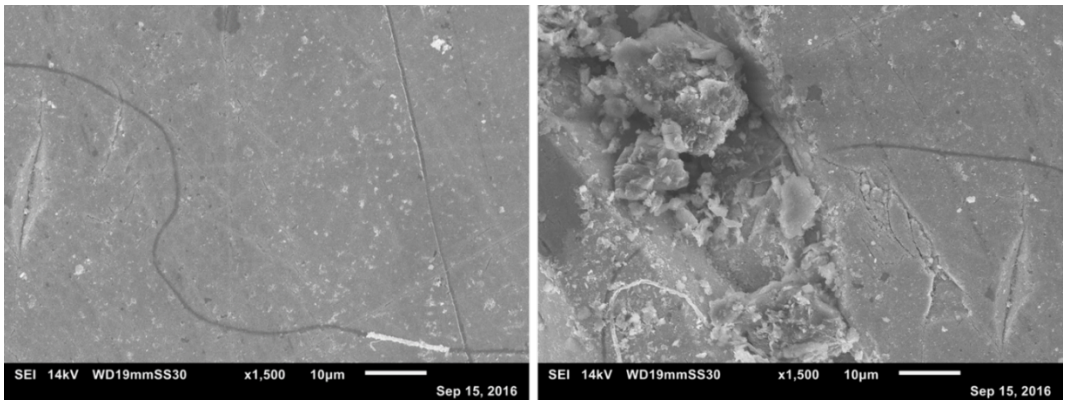

Figure 8.12¦ SEM image of microbial growth weathers the surface of pyrite after one year of burial at Assholm mine (single incubation). Dark etch lines are present underneath where microbial filamentous growth was present on the pyrite surface. These can be seen in both the images above. Remnants of the filament can be seen in the left-hand image.

One particular observation was made from the filamentous/hyphal growth across the surface of pyrite. Some filaments/hyphae could be seen to be broken and sections were absent from the surface, with remnants of the filament/hyphae still present. Dark lines etched into the mineral surface could be seen which would have been covered by these missing sections i.e. dark etch lines formed underneath the

filament/hyphae and became visible when these filaments were broken off from the surface (Fig. 8.12).

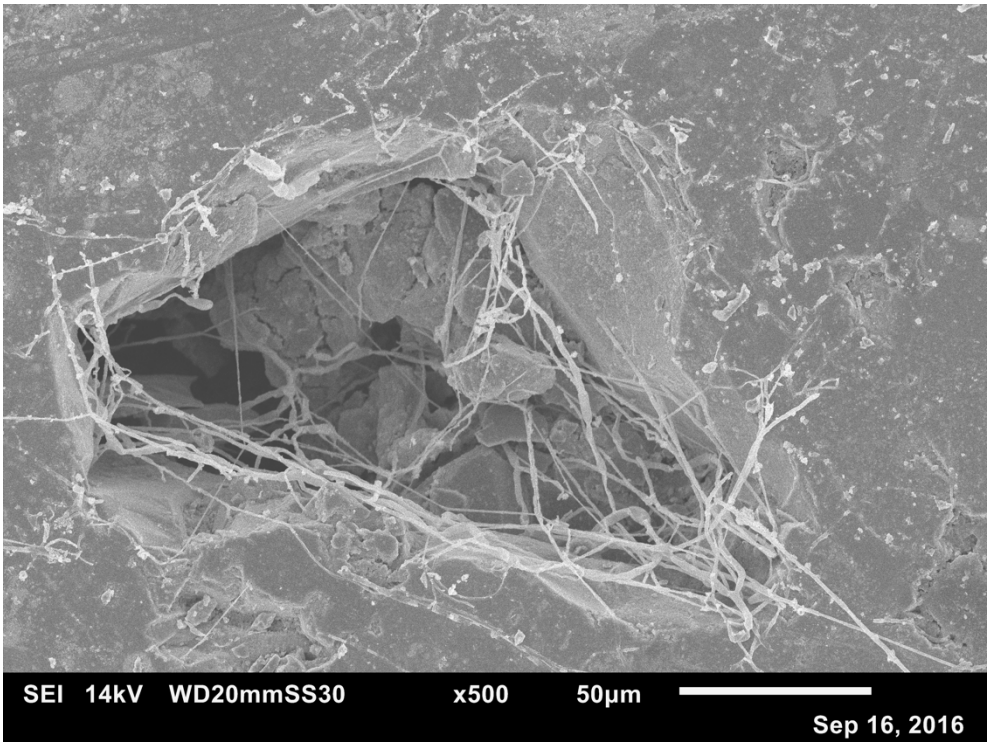

Figure 8.13¦ SEM image of filamentous growth surrounding a pit in the pyrite surface after burial at Assholm mine for one year (mixed incubation). Filaments can be seen deep inside the pit.

A final observation was made that filaments/hyphae were found abundantly within and surrounding pits on the pyrite surface (Fig. 8.13). Numerous filaments/hyphae could be seen extending into the pit cavity, although no evidence for macroscale pit (>5µm across) formation by biological activity was found.

Lower magnification images of the surface of pyrite incubated under mixed conditions revealed the heterogeneity of the microbial colonization on this mineral surface (Fig. 8.14 and 8.15). Microcolonies of densely packed cells of various sizes can be seen to be patchily distributed across the pyrite surface, in addition to interspersed branching filamentous growth.

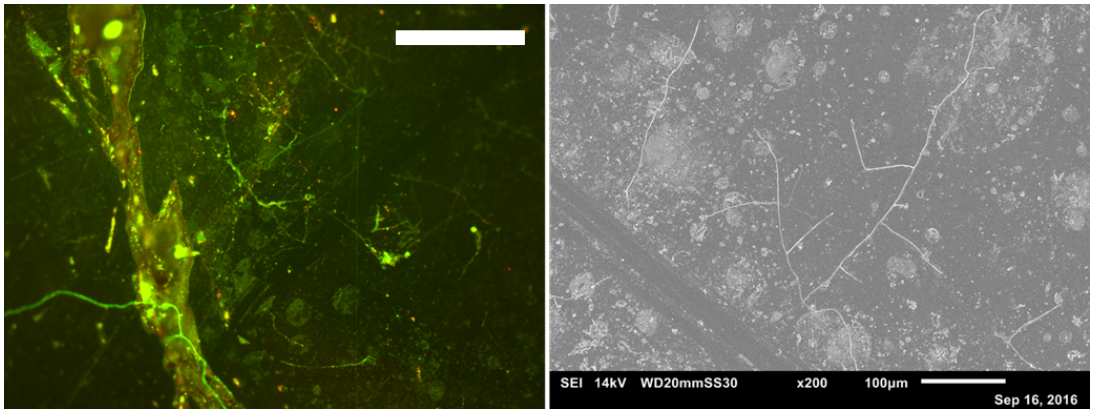

Figure 8.14¦ The surface of pyrite is heterogeneously colonised after one year of burial at Assholm mine (mixed), imaged both through fluorescence microscopy (left) and SEM (right). Microbial filaments can be seen extending across the mineral surface and the patchy distribution of microcolonies that vary in size. Scale bar in the left image is 100µm.

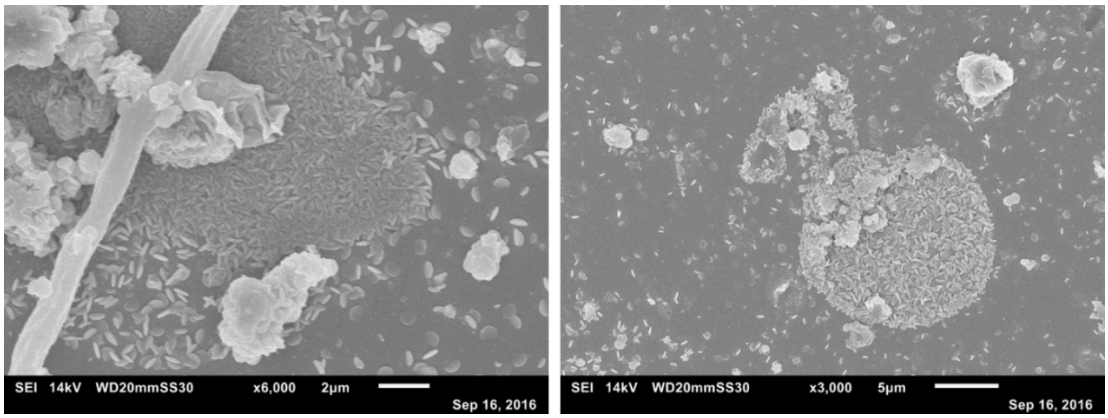

Figure 8.15¦Higher magnification SEM images of the microcolonies identified on the surface of the pyrite shown in Figure 8.14. In both images the tightly packed nature of the microbial cells can be seen, with distinct colony edges.

Higher magnification images of the microcolonies demonstrate the high density of cells that appear darker than surrounding cells (Fig. 8.15, left) as identified in the image of the microcolony on the surface of muscovite in the laboratory microcosm (Fig. 8.5b). The colony edge is distinct in the right-hand image of Figure 8.15, whereas the colony edge in the left-hand image of Figure 8.15 and the edge of the colony in Figure 8.5b reveals a less sharp cell density gradient across the surface.

8.4 Discussion

8.4.1 Microbial iron oxidation evident *in vitro*, but not *in situ*

Initial visual assessment of the *in vitro* incubations after 5.5 months indicated that the inoculum cultures used for each microcosm set contained active iron oxidizing microbes. This was primarily inferred by the strong presence of orange colouration both in the liquid medium and on the tubes of the biological incubations, which was either only weakly present or completely absent in the control tubes (Fig. 8.1a). This colouration was putatively identified as iron hydroxides/oxides, based on the observations of previous studies of biological iron oxidizing cultures grown using this media or similar media types (Kozubal *et al*., 2012; Wakeman *et al*., 2008).

In addition to the iron oxide precipitates on the tube walls, single biological incubations also had yellow-white deposits (Fig. 8.1b). Biological iron oxidation of pyrite releases sulfur which is readily oxidised to sulfuric acid, which can then further react to form sulfate-based minerals. Possible specific minerals that could comprise these yellow deposits include ferric hydroxysulphate, schwertmannite and jarosite (Konhauser, 1998).

The formation of sulfuric acid unless otherwise buffered will also significantly decrease the surrounding pH, something that was observed in the single biological incubations where these deposits were found (all single mineral incubations except calcite), relative to the sterile control (Biology ~pH 1.5, Control ~pH 2.5 - Fig. 8.3). This evidence is consistent with biological iron oxidation of pyrite (FeS_2), which liberates sulfur for oxidation to sulfuric acid (Konhauser, 1998). Iron oxidation can occur both via biotic and abiotic processes, however abiotic iron oxidation rate rapidly decreases with decreasing pH. As such, iron oxidation only becomes energetically favourable as a microbial metabolism below pH 4 (Hedrich *et al*., 2011), when organisms have sufficient access to available ferrous iron without competition from abiotic reactions. The initial acidity of Wakeman's medium (pH 3)

already makes biological iron oxidation favourable, and this is positively reinforced by pH reduction in biological cultures (Fig. 8.3).

In the single incubations with calcite, the pH was near to 7 and was not significantly different between the biological and control incubations, and a similar effect was identified in the mixed mineral conditions. This indicates that calcite is acting as a strong pH buffer in these solutions, raising the medium's initial pH (3) and neutralizing any acid produced by the microbial community in the biological incubation. Calcite is having this effect both in the single and mixed incubations, suggesting that calcite has a much greater contribution to solution pH than any of the other minerals tested (Fig. 8.3).

Biological activity also altered the surface colouring of pyrite incubated in both the single and mixed microcosms (Fig. 8.1b). These surfaces acquired an iridescent sheen, which appears morphologically analogous to "peacock" or "rainbow" pyrite in the literature (Cook, 1993; Baba-Kishi *et al*., 2005). These authors identified that the iridescent colouring of pyrite and related minerals (including chalcopyrite, $Cu_xFe_yS_2$) occurs when these minerals become oxidised. This suggests that biological activity acted to oxidise the pyrite surfaces, both in the single and mixed incubations. As the pH of the mixed incubation was above what is considered energetically favourable, this oxidative process may have been independent of metabolically driven iron oxidation.

Together, this evidence strongly indicates that microbial iron oxidation was taking place within the biological conditions of the *in vitro* microcosms. Although individual pieces of evidence could be explained by abiotic or alternative biological processes (for example, pH reduction could have been driven by biological organic acid production rather than sulfuric acid production from pyrite oxidation), it seems far more probable that the combined evidence points towards biological iron oxidation.

In contrast, none of the observations or evidence collected from the field microcosms indicates that iron oxidation (biotic or abiotic) occurred on the mineral surfaces at any appreciable level. Ferrous iron was available for iron oxidation both from the pyrite samples buried, and likely from the leachate of the surrounding shale rock.

There were no signs of orange crusts or yellow/white deposits on either the mineral surfaces or the bottle interior. The surfaces of the pyrite mineral cubes in all cases remained golden coloured, with no sign of iridescence. Although the pH of the actual mineral surfaces was not measured, the pH of the surrounding rocky material (as determined by immersion of samples in water) was above pH 5. This pH is above what is believed to energetically favourable for biological iron oxidation to occur. Although the pH of the mineral surfaces may have been lower this, the above evidence suggests iron oxidation was not occurring at a detectable level.

8.4.2 Distinct differential patterns of mineral colonization *in vitro*

The habitability of shale can be thought of as the extent to which shale rock supports the microbial community that inhabits the rock surface. Shale rock is an assemblage of its component minerals, metals and organic matter (kerogen), all of which will contribute to the rocks habitability. Via the use of the *in vitro* and *in situ* mineral incubations, the relative contribution of these minerals to shale habitability has been explored.

In the *in vitro* mineral incubations, clear differences in the levels of colonization (cells/mm^2) could be observed between minerals and between incubation conditions (Fig. 8.2a and 8.2b). The pattern of colonization across all three *in vitro* microcosm sets was similar, so mean average values obtained for each mineral from all three of the incubation sets set up (A-C) were calculated (Fig. 8.2b). Pyrite incubated under single mineral conditions was determined to be the most colonised mineral in the experiment, at 6.24 x 10^5 cells/mm^2. The least colonised mineral was calcite incubated under mixed mineralogical conditions, at 4.96 x 10^3 cells/mm^2 and under single mineral conditions calcite was colonised by 1.34 x 10^4 cells/mm^2. This data shows that levels of colonization varied by over two orders of magnitude between minerals and conditions combined, and by almost 1.5 orders of magnitude between minerals under the same conditions. Within the single mineral incubations the relative level of colonization of the minerals tested was in the order: pyrite>albite, muscovite>quartz>calcite, with pyrite being the most colonised and calcite the least (Fig. 8.2b).

A statistically significant reduction was observed in colonization levels between minerals incubated under single and mixed mineral conditions (K-W, across all microcosm sets (A-C), effect of condition on colonization, $Z=6.32$, $p<0.001$). The only sample where this is not the case is for calcite in microcosm set A (Fig. 8.2a). The reduction in community size between these conditions can likely be attributed to the higher pH experienced in the presence of calcite, being the least colonised mineral overall. The effect of pH on community size indicates that a significant subset of the community is comprised of acidophiles whose growth is reduced under pH neutral conditions.

The high level of pyrite colonization compared to other minerals tested supports the idea that these acidophiles are expected to be actively metabolising iron oxidizing microbes (Fig. 8.2b). SEM image analysis of the biologically incubated pyrite surface revealed abundant microbial cells adhered to the surface, supporting cell counts made with fluorescence microscopy (Fig. 8.2a and 8.4a). Biologically incubated pyrite showed distinct signs of having undergone surface weathering, including the presence of pits and crust formation (Fig. 8.4a-e). Together, this suggests that iron oxidizing microbial species were present in these microcosms and that their growth was supported by ferrous iron leaching out of the added pyrite granules or from the surface of pyrite mineral samples.

8.4.3 Pitting of pyrite and crust formation on mineral surfaces *in vitro*

Both cells and pits were largely isolated and were not found in aggregations on the pyrite surface. Pits were rectangular and roughly 2-3µm x 0.5µm in dimension, making them slightly longer than the numerous bacilli cells identified. The pits found in this study are analogous to those found on weathered pyrite in previous studies, within similar size ranges (McGuire *et al*., 2001; Edwards *et al*., 2001; Rojas-Chapana and Tributsch, 2004; Wacey *et al*., 2011). In a limited number of cases cells were found within pits (Fig. 8.4c), although a definitive conclusion on whether the cell within the pit can be attributed with its formation cannot be made (see Edwards *et al*., 2001). Pits appeared to be orientated by an unidentified planar feature within the crystal, potentially a twin plane, with these planes more heavily pitted than the

surrounding area (Fig. 8.4d). Such observations have been made in previous studies (Pisapia *et al*., 2008; Ndlovu and Monhemius, 2005; McGuire *et al*., 2001; Edwards *et al*., 1999; Edwards *et al*., 2001).

Crust formation was observed on all mineral types incubated under biological conditions, excluding calcite (Fig. 8.4e, 5a-d). This indicates that biological processes are responsible for crust formation. SEM-EDS was used to analyse the composition of the crusts, which showed them to be primarily composed of iron and sulfur like the unaltered surface. However, the crusts were enriched in oxygen compared to the pyrite surface, suggesting they are formed from the oxidised products of the mineral surface i.e. they are crusts of iron oxide/hydroxide (Fig. 8.6 panels A and B). The absence of crusts on calcite further corroborates that the crusts are likely to be iron oxide/hydroxide deposits formed from microbial iron oxidation activity that was supressed by the higher pH of the calcite microcosms.

Crusts were found abundantly on albite, muscovite and quartz incubated under biological conditions (Fig. 8.5a-d). These crusts covered a significant proportion of the surface of muscovite, although the distribution was patchy (Fig. 8.5a). Microbial colonization of muscovite and albite was distinguishable from the colonization of pyrite by the occurrence of both microcolonies and biofilms coating the surfaces of these minerals (Fig. 8.5b-d). The centre of these microcolonies appear darker on the SEM images (Fig. 8.5b), an observation also made by Torrentó *et al*. (2012) for colonies of *Thiobacillus denitrificans* on pyrite. They attribute this darkening as a thick organic film coating the cells (Torrentó *et al*., 2012).

Figure 8.5c demonstrates how these microbial biomasses could become coated in crusts, suggesting that cell surfaces or excreted EPS (as seen in Figure 8.4e) could act as nucleation sites for crust formation (Edwards *et al*., 2001; Mielke *et al*., 2003). Either dissolved iron oxides/hydroxides in the surrounding culture are precipitating onto these biological features, or these cells are actively oxidizing iron and precipitating the products onto their surface. In either case, crust formation was found to extensively cover biofilms coating the mineral surface, suggesting biofilms are a significant factor in crust formation (Fig. 8.5d). SEM-EDS analysis of crusts on the surface of muscovite showed that they were enriched in carbon as well as metals

including iron, potassium and calcium (Fig. 8.6 panels C and D). The presence of carbon further supports that biological material is present within the crusts, while the accumulation of metals has been found previously for iron oxide crusts (Carpenter and Hayes, 1980; Singh and Gilkes, 1992).

8.4.4 Surface colonization of shale-comprising minerals *in situ* and the surface weathering of pyrite by fungal hyphae

The results in the above sections identified that iron oxidizing enriched microbial communities isolated from weathered shale can differentially colonise minerals found in those environments. This community type was chosen specifically for this study based upon results presented in chapter 7, where iron oxidation was the only evident biological process occurring in simulated weathering conditions. Evidence from this chapter supports that the enriched communities actively weathered pyrite *in vitro* through redox reactions that resulted in pyrite dissolution and secondary mineral formation. To determine if biological iron oxidation is an important process *in situ*, mineral samples were buried in mesocosms within a weathered shale environment, the scree-comprised floor of Assholm mine (see Chapter 4 for images). This investigation also allowed more general observations to be made, including levels of mineral colonization, and other geochemical or biogeochemical processes that may contribute to morphological alterations of mineral surfaces.

Analysis of fluorescence microscopy counts taken from samples extracted from the mesocosms after one year revealed differential levels of colonization in the single mineral incubations, but not under mixed mineralogical conditions (Fig. 8.7) (. Muscovite was the most colonised mineral *in situ* (6×10^4 cells/mm^2), and was substantiallymore colonised compared to the least colonised mineral calcite (7.7×10^3 cells/mm^2) However, this difference was less than an order of magnitude. This suggests that mineral colonization was much more uniform *in situ* than it was *in vitro*, where colonization differed by over two orders of magnitude between pyrite and calcite (Fig. 8.2b). Furthermore, the order of colonization level which was the same between single and mixed conditions *in vitro* was not the same *in situ*, with some minerals more colonised under single than mixed conditions and vice versa (Fig. 8.7).

Combined fluorescence microscopy and scanning electron microscopy of mineral surfaces allowed microbiological and morphological features to be examined (Figs. 8.8-8.15). The surface of calcite was the most altered compared to the other minerals tested, showing characteristic signs of having undergone acid-driven dissolution (Fig. 8.8) (Trotignon *et al*., 2002; Lopez-Arce *et al*., 2005). The pH of the scree surroundingthe buried samples was mildly acidic (~pH 5), which supports acid-driven dissolution of the calcite surface. Both geochemical and biological processes could be responsible for producing this acidity, but the contribution of these separately was not assessed in this study.

Numerous microbial cell types were identified on the mineral surfaces imaged (Fig. 8.9-8.10). Bacterial cell shapes found include bacilli, coccobacilli (attached together at cell poles) and streptobacilli. Filaments of various widths were seen, which could represent either bacterial (actinomycetes) filaments or fungal hyphae. One way to distinguish between them is through filament width, with fungal hyphae ranging from 2-30μm (usually 5-10μm) whereas actinomycete filaments are normally less than 1μm (Deacon, 2006; Madigan *et al*., 2009). Based on these parameters, many of the filaments imaged are likely to be fungal hyphae (Fig. 8.9b, 8.13 and 8.15) although other, narrower filaments could be actinomycetes (Fig. 8.9b and 8.11). The unicellular, teardrop shaped cells have not been identified to any level, indicating that they could be non-biological formations. Figure 8.10 shows a collection of cells on the surface of albite that have a thick coating surrounding the cells. The fluorescence of these coatings under acridine orange staining (although less intense than the cell it surrounds) suggests that these coatings contain DNA (Fig. 8.10, left image). These coatings are likely to be comprised of EPS containing polysaccharides, DNA and other biological polymers. Such thick EPS capsules could be advantageous to these cells when colonizing the mineral surface. EPS is also believed to play an important role in mineral dissolution, through mechanisms such as metal complexation and oxidative attack (Welch and Vandevivere, 1994; Kinzler *et al*., 2003).

Biological material, in particular filaments of fungi/actinomycetes, were found to act as nucleation sites for crust formation and aggregation of particulates (Fig. 8.11). This effect is similar to that observed in the *in vitro* microcosms (Fig. 8.5a and 8.5c).

The composition of these materials is unknown, but crusts are likely to be formed from metals that have leached from the surrounding rock, become oxidised and then precipitated onto the cellular surfaces (Ferris *et al*., 1989). Accumulation of such materials will inherently alter the surface properties of the mineral, which could act to reduce or enhance surface weathering.

The most palpable alteration of a mineral surface observed in the *in situ* mesocosms was that of pyrite by fungal filaments (based on filament thickness, >1μm) (Fig. 8.12). In the process of sample preparation for SEM imaging, the mineral surfaces undergo several washing and liquid immersion steps that can dislodge cells and other material from the surface. In numerous images, broken fungal hyphae were observed revealing dark etchings on the mineral surface below where the hyphae had been present (Fig. 8.12). This indicates that fungal activity weathered the pyrite surface. Fungal/actinomycete filaments were found abundantly on the pyrite surface, demonstrating that this mechanism of biological weathering could have a significant effect on pyrite dissolution (Fig. 8.13 and 8.14). As far as the author is aware, no previous study has associated fungal activity with pyrite weathering (see reviews on geomycology, Gadd 2007, Gadd 2017). A putative mechanism for this observed weathering could be fungal release of organic acids that oxidise the pyrite surface, a mechanism that is known to play a key role in fungal rock and mineral weathering (Anjum *et al*., 2012; Gadd 2007). However, further research needs to be carried out to confirm this result and to elucidate the mechanisms used by these fungal species to cause these morphological alterations.

Fungi hyphal growth is also known to act as a biomechanical force, whereby the pressure exerted by growing fungal hyphae on mineral matrices they are in contact with can force weaknesses in the mineral matrices into cracks (Money 2004). Fungal hyphae were observed growing into pits and cracks within the pyrite surface (Fig. 8.13), indicating that weathering by this mechanism is possible, although no evidence to suggest its role was found.

No evidence of bacterial iron oxidation resulting in pit formation, as seen in the *in vitro* microcosms (Fig. 8.4a, 8.4c and 8.4d) was seen on the pyrite surfaces incubated *in situ* (Fig. 8.12-15). The pH of the surrounding scree (~pH 5), as well as the surface

pH of the incubated minerals, would be too high for biological iron oxidation to be metabolically favourable (Hedrich *et al*., 2011). However, the pH of microenvironments can be radically altered from that of the surrounding environment, particularly by microbial activity (Douglas and Beveridge 1998). Nevertheless, in addition to the lack of pitting there were no ubiquitous crusts found on the mineral surface, suggesting that microbial iron oxidation that caused crust formation was absent or at low, undetectable levels. Numerous microcolonies of bacteria were found on pyrite surfaces, similar to imaged colonies in the *in vitro* microcosms (Fig. 8.4b-c) and to microcolonies of *Thiobacillus denitrificans* on pyrite reported by Torrentó *et al*. (2012), but no evidence of surface dissolution surrounding these colonies was observed.

8.4.5 Conclusions

In this chapter, the habitability of shale comprising minerals was explored both *in vitro* and *in situ* and was found to be variable depending upon environmental conditions and the microbial community studied. *In vitro* pyrite was the most colonised mineral (Fig. 8.2), which supports a nutrient driven differential between mineral colonization where pyrite acts as a primary energy source for iron oxidizing microbes. The colonization and alteration of pyrite in this instance can be thought of as an active process that provides an adaptive advantage to the colonizing microbe. In contrast, no such colonization differential was seen in the *in situ* mesocosms (Fig. 8.7) suggesting that for these minerals, there were no clear defining factors in mineral colonization within the burial environment. This does not mean factors influencing colonization were not present, but that they could not be discerned by this study.

Through imaging and elemental analysis, this study demonstrates that microbial weathering and surface dissolution of pyrite occurs both *in vitro* and *in situ*, although via differing organisms and mechanisms (Fig. 8.4c-d and 8.12). The fungal weathering of pyrite was shown through dark etchings made below the hyphal growth, which can be putatively explained through organic acid secretion. This can be thought of as either a passive process, whereby the fungi produce organic acids that weather the pyrite as a by-product of their metabolism or for another adaptive

purpose, or as an active purpose to liberate the nutrients iron or sulfur. With surrounding rock leachate likely providing an abundant source of iron and sulfur, it seems a passive explanation is more probable.

While surface modifications, primarily through crust formation and particulate aggregation (Fig. 8.5a-d, 8.6 and 8.11), were observed on albite, muscovite and quartz, no direct evidence for microbially induced mineral dissolution was found either *in vitro* or *in situ*.

The findings of this chapter support those of the previous ones, where iron oxidizing microbes were found abundantly in acidic locations of weathered shale (Chapter 5) and microbial iron oxidation was the dominant process occurring within rock leaching experiments (Chapter 7). However, what is also clear from this chapter is that the level of this activity is based upon the geochemical environment. Despite iron oxidizing bacteria being successfully enriched from the wall of Assholm mine *in vitro*, these bacterial species were not active iron oxidisers within the scree comprised of chips eroded from that very wall *in situ*. This is believed to be due to differences in pH, although other environmental factors may be influential.

However, what is clear is that microbial species within natural weathered shale environments are both present and capable of active mineral weathering under the right conditions. In particular, this work has highlighted the role of fungi in pyrite weathering within a natural environment, a previously undocumented process.

Chapter 9 – Conclusions

9.1 Conclusions, synthesis and contribution to the field

The research presented in this thesis has made a significant contribution to our understanding of microbial rock weathering of shale in natural and historic, industrial environments. One aim of this work was to discern if rock weathering mechanisms not related to iron or sulfur redox reactions, were active in weathering shale rock (Chapter 1). Rock weathering bacteria were isolated from all samples tested, indicating that the potential for biotic weathering of shale rock is ubiquitous across weathered shale environments (Chapter 5). Furthermore, all weathering phenotypes tested for (iron oxidation, manganese oxidation, organic acid production, siderophore production and phosphatase production) were identified across multiple isolates. Of the 15 genera identified, the majority were either *Proteobacteria* (α and γ) or *Actinobacteria*, supporting previous studies that show these groups to be important members of shale weathering communities (Matlakowska and Sklodowska, 2009; Li *et al*., 2014; Jiang *et al*., 2015; Włodarczyk and Matlakowska, 2017).

A novel contribution to the field of microbial shale weathering includes the identification of three genera previously not associated with weathered shale environments: *Micromonospora*, *Moraxella*, and *Tetrasphaera* (Chapter 5). Furthermore, as far as the author is aware, this thesis is the most extensive survey of weathered shale isolates tested for rock weathering capabilities. This work therefore can validate the importance of these organisms in rock weathering processes, when they are identified in culture-independent weathered shale studies (Li *et al*., 2014; Jiang *et al*., 2015; Włodarczyk and Matlakowska, 2017).

Chapter 7 revealed microbial iron oxidation as the dominant biogeochemical process within simulated weathering experiments. Weathered shale chips incubated with a shale microbial enrichment community in water and M9 medium reduced liquid pH from circumneutral to acidic (~ pH 3) and mildly acidic (~ pH 5) respectively. Iron oxidation was evident in the water culture ((Fe) reduction from 25 ppm to 0.5 ppm)

but not observed in the M9 cultures. The pH buffering capacity of the M9 salts likely maintained culture pH above the threshold for energetically favourable iron oxidation (Hedrich *et al*., 2011).

Rock weathering phenotypes that can induce elemental leaching from rock were abundantly identified in Chapter 5, but no consistent evidence for biologically induced leaching was found in Chapter 7. Possible explanations for this finding include a) the specific experimental procedure used could not elucidate biological weathering activity, b) that rock weathering microbes were not present in the enrichment culture used to inoculate the experiment c) biologically induced leaching did occur, but could not be detected through concentration measurements due to absorption/precipitation of leached elements to solid phases within the cultures.

Concentrations of elements such as (Al) and (Si) were particularly variable between batch reactors in a pattern that did not correlate with incubation time, indicating possible sample heterogeneity (Chapter 7). Weathered shale chips were used as a rock source to simulate natural weathering conditions, but this likely resulted in sample heterogeneity that masked any biological effects on elemental leaching.

Within the M9 with added glucose batch reactors, bio-reduced leaching was observed rather than bio-enhanced leaching (Chapter 7). This widespread bio-reduced leaching is not seen in the M9 batch reactors lacking glucose, and biomass was lower in the absence of glucose. Absorption of leached elements to biomass across the experiment therefore could have masked any bio-enhanced leaching effects. Sample heterogeneity and/or absorption are proposed as possible explanations for lack of observable biological weathering activity. The data presented in Chapter 7 demonstrates the difficulty in designing biological weathering experiments, where a trade-off must be made between simulating natural conditions and obtaining consistent data.

Based on the results of Chapter 7, the microcosms of Chapter 8 were designed to identify the potential role of iron oxidizing microbes in weathering of shale-comprising minerals (albite, calcite, muscovite, pyrite and quartz). Colonization of mineral surfaces varied between mineral types, with pyrite being the most colonised and calcite the least. Microbial weathering of pyrite through pitting was evident from

all three microbial communities tested. However, none of the other minerals tested appeared biologically weathered after 5 months of incubation. The surfaces of these minerals however was altered through microbial colonization and production of EPS, which increased surface aggregation of particulates and the formation of iron oxyhydroxides.

In situ incubation of minerals within mesocosms for one year revealed that, unlike the *in vitro* microcosms, there was no differential surface colonization between mineral types (Chapter 8). Evidence for the surface weathering of pyrite by fungal hyphae was identified, with dark etchings shown below hyphae that become detached from the mineral surface. As far as the author is aware, this is the first evidence that fungi can weather pyrite, although the mechanism by which this occurs is unknown. Surface aggregation of particulates and crust formation (possibly precipitated mineral products) were found abundantly on mineral surfaces, particularly associated with bacterial cells and fungal hyphae.

However, no evidence for pitting, as observed *in vitro*, on the pyrite surface was found. Furthermore, no evidence for microbial surface weathering of any of the other minerals tested was identified *in situ*. These results highlight that pyrite is the most biologically reactive mineral within shale, having been weathered by microbial activity both *in vitro* and *in situ* (Chapter 8). This corroborates the main finding of Chapter 7, that iron oxidation is a dominant biogeochemical process within shale weathering environments. However, only four out of nine sites sampled in Chapter 5 yielded iron oxidizing isolates, suggesting that the role of microbial iron oxidation may be limited by geochemical and environmental parameters within weathered shale.

Chapter 6 investigated the growth and activity responses of the weathered shale isolate *Variovorax paradoxus* to organic carbon rich rocks, including shale. *V. paradoxus* was one of two isolates enriched in an extreme low nutrient medium lacking an added carbon source, and is a known degrader of recalcitrant organic sources (Satola *et al.*, 2013). The addition of crushed shale to growth medium enhanced the growth of *V. paradoxus* in liquid culture and increased colony size in swarming motility assays. Furthermore, *V. paradoxus* was found to colonise both

rock powder and shale-comprising mineral surfaces, producing pili to aid adherence to the geological substrate.

The addition of coal rock powder to liquid growth medium had a toxic effect on the growth of *V. paradoxus* and stimulated a stress response (Chapter 6). In the presence of coal rock powder, growth was reduced in M9 liquid medium lacking glucose (this reduction was not seen in M9 + glucose). Furthermore, cells plated onto agar displayed an increased frequency of colony morphology variation; colonies displayed enhanced production of surfactants that reduced surface tension within the colony, allowing cells to spread more thinly across the agar. Thiswas also observed in swarming motility assays, where the addition of coal powder to swarming media enhanced colony diameter. The effect of surfactant production on interfacial surface tension (IFT) was quantified in liquid culture and, although not statistically significant, cultures of *V. paradoxus* grown in the presence of coal powder did decrease the IFT values of resultant culture. Although not confirmed, non-soluble organic compounds within the coal could have induced the stress response identified in this work (Chapter 6).

This study is the first carried out to determine the physiological responses of *V. paradoxus* to geological environments. It has shown that shale can enhance and growth and motility, while coal rock powder induces a toxic stress response. This work is also the first to demonstrate that the surfactants produced by *V. paradoxus* reduce interfacial surface tension in liquid, and that this can be quantified using drop tensiometry (Chapter 6).

In Chapter 1, three central research questions were stated to be the focus of the work in this thesis. These aims are reiterated below, with a brief summary of how the findings in this thesis have addressed these questions.

1) What is the distribution of rock weathering microbes in natural and historic industrial weathered shale environments?

Fifteen different bacterial genera with rock weathering capabilities were identified across a range of weathered shale environments (Chapter 5). All rock weathering phenotypes (e.g. siderophore production) tested for were identified in at least one

environment, and some genera were identified for numerous weathering phenotypes (e.g. Pseudomonas). There was a non-even distribution of weathering phenotypes across the sampling sites tested, with co-association of some phenotypes (e.g. manganese and iron oxidation) and dis-association of others (e.g. siderophore production and iron oxidation) (Chapter 5).

2) Can microbial rock weathering activity in shale be demonstrated using *in vitro* and *in situ* methodologies?

Microbial rock weathering experiments *in vitro* provided a limited body of evidence for biologically enhanced leaching of elements such as Ni and Zn (Chapter 7). If representative of true biological activity, then this work identified that microbial rock weathering activity does occur in weathered shale, and that indicators of this activity are element specific. Microbial iron oxidation was the most pronounced biogeochemical process observed in these experiments (Chapter 7), and further *in vitro* work demonstrated that enriched iron oxidizing microbial communities could substantially weather the surface of the shale-comprising iron sulfide mineral pyrite (Chapter 8, section 8.3.1). *In situ* burial of pyrite in a shale weathering environment revealed evidence for biological mineral weathering (Chapter 8, section 8.3.2).

3) Investigate which physiological adaptations rock-dwelling microbes have to colonise and survive in weathered shale rock habitats?

Characterisation of the weathered shale inhabiting bacteria *Variovorax paradoxus* revealed numerous adaptations for survival and growth in a geological environment (Chapter 6). *V. paradoxus* is capable of growth under extreme nutrient limitation, storing intracellular carbon when nutrients are available. Addition of rock powder to growth media induces the excretion of extracellular polysaccharides in *V. paradoxus*, and is hypothesised to form part of a stress response to toxic geological components. The role of bacterial motility in responding to geochemical stimuli has been explored, with shale enhancing the swarming motility of *V. paradoxus* across agar surfaces.

Overall, this thesis demonstrates that microbes within weathered shale both alter, and respond to, their surrounding geological environment. These findings support the initial supposition made that microbial communities are active agents in the

weathering and breakdown of shale rock. Therefore, future work should focus on the rate at which these microbial agents weather shale, and the impact this has on shale cliff geomorphology and coastal erosion.

9.2 Future work

9.2.1 Methodological recommendation

The work presented in this thesis has focused on the use of culture and *in situ* based methodologies, to directly explore the activity of microbial rock weathering microorganisms on shale and shale-comprising minerals. The success of these approaches has varied, but in several cases have been effective in providing evidence of microbial activity in geological environments.

Combined used of *in vitro* and *in situ* mineral incubations in Chapter 8 allowed a direct comparison of the activity of enriched microbial communities in the laboratory, with the activity of natural microbial communities in the field. In the results presented in that Chapter, it revealed an unexpected conclusion – that the bacterial iron oxidation activity clearly demonstrated *in vitro* (Chapters 7 and 8) did not appear to occur *in situ* within the chosen study site (Assholm mine). The identification of cell-shaped pits on pyrite surfaces from three biological independent (enrichment cultures inoculated with material from three different sites) *in vitro* microcosms seemed to indicate the prevalence of this microbial activity in weathered shale. However, no evidence for any pitting of pyrite surfaces was detected *in situ* mesocosms. This demonstrates that even robust results of activity collected via *in vitro* experimentation need to be qualified by an assessment of that activity *in situ*.

In the conclusion of Chapter 7, a brief summary of the benefits and problems of *in vitro* simulated weathering conditions highlighted that the effect size of a factor could be maximised by highly constraining confounding variables. In the case of the experimental design for the *in vitro* microcosms in Chapter 8, this included providing an iron replete environment for the enrichment of iron oxidizing microbes. The enhanced effect of bacterial iron oxidation in this system likely decreased the activity, or chances of detection, of other microbial-mineral interactions such as the

fungal etching of pyrite detected *in situ* (Chapter 8). A pitfall therefore of highly constrained *in vitro* experimentation is that of limited detection of microbial activities from the diverse microbial processes that could occur within the environment. These conclusions should be taken into consideration when designing experimentation for future work to investigate microbial rock weathering processes in shale.

9.2.2 Quantifying rates of microbial rock weathering of shale

To evaluate the microbial contribution to geomorphological processes within shale cliffs, an assessment of the relative impact and rate of microbial mechanisms that contribute to erosive processes needs to be made. There are numerous difficulties in producing a reliable assessment of this type. Firstly, microbial weathering activity does not occur via a single process, but is comprised of numerous microbial species acting via a range of weathering mechanisms. Therefore, a single rate value for microbial rock weathering cannot be determined from a microbiological perspective. Many rock weathering mechanisms directly or indirectly contribute to mineral dissolution, resulting in elemental release. Therefore, elemental release from rock into the leachate solution (e.g. (Si) or (Al)), can provide measurable values for the extent of weathering within a system. However, the rate of leaching for each element is often different, making it difficult to provide a singular value for weathering extent.

In Chapter 7, elemental release from shale rock during weathering under biotic and abiotic conditions was measured using ICP-OES for 14 elements. The aim of this study was to provide elemental release rate values for the two conditions, in which biologically enhanced leaching could be identified. However, in practice this was not achieved due to complexities of the experimental system and the geochemistry of the weathering environment. Other biological shale weathering studies have determined rates of elemental release (Anjum *et al.*, 2010; Matlakowska *et al.*, 2010a; Włodarczyk *et al.*, 2015), but they have often used highly artificial conditions such as elevated temperature (e.g. 35 ^{o}C), shaking/stirred cultures or incubation with a single organism rather than a microbial community. Therefore, the relevance of

these acquired rates to the rates of microbial rock weathering natural environments islimited.

Based on the work of these thesis, the role of microbial iron oxidation as a dominant biogeochemical process within weathered shale environments has been supported. Therefore, the author would suggest that future work determines the following two factors: a) the rate of microbial iron oxidation by indigenous microbial communities within weathered shale b) quantify the impact that pyrite dissolution and subsequent secondary mineral formation (e.g. iron oxyhydroxides) has on structurally weakening shale rock.

Part a) would require geomicrobiological techniques such as geochemical tests (e.g. ferrozine assay) to quantify iron oxidation within a simulated weathering environment. The range of conditions under which microbial iron oxidation can occur would also need to be determined. The frequency at which these conditions are met within weathered shale environments would then add an upper bound on the impact this microbial iron oxidation could have *in situ*.

To determine the impact iron oxidation has on structurally weakening shale rock, geotechnical and engineering approaches could be used. Shale rock would need to be artificially weathered under conditions which facilitated iron oxidation. Rock strength analyses such as slake durability (qualitative), surface strength or unconfined compressive strength tests (quantitative) could be used to determine the impact that artificial weathering had on rock structure (Koncagül *et al*., 1999; Hobbs *et al*., 2012; Islam and Skalle, 2013). The relative impact of iron oxidative processes would need to be distinguished from other rock weakening processes such as hydration, so appropriate controls would be required.

By combining these two approaches, a quantifiable value could be placed on the impact of microbial iron oxidation on shale structural weakness and breakdown.

Another microbial process that has not been addressed in this thesis is that of sulfur oxidation that occurs when sulfur is liberated from pyrite during iron oxidation. The oxidation of sulfur has a two-part effect on weathering and structurally weakening shale rock: a) sulfuric acid is produced as an end-product of sulfur transformation,

which can act to dissolve minerals and matrix within shale rock and b) secondary sulfate minerals formed from sulfuric acid reacting with calcite (gypsum) and aluminosilicate minerals (jarosite) causing volumetric expansion (pyritic heaving) (Hawkins, 2014).

Future work could determine the relative contribution of microbial oxidative processes to sulfur oxidation (which also occurs via purely geochemical mechanisms) within weathering shale environments. This could be achieved by enumerating the number of sulfur oxidizing microbial cells within weathered shale, and determining the rate of sulfur oxidation within a weathered shale microbial community. Further geomicrobiological characterisation of microbial sulfur oxidation within natural weathered shale environments would provide a useful background for future research. These findings could then be applied in a similar approach outlined above for microbial iron oxidation, to determine the impact microbial sulfur oxidation has on shale rock degradation.

9.2.3 Continuation of work within this thesis

The suggestions made in section 9.2.1 above are relatively advanced beyond the work of this thesis, and would likely require additional research into the geomicrobiology of shale weathering environments before they could be carried out. The following suggestions for future work are direct continuations from the findings presented in this thesis:

1) Obtain rock weathering microbial isolates using the methodology outlined in Chapter 5, and then quantify the relative rock weathering capacity of those isolates. For example, siderophore production by isolates could be determined in shale rock batch cultures, and the relative impact on rock dissolution quantified. This would enable a more accurate interpretation of microbial weathering potential within weathered shale environments.

2) Use organic geochemical approaches (e.g. PLFA analysis or radioactive isotope labelling) to determine if *V. paradoxus* can degrade and utilise shale bound organic matter. *V. paradoxus* has been extensively characterised for its ability to degrade and metabolise recalcitrant organic compounds (Satola *et al.*, 2013). It has recently been

identified in other weathered shale studies (Włodarczyk and Matlakowska, 2017), so *V. paradoxus* could be an important member of kerogen-degrading microbial communities within weathered shale.

3) Isolate and identify fungal species that can oxidise pyrite or modify pyrite surfaces. The mechanisms of action behind these processes could then be determined. Fungi have not previously been indicated in pyrite weathering activity, so experiments along this line would provide interesting insight into the geomycology of shale weathering.

References

Abdulla, H., May, E., Bahgat, M., & Dewedar, A. (2008). Characterization of actinomycetes isolated from ancient stone and their potential for deterioration. *Polish Journal of Microbiology*, *57*(3), 213-220.

Abou-Shanab, R. A. I., Van Berkum, P., & Angle, J. S. (2007). Heavy metal resistance and genotypic analysis of metal resistance genes in gram-positive and gram-negative bacteria present in Ni-rich serpentine soil and in the rhizosphere of Alyssum murale. *Chemosphere*, *68*(2), 360-367

Achten, C., Cheng, S., Straub, K. L., & Hofmann, T. (2011). The lack of microbial degradation of polycyclic aromatic hydrocarbons from coal-rich soils. *Environmental Pollution*, *159*(2), 623-629.

Adams, L. F., & Ghiorse, W. C. (1987). Characterization of extracellular Mn^{2+}-oxidizing activity and isolation of an Mn^{2+}-oxidizing protein from *Leptothrix discophora* SS-1. *Journal of Bacteriology*, 169(3), 1279-1285.

Agar, R. (1960). Post-glacial erosion of the North Yorkshire coast from the Tees estuary to Ravenscar. In *Proceedings of the Yorkshire geological and Polytechnic Society*, 32 (4), 409-427.

Ahmed, E., & Holmström, S. J. (2014). Siderophores in environmental research: roles and applications. *Microbial Biotechnology*, *7*(3), 196-208.

Akob, D. M., & Küsel, K. (2011). Where microorganisms meet rocks in the Earth's Critical Zone. *Biogeosciences*, *8*(12), 3531-3543.

Allied Market Research (2016) Shale Gas Market by End User (Industrial, Power generation, Residential, Commercial, Transportation) - Global Opportunity Analysis and Industry Forecast, 2014 – 2022. Accessed at (29/08/2017): https://www.alliedmarketresearch.com/shale-gas-market

Amiotte Suchet, P., Probst, J. L., & Ludwig, W. (2003). Worldwide distribution of continental rock lithology: Implications for the atmospheric/soil CO2 uptake by continental weathering and alkalinity river transport to the oceans. *Global Biogeochemical Cycles*, *17*(2), doi:10.1029/2002GB001891

An, Y. H., & Friedman, R. J. (1998). Concise review of mechanisms of bacterial adhesion to biomaterial surfaces. *Journal of Biomedical Materials Research*, *43*(3), 338-348.

Anderson, W. H. (2008). *Foundation problems and pyrite oxidation in the Chattanooga Shale, Estill County, Kentucky*. Kentucky Geological Survey, University of Kentucky

Anjum, F., Bhatti, H. N., Asgher, M., & Shahid, M. (2010). Leaching of metal ions from black shale by organic acids produced by *Aspergillus niger*. *Applied Clay Science*, *47*(3), 356-361.

Anjum, F., Bhatti, H. N., Ghauri, M. A., Bhatti, I. A., Asgher, M., & Asi, M. R. (2009). Bioleaching of copper, cobalt and zinc from black shale by *Penicillium notatum*. *African Journal of Biotechnology*, *8*(19).

Anjum, F., Shahid, M., & Akcil, A. (2012). Biohydrometallurgy techniques of low grade ores: A review on black shale. *Hydrometallurgy*, *117*, 1-12.

Arora, N. K., Kang, S. C., & Maheshwari, D. K. (2001). Isolation of siderophore producing strains of *Rhizobium meliloti* and their biocontrol potential against *Macrophomina phaseolina* that causes charcoal rot of groundnut. *Current Science*, *81*(6), 673-677.

Baba-Kishi, K. Z., Lee, M. K., & Tai, C. W. (2005). Observation of the structure of iridescent surface layer on Chalcopyrite. *Microscopy and Microanalysis*, *11*(S02), 1770-1771.

Baker, B. J., & Banfield, J. F. (2003). Microbial communities in acid mine drainage. *FEMS Microbiology Ecology*, *44*(2), 139-152.

Baker, E. W., & Louda, J. W. (1986). Porphyrin geochemistry of Atlantic Jurassic-Cretaceous black shales. *Organic Geochemistry*, *10*(4), 905-914.

Balci, N., Shanks, W. C. III, Mayer, B, & Mandernack, K. W. (2007) Oxygen and sulfur isotope systematics of sulfate produced during bacterial and abiotic oxidation of pyrite. *Geochimica Cosmochimica Acta,* 71, 3796–3811.

Banfield, J. F., Barker, W. W., Welch, S. A., & Taunton, A. (1999). Biological impact on mineral dissolution: application of the lichen model to understanding mineral weathering in the rhizosphere. *Proceedings of the National Academy of Sciences*, 96(7), 3404-3411.

Barker, W. W., Welch, S. A., Chu, S., & Banfield, J. F. (1998). Experimental observations of the effects of bacteria on aluminosilicate weathering. *American Mineralogist*, *83*(11), 1551-1563.

Battaglia-Brunet, F., Itard, Y., Garrido, F., Delorme, F., Crouzet, C., Greffié, C., & Joulian, C. (2006). A simple biogeochemical process removing arsenic from a mine drainage water. *Geomicrobiology Journal*, *23*(3-4), 201-211.

Bax, S., Lotherington, R. & Scott, S. (2015) Archaeological Excavation and Survey of Scheduled Coastal Alum Working Sites at Boulby, Kettleness, Sandsend and Saltwick, North Yorkshire, *Archaeological Research Services Ltd*, Report No-2015/42

Beaulieu, E., Goddéris, Y., Donnadieu, Y., Labat, D., & Roelandt, C. (2012). High sensitivity of the continental-weathering carbon dioxide sink to future climate change. *Nature Climate Change*, *2*(5), 346.

Behar, F., & Vandenbroucke, M. (1986). Chemical modeling of the structure of kerogens and asphaltenes as a function of their origin and evolution stage. *Revue de l'institut Francais du Petrole*, *41*(2), 173-188.

Belimov, A. A., Hontzeas, N., Safronova, V. I., Demchinskaya, S. V., Piluzza, G., Bullitta, S., & Glick, B. R. (2005). Cadmium-tolerant plant growth-promoting bacteria associated with the roots of Indian mustard (*Brassica juncea L. Czern*.). *Soil Biology and Biochemistry*, *37*(2), 241-250.

Benner, S. G., Gould, W. D., & Blowes, D. W. (2000). Microbial populations associated with the generation and treatment of acid mine drainage. *Chemical Geology*, *169*(3), 435-448.

Bennett, P. C. (1991). Quartz dissolution in organic-rich aqueous systems. *Geochimica et Cosmochimica Acta*, *55*(7), 1781-1797.

Bennett, P. C., Rogers, J. R., Choi, W. J., & Hiebert, F. K. (2001). Silicates, silicate weathering, and microbial ecology. *Geomicrobiology Journal*, 18(1), 3-19.

Berlendis, S., Beyssac, O., Derenne, S., Benzerara, K., Anquetil, C., Guillaumet, M., Esteve, I. and Capelle, B. (2014) Comparative mineralogy, organic geochemistry and microbial diversity of the Autun black shale and Graissessac coal (France). *International Journal of Coal Geology*, *132*, 147-157.

Bini, C., & Wahsha, M. (2014). Potentially harmful elements and human health. In PHEs, Environment and Human Health (pp. 401-463). Springer Netherlands.

Bhattarai, P., Marui, H., Tiwari, B., Watanabe, N., Tuladhar, G. R., & Aoyama, K. (2006). Influence of weathering on physical and mechanical properties of mudstone. In *Proc., int. symp. on disaster mitigation of debris flows, slope failures and landslides* (pp. 467-479). Tokyo: Universal Academy Press.

Boggs, S. (2009). *Petrology of Sedimentary Rocks*. Cambridge University Press.

Boston, P. J., Hose, L. D., Northup, D. E., & Spilde, M. N. (2006). The microbial communities of sulfur caves: a newly appreciated geologically driven system on Earth and potential model for Mars. *Geological Society of America Special Papers*, *404*, 331-344.

Boston, P.J., Spilde, M.N., Northup, D.E., Melim, L.A., Soroka, D.S., Kleina, L.G., Lavoie, K.H., Hose, L.D., Mallory, L.M., Dahm, C.N. and Crossey, L.J., (2001). Cave biosignature suites: microbes, minerals, and Mars. *Astrobiology*, *1*(1), 25-55.

Botero, A. E. C., Torem, M. L., & de Mesquita, L. M. S. (2008). Surface chemistry fundamentals of biosorption of *Rhodococcus opacus* and its effect in calcite and magnesite flotation. *Minerals Engineering*, 21(1), 83-92.

Bouchez, J., Beyssac, O., Galy, V., Gaillardet, J., France-Lanord, C., Maurice, L., & Moreira-Turcq, P. (2010). Oxidation of petrogenic organic carbon in the Amazon floodplain as a source of atmospheric CO2. *Geology*, *38*(3), 255-258.

Brain, M. J., Rosser, N. J., Norman, E. C., & Petley, D. N. (2014). Are microseismic ground displacements a significant geomorphic agent? *Geomorphology*, *207*, 161-173.

Brandt, U., Hiessl, S., Schuldes, J., Thürmer, A., Wübbeler, J. H., Daniel, R., & Steinbüchel, A. (2014). Genome- guided insights into the versatile metabolic capabilities of the mercaptosuccinate- utilizing β- proteobacterium *Variovorax paradoxus* strain B4. *Environmental Microbiology*, *16*(11), 3370-3386.

Brantley, S. L., Liermann, L., Bau, M., & Wu, S. (2001). Uptake of trace metals and rare Earth elements from hornblende by a soil bacterium. *Geomicrobiology Journal*, *18*(1), 37-61.

Brehm, U., Gorbushina, A., & Mottershead, D. (2005). The role of microorganisms and biofilms in the breakdown and dissolution of quartz and glass. *Palaeogeography, Palaeoclimatology, Palaeoecology*, *219*(1), 117-129.

Brofft, J. E., McArthur, J. V., & Shimkets, L. J. (2002). Recovery of novel bacterial diversity from a forested wetland impacted by reject coal. *Environmental Microbiology*, *4*(11), 764-769.

Bryce, B. C, Bihan T. L., Martin S. F., Harrison J. P., Bush T., Spears B., Moore A., Leys N., Byloos B., and Cockell C. S. (2016). Rock geochemistry induces stress and starvation responses in the bacterial proteome. *Environmental Microbiology* 18, 4: 1110-1121.

Buss, H. L., Bruns, M. A., Schultz, M. J., Moore, J., Mathur, C. F., & Brantley, S. L. (2005). The coupling of biological iron cycling and mineral weathering during saprolite formation, Luquillo Mountains, Puerto Rico. *Geobiology*, *3*(4), 247-260.

Buss, H. L., Lüttge, A., & Brantley, S. L. (2007). Etch pit formation on iron silicate surfaces during siderophore-promoted dissolution. *Chemical Geology*, *240*(3), 326-342.

Caiazza, N. C., Shanks, R. M., & O'Toole, G. A. (2005). Rhamnolipids modulate swarming motility patterns of *Pseudomonas aeruginosa*. *Journal of Bacteriology*, *187*(21), 7351-7361.

Calvert, S. E., & Pedersen, T. F. (1996). Sedimentary geochemistry of manganese; implications for the environment of formation of manganiferous black shales. *Economic Geology*, *91*(1), 36-47.

Carmichael, M. J., Carmichael, S. K., Santelli, C. M., Strom, A., & Bräuer, S. L. (2013). Mn (II)-oxidizing bacteria are abundant and environmentally relevant members of ferromanganese deposits in caves of the upper Tennessee River Basin. *Geomicrobiology Journal*, *30*(9), 779-800.

Carpenter, R. H., & Hayes, W. B. (1980). Annual accretion of Fe− Mn-oxides and certain associated metals in a stream environment. *Chemical Geology*, *29*(1-4), 249-259.

Castle, D. M., Montgomery, M. T., & Kirchman, D. L. (2006). Effects of naphthalene on microbial community composition in the Delaware estuary. *FEMS Microbiology Ecology*, *56*(1), 55-63.

Cerrato, J. M., Falkinham, J. O., Dietrich, A. M., Knocke, W. R., McKinney, C. W., & Pruden, A. (2010). Manganese-oxidizing and-reducing microorganisms isolated from biofilms in chlorinated drinking water systems. *Water Research*, 44(13), 3935-3945.

Chan, C. S., Fakra, S. C., Edwards, D. C., Emerson, D., & Banfield, J. F. (2009). Iron oxyhydroxide mineralization on microbial extracellular polysaccharides. *Geochimica et Cosmochimica Acta*, 73(13), 3807-3818

Chapelle, F. H., & Lovley, D. R. (1990). Rates of microbial metabolism in deep coastal plain aquifers. *Applied and Environmental Microbiology*, *56*(6), 1865-1874.

Chigira, M., & Oyama, T. (2000). Mechanism and effect of chemical weathering of sedimentary rocks. *Engineering Geology*, *55*(1), 3-14.

Cockell, C. S., & Herrera, A. (2008). Why are some microorganisms boring? *Trends in Microbiology*, *16*(3), 101-106.

Cockell, C. S., Kelly, L. C., & Marteinsson, V. (2013). *Actinobacteria*—an ancient phylum active in volcanic rock weathering. *Geomicrobiology Journal*, *30*(8), 706-720.

Cockell, C. S., Olsson, K., Knowles, F., Kelly, L., Herrera, A., Thorsteinsson, T., & Marteinsson, V. (2009). Bacteria in weathered basaltic glass, Iceland. *Geomicrobiology Journal*, 26(7), 491-507.

Cockell, C. S., Pybus, D., Olsson-Francis, K., Kelly, L., Petley, D., Rosser, N., Howard, K., & Mosselmans, F. (2011). Molecular characterization and geological microenvironment of a microbial community inhabiting weathered receding shale cliffs. *Microbial Ecology*, 61(1), 166-181.

Cold Spring Harbour Laboratory Protocols (2006), Recipe for phosphate-buffered saline, Cold Spring Harbour Laboratory Press, doi:10.1101/pdb.rec8247

Collignon, C., Uroz, S., Turpault, M. P., & Frey-Klett, P. (2011). Seasons differently impact the structure of mineral weathering bacterial communities in beech and spruce stands. *Soil Biology and Biochemistry*, *43*(10), 2012-2022.

Colosimo, F., Thomas, R., Lloyd, J.R., Taylor, K.G., Boothman, C., Smith, A.D., Lord, R. and Kalin, R.M. (2016) Biogenic methane in shale gas and coal bed methane: a review of current knowledge and gaps. *International Journal of Coal Geology*, *165*, pp.106-120.

Cook, R. B. (1993). Connoisseur's Choice Pyrite: Park City District, Utah. *Rocks & Minerals*, *68*(6), 394-396.

Coombes, M. A. (2016). Biogeomorphology: diverse, integrative and useful. *Earth Surface Processes and Landforms*, *41*(15), 2296-2300.

Coveney, R. M., Leventhal, J. S., Glascock, M. D., & Hatch, J. R. (1987). Origins of metals and organic matter in the Mecca Quarry Shale Member and stratigraphically equivalent beds across the Midwest. *Economic Geology*, *82*(4), 915-933.

Cowan, D. A., Russell, N. J., Mamais, A., & Sheppard, D. M. (2002). Antarctic Dry Valley mineral soils contain unexpectedly high levels of microbial biomass. *Extremophiles*, *6*(5), 431-436.

Crabb, E., & Moore, E. A. (2010). *Metals and life*, Royal Society of Chemistry Publishing, London

Cserháti, T., Forgács, E., & Oros, G. (2002). Biological activity and environmental impact of anionic surfactants. *Environment International*, *28*(5), 337-348.

Cvetkovic, O., Curiale, J. A., Dragutinovic, V., Jarvie, D. A. N. I. E. L., Vrvic, M. M., & Vitorovic, D. (2001). Evidence of stability of sedimentary organic matter during bacterial desilicification of an oil shale. *Journal-Serbian Chemical Society*, *66*(2), 95-100.

Daniels, R., Reynaert, S., Hoekstra, H., Verreth, C., Janssens, J., Braeken, K., Fauvart, M., Beullens, S., Heusdens, C., Lambrichts, I., De Vos, D., Vanderleyden, J., Vermant, J. & Michiels J. (2006). Quorum signal molecules as biosurfactants affecting swarming in *Rhizobium etli*. *Proceedings of the National Academy of Sciences*, *103*(40), 14965-14970.

Das, S., & Hendry, M. J. (2011). Application of Raman spectroscopy to identify iron minerals commonly found in mine wastes. *Chemical Geology*, *290*(3), 101-108.

Davey, M. E., & O'toole, G. A. (2000). Microbial biofilms: from ecology to molecular genetics. *Microbiology and Molecular Biology Reviews*, *64*(4), 847-867.

Davis, D. H., Doudoroff, M., Stanier, R. Y., & Mandel, M. (1969). Proposal to reject the genus *Hydrogenomonas*: taxonomic implications. *International Journal of Systematic and Evolutionary Microbiology*, *19*(4), 375-390.

Deacon, J. W. (2006). *Fungal biology*. Malden, MA: Blackwell Pub.

Douglas, S., & Beveridge, T. J. (1998). Mineral formation by bacteria in natural microbial communities. *FEMS Microbiology Ecology*, *26*(2), 79-88.

Dragutinović, V., Vrvić, M. M., Swiecicka, I., Cvetković, O., Berić, T., & Stanković, S. (2012). Characterisation of new *Bacillus circulans* strain isolated from oil shale. *Food Technology and Biotechnology*, *50*(1), 123-127.

Drever, J. I., & Stillings, L. L. (1997). The role of organic acids in mineral weathering. *Colloids and Surfaces A:Physicochemical and Engineering aspects*, *120*(1-3), 167-181.

Drozdova, O. Y., Pokrovsky, O. S., Lapitskiy, S. A., Shirokova, L. S., González, A. G., & Demin, V. V. (2014). Decrease in zinc adsorption onto soil in the presence of EPS-rich and EPS-poor *Pseudomonas aureofaciens*. *Journal of Colloid and Interface Science*, 435, 59-66.

Dziewit, L., Pyzik, A., Szuplewska, M., Matlakowska, R., Mielnicki, S., Wibberg, D., Schlüter, A., Pühler, A. and Bartosik, D. (2015). Diversity and role of plasmids in adaptation of bacteria inhabiting the Lubin copper mine in Poland, an environment rich in heavy metals. *Frontiers in Microbiology*, 6, 152.

Edwards, K. J., Goebel, B. M., Rodgers, T. M., Schrenk, M. O., Gihring, T. M., Cardona, M. M., McGuire, M. M., Hamers, R. J., Pace, N. R. & Banfield, J. F. (1999). Geomicrobiology of pyrite (FeS2) dissolution: case study at Iron Mountain, California. *Geomicrobiology Journal*, *16*(2), 155-179.

Edwards, K. J., Hu, B., Hamers, R. J., & Banfield, J. F. (2001). A new look at microbial leaching patterns on sulfide minerals. *FEMS Microbiology Ecology*, *34*(3), 197-206.

Edwards, K. J., Schrenk, M. O., Hamers, R., & Banfield, J. F. (1998). Microbial oxidation of pyrite: experiments using microorganisms from an extreme acidic environment. *American Mineralogist*, *83*(11), 1444-1453.

Ehrlich, H. L. (1998). Geomicrobiology: its significance for geology. *Earth-Science Reviews*, *45*(1), 45-60.

Ehrlich, H. L., Newman, D. K., & Kappler, A. (Eds.). (2015). Ehrlich's Geomicrobiology. CRC press.

Emerson, D., Fleming, E. J., & McBeth, J. M. (2010). Iron-oxidizing bacteria: an environmental and genomic perspective. *Annual Review of Microbiology*, *64*, 561-583.

Espana, J. S., Pamo, E. L., Santofimia, E., Aduvire, O., Reyes, J., & Barettino, D. (2005). Acid mine drainage in the Iberian Pyrite Belt (Odiel river watershed, Huelva, SW Spain): geochemistry, mineralogy and environmental implications. *Applied Geochemistry*, *20*(7), 1320-1356.

Fakoussa, R. M., & Hofrichter, M. (1999). Biotechnology and microbiology of coal degradation. *Applied Microbiology and Biotechnology*, *52*(1), 25-40.

Falkowski, P. G., Fenchel, T., & Delong, E. F. (2008). The microbial engines that drive Earth's biogeochemical cycles. *Science*, *320*(5879), 1034-1039.

Farbiszewska, T., Farbiszewska-Kiczma, J., & Bąk, M. (2003). Biological extraction of metals from a Polish black shale. *Physicochemical Problems of Mineral Processing*, *37*, 51-56.

Farbiszewska, T., Farbiszewska-Kiczma, J., Jażdżyk, E., Sadowski, Z., & Szubert, A. (2006). Kinetic study of biodegradation of organic matter extracted from black shale ore. *Physicochemical Problems of Mineral Processing*, *40*, 317-325.

Farbiszewska-Kiczma, J., & Farbiszewska, T. (2005). Isolation of bacteria that degrade organometallic compounds from metallic wastes. *Physicochemical Problems of Mineral Processing*, *39*, 263-267.

Farbiszewska-Kiczma, J., Farbiszewska, T., & Bąk, M. (2004). Bioleaching of metals from polish black shale in neutral medium. *Physicochemical Problems of Mineral Processing*, *38*, 273-280.

Ferris, F. G., Schultze, S., Witten, T. C., Fyfe, W. S., & Beveridge, T. J. (1989). Metal interactions with microbial biofilms in acidic and neutral pH environments. *Applied and Environmental Microbiology*, *55*(5), 1249-1257.

Findley, J., Appleman, M. D., & Yen, T. F. (1974). Degradation of oil shale by sulfur-oxidizing bacteria. *Applied Microbiology*, *28*(3), 460-464.

Fischer, C., & Gaupp, R. (2005). Change of black shale organic material surface area during oxidative weathering: Implications for rock-water surface evolution. *Geochimica et Cosmochimica Acta*, *69*(5), 1213-1224.

Fletcher, M., & Loeb, G. I. (1979). Influence of substratum characteristics on the attachment of a marine *pseudomonad* to solid surfaces. *Applied and Environmental Microbiology*, *37*(1), 67-72.

Fox-Strangways, C., Barrow, G., & Buckman, S. S. (1915). *The geology of the country between Whitby and Scarborough* (Vol. 35). HM Stationery Office.

Francis, A. J., Dodge, C. J., Rose, A. W., & Ramirez, A. J. (1989). Aerobic and anaerobic microbial dissolution of toxic metals from coal wastes: mechanism of action. *Environmental Science & Technology*, *23*(4), 435-441.

Francis, C. A., Casciotti, K. L., & Tebo, B. M. (2002). Localization of Mn (II)-oxidizing activity and the putative multicopper oxidase, MnxG, to the exosporium of the marine *Bacillus* sp. strain SG-1. *Archives of Microbiology*, *178*(6), 450-456.

François, F., Lombard, C., Guigner, J. M., Soreau, P., Brian-Jaisson, F., Martino, G., Vandervennet, M., Garcia, D., Molinier, A., Pignol, D., Peduzzi, J., Zirah, S. & Rebuffat S. (2012). Isolation and characterization of environmental bacteria capable of extracellular biosorption of mercury. *Applied and Environmental Microbiology*, *78*(4), 1097-1106.

Franzetti, A., Gandolfi, I., Raimondi, C., Bestetti, G., Banat, I. M., Smyth, T. J., Papacchini, M., Cavallo, M., & Fracchia, L. (2012). Environmental fate, toxicity,

characteristics and potential applications of novel bioemulsifiers produced by *Variovorax paradoxus* 7bCT5. *Bioresource Technology*, *108*, 245-251.

Frazier, W. C., & Rupp, P. (1928). Studies on the proteolytic bacteria of milk I. A medium for the direct isolation of caseolytic milk bacteria. *Journal of Bacteriology*, 16(1), 57.

Frey, B., Rieder, S. R., Brunner, I., Plötze, M., Koetzsch, S., Lapanje, A., Brandl, H. & Furrer, G. (2010). Weathering-associated bacteria from the Damma glacier forefield: physiological capabilities and impact on granite dissolution. *Applied and Environmental Microbiology*, 76(14), 4788-4796.

Friedman, I., & Murata, K. J. (1979). Origin of dolomite in Miocene Monterey Shale and related formations in the Temblor Range, California. *Geochimica et Cosmochimica Acta*, *43*(8), 1357-1365.

Fru, E.C., Rodríguez, N.P., Partin, C.A., Lalonde, S.V., Andersson, P., Weiss, D.J., El Albani, A., Rodushkin, I. and Konhauser, K.O., (2016) Cu isotopes in marine black shales record the Great Oxidation Event. *Proceedings of the National Academy of Sciences*, *113*(18), 4941-4946.

Gad, M. A., Catt, J. A., & Le Riche, H. H. (1968). Geochemistry of the Whitbian (Upper Lias) sediments of the Yorkshire coast. In *Proceedings of the Yorkshire Geological and Polytechnic Society* (Vol. 37, No. 1, pp. 105-140). Geological Society of London.

Gadd, G. M. (2004). Microbial influence on metal mobility and application for bioremediation. *Geoderma*, *122*(2), 109-119.

Gadd, G. M. (2007). Geomycology: biogeochemical transformations of rocks, minerals, metals and radionuclides by fungi, bioweathering and bioremediation. *Mycological Research*, *111*(1), 3-49.

Gadd, G. M. (2010). Metals, minerals and microbes: geomicrobiology and bioremediation. *Microbiology*, *156*(3), 609-643.

Gadd, G. M. (2017). Fungi, Rocks, and Minerals. *Elements*, *13*(3), 171-176.

Geszvain, K., Butterfield, C., Davis, R. E., Madison, A. S., Lee, S. W., Parker, D. L., Soldatova, A., Spiro, T.G., Luther, G.W. & Tebo, B. M. (2012). The molecular biogeochemistry of manganese (II) oxidation. *Biochemical Society Transactions*, 40(6)

Ghiorse, W. C. (1984). Biology of iron-and manganese-depositing bacteria. *Annual Reviews in Microbiology*, 38(1), 515-550.

Gorbushina, A. A., Krumbein, W. E., & Volkmann, M. (2002). Rock surfaces as life indicators: new ways to demonstrate life and traces of former life. *Astrobiology*, *2*(2), 203-213.

Gorbushina, A. A. (2007). Life on the rocks. *Environmental Microbiology*, *9*(7), 1613-1631.

Gordillo, F., Chávez, F. P., & Jerez, C. A. (2007). Motility and chemotaxis of *Pseudomonas* sp. B4 towards polychlorobiphenyls and chlorobenzoates. *FEMS Microbiology Ecology*, *60*(2), 322-328.

Grattan-Bellew, P. E., & Eden, W. J. (1975). Concrete deterioration and floor heave due to biogeochemical weathering of underlying shale. *Canadian Geotechnical Journal*, *12*(3), 372-378.

Grimm, A. C., & Harwood, C. S. (1997). Chemotaxis of *Pseudomonas* spp. to the polyaromatic hydrocarbon naphthalene. *Applied and Environmental Microbiology*, *63*(10), 4111-4115.

Grobelski, T., Farbiszewska-Kiczma, J., & Farbiszewska, T. (2007). Bioleaching of Polish black shale. *Physicochemical Problems of Mineral Processing*, *41*, 259-264.

Grote, G., & Krumbein, W. E. (1992). Microbial precipitation of manganese by bacteria and fungi from desert rock and rock varnish. *Geomicrobiology Journal*, 10(1), 49-57.

Groudev, S. (1979). Mechanism of bacterial oxidation of pyrite. *Microbiology*, *16*, 75-87.

Grube, M., Cardinale, M., de Castro, J. V., Müller, H., & Berg, G. (2009). Species-specific structural and functional diversity of bacterial communities in lichen symbioses. *The ISME Journal*, 3(9), 1105-1115.

Guibaud, G., Tixier, N., Bouju, A., & Baudu, M. (2004). Use of a polarographic method to determine copper, nickel and zinc constants of complexation by extracellular polymers extracted from activated sludge. *Process Biochemistry*, 39(7), 833-839.

Haddadin, M. S., Arqoub, A. A. A., Reesh, I. A., & Haddadin, J. (2009). Kinetics of hydrocarbon extraction from oil shale using biosurfactant producing bacteria. *Energy Conversion and Management*, *50*(4), 983-990.

Hallam, A. (1997). Estimates of the amount and rate of sea-level change across the Rhaetian—Hettangian and Pliensbachian—Toarcian boundaries (latest Triassic to early Jurassic). *Journal of the Geological Society*, *154*(5), 773-779.

Hallberg, K. B., Hedrich, S., & Johnson, D. B. (2011). *Acidiferrobacter thiooxydans*, gen. nov. sp. nov.; an acidophilic, thermo-tolerant, facultatively anaerobic iron-and sulfur-oxidiser of the family *Ectothiorhodospiraceae*. *Extremophiles*, *15*(2), 271-279.

Hall-Stoodley, L., Costerton, J. W., & Stoodley, P. (2004). Bacterial biofilms: from the natural environment to infectious diseases. *Nature Reviews. Microbiology*, *2*(2), 95.

Hamdali, H., Bouizgarne, B., Hafidi, M., Lebrihi, A., Virolle, M. J., & Ouhdouch, Y. (2008). Screening for rock phosphate solubilizing *Actinomycetes* from Moroccan phosphate mines. *Applied Soil Ecology*, *38*(1), 12-19.

Hameeda, B., Reddy, Y. H. K., Rupela, O. P., Kumar, G. N., & Reddy, G. (2006). Effect of carbon substrates on rock phosphate solubilization by bacteria from composts and macrofauna. *Current Microbiology*, 53(4), 298-302.

Han, J. I., Choi, H. K., Lee, S. W., Orwin, P. M., Kim, J., LaRoe, S. L., Kim, T.G., O'Neil, J., Leadbetter, J.R., Lee, S.Y.& Hur, C. G. (2011). Complete genome sequence of the metabolically versatile plant growth-promoting endophyte *Variovorax paradoxus* S110. *Journal of Bacteriology*, *193*(5), 1183-1190.

Han, J. I., Spain, J. C., Leadbetter, J. R., Ovchinnikova, G., Goodwin, L. A., Han, C. S., Woyke, T., Davenport, K., & Orwin, P. M. (2013). Genome of the root-associated plant growth-promoting bacterium *Variovorax paradoxus* strain EPS. *Genome announcements*, *1*(5), e00843-13.

Hand, V. L., Lloyd, J. R., Vaughan, D. J., Wilkins, M. J., & Boult, S. (2008). Experimental studies of the influence of grain size, oxygen availability and organic carbon availability on bioclogging in porous media. *Environmental Science & Technology*, 42(5), 1485-1491.

Harshey, R. M., & Matsuyama, T. (1994). Dimorphic transition in *Escherichia coli* and *Salmonella typhimurium*: surface-induced differentiation into hyperflagellate swarmer cells. *Proceedings of the National Academy of Sciences*, *91*(18), 8631-8635.

Havig, J. R., Grettenberger, C., & Hamilton, T. L. (2017). Geochemistry and microbial community composition across a range of acid mine drainage impact and implications for the Neoarchean- Paleoproterozoic transition. *Journal of Geophysical Research: Biogeosciences*, doi: 10.1002/2016JG003594

Hawkins, A. B. (2014). Engineering implications of the oxidation of pyrite: An overview, with particular reference to Ireland. In *Implications of pyrite oxidation for engineering works* (pp. 1-98). Springer International Publishing.

Hayes, P. R. (1963). Studies on marine flavobacteria. *Microbiology*, *30*(1), 1-19.

Hedges, J. I., & Oades, J. M. (1997). Comparative organic geochemistries of soils and marine sediments. *Organic Geochemistry*, *27*(7), 319-361.

Hedrich, S., Schlömann, M., & Johnson, D. B. (2011). The iron-oxidizing *proteobacteria*. *Microbiology*, *157*(6), 1551-1564.

Hemingway, J. E., Wilson, V., & Wright, C. W. (1968). *Geology of the Yorkshire coast*. Benham.

Herrera, L. K., Arroyave, C., Guiamet, P., de Saravia, S. G., & Videla, H. (2004). Biodeterioration of peridotite and other constructional materials in a building of the Colombian cultural heritage. *International Biodeterioration & Biodegradation*, *54*(2), 135-141.

Hider, R. C., & Kong, X. (2010). Chemistry and biology of siderophores. *Natural Product Reports*, *27*(5), 637-657.

Hiebert, F. K., & Bennett, P. C. (1992). Microbial control of silicate weathering in organic-rich ground water. *Science, 258*(5080), 278.

Hirsch, P., Eckhardt, F. E. W., & Palmer, R. J. (1995). Methods for the study of rock-inhabiting microorganisms—a mini review. *Journal of Microbiological Methods*, 23(2), 143-167.

Hirst, I. D., Hastings, T. S., & Ellis, A. E. (1991). Siderophore production by *Aeromonas salmonicida*. *Microbiology*, *137*(5), 1185-1192.

Hobbs, P.R.N., Entwisle, D.C., Northmore, K.J., Sumbler, M.G., Jones, L.D., Kemp, S., Self, S., Barron, M. and Meakin, J.L. (2012). Engineering geology of British rocks and soils: Lias Group.

Hong, Z., Rong, X., Cai, P., Dai, K., Liang, W., Chen, W., & Huang, Q. (2012). Initial adhesion of *Bacillus subtilis* on soil minerals as related to their surface properties. *European Journal of Soil Science*, *63*(4), 457-466.

Hoover, S. E., & Lehmann, D. (2009). The expansive effects of concentrated pyritic zones within the Devonian Marcellus Shale Formation of North America. *Quarterly Journal of Engineering Geology and Hydrogeology*, *42*(2), 157-164.

Hori, K., & Matsumoto, S. (2010). Bacterial adhesion: from mechanism to control. *Biochemical Engineering Journal*, *48*(3), 424-434.

Hou, X., Amais, R. S., Jones, B. T., & Donati, G. L. (2000). Inductively coupled plasma optical emission spectrometry. *Encyclopedia of Analytical Chemistry*.

Howarth, M. K. (1962). The jet rock series and the alum shale series of the Yorkshire coast. In *Proceedings of the Yorkshire Geological and Polytechnic Society* (Vol. 33, No. 4, pp. 381-422). Geological Society of London.

Huang, S. L., Speck, R. C., & Wang, Z. (1995, April). The temperature effect on swelling of shales under cyclic wetting and drying. In *International Journal of Rock Mechanics and Mining Sciences & Geomechanics Abstracts* (Vol. 32, No. 3, pp. 227-236). Pergamon.

Huckriede, H., & Meischner, D. (1996). Origin and environment of manganese-rich sediments within black-shale basins. *Geochimica et Cosmochimica Acta*, *60*(8), 1399-1413.

Hungate, R. E. (1946). Studies on Cellulose Fermentation: II. An Anaerobic Cellulose-decomposing Actinomycete, Micromonospora propionici, N. Sp. *Journal of Bacteriology*, *51*(1), 51.

Hutchens (2009) Microbial selectivity on mineral surfaces: possible implications for weathering processes. *Fungal Biology Reviews*, 23(4), 115-121.

Ilgen, A.G., Heath, J.E., Akkutlu, I.Y., Bryndzia, L.T., Cole, D.R., Kharaka, Y.K., Kneafsey, T.J., Milliken, K.L., Pyrak-Nolte, L.J. and Suarez-Rivera, R. (2017). Shales at all scales: Exploring coupled processes in mudrocks. *Earth-Science Reviews.* 166: 132-152

Islam, M. A., & Skalle, P. (2013). An experimental investigation of shale mechanical properties through drained and undrained test mechanisms. *Rock Mechanics and Rock Engineering*, *46*(6), 1391-1413.

Ivshina, I. B., Kuyukina, M. S., Philp, J. C., & Christofi, N. (1998). Oil desorption from mineral and organic materials using biosurfactant complexes produced by *Rhodococcus* species. *World Journal of Microbiology and Biotechnology*, *14*(5), 711-717.

Jacobs, J. A., Testa, S. M., Alpers, C. N., & Nordstrom, D. K. An Overview of Environmental Impacts and Mine Reclamation Efforts at Iron Mountain, Shasta County, California.

Jamieson, W. D., Pehl, M. J., Gregory, G. A., & Orwin, P. M. (2009). Coordinated surface activities in *Variovorax paradoxus* EPS. *BMC Microbiology*, *9*(1), 124.

Jecock, M. (2009). A fading memory: the North Yorkshire coastal alum industry in the light of recent analytical field survey by English Heritage. *Industrial Archaeology Review*, *31*(1), 54-73.

Jendrossek, D., Selchow, O., & Hoppert, M. (2007). Poly (3-hydroxybutyrate) granules at the early stages of formation are localised close to the cytoplasmic membrane in *Caryophanon latum*. *Applied and Environmental Microbiology*, *73*(2), 586-593.

Jiang, S., Wang, W., Xue, X., Cao, C., & Zhang, Y. (2016). Fungal diversity in major oil-shale mines in China. *Journal of Environmental Sciences*, *41*, 81-89.

Jiang, S., Wang, W., Xue, X., Cao, C., Zhang, Y., & Hou, X. (2015). Bacterial Diversity in Major Oil Shale Mines in China. *Fresenius Environmental Bulletin*, *24*(10), 3176-3188.

Jin, L., Mathur, R., Rother, G., Cole, D., Bazilevskaya, E., Williams, J., Carone, A., & Brantley, S. (2013). Evolution of porosity and geochemistry in Marcellus Formation black shale during weathering. *Chemical Geology*, *356*, 50-63.

Jin, L., Ogrinc, N., Yesavage, T., Hasenmueller, E.A., Ma, L., Sullivan, P.L., Kaye, J., Duffy, C. and Brantley, S.L., (2014) The CO_2 consumption potential during gray

shale weathering: insights from the evolution of carbon isotopes in the Susquehanna Shale Hills critical zone observatory. *Geochimica et Cosmochimica Acta*, *142*: 260-280.

Jin, L., Ravella, R., Ketchum, B., Bierman, P. R., Heaney, P., White, T., & Brantley, S. L. (2010). Mineral weathering and elemental transport during hillslope evolution at the Susquehanna/Shale Hills Critical Zone Observatory. *Geochimica et Cosmochimica Acta*, *74*(13), 3669-3691.

Joe, S. J., Suto, K., Inoie, C., & Chida, T. (2007). Isolation and characterization of acidophilic heterotrophic iron-oxidizing bacterium from enrichment culture obtained from acid mine drainage treatment plant. *Journal of Bioscience and Bioengineering*, 104(2), 117-123.

Joeckel, R. M., Clement, B. A., & Bates, L. V. (2005). Sulfate-mineral crusts from pyrite weathering and acid rock drainage in the Dakota Formation and Graneros Shale, Jefferson County, Nebraska. *Chemical Geology*, *215*(1), 433-452.

Johnson, D. B. (1995). Selective solid media for isolating and enumerating acidophilic bacteria. *Journal of Microbiological Methods*, 23(2), 205-218.

Johnson, D. B., & Hallberg, K. B. (2005). Acid mine drainage remediation options: a review. *Science of the Total Environment*, *338*(1), 3-14.

Johnson, D. B., Ghauri, M. A., & Said, M. F. (1992). Isolation and characterization of an acidophilic, heterotrophic bacterium capable of oxidizing ferrous iron. *Applied and Environmental Microbiology*, 58(5), 1423-1428.

Johnson, K. W., Carmichael, M. J., McDonald, W., Rose, N., Pitchford, J., Windelspecht, M., Karatan, E., & Bräuer, S. L. (2012). Increased abundance of *Gallionella* spp., *Leptothrix* spp. and total bacteria in response to enhanced Mn and Fe concentrations in a disturbed southern Appalachian high elevation wetland. *Geomicrobiology Journal*, *29*(2), 124-138.

Johnston, D., & Rolley, S. (2008). Abandoned mines and the water framework directive in the United Kingdom. *Proc. mine water and the environment. VSB–Technical University of Ostrava, Czech Republic*, 529-532.

Jones, E. V., Rosser, N. J., Brain, M. J., & Petley, D. N. (2015). Quantifying the environmental controls on erosion of a hard rock cliff. *Marine Geology*, *363*, 230-242.

Kable (2017) KGHM Copper, Poland, accessed at (29/08/2017): http://www.mining-technology.com/projects/kghm/

Kalinowski, B. E., Liermann, L. J., Brantley, S. L., Barnes, A., & Pantano, C. G. (2000). X-ray photoelectron evidence for bacteria-enhanced dissolution of hornblende. *Geochimica et Cosmochimica Acta*, *64*(8), 1331-1343.

Kalinowski, B. E., Johnsson, A., Arlinger, J., Pedersen, K., Ödegaard-Jensen, A., & Edberg, F. (2006). Microbial mobilization of uranium from shale mine waste. *Geomicrobiology Journal*, *23*(3-4), 157-164.

Kanehisa, M., & Goto, S. (2000). KEGG: Kyoto encyclopedia of genes and genomes. *Nucleic Acids Research*, *28*(1), 27-30.

Kanehisa, M., Sato, Y., Kawashima, M., Furumichi, M., & Tanabe, M. (2015). KEGG as a reference resource for gene and protein annotation. *Nucleic Acids Research*, gkv1070.

Karavaiko, G.I., Tat'yana, P.T., Kondrat'eva, T.F., Lysenko, A.M., Tat'yana, V.K., Ageeva, S.N., Muntyan, L.N. and Tat'yana, A.P., 2003. Phylogenetic heterogeneity of the species *Acidithiobacillus ferrooxidans*. *International Journal of Systematic and Evolutionary Microbiology*, *53*(1), pp.113-119.

Karpiński, B., & Szkodo, M. (2015). Clay Minerals–Mineralogy and Phenomenon of Clay Swelling in Oil & Gas Industry. *Advances in Materials Science*, *15*(1), 37-55.

Kearns, D. B. (2010). A field guide to bacterial swarming motility. *Nature Reviews Microbiology*, *8*(9), 634-644.

Kelly, D. P., & Wood, A. P. (2000). Reclassification of some species of *Thiobacillus* to the newly designated genera *Acidithiobacillus* gen. nov., *Halothiobacillus* gen. nov. and *Thermithiobacillus* gen. nov. *International Journal of Systematic and Evolutionary Microbiology*, *50*(2), 511-516.

Kinzler, K., Gehrke, T., Telegdi, J., & Sand, W. (2003). Bioleaching—a result of interfacial processes caused by extracellular polymeric substances (EPS). *Hydrometallurgy*, *71*(1), 83-88.

Klein, C., & Philpotts, A. R. (2012). Earth materials: introduction to mineralogy and petrology. *Cambridge University Press*.

Köhler, T., Curty, L. K., Barja, F., Van Delden, C., & PecheRe, J. C. (2000). Swarming of *Pseudomonas aeruginosa* is dependent on cell-to-cell signaling and requires flagella and pili. *Journal of Bacteriology*, *182*(21), 5990-5996.

Kolowith, L. C., & Berner, R. A. (2002). Weathering of phosphorus in black shales. *Global Biogeochemical Cycles*, 16(4), doi:10.1029/2001GB001887

Koncagül, E. C. (1998). Comparison of uniaxial compressive strength test and slake durability index values of shale samples from the Breathitt Formation, Kentucky.

Koncagül, E. C., & Santi, P. M. (1999). Predicting the unconfined compressive strength of the Breathitt shale using slake durability, Shore hardness and rock structural properties. *International Journal of Rock Mechanics and Mining Sciences*, *36*(2), 139-153.

Konhauser, K. O. (1998). Diversity of bacterial iron mineralization. *Earth-Science Reviews*, *43*(3), 91-121.

Konhauser, K. O. (2006). Introduction to geomicrobiology. *John Wiley & Sons*.

Konhauser, K. O., Lalonde, S. V., Planavsky, N. J., Pecoits, E., Lyons, T. W., Mojzsis, S. J., Rouxel, O.J., Barley, M.E., Rosìere, C., Fralick, P.W. & Kump, L. R. (2011). Aerobic bacterial pyrite oxidation and acid rock drainage during the Great Oxidation Event. *Nature*, *478*(7369), 369.

Kostudis, S., Bachmann, K., Kutschke, S., Pollmann, K., & Gutzmer, J. (2015). Leaching of copper from Kupferschiefer by glutamic acid and heterotrophic bacteria. *Minerals Engineering*, *75*, 38-44.

Kozubal, M. A., Macur, R. E., Jay, Z. J., Beam, J. P., Malfatti, S. A., Tringe, S. G., Kocar. B. D., Borch. T. & Inskeep, W. P. (2012). Microbial iron cycling in acidic geothermal springs of Yellowstone National Park: integrating molecular surveys, geochemical processes, and isolation of novel Fe-active microorganisms, *Frontiers in Microbiology,* 109(3), 1-16.

Kristiansen, R., Nguyen, H.T.T., Saunders, A.M., Nielsen, J.L., Wimmer, R., Le, V.Q., McIlroy, S.J., Petrovski, S., Seviour, R.J., Calteau, A. and Nielsen, K.L. (2013). A metabolic model for members of the genus *Tetrasphaera* involved in enhanced biological phosphorus removal. *The ISME Journal*, *7*(3), p.543.

Krumbein, W. E., & Altmann, H. J. (1973). A new method for the detection and enumeration of manganese oxidizing and reducing microorganisms. *Helgoländer wissenschaftliche Meeresuntersuchungen*, *25*(2-3), 347-356.

Krumholz, L. R., Harris, S. H., & Suflita, J. M. (2002). Anaerobic microbial growth from components of Cretaceous shales. *Geomicrobiology Journal*, *19*(6), 593-602.

Krumholz, L. R., McKinley, J. P., Ulrich, G. A., & Suflita, J. M. (1997). Confined subsurface microbial communities in Cretaceous rock. *Nature*, *386*(6620), 64.

Kuhlman, K. R., Fusco, W. G., La Duc, M. T., Allenbach, L. B., Ball, C. L., Kuhlman, G. M., & Strap, J. L. (2006). Diversity of microorganisms within rock varnish in the Whipple Mountains, California. *Applied and Environmental Microbiology*, *72*(2), 1708-1715

Kutschke, S., Guezennec, A.G., Hedrich, S., Schippers, A., Borg, G., Kamradt, A., Gouin, J., Giebner, F., Schopf, S., Schlömann, M. and Rahfeld, A. (2015) Bioleaching of Kupferschiefer black shale–A review including perspectives of the Ecometals project. *Minerals Engineering*, *75*, pp.116-125.

Kwong, Y. J., Whitley, G., & Roach, P. (2009). Natural acid rock drainage associated with black shale in the Yukon Territory, Canada. *Applied Geochemistry*, *24*(2), 221-231.

Lacey, D. T., & Lawson, F. (1970). Kinetics of the liquid- phase oxidation of acid ferrous sulfate by the bacterium *Thiobacillus ferrooxidens*. *Biotechnology and Bioengineering*, *12*(1), 29-50.

Langan, S. J., Reynolds, B., & Bain, D. C. (1996). The calculation of base cation release from mineral weathering in soils derived from Palaeozoic greywackes and shales in upland UK. *Geoderma*, *69*(3-4), 275-285.

Larkin, M. J., Kulakov, L. A., & Allen, C. C. (2005). Biodegradation and *Rhodococcus*–masters of catabolic versatility. *Current opinion in Biotechnology*, *16*(3), 282-290.

Larsson, L., Olsson, G., Holst, O., & Karlsson, H. T. (1990). Pyrite oxidation by thermophilic archaebacteria. *Applied and Environmental Microbiology*, *56*(3), 697-701.

Lash, G. G., & Blood, D. R. (2004). Origin of shale fabric by mechanical compaction of flocculated clay: evidence from the Upper Devonian Rhinestreet Shale, western New York, USA. *Journal of Sedimentary Research*, *74*(1), 110-116.

Lavina, B., Dera, P. and Downs, R.T. (2014) Modern X-ray diffraction methods in mineralogy and geosciences. *Reviews in Mineralogy and Geochemistry*, *78*(1), 1-31.

Lee, B. B., Ravindra, P., & Chan, E. S. (2008). A critical review: surface and interfacial tension measurement by the drop weight method. *Chemical Engineering Communications*, *195*(8), 889-924.

Lee, J. U., Kim, S. M., Kim, K. W., & Kim, I. S. (2005). Microbial removal of uranium in uranium-bearing black shale. *Chemosphere*, *59*(1), 147-154.

Lee, S. T., Lee, S. B., & Park, Y. H. (1991). Characterization of a pyridine-degrading branched Gram-positive bacterium isolated from the anoxic zone of an oil shale column. *Applied Microbiology and Biotechnology*, *35*(6), 824-829.

Lee, S. L. (1991) Bacterial polyhydroxyalkanoates, *Biotechnology and Bioengineering* 49,1: 1-14.

Leventhal, J. S. (1991). Comparison of organic geochemistry and metal enrichment in two black shales: Cambrian Alum Shale of Sweden and Devonian Chattanooga Shale of United States. *Mineralium Deposita*, *26*(2), 104-112.

Leventhal, J. S., & Hosterman, J. W. (1982). Chemical and mineralogical analysis of Devonian black-shale samples from Martin County, Kentucky; Carroll and Washington counties, Ohio; Wise County, Virginia; and Overton County, Tennessee, USA. *Chemical Geology*, *37*(3-4), 239-264.

Li, J., Sun, W., Wang, S., Sun, Z., Lin, S., & Peng, X. (2014). Bacteria diversity, distribution and insight into their role in S and Fe biogeochemical cycling during black shale weathering. *Environmental Microbiology*, *16*(11), 3533-3547.

Li, Y., & Li, H. (2014). Type IV pili of *Acidithiobacillus ferrooxidans* can transfer electrons from extracellular electron donors. *Journal of Basic Microbiology*, *54*(3), 226-231.

Li, Y., & Strohl, W. R. (1996). Cloning, purification, and properties of a phosphotyrosine protein phosphatase from *Streptomyces coelicolor* A3 (2). *Journal of Bacteriology*, *178*(1), 136-142.

Liermann, L. J., Kalinowski, B. E., Brantley, S. L., & Ferry, J. G. (2000). Role of bacterial siderophores in dissolution of hornblende. *Geochimica et Cosmochimica Acta*, *64*(4), 587-602.

Liermann, L. J., Mathur, R., Wasylenki, L. E., Nuester, J., Anbar, A. D., & Brantley, S. L. (2011). Extent and isotopic composition of Fe and Mo release from two Pennsylvania shales in the presence of organic ligands and bacteria. *Chemical Geology*, *281*(3), 167-180.

Lim, C. H., Ozkanca, R., & Flint, K. P. (1996). The effects of osmotic stress on survival and alkaline phosphatase activity of *Aeromonas hydrophila*. *FEMS Microbiology Letters*, *137*(1), 19-24.

Lim, M., Petley, D. N., Rosser, N. J., Allison, R. J., Long, A. J., & Pybus, D. (2005). Combined digital photogrammetry and time- of- flight laser scanning for monitoring cliff evolution. *The Photogrammetric Record*, *20*(110), 109-129.

Lim, M., Rosser, N. J., Allison, R. J., & Petley, D. N. (2010). Erosional processes in the hard rock coastal cliffs at Staithes, North Yorkshire. *Geomorphology*, *114*(1), 12-21.

Littke, R., Klussmann, U., Krooss, B., & Leythaeuser, D. (1991). Quantification of loss of calcite, pyrite, and organic matter due to weathering of Toarcian black shales and effects on kerogen and bitumen characteristics. *Geochimica et Cosmochimica Acta*, *55*(11), 3369-3378.

London, D. (1992). Phosphorus in S-type magmas: the P_2O_5 content of feldspars from peraluminous granites, pegmatites, and rhyolites. *American Mineralogist*, *77*(1-2), 126-145.

Lopez- Arce, P., Benavente, D., & Garcia- Guinea, J. (2005). Durability improvement of ancient bricks by cementation of porous media. *Journal of the American Ceramic Society*, *88*(9), 2564-2572.

Lors, C., Ryngaert, A., Périé, F., Diels, L., & Damidot, D. (2010). Evolution of bacterial community during bioremediation of PAHs in a coal tar contaminated soil. *Chemosphere*, *81*(10), 1263-1271.

Loucks, R. G., Reed, R. M., Ruppel, S. C., & Jarvie, D. M. (2009). Morphology, genesis, and distribution of nanometer-scale pores in siliceous mudstones of the Mississippian Barnett Shale. *Journal of Sedimentary Research*, *79*(12), 848-861.

Ma, L., Chabaux, F., Pelt, E., Blaes, E., Jin, L., & Brantley, S. (2010). Regolith production rates calculated with uranium-series isotopes at Susquehanna/Shale Hills Critical Zone Observatory. *Earth and Planetary Science Letters*, *297*(1), 211-225.

Macur, R. E., Jackson, C. R., Botero, L. M., Mcdermott, T. R., & Inskeep, W. P. (2004). Bacterial populations associated with the oxidation and reduction of arsenic in an unsaturated soil. *Environmental Science & Technology*, *38*(1), 104-111.

Madigan, M. T., Martinko, J. M., Bender, K. S., Buckley, D. H., & Stahl, D. A. (2015). *Brock biology of microorganisms* (Fourteenth edition.). Boston: Pearson

Majumdar, M. K., & Majumdar, S. K. (1971). Relationship between alkaline phosphatase and neomycin formation in *Streptomyces fradiae*. *Biochemical Journal*, *122*(4), 397-404.

Manceau, A., Lanson, M., & Geoffroy, N. (2007). Natural speciation of Ni, Zn, Ba, and As in ferromanganese coatings on quartz using X-ray fluorescence, absorption, and diffraction. *Geochimica et Cosmochimica Acta*, *71*(1), 95-128.

Marnocha, C. L., & Dixon, J. C. (2013). Bacterial communities in Fe/Mn films, sulphate crusts, and aluminium glazes from Swedish Lapland: implications for astrobiology on Mars. *International Journal of Astrobiology*, *12*(4), 345-356.

Marshall, K. C. (1979). Biogeochemistry of manganese minerals. *Studies in Environmental Science*, *3*, 253-292.

Martini, A. M., Walter, L. M., & McIntosh, J. C. (2008). Identification of microbial and thermogenic gas components from Upper Devonian black shale cores, Illinois and Michigan basins. *Aapg Bulletin*, *92*(3), 327-339.

Marx, R. B., & Aitken, M. D. (2000). Bacterial chemotaxis enhances naphthalene degradation in a heterogeneous aqueous system. *Environmental Science & Technology*, *34*(16), 3379-3383.

Maskow, T., & Babel, W. (2001). A calorimetrically based method to convert toxic compounds into poly-3-hydroxybutyrate and to determine the efficiency and velocity of conversion. *Applied Microbiology and Biotechnology*, *55*(2), 234-238.

Maslova, M. V., Gerasimova, L. G., & Forsling, W. (2004). Surface properties of cleaved mica. *Colloid Journal*, *66*(3), 322-328.

Matlakowska, R., & Sklodowska, A. (2009). The culturable bacteria isolated from organic- rich black shale potentially useful in biometallurgical procedures. *Journal of Applied Microbiology*, *107*(3), 858-866.

Matlakowska, R., & Sklodowska, A. (2010). Uptake and degradation of copper and cobalt porphyrins by indigenous microorganisms of Kupferschiefer (Fore-Sudetic Monocline, Poland). *Hydrometallurgy*, *104*(3), 501-505.

Matlakowska, R., & Sklodowska, A. (2011). Biodegradation of Kupferschiefer black shale organic matter (Fore-Sudetic Monocline, Poland) by indigenous microorganisms. *Chemosphere*, *83*(9), 1255-1261.

Matlakowska, R., Drewniak, L., & Sklodowska, A. (2008). Arsenic-hypertolerant *Pseudomonads* isolated from ancient gold and copper-bearing black shale deposits. *Geomicrobiology Journal*, *25*(7-8), 357-362.

Matlakowska, R., Narkiewicz, W., & Sklodowska, A. (2010). Biotransformation of organic-rich copper-bearing black shale by indigenous microorganisms isolated from lubin copper mine (Poland). *Environmental Science & Technology*, *44*(7), 2433-2440.

Matlakowska, R., Ruszkowski, D., & Sklodowska, A. (2013). Microbial transformations of fossil organic matter of Kupferschiefer black shale–elements mobilization from metalloorganic compounds and metalloporphyrins by a community of indigenous microorganisms. *Physicochemical Problems of Mineral Processing*, *49*(1), 223-231.

Matlakowska, R., Skłodowska, A., & Nejbert, K. (2012). Bioweathering of Kupferschiefer black shale (Fore-Sudetic Monocline, SW Poland) by indigenous bacteria: implication for dissolution and precipitation of minerals in deep underground mine. *FEMS Microbiology Ecology*, *81*(1), 99-110.

Matlakowska, R., Wlodarczyk, A., Slominska, B., & Sklodowska, A. (2014). Extracellular elements-mobilizing compounds produced by consortium of indigenous bacteria isolated from kupferschiefer black shale–implication for metals biorecovery from neutral and alkaline polymetallic ores. *Physicochemical Problems of Mineral Processing*, *50*.

Mautner, M. N., Leonard, R. L., & Deamer, D. W. (1995). Meteorite organics in planetary environments: hydrothermal release, surface activity, and microbial utilization. *Planetary and Space Science*, *43*(1), 139-147.

McGuire, M. M., Edwards, K. J., Banfield, J. F., & Hamers, R. J. (2001). Kinetics, surface chemistry, and structural evolution of microbially mediated sulfide mineral dissolution. *Geochimica et Cosmochimica Acta*, *65*(8), 1243-1258.

McLennan, A., Bates, A., Turner, P., & White, M. (2012). *Bios instant notes in molecular biology*. Taylor & Francis.

Méndez-García, C., Peláez, A. I., Mesa, V., Sánchez, J., Golyshina, O. V., & Ferrer, M. (2015). Microbial diversity and metabolic networks in acid mine drainage habitats. *Frontiers in Microbiology*, *6*

Meslé, M., Dromart, G., & Oger, P. (2013). Microbial methanogenesis in subsurface oil and coal. *Research in Microbiology*, *164*(9), 959-972

Meyer, W. C., & Yen, T. F. (1976). Enhanced dissolution of oil shale by bioleaching with *Thiobacilli*. *Applied and environmental microbiology*, *32*(4), 610-616.

Mielke, R. E., Pace, D. L., Porter, T., & Southam, G. (2003). A critical stage in the formation of acid mine drainage: Colonization of pyrite *by Acidithiobacillus ferrooxidans* under pH- neutral conditions. *Geobiology*, *1*(1), 81-90.

Miller, J. H. (1972). Experiments in molecular genetics. Cold Spring Laboratory Press.

Mills, A. L., Herman, J. S., Hornberger, G. M., & DeJesús, T. H. (1994). Effect of solution ionic strength and iron coatings on mineral grains on the sorption of bacterial cells to quartz sand. *Applied and Environmental Microbiology*, *60*(9), 3300-3306.

Mishra, A. K., Roy, P., Mahapatra, S. S. R., & Chandra, D. (1984). Low grade pyrites and their possible beneficiation by *Thiobacillus ferrooxidans*. *Proceedings of the Indian National Science Academy. Part B: Biological Sciences*.

Money, N. P. (2004). The fungal dining habit: a biomechanical perspective. *Mycologist*, *18*(2), 71-76.

Morris, C H and Whitlock, S (2005) Boulby Alum Works Tunnel Revisited, *Cleveland Industrial Archaeologist, 30*, 29-45

Mozley, P. S., & Wersin, P. (1992). Isotopic composition of siderite as an indicator of depositional environment. *Geology*, *20*(9), 817-820.

Mustin, C., Berthelin, J., Marion, P., & de Donato, P. (1992). Corrosion and electrochemical oxidation of a pyrite by *Thiobacillus ferrooxidans*. *Applied and Environmental Microbiology*, *58*(4), 1175-1182.

Naicker, K., Cukrowska, E., & McCarthy, T. S. (2003). Acid mine drainage arising from gold mining activity in Johannesburg, South Africa and environs. *Environmental Pollution*, *122*(1), 29-40.

Ndlovu, S., & Monhemius, A. J. (2005). The influence of crystal orientation on the bacterial dissolution of pyrite. *Hydrometallurgy*, *78*(3), 187-197.

Nichols, G. (2009). *Sedimentology and stratigraphy*. John Wiley & Sons.

Nogueira, M. A., Nehls, U., Hampp, R., Poralla, K., & Cardoso, E. J. B. N. (2007). Mycorrhiza and soil bacteria influence extractable iron and manganese in soil and uptake by soybean. *Plant and Soil*, *298*(1-2), 273-284.

Nordstrom, D. K., & Southam, G. (1997). Geomicrobiology of sulfide mineral oxidation. *Reviews in Mineralogy*, *35*, 361-390.

Northup, D. E., Barns, S. M., Yu, L. E., Spilde, M. N., Schelble, R. T., Dano, K. E., Crossey, L. J., Connolly, C. A., Boston, P. J., Natvig, D. O., & Dahm, C. N. (2003). Diverse microbial communities inhabiting ferromanganese deposits in Lechuguilla and Spider Caves. *Environmental Microbiology*, *5*(11), 1071-1086.

Northup, D. E., Dahm, C. N., Melim, L. A., Spilde, M. N., Crossey, L. J., Lavoie, K. H., Mallory, L. M., Boston, P. J., Cunningham, K. I., & Barns, S. M. (2000). Evidence for geomicrobiological interactions in Guadalupe caves. *Journal of Cave and Karst Studies*, 62(2), 80-90.

Nouren, S., Bhatti, H. N., & Ilyas, S. (2011). Bioleaching of copper, aluminum, magnesium and manganese from brown shale by *Ganoderma lucidum*. *African Journal of Biotechnology*, *10*(52), 10664-10673.

Ofek, I. T. Z. H. A. K., Whitnack, E. L. L. E. N., & Beachey, E. H. (1983). Hydrophobic interactions of group A streptococci with hexadecane droplets. *Journal of Bacteriology*, *154*(1), 139-145.

Ohmura, N., Kitamura, K., & Saiki, H. (1993). Selective adhesion of *Thiobacillus ferrooxidans* to pyrite. *Applied and Environmental Microbiology*, *59*(12), 4044-4050.

Olsson- Francis, K., Simpson, A. E., Wolff- Boenisch, D., & Cockell, C. S. (2012). The effect of rock composition on cyanobacterial weathering of crystalline basalt and rhyolite. *Geobiology*, *10*(5), 434-444.

Pacheco, F. A., & Alencoão, A. M. (2006). Role of fractures in weathering of solid rocks: narrowing the gap between laboratory and field weathering rates. *Journal of Hydrology*, *316*(1), 248-265.

Palleroni, N. J., & Bradbury, J. F. (1993). *Stenotrophomonas*, a new bacterial genus for *Xanthomonas maltophilia* (Hugh 1980) Swings *et al.* 1983. *International Journal of Systematic and Evolutionary Microbiology*, *43*(3), 606-609.

Palmer Jr, R. J., Siebert, J., & Hirsch, P. (1991). Biomass and organic acids in sandstone of a weathering building: production by bacterial and fungal isolates. *Microbial Ecology*, 21(1), 253-266.

Pandey, G., & Jain, R. K. (2002). Bacterial chemotaxis toward environmental pollutants: role in bioremediation. *Applied and Environmental Microbiology*, *68*(12), 5789-5795.

Parales, R. E., & Harwood, C. S. (2002). Bacterial chemotaxis to pollutants and plant-derived aromatic molecules. *Current Opinion in Microbiology*, *5*(3), 266-273.

Pehl, M. J., Jamieson, W. D., Kong, K., Forbester, J. L., Fredendall, R. J., Gregory, G. A., McFarland, J.E., Healy, J.M & Orwin, P. M. (2012). Genes that influence swarming motility and biofilm formation in *Variovorax paradoxus* EPS. *PLoS One*, *7*(2), e31832.

Penner, E., Gillott, J. E., & Eden, W. J. (1970). Investigation of heave in Billings shale by mineralogical and iogeochemical methods. *Canadian Geotechnical Journal*, *7*(3), 333-338.

Percak- Dennett, E., He, S., Converse, B., Konishi, H., Xu, H., Corcoran, A., Noguera, D., Chan, C., Bhattacharyya, A., Borch, T. and Boyd, E. (2017) Microbial acceleration of aerobic pyrite oxidation at circumneutral pH. *Geobiology*, 1-14

Petsch, S. T., Edwards, K. J., & Eglinton, T. I. (2003). Abundance, distribution and δ13C analysis of microbial phospholipid-derived fatty acids in a black shale weathering profile. *Organic Geochemistry*, *34*(6), 731-743.

Petsch, S. T., Edwards, K. J., & Eglinton, T. I. (2005). Microbial transformations of organic matter in black shales and implications for global biogeochemical cycles. *Palaeogeography, Palaeoclimatology, Palaeoecology*, *219*(1), 157-170.

Petsch, S. T., Eglinton, T. I., & Edwards, K. J. (2001a). 14C-dead living biomass: evidence for microbial assimilation of ancient organic carbon during shale weathering. *Science*, *292*(5519), 1127-1131.

Petsch, S. T., Smernik, R. J., Eglinton, T. I., & Oades, J. M. (2001b). A solid state 13 C-NMR study of kerogen degradation during black shale weathering. *Geochimica et Cosmochimica Acta*, *65*(12), 1867-1882.

Pisapia, C., Humbert, B., Chaussidon, M., & Mustin, C. (2008). Perforative corrosion of pyrite enhanced by direct attachment of *Acidithiobacillus ferrooxidans*. *Geomicrobiology Journal*, *25*(6), 261-273.

Pizzarello, S., Cooper, G. W., & Flynn, G. J. (2006). The nature and distribution of the organic material in carbonaceous chondrites and interplanetary dust particles. *Meteorites and the Early Solar System II*, *1*, 625-651.

Polgári, M., Hein, J.R., Vigh, T., Szabó-Drubina, M., Fórizs, I., Bíró, L., Müller, A. and Tóth, A.L., (2012) Microbial processes and the origin of the Úrkút manganese deposit, Hungary. *Ore Geology Reviews*, *47*, 87-109.

Post, J. E. (1999). Manganese oxide minerals: Crystal structures and economic and environmental significance. *Proceedings of the National Academy of Sciences*, *96*(7), 3447-3454.

Powell, J. H. (1984). Lithostratigraphical nomenclature of the Lias Group in the Yorkshire Basin. In *Proceedings of the Yorkshire geological and polytechnic Society* (Vol. 45, No. 1-2, pp. 51-57). Geological Society of London.

Powell, J. H. (2010). Jurassic sedimentation in the Cleveland Basin: a review. *Proceedings of the Yorkshire Geological Society*, *58*(1), 21-72.

Puente, M. E., Bashan, Y., Li, C. Y., & Lebsky, V. K. (2004). Microbial populations and activities in the rhizoplane of rock-weathering desert plants. I. Root colonization and weathering of igneous rocks. *Plant Biology*, 6(05), 629-642.

Pye, K., & Miller, J. A. (1990). Chemical and biochemical weathering of pyritic mudrocks in a shale embankment. *Quarterly Journal of Engineering Geology and Hydrogeology*, *23*(4), 365-382.

Quigley, R. M., Zajic, J. E., McKyes, E., & Yong, R. N. (1973). Biochemical alteration and heave of black shale; detailed observations and interpretations. *Canadian Journal of Earth Sciences*, *10*(6), 1005-1015.

Rajpert, L., Skłodowska, A., & Matlakowska, R. (2013). Biotransformation of copper from Kupferschiefer black shale (Fore-Sudetic Monocline, Poland) by yeast Rhodotorula mucilaginosa LM9. *Chemosphere*, *91*(9), 1257-1265.

Rawson, P.F., Wright, J.K., Starmer, I.C., Whitham, F., Hemingway, J.E. and Greensmith, J.T., 2000. *The Yorkshire Coast* (No. 34). Geologists' Association.

Reddy, C. S. K., Ghai, R., & Kalia, V. (2003). Polyhydroxyalkanoates: an overview. *Bioresource Technology*, *87*(2), 137-146.

Rehder, D. (2015). The role of vanadium in biology. *Metallomics*, *7*(5), 730-742.

Reichelt, R. (2007). Scanning electron microscopy. In *Science of Microscopy* (pp. 133-272). Springer New York.

Rhine, E. D., Onesios, K. M., Serfes, M. E., Reinfelder, J. R., & Young, L. Y. (2008). Arsenic transformation and mobilization from minerals by the arsenite oxidizing strain WAO. *Environmental Science & Technology*, *42*(5), 1423-1429.

Richardson, A. E., & Hadobas, P. A. (1997). Soil isolates of *Pseudomonas* spp. that utilise inositol phosphates. *Canadian Journal of Microbiology*, *43*(6), 509-516.

Robinson, L. A. (1977a). Marine erosive processes at the cliff foot. *Marine Geology*, *23*(3), 257-271.

Robinson, L. A. (1977b). Erosive processes on the shore platform of northeast Yorkshire, England. *Marine Geology*, *23*(4), 339-361.

Robinson, L. A. (1977c). The morphology and development of the northeast Yorkshire shore platform. *Marine Geology*, *23*(3), 237-255.

Rodrıguez, Y., Ballester, A., Blazquez, M. L., Gonzalez, F., & Munoz, J. A. (2003). New information on the sphalerite bioleaching mechanism at low and high temperature. *Hydrometallurgy*, *71*(1-2), 57-66.

Rogers, J. R., & Bennett, P. C. (2004). Mineral stimulation of subsurface microorganisms: release of limiting nutrients from silicates. *Chemical Geology*, *203*(1), 91-108.

Rogers, J. R., Bennett, P. C., & Choi, W. J. (1998). Feldspars as a source of nutrients for microorganisms. *American Mineralogist*, *83*(11), 1532-1540.

Rojas-Chapana, J. A., & Tributsch, H. (2004). Interfacial activity and leaching patterns of *Leptospirillum ferrooxidans* on pyrite. *FEMS Microbiology Ecology*, *47*(1), 19-29.

Rossbach, S., Wilson, T. L., Kukuk, M. L., & Carty, H. A. (2000). Elevated zinc induces siderophore biosynthesis genes and a zntA-like gene in *Pseudomonas fluorescens*. *FEMS Microbiology Letters*, 191(1), 61-70.

Rosser, N. J., Brain, M. J., Petley, D. N., Lim, M., & Norman, E. C. (2013). Coastline retreat via progressive failure of rocky coastal cliffs. *Geology*, *41*(8), 939-942.

Rosser, N. J., Petley, D. N., Lim, M., Dunning, S. A., & Allison, R. J. (2005). Terrestrial laser scanning for monitoring the process of hard rock coastal cliff erosion. *Quarterly Journal of Engineering Geology and Hydrogeology*, *38*(4), 363-375.

Rozycki, H., & Strzelczyk, E. (1986). Organic acids production by *Streptomyces* spp. isolated from soil, rhizosphere and mycorrhizosphere of pine (*Pinus sylvestris L.*). *Plant and Soil*, *96*(3), 337-345.

Saarikoski, S., Timonen, H., Saarnio, K., Aurela, M., Järvi, L., Keronen, P., Kerminen, V-M., & Hillamo, R. (2008). Sources of organic carbon in fine particulate matter in northern European urban air. *Atmospheric Chemistry and Physics, 8*(20), 6281-6295.

Sadisun, I. A., Shimada, H., & Matsui, K. (2000). Characterization of weathered claystone and their engineering significance. In *Indonesian Scientific Meeting, Fukuoka, Japan. ISSN*, 1343-2451.

Saha, R., Saha, N., Donofrio, R. S., & Bestervelt, L. L. (2013). Microbial siderophores: a mini review. *Journal of Basic Microbiology*, *53*(4), 303-317.

Sand, W., Gehrke, T., Jozsa, P. G., & Schippers, A. (2001). (Bio) chemistry of bacterial leaching—direct vs. indirect bioleaching. *Hydrometallurgy*, *59*(2), 159-175.

Satola, B., Wübbeler, J. H., & Steinbüchel, A. (2013). Metabolic characteristics of the *species Variovorax paradoxus. Applied Microbiology and Biotechnology*, *97*(2), 541-560.

Schillawski, S., & Petsch, S. (2008). Release of biodegradable dissolved organic matter from ancient sedimentary rocks. *Global Biogeochemical Cycles*, *22*(3), doi:10.1029/2007GB002980

Schippers, A., Hedrich, S., Vasters, J., Drobe, M., Sand, W., & Willscher, S. (2013). Biomining: metal recovery from ores with microorganisms. In *Geobiotechnology I* (pp. 1-47). Springer Berlin Heidelberg.

Schippers, A., Jozsa, P., & Sand, W. (1996). Sulfur chemistry in bacterial leaching of pyrite. *Applied and Environmental Microbiology*, *62*(9), 3424-3431.

Schlegel, M. E., McIntosh, J. C., Petsch, S. T., Orem, W. H., Jones, E. J., & Martini, A. M. (2013). Extent and limits of biodegradation by *in situ* methanogenic consortia in shale and formation fluids. *Applied Geochemistry*, *28*, 172-184.

Schmalenberger, A., Hodge, S., Bryant, A., Hawkesford, M. J., Singh, B. K., & Kertesz, M. A. (2008). The role of *Variovorax* and other *Comamonadaceae* in sulfur transformations by microbial wheat rhizosphere communities exposed to different sulfur fertilization regimes. *Environmental Microbiology*, *10*(6), 1486-1500.

Scholl, M. A., Mills, A. L., Herman, J. S., & Hornberger, G. M. (1990). The influence of mineralogy and solution chemistry on the attachment of bacteria to representative aquifer materials. *Journal of Contaminant Hydrology*, *6*(4), 321-336.

Schwyn, B., & Neilands, J. B. (1987). Universal chemical assay for the detection and determination of siderophores. *Analytical Biochemistry*, 160(1), 47-56.

Seewald, J. S. (2003). Organic-inorganic interactions in petroleum-producing sedimentary basins. *Nature*, *426*(6964), 327.

Sethurajan, M., Aruliah, R., Karthikeyan, O. P., & Balasubramanian, R. (2012). Bioleaching of copper from black shale ore using mesophilic mixed populations in an air up-lift bioreactor. *Environmental Engineering and Management Journal*, *11*(10), 1839-1848.

Sharma, P. K., & Rao, K. H. (2003). Adhesion of *Paenibacillus polymyxa* on chalcopyrite and pyrite: surface thermodynamics and extended DLVO theory. *Colloids and Surfaces B: Biointerfaces*, *29*(1), 21-38.

Shrout, J. D., Chopp, D. L., Just, C. L., Hentzer, M., Givskov, M., & Parsek, M. R. (2006). The impact of quorum sensing and swarming motility on *Pseudomonas aeruginosa* biofilm formation is nutritionally conditional. *Molecular Microbiology*, *62*(5), 1264-1277.

Silverman, M. P. (1967). Mechanism of bacterial pyrite oxidation. *Journal of Bacteriology*, *94*(4), 1046-1051.

Simate, G. S., & Ndlovu, S. (2014). Acid mine drainage: Challenges and opportunities. *Journal of Environmental Chemical Engineering*, *2*(3), 1785-1803.

Singer, P. C., & Stumm, W. (1970). Acidic mine drainage: the rate-determining step. *Science*, *167*(3921), 1121-1123.

Singh, B., & Gilkes, R. J. (1992). Properties and distribution of iron oxides and their association with minor elements in the soils of south- western Australia. *European journal of Soil Science*, *43*(1), 77-98.

Skidmore, M., Anderson, S. P., Sharp, M., Foght, J., & Lanoil, B. D. (2005). Comparison of microbial community compositions of two subglacial environments reveals a possible role for microbes in chemical weathering processes. *Applied and Environmental Microbiology*, *71*(11), 6986-6997.

Skinner, H. C. W. (1993). A review of apatites, iron and manganese minerals and their roles as indicators of biological activity in black shales. *Precambrian Research*, *61*(3-4), 209-229.

Sonnleitner, R., Redl, B., Pipal, A., & Schinner, F. (2011). Chemolithotrophic Metal Mobilization from Dolomite. *Geomicrobiology Journal*, *28*(8), 651-659.

Spilde, M. N., Northup, D. E., Boston, P. J., Schelble, R. T., Dano, K. E., Crossey, L. J., & Dahm, C. N. (2005). Geomicrobiology of cave ferromanganese deposits: a field and laboratory investigation. *Geomicrobiology Journal*, *22*(3-4), 99-116.

Spink, T. W., & Norbury, D. R. (1993). The engineering geological description of weak rocks and overconsolidated soils. *Engineering Geology Special Publication*, 289-289.

Spring, S., Kampfer, P., Ludwig, W., & Schleifer, K. H. (1996). Polyphasic Characterization of the Genus *Leptothrix*: New Descriptions of *Leptothrix mobilis* sp. nov. and *Leptothrix discophora* sp. nov. nom. rev. and Emended Description of *Leptothrix cholodnii* emend. *Systematic and Applied Microbiology*, *19*(4), 634-643.

Stasiuk, R., Włodarczyk, A., Karcz, P., Janas, M., Skłodowska, A., & Matlakowska, R. (2017). Bacterial weathering of fossil organic matter and organic carbon mobilization from subterrestrial K upferschiefer black shale: long- term laboratory studies. *Environmental Microbiology Reports*, 9(4), 459-466.

Stein, L. Y., La Duc, M. T., Grundl, T. J., & Nealson, K. H. (2001). Bacterial and archaeal populations associated with freshwater ferromanganous micronodules and sediments. *Environmental Microbiology*, *3*(1), 10-18.

Stenström, T. A. (1989). Bacterial hydrophobicity, an overall parameter for the measurement of adhesion potential to soil particles. *Applied and Environmental Microbiology*, *55*(1), 142-147.

Stewart, E. J. (2012). Growing unculturable bacteria. *Journal of Bacteriology*, *194*(16), 4151-4160.

Strąpoć, Dariusz, Maria Mastalerz, Katherine Dawson, Jennifer Macalady, Amy V. Callaghan, Boris Wawrik, Courtney Turich, and Matthew Ashby (2011) Biogeochemistry of microbial coal-bed methane, *Annual Review of Earth and Planetary Sciences* 39, 617–656

Sudek, L. A., Templeton, A. S., Tebo, B. M., & Staudigel, H. (2009). Microbial ecology of Fe (hydr) oxide mats and basaltic rock from Vailulu'u Seamount, American Samoa. *Geomicrobiology Journal*, *26*(8), 581-596.

Sure, S., Ackland, M. L., Torriero, A. A., Adholeya, A., & Kochar, M. (2016). Microbial nanowires: an electrifying tale. *Microbiology*, *162*(12), 2017-2028.

Suzuki, I. (2001). Microbial leaching of metals from sulfide minerals. *Biotechnology Advances*, *19*(2), 119-132.

Szubert, A., Sadowski, Z., Gros, C. P., Barbe, J. M., & Guilard, R. (2006). Identification of metalloporphyrins extracted from the copper bearing black shale of Fore Sudetic Monocline (Poland). *Minerals Engineering*, 19(11), 1212-1215.

Tasa, A., Vuorinen, A., Garcia Jr, O., & Tuovinen, O. H. (1997). Biologically enhanced dissolution of a pyrite- rich black shale concentrate. *Journal of Environmental Science & Health part A*, *32*(9-10), 2683-2695.

Taunton, A. E., Welch, S. A., & Banfield, J. F. (2000). Microbial controls on phosphate and lanthanide distributions during granite weathering and soil formation. *Chemical Geology*, *169*(3-4), 371-382.

Taylor, R. K. (1988). Coal Measures mudrocks: composition, classification and weathering processes. *Quarterly Journal of Engineering Geology and Hydrogeology*, *21*(1), 85-99.

Tebo, B. M., Bargar, J. R., Clement, B. G., Dick, G. J., Murray, K. J., Parker, D., Verity, R. & Webb, S. M. (2004). Biogenic manganese oxides: properties and mechanisms of formation. *Annual Reviews in Earth Planetary Sciences*, *32*, 287-328.

Tebo, B. M., Ghiorse, W. C., Van Waasbergen, L. G., Siering, P. L., & Caspi, R. (1997). Bacterially mediated mineral formation; insights into manganese (II) oxidation from molecular genetic and biochemical studies. *Reviews in Mineralogy and Geochemistry*, *35*(1), 225-266.

Tebo, B. M., Johnson, H. A., McCarthy, J. K., & Templeton, A. S. (2005). Geomicrobiology of manganese (II) oxidation. *Trends in Microbiology*, 13(9), 421-428.

The Irish Times (2017), Pyrite costs in Dublin social housing estates exceed €12m, Friday July 7th 2017, accessed at: https://www.irishtimes.com/news/environment/pyrite-costs-in-dublin-social-housing-estates-exceed-12m-1.3145922

Torrentó, C., Urmeneta, J., Edwards, K. J., & Cama, J. (2012). Characterization of attachment and growth of *Thiobacillus denitrificans* on pyrite surfaces. *Geomicrobiology Journal*, *29*(4), 379-388.

Tributsch, H. (1999). Direct versus indirect bioleaching. *Process Metallurgy*,*9*, 51-60.

Tributsch, H. (2001). Direct versus indirect bioleaching. *Hydrometallurgy*,*59*(2), 177-185.

Trotignon, L., Michaud, V., Lartigue, J. E., Ambrosi, J. P., Eisenlohr, L., Griffault, L., Combarieu. M. & Daumas, S. (2002). Laboratory simulation of an oxidizing perturbation in a deep granite environment. *Geochimica et Cosmochimica Acta*, *66*(14), 2583-2601.

Trujillo, M. E., Kroppenstedt, R. M., Fernández-Molinero, C., Schumann, P., & Martínez-Molina, E. (2007). *Micromonospora lupini* sp. nov. and *Micromonospora saelicesensis* sp. nov., isolated from root nodules of *Lupinus angustifolius*. *International Journal of Systematic and Evolutionary Microbiology*, *57*(12), 2799-2804.

Tuson, H. H., & Weibel, D. B. (2013). Bacteria–surface interactions. *Soft matter*, *9*(17), 4368-4380.

Tuttle, M. L., & Breit, G. N. (2009). Weathering of the New Albany Shale, Kentucky, USA: I. Weathering zones defined by mineralogy and major-element composition. *Applied Geochemistry*, *24*(8), 1549-1564.

Tuttle, M. L., Breit, G. N., & Goldhaber, M. B. (2009). Weathering of the New Albany Shale, Kentucky: II. Redistribution of minor and trace elements. *Applied Geochemistry*, *24*(8), 1565-1578.

Uroz, S., Calvaruso, C., Turpault, M. P., & Frey-Klett, P. (2009). Mineral weathering by bacteria: ecology, actors and mechanisms. *Trends in Microbiology*, *17*(8), 378-387.

Vandamme, P., Bernardet, J. F., Segers, P., Kersters, K., & Holmes, B. (1994). NOTES: New Perspectives in the Classification of the Flavobacteria: Description of Chryseobacterium gen. nov., Bergeyella gen. nov., and Empedobacter nom. rev. *International Journal of Systematic and Evolutionary Microbiology*, *44*(4), 827-831.

Vandenabeele, P. (2013). *Practical Raman spectroscopy: an introduction*. John Wiley & Sons.

Vandenbroucke, M. (2003). Kerogen: from types to models of chemical structure. *Oil & Gas Science and Technology*, *58*(2), 243-269.

Vann Jones, E. V., Rosser, N. J., Brain, M. J., & Petley, D. N. (2015). Quantifying the environmental controls on erosion of a hard rock cliff. *Marine Geology*, *363*, 230-242.

Vengosh, A., Jackson, R. B., Warner, N., Darrah, T. H., & Kondash, A. (2014). A critical review of the risks to water resources from unconventional shale gas development and hydraulic fracturing in the United States. *Environmental Science & Technology*, *48*(15), 8334-8348.

Vera, M., Schippers, A., & Sand, W. (2013). Progress in bioleaching: fundamentals and mechanisms of bacterial metal sulfide oxidation—part A. *Applied Microbiology and Biotechnology*, *97*(17), 7529-7541.

Viles, H. (2016). Technology and geomorphology: Are improvements in data collection techniques transforming geomorphic science? *Geomorphology*, *270*, 121-133.

Viles, H. A. (2012). Microbial geomorphology: a neglected link between life and landscape. *Geomorphology*, *157*, 6-16.

Vine, J.D., Tourtelot, E.B. (1970). Geochemistry of black shale deposits—a summary report. *Economic Geology.* 65, 253–272.

Visca, P. A. O. L. O., Colotti, G., Serino, L., Verzili, D., Orsi, N., & Chiancone, E. (1992). Metal regulation of siderophore synthesis in *Pseudomonas aeruginosa* and functional effects of siderophore-metal complexes. *Applied and Environmental Microbiology*, *58*(9), 2886-2893.

Vrvić, M. M., Djordjević, V., Savković, O., Vučetić, J., & Vitorović, D. (1988). Preparation of rich kerogen concentrates: removal of pyrite with *Thiobacillus ferrooxidans*. *Organic Geochemistry*, *13*(4-6), 1109-1114.

Vrvić, M. M., Matić, V., Vučetić, J., & Vitorović, D. (1989). Demineralization of an oil shale by Bacillus circulans ("siliceous bacteria"). *Organic Geochemistry*, *16*(4-6), 1203-1209.

Vupputuri, S., Fathepure, B. Z., Wilber, G. G., Sudoi, E., Nasrazadani, S., Ley, M. T., & Ramsey, J. D. (2015). Isolation of a sulfur-oxidizing Streptomyces sp. from deteriorating bridge structures and its role in concrete deterioration. *International Biodeterioration & Biodegradation*, *97*, 128-134.

Wacey, D., Saunders, M., Brasier, M. D., & Kilburn, M. R. (2011). Earliest microbially mediated pyrite oxidation in~ 3.4 billion-year-old sediments. *Earth and Planetary Science Letters*, *301*(1), 393-402.

Wai, S. N., Mizunoe, Y., Takade, A., Kawabata, S. I., & Yoshida, S. I. (1998). *Vibrio cholerae* O1 strain TSI-4 produces the exopolysaccharide materials that determine colony morphology, stress resistance, and biofilm formation. *Applied and Environmental Microbiology*, *64*(10), 3648-3655.

Wakeman, K., Auvinen, H., & Johnson, D. B. (2008). Microbiological and geochemical dynamics in simulated- heap leaching of a polymetallic sulfide ore. *Biotechnology and Bioengineering*, *101*(4), 739-750.

Wang, Q., Chen, X., Jha, A. N., & Rogers, H. (2014). Natural gas from shale formation–the evolution, evidences and challenges of shale gas revolution in United States. *Renewable and Sustainable Energy Reviews*, *30*, 1-28.

Wang, Z., & Krupnick, A. (2013). A retrospective review of shale gas development in the United States: What led to the boom?, Resources For the Future, Discussion Paper

Watling, H. R. (2014). Review of biohydrometallurgical metals extraction from polymetallic mineral resources. *Minerals*, *5*(1), 1-60.

Watling, H. R. (2015). Review of Biohydrometallurgical Metals Extraction from Polymetallic Mineral Resources. *Minerals*, *5*(1), 1-60.

Welch, S. A., & Vandevivere, P. (1994). Effect of microbial and other naturally occurring polymers on mineral dissolution. *Geomicrobiology Journal*, *12*(4), 227-238.

Welch, S. A., Barker, W. W., & Banfield, J. F. (1999). Microbial extracellular polysaccharides and plagioclase dissolution. *Geochimica et Cosmochimica Acta*, *63*(9), 1405-1419.

Wengel, M., Kothe, E., Schmidt, C. M., Heide, K., & Gleixner, G. (2006). Degradation of organic matter from black shales and charcoal by the wood-rotting fungus *Schizophyllum commune* and release of DOC and heavy metals in the aqueous phase. *Science of the Total Environment*, *367*(1), 383-393.

White, A. F., & Brantley, S. L. (2003). The effect of time on the weathering of silicate minerals: why do weathering rates differ in the laboratory and field? *Chemical Geology*, 202(3), 479-506.

Willems, A., De Ley, J., Gillis, M., & Kersters, K. (1991). Notes: *comamonadaceae*, a new family encompassing the *acidovorans* rRNA complex, including *Variovorax paradoxus* gen. nov., comb. nov., for *Alcaligenes paradoxus* (Davis 1969). *International Journal of Systematic and Evolutionary Microbiology*, *41*(3), 445-450.

Wilson, E. J. (1987). Pyritic shale heave in the Lower Lias at Barry, Glamorgan. *Quarterly Journal of Engineering Geology and Hydrogeology*, *20*(3), 251-253.

Włodarczyk, A., & Matlakowska, R. (2017). Mikrobiologiczne procesy utleniania kopalnej materii organicznej miedzionośnego łupka bitumicznego Kupferschiefer (monoklina przedsudecka) – In Polish.

Włodarczyk, A., Stasiuk, R., Skłodowska, A., & Matlakowska, R. (2015). Extracellular compounds produced by bacterial consortium promoting elements mobilization from polymetallic Kupferschiefer black shale (Fore-Sudetic Monocline, Poland). *Chemosphere*, *122*, 273-279.

Włodarczyk, A., Szymańska, A., Bąkowska, A., Skłodowska, A., & Matlakowska, R. (2016). Extracellular membrane structures–a component of the epilithic biofilm on the Kupferschiefer black shale. *Geomicrobiology Journal,* 0(0), 1–10.

Workentine, M. L., Harrison, J. J., Weljie, A. M., Tran, V. A., Stenroos, P. U., Tremaroli, V., Vogel. H., Ceri. H., & Turner, R. J. (2010). Phenotypic and metabolic profiling of colony morphology variants evolved from *Pseudomonas fluorescens biofilms*. *Environmental Microbiology*, *12*(6), 1565-1577.

Xiao, C. Q., Chi, R. A., He, H., & Zhang, W. X. (2009). Characterization of tricalcium phosphate solubilization by *Stenotrophomonas maltophilia* YC isolated from phosphate mines. *Journal of Central South University of Technology*, *16*, 581-587.

Yang, W., Zhang, Z., Zhang, Z., Chen, H., Liu, J., Ali, M., Liu, F., & Li, L. (2013). Population structure of manganese-oxidizing bacteria in stratified soils and properties of manganese oxide aggregates under manganese–complex medium enrichment. *PLoS One*, *8*(9), e73778.

Yesavage, T., Fantle, M. S., Vervoort, J., Mathur, R., Jin, L., Liermann, L. J., & Brantley, S. L. (2012). Fe cycling in the Shale Hills Critical Zone Observatory, Pennsylvania: an analysis of biogeochemical weathering and Fe isotope fractionation. *Geochimica et Cosmochimica Acta*, *99*, 18-38.

Young, G., & Bird, J. (1822). *A geological survey of the Yorkshire Coast*, Printed by R. Kirby, Whitby, England.

Zaitsev, G. M., Uotila, J. S., & Häggblom, M. M. (2007). Biodegradation of methyl tert-butyl ether by cold-adapted mixed and pure bacterial cultures. *Applied Microbiology and Biotechnology*, *74*(5), 1092-1102.

Zhang, J., Lion, L. W., Nelson, Y. M., Shuler, M. L., & Ghiorse, W. C. (2002). Kinetics of Mn (II) oxidation by *Leptothrix discophora* SS1. *Geochimica et Cosmochimica Acta*, 66(5), 773-781.

Zhang, S., Wan, R., Wang, Q., & Xie, S. (2011). Identification of anthracene degraders in leachate-contaminated aquifer using stable isotope probing. *International Biodeterioration & Biodegradation*, *65*(8), 1224-1228.

Zhang, x. Q., & Li, y. S. (2017). Changes in shale oil composition and yield after bioleaching by *Bacillus mucilaginosus* and *Thiobacillus ferrooxidans*. *Oil Shale*, *34*(2).

Zhang, X. Q., Ren, H. J., Liu, N., Zhang, L. Y., & Zhou, R. (2013). Changes in texture and retorting yield in oil shale during its bioleaching by *Bacillus Mucilaginosus*. *Chemical Research in Chinese Universities*, *29*(2), 294-298.

Zhao, F., Qiu, G., Huang, Z., He, L., & Sheng, X. (2013). Characterization of *Rhizobium* sp. *Q32* isolated from weathered rocks and its role in silicate mineral weathering. *Geomicrobiology Journal*, *30*(7), 616-622.

Zhou, H. B., Zeng, W. M., Yang, Z. F., Xie, Y. J., & Qiu, G. Z. (2009). Bioleaching of chalcopyrite concentrate by a moderately thermophilic culture in a stirred tank reactor. *Bioresource Technology*, *100*(2), 515-520.

Zhu, W., & Reinfelder, J. R. (2012). The microbial community of a black shale pyrite biofilm and its implications for pyrite weathering. *Geomicrobiology Journal*, *29*(2), 186-193.

Zhu, W., Young, L. Y., Yee, N., Serfes, M., Rhine, E. D., & Reinfelder, J. R. (2008). Sulfide-driven arsenic mobilization from arsenopyrite and black shale pyrite. *Geochimica et Cosmochimica Acta*, *72*(21), 5243-5250.